Defining the Role of the Actin Cytoskeleton in Cellular Uptake of Cell Penetrating Peptides

A thesis submitted for the degree of
Philosophiae Doctor in Cardiff University

By

Lin He

March 2016

Cardiff School of Pharmacy and Pharmaceutical Sciences
Cardiff University

Abstract

The increased need for macromolecular therapeutics, such as proteins and nucleotides, to reach intracellular targets asks for more effective delivery vectors and a higher level of understanding of their mechanism of action. Cell Penetrating Peptides (CPPs) have been shown to deliver a range of macromolecules into cells either through direct plasma membrane translocation or by endocytosis. All known endocytic pathways involve cell-cortex remodelling, a process shown to be regulated by reorganisation of the actin cytoskeleton. Links between actin remodelling and CPP uptake has been shown but more information is required to determine the extent of this association and how it could influence further research into improving the delivery capacity of these entities. This project, by using the CPP octaarginine (R8) investigated how actin disorganisation influences the cellular entry of this peptide when attached to a model fluorophore Alexa 488 or Enhanced Green Fluorescent Protein (EGFP).

A confocal microscopy technique was initially developed, allowing for high-resolution and spatial characterization of the actin cytoskeleton at different cell depths. Analysis using this developed method was used to highlight that serum starvation has a strong influence on the capacity of R8 to cause membrane blebs and possibly macropinocytosis. Using a range of direct or indirect actin inhibitors this work also highlighted how they can rapidly cause dramatic cellular deformities beyond the level of actin or more subtly affect actin organisation. Further confocal studies revealed that choice of cell line significantly affects the effect of actin disruption on CPP entry and that this is highly dependent on the nature of the probe. This was exemplified by results showing inhibition of EGFP-R8 uptake in HeLa cells treated with cytochalasin D, latrunculin B and jasplakinolide but a dramatic increase in uptake in A431 cells when they were treated with these drugs.

The regulation of actin dynamics involves various kinases including Rho–associated kinases ROCKs, and Src family kinases. The ROCK inhibitor Y27632 induced the formation of actin needles running perpendicular to the plasma membrane of A431 cells and increased EGFP-R8 internalisation. By contrast, Src inhibitor PP2 had little effect on both the actin cytoskeleton and EGFP-R8 uptake but completely abrogated the effects of Cyt D on cellular uptake. This demonstrates for the first time that pre-treatment of actin with one inhibitor can negate the endocytic effects of another actin inhibitor working on a different target.

Overall this study highlights the importance of analysing actin in detail to identify how CPPs and possibly other drug delivery vectors and formulations interact with cells to gain entry. Under defined experimental conditions R8 can modify the actin cytoskeleton and requires a functional or dysfunctional actin network to allow for maximal cellular entry.

Acknowledgements

First and foremost I would like to thank my principal supervisor Prof. Arwyn Jones for giving me the opportunity to undertake this PhD project and for providing me with invaluable guidance and inspiration over the past four years. Without his unwavering support and incredible patience, I would not have been able to complete the project and by extension the thesis. Furthermore, I would like to extend my thanks to my co-supervisor Dr. Peter Watson for his wisdom, mentoring and input throughout this project, from inception to completion.

I must also thank and acknowledge my current and former lab members that I have had the incredible joy and pleasure of working with: Dr. Edd Sayers, Dr. Jenny Wymant, Dr. Helen Wiggins, Dr. Noura Elissa, Hope Roberts-Dalton and Dr. Paul Moody for their advice, support and friendship. They were always open to assist me whenever I was stuck. In addition, I would like to gratefully acknowledge the contribution of my other colleagues and friends from the School of Pharmacy and the School of BioSciences: Harsha Siani, Dr. Xin Zhao and Dr. Kez Cleal whose friendship, encouragement and technical assistance have been very much appreciated.

Lastly and personally, I would like to express my deepest gratitude to my family for their constant and overwhelming support over the course of my PhD. Thank you to my Mum and Dad, who have been with me through every step of my life journey.

Declaration

This work has not been submitted in substance for any other degree or award at this or any other university or place of learning, nor is being submitted concurrently in candidature for any degree or other award.

Signed ……………He Lin…………………………… (candidate)

Date …14-09-2016…………

STATEMENT 1

This thesis is being submitted in partial fulfillment of the requirements for the degree of PhD.

Signed ……………He Lin…………………………… (candidate)

Date …14-09-2016…………

STATEMENT 2

This thesis is the result of my own independent work/investigation, except where otherwise stated.
Other sources are acknowledged by explicit references. The views expressed are my own.

Signed ……………He Lin…………………………… (candidate)

Date …14-09-2016…………

STATEMENT 3: PREVIOUSLY APPROVED BAR ON ACCESS

I hereby give consent for my thesis, if accepted, to be available online in the University's Open Access repository and for inter-library loans after expiry of a bar on access previously approved by the Academic Standards & Quality Committee.

Signed ……………He Lin…………………………… (candidate)

Date …14-09-2016…………

Table of Contents

List of Figures and Tables

List of Publications and Conference Abstract

Publications

He, L., Watson, P.D. and Jones, A.T. 2015. **Visualizing actin architectures in cells incubated with cell-penetrating peptides.** *Methods in Molecular Biology.* 1324, p. 247-259.

Cleal, K., He, L., Watson, P.D. and Jones, A.T. 2013. **Endocytosis, intracellular traffic and fate of cell penetrating peptide based conjugates and nanoparticles.** *Current Pharmaceutical Design.* 19(16), p. 2878-2894.

Al Soraj, M., He, L., Peynshaert, K., Cousaert, J., Vercauteren, D., Braeckmans, K., De Smedt, S.C. and Jones, A.T. 2012. **siRNA and pharmacological inhibition of endocytic pathways to characterize the differential role of macropinocytosis and the actin cytoskeleton on cellular uptake of dextran and cationic cell penetrating peptides octaarginine (R8) and HIV-Tat.** *Journal of Controlled Release.* 161(1), p. 132-141.

Conference abstract

He, L., Al Soraj, M., Riester, P., Watson, P.D. and Jones, A.T. 2014. **Optimisation of methods for assessing the role of the actin cytoskeleton in endocytic uptake of drug delivery vectors.** 13th European Symposium on Controlled Drug Delivery (ESCDD2014), Egmond aan Zee, The Netherlands.

Abbreviations

AAV	Adeno-associated virus
ABP	Actin-binding protein
ADF	Actin depolymerising factor
AP2	Adaptor Protein-2
APC	Adenomatous polyposis coli
APS	Ammonium persulphate
ARP2/3	Actin-related protein 2/3 complex
BSA	Bovine serum albumin
$CaCl_2$	Calcium chloride
CBA	Cell Body and Apex
CCV	Clathrin-coated vesicle
CHC	Clathrin heavy chain
CLC	Clathrin light chain
CLIC	Clathrin-independent carrier
CME	Clathrin-mediated endocytosis
CPP	Cell penetrating peptide
CT	Cholera toxin
CTxB	Cholera toxin B subunit
Cyt D	Cytochalasin D
DDV	Drug delivery vector
DIC	Differential interference contrast microscopy
DMEM	Dulbecco's Modified Eagle's medium
DMSO	Dimethyl sulphoxide
DTT	Dithiothreitol
EDTA	Ethylenediaminetetraacetic acid
EGF	Epidermal growth factor
EGFR	Epidermal growth factor receptor
EGFP	Enhanced green fluorescent protein
EIPA	5-(N-ethyl-N-isopropyl) amiloride
EPS15	EGFR pathway substrate 15
ER	Endoplasmic reticulum
F-actin	Actin filament
FBS	Fetal bovine serum
FH	Formin homology
FRK	Fyn-related kinase
G-actin	Globular actin
GAG	Glycosaminoglycan
GBD	GTPase-binding domain
GEEC	GPI-enriched early endosomal compartment
GFP	Green fluorescent protein
GPI	Glycosylphosphatidylinositol
GSL	Glycosohingolipid
GUV	Giant unilamellar vesicle
HIV-1	Human immunodeficiency virus 1
HSC70	Heat shock cognate 70
HSV-1	Herpes simplex-1virus
IF	Intermediate filament
IPTG	Isopropyl β-D-1-thiogalactopyranoside

JAS	Jasplakinolide
JMY	Junction-mediating regulatory protein
Lat B	Latrunculin B
LDL	Low density lipoprotein
MAP	Model amphipathic peptide
MVB	Multivesicular body
$MgCl_2$	Magnesium chloride
NaCl	Sodium chloride
NaOH	Sodium hydroxide
NDDS	Nanoscale drug delivery system
NLS	Nuclear localisation sequence
NP	Nanoparticle
NPF	Nucleation promoting factor
NRTK	Non-receptor tyrosine kinases
NTA	Nitrilotriacetic acid
NV-DDM	Non-viral drug delivery method
PAK-1	p21-activated kinase-1
Pas	Penetration accelerating sequence
PDGF	Platelet-derived growth factor
PDGFR	Platelet-derived growth factor receptor
PEG	Polyethylene glycol
PI3K	Phosphatidylinositol-3 kinase
PKC	Protein kinase C
PRK2	Protein kinase C-related protein kinase 2
PtdIns	Phospholipid phosphatidylinositol
$PtdIns(3,4)P_2$	Phosphatidylinositol (3,4)-bisphosphate
$PtdIns(3,4,5)P_3$	Phosphatidylinositol (3,4,5)-trisphosphate
$PtdIns(4,5)P_2$	Phosphatidylinositol (4,5)-bisphosphate
PVDF	Polyvinylidene fluoride
Rh-P	Rhodamine-conjugated phalloidin
RN-Tre	Related protein N-terminal threonine
RTK	Receptor tyrosine kinase
SDS	Sodium dodecyl sulfate
SFK	Src-family kinase
SH3	SRC homology 3
SNX5	Sorting nexin 5
SNX9	Sorting nexin 9
SV40	Simian virus 40
Tat	Trans-activator of transcription
TEMED	Tetramethylethylenediamine
TfR	Transferrin receptor
TGN	Trans-Golgi network
TP10	Transportan 10
WASP	Wiskott-Aldrich syndrome protein
WAVE	WASP-family verprolin homologue isoforms
WASH	WASP and WAVE homologue
WH2	WASP homology 2
WHAMM	WASP homologue associated with actin, membranes and microtubules
YFP	Yellow fluorescent protein

Chapter 1: Introduction

1.1 Therapeutic macromolecules and drug delivery vectors (DDVs)

Therapeutic macromolecules, such as nucleic acids, peptides and high-purity recombinant proteins, are a class of clinically applicable compounds with high molecular weight that can be defined as macromolecular therapeutics. Also termed macro biopharmaceuticals, these are receiving increasing research interest and show significant potential in the treatment of acquired diseases such as cancer and also hereditary genetic disorders. However, the efficacy of newly discovered macromolecules is still impeded by several physiological and cellular barriers, non-specific bio-distribution and poor bioavailability caused by clearance in the body (Wassef et al., 1991). Therefore it is of crucial importance to design and develop new approaches for efficient and safe macromolecular delivery to target sites.

In *in vitro* studies, the first major obstacle to efficient delivery of macromolecules to intracellular targets or locations is the plasma membrane (Cleal et al., 2013). The lipid-based bilayer of the plasma membrane forms a highly effective barrier that separates the intracellular environment from the extracellular space. As a result, the intracellular entry of most macromolecules is blocked due to impermeability of the plasma membrane to these large entities (Copolovici et al., 2014). The fact that most of the therapeutic macromolecules are hydrophilic is also a further hindrance. One of the most widely investigated approaches to translocate macromolecules across the plasma membrane is to create complexes or conjugates with vectors that have some kind of specific or non-specific affinity for the plasma membrane that will then allow entry into the cell via endocytosis. Such drug delivery approaches include vectors that may be of biological origin such as viruses (Giacca and Zacchigna, 2012), peptides and proteins (Bechara and Sagan, 2013) or artificial systems such as polymer-based nanoparticles (NPs) (Cleal et al., 2013).

1.2 Viral delivery vectors

In 1976, Paul Berg harnessed the modified SV40 virus to deliver DNA segments into cultured monkey kidney cells (Goff and Berg, 1976). Since this breakthrough, viral vectors have attracted extensive attention in the field of gene therapy. By exploiting viral infection pathways, the genetic materials of choice can be co-transported with viral DNA or RNA genomes into infected host cells. Certain viral coding regions whose subsequent expression in the host accounts for viral replication and toxicity are deleted from the original viral genome. The exogenous DNA of interest is then incorporated into the viral backbone in place of the deleted sequences. The sequences that are essential for encapsulating the vector genes into the viral capsid or integrating vector genome into the chromatin of infected cells are, necessarily, kept intact. To reproduce recombinant viral vectors in a host cell, a separate helper virus is also required to provide the transduced cells with viral genes encoding capsid proteins or replication-associated proteins (Thomas et al., 2003).

In the field of gene therapy, the majority of the clinically relevant virus vectors originate from five major classes: oncoretroviruses, lentiviruses, adenoviruses, adeno-associated viruses (AAVs) and herpes simplex virus type 1 (HSV-1) (Giacca and Zacchigna, 2012). As each of these classes holds their own unique set of properties and their disease targets are diverse, no single class is suitable for all clinical applications. Although viral vectors of different classes have proven to be useful tools for gene transfer in animal models and even clinical trials, some characteristics they hold limit their wider therapeutic use (Thomas et al., 2003). Oncoretrovirus and lentivirus vectors perform genetic alterations by integrating their genomes into the host cellular chromatin. These integrating vectors are preferred if stable genetic modification needs to be maintained in proliferating cells, although stable transgene expression from the integrated genomes can not be guaranteed due to gradual silencing over time (Pannell and Ellis, 2001). However, oncoretrovirus can only access the cell nucleus when the nuclear membrane breaks down. Lentivirus can breach the intact nuclear membrane of some cell types, but not all non-dividing cells are susceptible to gene transfer by these vectors (Park et al., 2000). The major obstacle using adenovirus vectors to deliver genes into the cell nucleus is their potent immunogenicity. These viruses have been shown to induce strong inflammatory responses (Thomas et al., 2003). Another challenge that faces all classes of viral vectors is the pre-existing humoral immune responses to the parental wild type viruses. These humoral responses lead to the production of virus–specific antibodies by B lymphocytes, which impede efficient translocation mediated by viral vectors or the subsequent secretion of therapeutic proteins, therefore preclude the long-term therapy of certain disorders (Sun et al., 2003, Mingozzi and High, 2013, Halbert et al., 2000). Other shortcomings of viral vectors include short-lived transgene expression, limited DNA carrying capacity and vector tropism (infectable cell types). These limitations necessitate the design and development of new non-viral based approaches to introduce exogenous nucleic acids and other macromolecular therapeutics into cells with maximum efficiency and minimal toxicity.

1.3 Non-viral drug delivery methods (NV-DDMs)

Non-viral delivery methods for drug delivery represent promising alternatives to viral vectors since they can offer localised or targeted drug delivery with easier preparation, larger drug-load, longer release period and lower immunogenicity (Yin et al., 2014).

At present, non-viral drug delivery methods (NV-DDMs) can be generally divided into two main classes according to the technology they exploit. Physical methods include electroporation, microinjection and magnetofection, and biochemical delivery systems engineered by nanotechnology include liposomes, dendrimers, polymeric micelles and nanoparticles. Although the physical approaches can offer highly efficient drug or gene delivery, these methods also have some significant drawbacks as they can cause damage and death to the targeted cells. In the past decades, nanoscale drug delivery systems (NDDS) have received widespread attention, and a variety of materials have been utilised in their manufacture. The concept of NDDS was derived with the description of lipid vesicles (later known as liposomes) in the 1960s along with polymer-drug conjugates in the 1970s (Bangham et al., 1965, Ringsdorf, 1975). Liposomes are spherical nanostructures that are formed by self-assembly of single or multiple lipid bilayers in aqueous systems. This construction allows for entrapment of hydrophilic molecules within the internal aqueous phase and hydrophobic compounds in the bilayer membrane (Vemuri and Rhodes, 1995). In spite of several desired advantages such as biocompatibility and biodegradability, the major problems for liposome vehicles used in pharmaceutics are their relatively low stability and short circulation half-life (Mufamadi et al., 2011). To combat this, liposomes can be conjugated with biocompatible polymers such as polyethylene glycol (PEG). PEGylation protects liposomes from clearance by the reticuloendothelial system; otherwise conventional liposomes can be easily phagocytosed by specialist cells found within the reticular connective tissue in the liver, spleen and lymph nodes (Felice et al., 2014).

To date, the NDDS family has been undergoing significant expansion and more nanotechnology platforms have emerged for drug delivery applications. For example, an alternative to covalent binding of cargo to polymer, they can also be physically entrapped in the polymer structures. The resulting products prepared by either method may present as polymeric capsules, polymeric nanoparticles, polymeric micelles with amphiphilic interior or exterior, or hyperbranched dendrimers (Cho et al., 2008). Carbon nanotubes, magnetic nanoparticles and silica nanocarriers have also gained great interest as potential drug delivery vehicles (Wilczewska et al., 2012). Currently, there are a number of NDDS-based therapeutic agents under preclinical evaluation but only relatively few nanotherapeutics have been launched in the pharmaceutical market. A variety of limitations have impeded the clinical use and success of nanosized carriers. For example, most of the delivery achieved by NDDS relies on the passive accumulation of carriers in pathological sites, which leads to low efficiency of cargo delivery to specific cells or particular intracellular regions (Koren and Torchilin, 2012).

1.4 Cell penetrating peptides (CPPs) as drug delivery vectors

As discussed previously, viral vectors are still considered to be the most efficient vehicles for gene delivery, despite the associated negative side effects. This has inspired some investigators to develop proteins and peptides that mimic viral cell entry and also exploit the mechanisms by which some plant and bacterial toxins can translocate across membrane barriers. In the past 15 years, a group of peptides called cell penetrating peptides (CPPs) has been discovered and developed for intracellular delivery of genetic material, peptides, proteins and other macro entities (Gupta et al., 2005, Raucher and Ryu, 2015, Margus et al., 2012).

The initial observations about the potential of membrane-penetrating proteins or amino acid sequences to carry macromolecular cargo and enhance their cellular uptake were published in 1965 (Ryser and Hancock, 1965). In this report, histones and poly amino acids (polyamines) were shown to be capable of accelerating albumin uptake by cultured tumour cells. Very little was then published on the cell-penetrating properties of peptides/proteins until 1988. The transcription-transactivating (Tat) protein of the human immunodeficiency virus 1 (HIV-1) and a chemically synthesized version of Tat were observed to have the ability to rapidly translocate across the plasma membrane and even into the nucleus (Frankel and Pabo, 1988, Green and Loewenstein, 1988). The two independent publications triggered great interest in the drug delivery field and are generally considered to be the first documented CPPs. In 1991, Prochiantz and colleagues reported that *Drosophila* antennapedia homeodomain, a 60-amino acid polypeptide pAntp, could be internalised by mammalian neuronal cells (Joliot et al., 1991). This work subsequently led to the identification of a shorter polypeptide (16 amino acid in length), penetratin, corresponding to the third helix of pAntp (Derossi et al., 1994). Table 1.1 describes a list of studied CPPs including penetratin and their amino acid sequences. In 1997, Vives *et al.* delineated a minimal amino acid region required for Tat protein translocation after intensive studies on different truncated versions of Tat (Vivès et al., 1997). These initial descriptions about CPPs have subsequently demonstrated significant efficacy in the delivery of biologically active entities into cells or various subcellular compartments.

Table 1.1 Representative CPPs: sequences, subtypes and origins.

CPP	CPP sequence	Subtype	Origin	Ref.
Oligoarginines	R(n)	Poly-cationic	Synthetic	(Rothbard et al., 2000)
HIV-1 Tat (48-60)	GRKKRRQRRRPPQ		Protein derived	(Richard et al., 2005)
TP10	AGYLLGKINLKALAALAKKIL	Primary amphipathic	Chimeric	(Soomets et al., 2000)
Transportan	GWTLNSAGYLLGKINLKALAALAKKIL		Chimeric	(Pooga et al., 1998)
MPG	GALFLGFLGAAGSTMGAWSQPKS		Chimeric	(Morris et al., 1997)
Pep-1	KETWWETWWTEWSQPKKKRKV		Synthetic	(Deshayes et al., 2004a)
Pep-2	KETWFETWFTEWSQPKKKRKV		Synthetic	(Kurzawa et al., 2010)
Pep-3	KWFETWFTEWPKKRK		Synthetic	(Kurzawa et al., 2010)
CADY	GLWRALWRLLRSLWRLLWRA	Secondary amphipathic	Synthetic	(Crombez et al., 2009)
CADY2	GLWWRLWWRLRSWFRLWFRA		Synthetic	(Kurzawa et al., 2010)
MAP	KLALKLALKALKAALKLA		Synthetic	(Oehlke et al., 1998)
pVec	LLIILRRRIRKQAHAHSK		Protein derived	(Elmquist et al., 2001)
Penetratin	RQIKIWFQNRRMKWKK		Protein derived	(Derossi et al., 1994)

1.4.1 Classifications of CPPs

More than 100 diverse cell penetrating sequences containing 5-40 amino acids have now been described as carriers of various cargos including small entities, macromolecules and even nanoparticles (Koren and Torchilin, 2012). Although CPPs have a great variety of sequence profiles, it is possible to classify them on the basis of specific parameters. According to their origin, CPPs can be broadly distinguished into three major groups: protein derived peptides, synthetic sequences that are designed to mimic the structures of pre-existing peptides for optimised activity, and chimeric CPPs that are fusion of two natural sequences (usually a hydrophobic and a hydrophilic domain of different proteins) (Zorko and Langel, 2005).

The physico-chemical characteristics of CPP sequences can also be used to subcategorize CPPs into three main subclasses: cationic, amphipathic and hydrophobic. Most of the known CPPs (~83%) are net positively charged (Milletti, 2012). Among them, it has been well accepted that only those that are highly charged without displaying any amphipathic arrangement can be classified as cationic CPPs (Figure 1.1A). There are also some peptides that have both a net positive charge and which are hydrophobic. Such peptides are identified cationic if their uptake primarily relies on the stretch of positive charges (usually contributed by arginine and/or lysine) at physiological pH (Milletti, 2012).

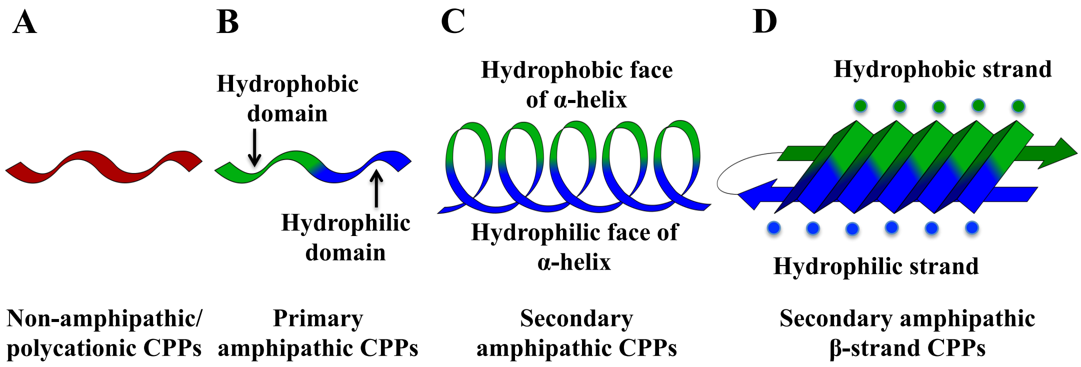

Figure 1.1 CPP models showing different structural properties. A) Non-amphipathic/polycationic CPPs have no defined secondary structures. **B)** Primary amphipathic CPPs comprise a hydrophobic and a hydrophilic domain. **C)** The secondary amphipathic CPPs form a secondary structure α-helix with dual faces: a hydrophobic and a hydrophilic face. **D)** In amphipathic β-strand CPPs, β-strands are designated as parallel or antiparallel according to the relative direction of the two β-strands associated by hydrogen bonding. The side chains (indicated by green or blue dots) of the amino acids of a strand in a β-sheet are located on opposite sides of the sheet, leading to the formation of amphipathic regions.

The first described cationic CPP is a short region derived from HIV-1 Tat protein and containing both arginines and lysines (Green et al., 1989). Subsequent studies suggested that the number of positive charges is crucial for efficient cellular internalisation of cationic CPPs. In some cases, at least eight positive charges are thought to be required, and for polyarginine peptides (R_n), the level of uptake increases with the addition of more arginines to the amino acid sequence (Futaki et al., 2001, Tünnemann et al., 2008). The guanidinium head groups of arginine-rich peptides can electrostatically interact with the carboxylates and sulfates provided by cell surface glycosaminoglycans (GAGs) or other negatively charged phosphate head groups on the membrane, which leads to the formation of bidentate hydrogen bonding (Figure 1.2A). This is thought to be responsible for the initial generation of plasma membrane curves or protrusions towards the extracellular space (Mishra et al., 2011). However, the amine groups of lysine can only form monodentate hydrogen bonding with their counterparts (Figure 1.2B), which is unfavorable to the formation of membrane curvature (Mishra et al., 2011). If the correlation between the membrane curvature and membrane perturbation is true, it can be considered as a convincing explanation why arginine is more promising than lysine in CPP uptake. Additionally, polycationic CPPs were also observed to mediate the aggregation of GAGs on cell surface, leading to actin rearrangement and a selective activation of protein kinase C and Rho/Rac GTPases to produce an endocytic signal (Ziegler and Seelig, 2008, Duchardt et al., 2007). As a membrane destabilisation reagent, pyrenebutyrate can insert into the lipid bilayer via its hydrophobic region. Also it can electrostatically bind the positively charged head groups of arginine, increasing the hydrophobicity of the CPP (Perret et al., 2005). The addition of hydrophobicity to the hydrophilic oligoarginine peptides using the hydrophobic counter-anion pyrenebutyrate was shown to promote the interactions between the peptides and the lipid bilayer, leading to direct cell entry into the cytoplasm and cytosol (Takeuchi et al., 2006, Guterstam et al., 2009). Such an enhancement on the cellular penetration mediated by hydrophobicity was further investigated by adding a penetration accelerating sequence (Pas) to oligoarginine (Takayama et al., 2012). Compared with R8 alone, the attachment of the hydrophobic sequence (FFLIPKG) Pas to R8 (PasR8) was observed to increase the cellular internalisation of the peptide. Probably, the increased hydrophobicity in PasR8 strengthens the interaction between the peptide and the plasma membrane, which results in a further membrane destabilisation. Further work from our laboratory has shown that adding a phenylalanine group several residues away from the CPP sequence can also have quite dramatic effects on cell binding and uptake (Watkins et al., 2011, Sayers et al., 2014).

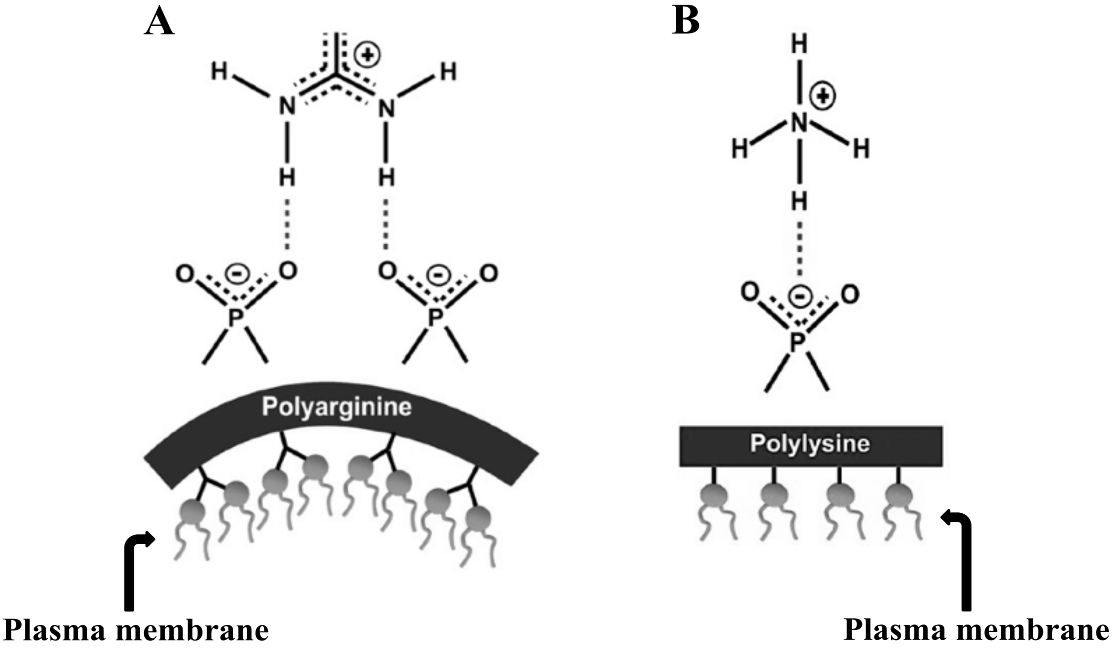

Figure 1.2 Interactions between polyarginine or polylysine and phospholipid head groups. Adapted from (Mishra et al., 2011). **A)** Multidentate hydrogen bonding formed by interactions between the membrane's phosphate head groups and arginine's guanidinium side chain, induces positive curvature strain along the peptide. **B)** Monodentate coordination of lysine's amino side chain does not induce positive curvature.

The largest subgroup termed amphipathic CPPs can be further identified as primary amphipathic, secondary amphipathic and proline-rich amphipathic (Milletti, 2012). Primary amphipathic CPPs are formed by the fusion of hydrophobic and hydrophilic domains in their primary sequence (Figure 1.1B). Most of the primary amphipathic peptides, such as MPG and Pep families (Table 1.1), have hydrophobic sequences of different origins but share a common hydrophilic motif, i.e. the nuclear localisation sequence (NLS) of Simian virus 40 (SV40) T-antigen: PKKKRKV (Deshayes et al., 2006). NLSs are short amino acid sequences, rich in arginine and lysine, that tag proteins for transportation into the nucleus. NLSs themselves, to some extent, can be considered cationic CPPs. However, the lack of sufficient positive charge means that most NLSs (alone) are inadequate for cellular uptake (Mueller et al., 2008). NLSs can and have been covalently fused with certain highly hydrophobic signal peptides to obtain amphipathic peptides that efficiently penetrate the plasma membrane and enter cells (Lin et al., 1995, Chaloin et al., 1997).

Unlike primary amphipathic CPPs, secondary amphipathic peptides only become truly amphipathic when in a α-helical or β-sheet confirmation (Figure 1.1C or D). For example, in model amphipathic peptides (MAPs) and CADY family of peptides, hydrophobic and hydrophilic residues are clustered on separate sides of the peptide helix, resulting in one highly hydrophobic face and the other face cationic, anionic or polar (Milletti, 2012). β-sheet amphipathic CPPs reveal their amphipathic character upon interaction with a phospholipid membrane, through the formation of a hydrophobic and a hydrophilic stretch of amino acids. Although the majority of amphipathic CPPs are also cationic, there is also a significant body of evidence to suggest that the membrane translocation of amphipathic CPPs is actually a result of the amphipathic conformation they adopt under certain circumstances, rather than directly due to the presence of positively charged residues (Oehlke et al., 1998, Scheller et al., 1999, Oehlke et al., 2002). However, in some other studies on the mutants of MAP and another amphipathic CPP transportan, the ability of the peptides to translocate across the plasma membrane was significantly impaired by single mutations or deletions even though some degree of amphipathicity still remained (Scheller et al., 1999, Soomets et al., 2000). Thus, further investigations are required to understand the role and necessity of amphipathicity in the cellular uptake of amphipathic CPPs.

Positively charged residues and amphipathicity are not thought to be obligate for cell penetration and efficient internalisation. And recently a few CPP sequences comprised of hydrophobic amino acids have been identified. Most of hydrophobic CPPs in this class are constructed from natural amino acids. Examples include short sequence PFVYLI, a truncated version of the longer peptide C105Y (Rhee and Davis, 2006, Watkins et al., 2009) and the signal sequence from integrin beta 3 (VTVLALGALAGVGVG) (Liu et al., 1996). Recent data indicate that some hydrophobic CPPs such as PFVYLI can drive their cellular uptake through an ATP-independent, non-endocytic pathway (Watkins et al., 2009, Marks et al., 2011). In some cases this confers an advantage as CPPs internalised via a non-endocytic route can be immediately available in the cytosol and should avoid endo-lysosomal entrapment/degradation. Some other hydrophobic CPPs can be produced by chemical modifications such as ring-closing olefin metathesis (Schafmeister et al., 2000) and prenylation that involved the covalent addition of hydrophobic lipid prenyl (C_{15} or C_{20}) groups onto cysteine residues of peptides (Ochocki et al., 2011). The prenylation modification serves to aid peptide penetration via enhancing hydrophobic interaction with cell membranes. A number of membrane interacting proteins including Rab GTPases are modified via prenylation (Pereira-Leal et al., 2001, Wang and Casey, 2016). A more recent group of CPPs termed Pepfects, are chemically modified derivatives of transportan 10 (TP10). This peptide family are formed through the introduction of the stearyl moiety at different positions such as the C-terminus of TP10, and have been shown to efficiently deliver DNA and siRNA *in vitro* and *in vivo* without the risks of toxicity and inflammations (Ezzat et al., 2011, Suhorutsenko et al., 2011).

1.4.2 Cellular uptake mechanisms of CPPs

A key research question in the CPP field is what mechanism(s) do these peptides use to enter into cells. Early mechanistic studies in the 1990s suggested that most CPPs achieved plasma membrane translocation by non-endocytic, energy- and temperature-independent, direct passage (Derossi et al., 1994). In most early analysis the cells were fixed to allow microscopical analysis of fluorescent CPPs or CPPs attached to GFP in cells. This fixing procedure was later found to completely alter the localisation of the CPP often towards the negative DNA in the nucleus (Lundberg and Johansson, 2002, Richard et al., 2003). Since the publication of these very important papers, a number of subsequent studies have led to the general consensus that CPPs under certain conditions and with low molecular weight cargo can translocate the plasma membrane in the presence or absence of energy (Bechara and Sagan, 2013). However a number of endocytic pathways have also been shown to be utilized by CPPs with small and large molecular weight cargos to reach the cytoplasm. The mechanism by which they then mediate escape from endosomal organelles to reach the cytosol still remains a mystery.

Despite the significant investment of effort that has been made to unveil the mechanisms of CPP translocation across the plasma membrane, the exact uptake pathways still remain elusive. It should however be noted that finding one mechanism that fits all CPPs with or without attached cargo is impossible to achieve. As mentioned earlier it is now well accepted that two modes of cell entry exist to accomplish entry into the cytoplasm of cells: direct translocation and uptake via endocytosis. The endocytic pathways involved in CPP cell entry relate to the pinocytosis process, which can be broadly grouped into four main pathways: clathrin-dependent endocytosis, caveolae/lipid raft-mediated endocytosis, clathrin/caveolae-independent endocytosis and macropinocytosis (Doherty and McMahon, 2009, Sigismund et al., 2012). Under certain experimental/biological conditions, some CPPs, alone and attached to low molecular weight cargo can translocate directly through the lipid bilayer. This is initiated by and is thought to depend on the electrostatic interactions between CPP and membrane components or via hydrogen bonding (Herbig et al., 2005, Mai et al., 2002). The majority of CPPs attached to cargo molecules, especially to those of high molecular weight (e.g. proteins, liposomes and nanoparticles) have to utilize single or multiple endosomal routes to gain entry to cells and to different subcellular compartments (Duchardt et al., 2007). The specific pathway(s) used by a CPP to gain cell entry depends on a number of key peptide parameters: the physico-chemical characters of the CPP sequences, their concentrations and the properties of the associated cargos. The cell type targeted for delivery is also critically important as this determines the plasma membrane composition and the cell's endocytic capacity and profile.

1.4.2.1 Direct translocation

The mechanisms of energy-independent direct translocation of CPP cargos have been described in several models that include inverted micelle formation, pore formation and the carpet-like model (Derossi et al., 1996, Matsuzaki et al., 1996, Pouny et al., 1992). Almost all these proposed mechanisms highly depend on the properties of peptide sequences, their concentrations (usually above a threshold) and even the membrane composition of the studied cells. No matter which of these mechanisms the CPP cargo uses to penetrate the bilayer, the first step is thought to involve interactions of the positively charged amino acids in the peptide, with negatively charged membrane components such as extracellular GAGs, e.g. heparan sulfate and heparin, and phospholipids. As a consequence, the plasma membrane may experience stable or transient destabilisation, which provides CPPs with opportunities to pass through into the cell (Thorén et al., 2003, Rothbard et al., 2004). Not all the known CPPs are capable of direct translocation, however cationic or amphipathic CPPs, such as Tat, R8/9 or MPG, have been shown to perform this process under certain conditions (Thorén et al., 2003, Deshayes et al., 2006, Fretz et al., 2007, Duchardt et al., 2007).

Following Tat's first contact with negatively charged phospholipids, part of the plasma membrane can be transformed into an inverted micelle structure (Figure 1.3A: I) which can open on either the extracellular or the intracellular layer of the membrane (Vivès et al., 2003). For the secondary amphipathic penetratin, in addition to the initial electrostatic interaction between the peptide and the membrane, the subsequent interaction between hydrophobic amino acids of peptide sequence and the hydrophobic components of the lipid bilayer also takes part in this inverted micelle mechanism (Alves et al., 2008).

Several more recent studies based on giant unilamellar vesicles (GUVs) indicated that the rapid and tight binding of cationic CPPs to anionic extracellular GAGs might not be essential for CPP uptake, since effective translocation across GUVs in the absence of these components can be observed (Mishra et al., 2011, Swiecicki et al., 2014). However, these studies also highlighted the importance of the direct interaction between the positive charges of cationic CPPs and phospholipid phosphate groups for efficient peptide internalisation via a model phospholipid membrane or biological membrane. Cationic CPPs are also thought to induce an internalisation platform in a defined region of the plasma membrane that then leads to rapid rush of the peptide into the cytosol (Duchardt et al., 2007, Hirose et al., 2012).

In a theoretical model proposed by Herce *et. al* (Figure 1.3B), a transmembrane pore is formed to facilitate the translocation of highly cationic CPPs such as Tat and other arginine/lysine-rich peptides (Herce and Garcia, 2007, Herce et al., 2009). The charged amino acids of the peptides are initially attracted by the phosphate groups of the phospholipid bilayer and bind to them, mainly through the side chains of arginines and/or lysines. Along with the increase of the surface concentration of the peptides, the strength of the peptide-phosphate interactions also builds up. This subsequently leads to the distortion of the arrangement of local membrane region compared with their resting structure. When the peptide concentration is greater than a certain threshold, which is peptide-specific, an arginine/lysine side chain may penetrate into the distal layer and nucleate the formation of an aqueous pore. This transient pore then provides an entry point for more peptides to diffuse across the bilayer, and the translocation ends with pore closure.

The research group of A.E. Mark described the toroidal model (Figure 1.3A: II) for the mechanism of pore formation, which is also applicable to the amphipathic CPP penetratin (Yesylevskyy et al., 2009). The initial interactions between penetratin and model lipid bilayer depresses the upper monolayer of the plasma membrane while the lower monolayer is unaffected. Driven by the increased restraining potential, the peptide moves toward the bilayer interior, gradually increasing the deformation of the upper monolayer. When the deformation reaches a critical point, a hydrophilic toroidal pore appears and its surface is occupied by lipid head groups, which is the major difference from the model proposed by Herce *et. al*.

The carpet-like model (Figure 1.3A: III) describes a mechanism where peptides accumulate on, and bind parallel to, the plane of the lipid bilayer, coating the local membrane area with a carpet-like extra layer (Deshayes et al., 2004). When the peptide concentration reaches a given threshold, the peptide sheet can initiate the formation of micelles or membrane pores, allowing for subsequent peptide translocation.

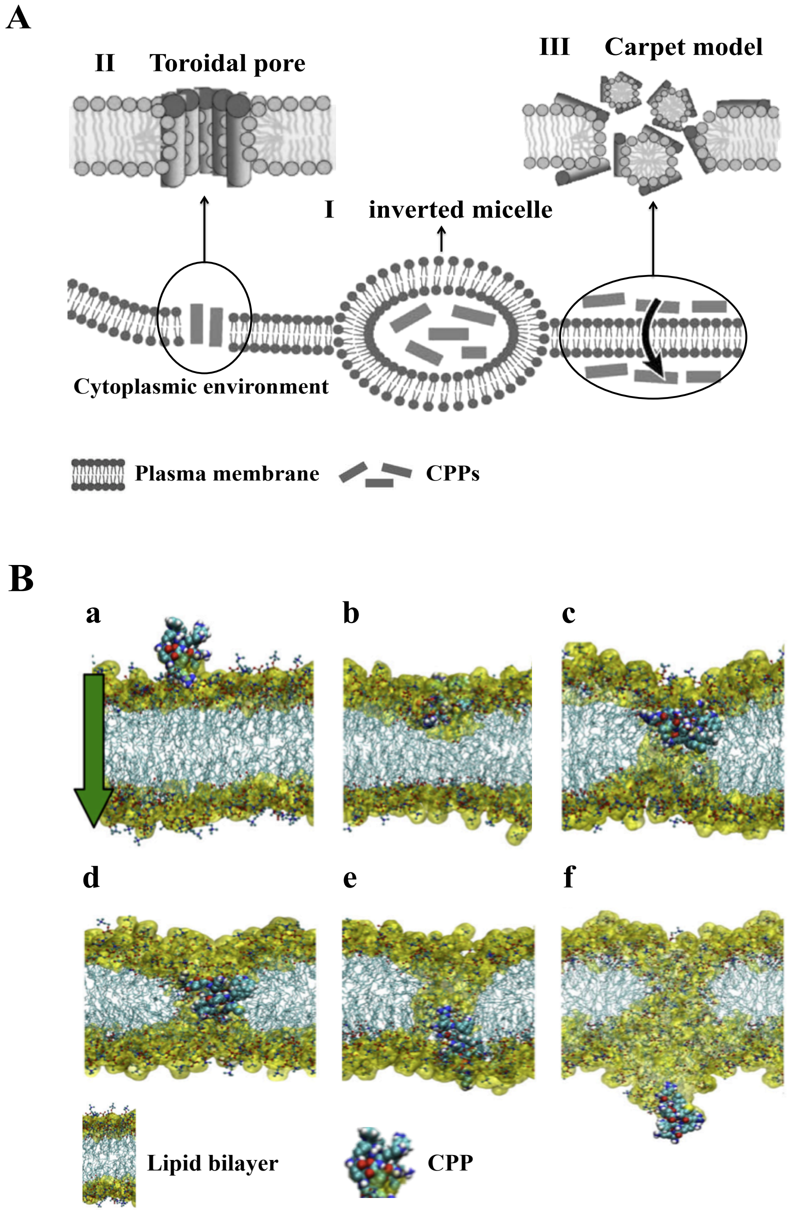

Figure 1.3 A variety of possible models for CPP-mediated direct penetration. The inverted micelle **(A:I)** (Järver et al., 2010) is described as a kind of hydrophilic cavity that forms within the lipid bilayer leaflets following interaction between the positively charged residues of CPPs and the phospholipid headgroups. This causes membrane distortion. The accommodated CPPs are then released directly from the transient micelles to the cytoplasmic region. In the toroidal model **(A:II)** (Nguyen et al., 2011), the peptides insert perpendicular into the sheet of lipid bilayer, with interaction between their hydrophobic motifs and the membrane lipid core and association between the polar head groups of phospholipid via the hydrophilic regions of the peptides. During such insertion, the membrane is also bent inward to line the pore, thus the lipid headgroups form contacts with the transmembrane peptides throughout. The formed toroidal structure is then stabilised by the peptides. According to the carpet model **(A:III)** (Nguyen et al., 2011), the peptides accumulate and clustered on the lipid bilayer in a parallel fashion, coating the local membrane region with a carpet-like layer. When the coating peptide concentration reaches a given threshold, the panel of peptides can initiate the formation of micelles and membrane pores to allow cell entry. **B)** Following the order from a to f, the binding and aggregation of CPPs onto the membrane trigger a slight depression within the upper monolayer. The formation of a hydrophilic toroidal-like pore structure occurs as a consequence of both the movement of the peptide towards the bilayer core and the distortion within the bilayer. Then the peptide passes through the transient pore and is pulled out of the structure into the cytosol. The green arrow indicates the direction of the CPP internalisation (Yesylevskyy et al., 2009).

1.4.2.2 Endocytosis

Endocytosis is a highly regulated activity by which cells internalise solutes and fluid from the extracellular matrix. Endocytosis is an umbrella term that includes phagocytosis, a process that is mainly used to internalise large particles such as viruses, bacteria and other cells, and several other routes that fall under the classification of pinocytosis (Figure 1.4 and legend to this figure). In this introduction a few of these pathways are described further and this will then lead to roles that have been proposed for them in the uptake of CPPs.

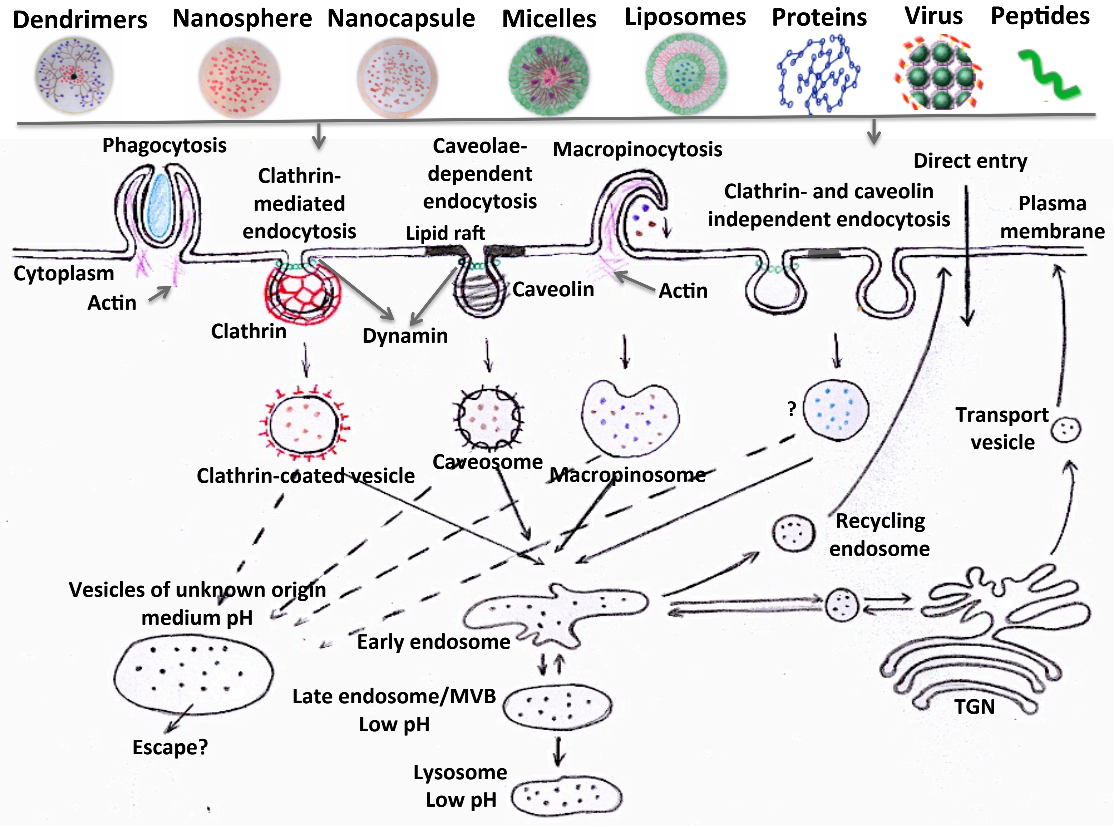

Figure 1.4 Endocytic pathways and the delivery of therapeutic macromolecules using vector systems. A variety of (nano) carriers including viruses, liposomes, micelles, dendrimers and CPPs, whose sizes vary from low nanometers (peptides) to micrometers, have been shown to facilitate intracellular delivery of a wide range of therapeutic macromolecules. All of these pinocytic pathways (clathrin-mediated endocytosis, caveolae-mediated endocytosis, clathrin/caveolin-independent endocytosis and macropinocytosis) have been shown to be involved in the CPP-mediated delivery. Some CPPs are able to directly translocate through the plasma membrane. The intracellular endocytic vesicles entrapping the CPP complexes may be targeted to recycling endosomes or the endo-lysosomal pathway or CPPs may be directed to other locations such as the *trans*-Golgi Network (TGN).

1.4.2.2.1 Clathrin-mediated endocytosis (CME)

Clathrin-mediated endocytosis is a relatively well-described internalisation pathway that occurs constitutively in all known eukaryotic cells. CME involves material uptake through clathrin coated vesicles (CCVs) formed as invaginations from the plasma membrane; CCVs can also bud from other membrane compartments using different adaptor proteins (McMahon and Boucrot, 2011). CME has been reported to be an important regulatory process for several cellular activities, such as bringing essential nutrients into cells, regulating the activation of signalling pathways, and intercellular communication in tissue or organ development (Conner and Schmid, 2003). Based on the ultrastructural and biological observations, the formation of CCVs has been clearly described, and many adaptor proteins have been identified that, along with clathrin, make significant contributions to the formation of clathrin coated pits and vesicles (McMahon and Boucrot, 2011). CME utilizes a variety of cargo adaptors and accessory proteins serving to package distinct cargos or cargo sets into different cells (Schmid and McMahon, 2007). However, it is worth noting that there is overlapping and sharing of functions among different cargo adaptors and accessory proteins.

The CME-mediated uptake usually involves five stages including initiation, cargo selection, coat assembly, scission and uncoating. CME can be stimulated by ligand binding to specific transmembrane receptors. However, for some other receptors such as the transferrin receptor (TfR), their internalisation via CME is constitutive (Hopkins et al., 1985). CME internalisation begins with membrane curvature that was originally thought to be triggered by local recruitment of the highly conserved Adaptor Protein-2 (AP2) complex. AP2 binds to the cytoplasmic tails of receptors destined for internalisation and to the plasma membrane-specific lipid phosphatidylinositol-4,5-bisphosphate (PtdIns(4,5)P_2) (Ohno et al., 1995, Höning et al., 2005). However, the role of AP2 in initiation of membrane curvature was challenged by some recent studies in mammalian cells, which indicate that membrane deformation may result from the action of a putative nucleation protein module. The proposed module contains FCH domain only (FCHO) proteins, EGFR pathway substrate 15 (EPS15) and intersectins, and is suggested to be required for the recruitment of AP2 (Henne et al., 2010). The recruited AP2 complex then can bind to cargo to be internalised via its core domain and can anchor on the plasma membrane through the binding to PtdIns(4,5)P_2); its appendage domains (ears) can bind to most of the cargo-specific accessory adaptor proteins and to clathrin (Collins et al., 2002). Adaptor proteins are also thought to induce membrane curvature effectors that ensure membrane-deformation regardless of the identity of the cargo (McMahon and Boucrot, 2011). Clathrin coat assembly proceeds at specific regions of the plasma membrane wherein selected cargo is bound to either AP2 or adaptor proteins.

Clathrin is a triskelion-like structure comprising three identical clathrin heavy chains (CHCs) and other three tightly associated clathrin light chains (CLCs) (Fotin et al., 2004). Clathrin triskelia are recruited by AP2 and also by other accessory adaptor proteins directly from the cell cytosol to the sites where coated vesicles will mature. The recruited clathrin triskelia are then self-polymerised into cage-shaped lattice, which consequently stabilises the curvature of the attached membrane. Clathrin assembly itself is insufficient to drive membrane deformation as the coated pit invaginates, curvature effectors such as epsin family proteins can help mediate membrane bending in the assembling clathrin-coated pit for a fully invaginated CCV to form (Ungewickell et al., 1995, Ford et al., 2002).

A class of BAR domain-containing proteins such as amphiphysin and sorting nexin 9 (SNX9) aid in the formation and constriction of the budding vesicle neck (Wigge et al., 1997, Ferguson et al., 2009). Another important function of these accessory proteins is to recruit the membrane scission protein dynamin to the vesicle neck through the binding of their SRC homology 3 (SH3) domains to the pro-rich domain of dynamin (Ringstad et al., 1997). The large GTPase dynamin is then concentrated and polymerised into helical structures around the vesicle neck. Upon GTP hydrolysis, the dynamin polymers induce vesicle scission from the parent plasma membrane, which leads to the release of CCVs into cytosol (Praefcke and McMahon, 2004). The clathrin coat is subsequently disassembled from lattice back to triskelia by ATPase heat shock cognate 70 (HSC70) and its cofactor auxilin (Schlossman et al., 1984, Ungewickell et al., 1995). The detached and naked vesicles are then trafficked to and fuse with early endosomes. The rapid disassembly of the clathrin coat allows the recycling/reuse of the clathrin machinery in further rounds of CCV budding.

1.4.2.2.2 Caveolae-dependent endocytosis

It has been observed that certain compounds introduced to cells can be directed into lipid rafts and subsequently endocytosed via a pathway distinct from the classical clathrin-dependent pathway. Additionally, constitutive uptake of many types of cargos in CME-inhibited cells is not negatively affected, providing more evidence for the existence of clathrin-independent internalisation pathways (Nichols and Lippincott-Schwartz, 2001). One such pathway is caveolae-dependent endocytosis. Caveolae are membrane invaginations generated from specialized type of microdomain and characterized initially by having the presence of caveolin proteins (described later). These flask-shaped membrane structures were first observed in the 1950s (Palade, 1953), but were not extensively investigated until the identification of caveolin proteins in 1992 (Kurzchalia et al., 1992, Rothberg et al., 1992). Since then a large number of studies have highlighted the importance of caveolae and caveolins in a diverse array of cellular functions ranging from lipid turnover, transport processes, cell growth and regulation of signalling molecules (Schnitzer, 2001, Parton and del Pozo, 2013). Caveolae have been shown to provide a vehicle for the cellular entry of many entities including bacteria, bacterial toxins bound to surface glycolipids, certain viruses such as SV40 and glycosphingolipid lactosylceramide (Nabi and Le, 2003, Pelkmans and Helenius, 2002, Wolf et al., 1998, Pelkmans, 2005, Vercauteren et al., 2010). However, its contribution to cellular endocytosis may be significantly dependent on cell types and conditions, implying tissue specific distribution and, probably functions, of caveolae.

Under the electron microscope, caveolae appear as uncoated flask-shaped invaginations, which are typically ~50-100nm in diameter, with spiral or striations around the invagination. These bulb structures are invaginated from specific plasma membrane microdomains which are rich in cholesterol, glycosphingolipids (GSLs) and glycosylphosphatidylinositol (GPI)-linked proteins (known as glycolipid rafts) (Anderson, 1998). Caveolae are an abundant feature of many mammalian cell types including adipocytes, endothelial cells, smooth muscle and fibroblasts, but have not been detected in neurons and leukocytes that lack expression of caveolin proteins (Fra et al., 1994). This highlights that the formation of caveolae is dependant on the expression of the integral membrane protein caveolin-1 in nonmuscle cells and on muscle specific isoform caveolin-3 in myocytes (Drab et al., 2001, Galbiati et al., 2001). Caveolae are commonly thought to be specialized, morphologically distinguishable forms of lipid raft domains, whose shape is sculpted by caveolin and several other proteins. Although caveolin-2 is usually coexpressed and heterooligomerizes with caveolin-1 in many nonmuscle cell types and may be involved in some caveolae-like structures, it appears not to be obligate for caveolar biogenesis (Razani et al., 2002).

Caveolin-1 adopts a hairpin-like loop conformation and embeds in the plasma membrane with both N- and C- terminals exposed to the cytoplasm. It binds cholesterol and fatty acids and is able to form caveolin homooligomers, which may provide attachment sites for caveolin-interacting molecules, concentrating them within caveolae (Sargiacomo et al., 1995). Initial reports attributed the assembly of the spiral or striated "coat" encircling the cytoplasmic surface of caveolae to the membrane embedded caveolin oligomers (Monier et al., 1995). However, a number of recent studies on caveolae structure suggest that in addition to caveolin oligomers, polymerised cavin proteins are another major component of the unique spiral caveolar "coat" (Kovtun et al., 2014, Gambin et al., 2014). The peripheral membrane protein family cavins contain four isoforms, cavin 1-4, and are thought to be a key structural component of caveolae. The caveolin and cavin families together appear to be sufficient to mediate caveolae formation in a cooperative manner (Kovtun et al., 2015). Analysis of the caveolae ultrastructure by electron microscopy showed that caveolin proteins are also concentrated circumferentially around the narrow neck (Thorn et al., 2003). In addition to caveolin, dynamin GTPase, the dynamin-like ATPase EHD2, and the BAR domain-containing protein Syndapin2 are also enriched at the caveolae neck region, influencing the caveolar morphology and dynamics, but these proteins are not essentially required for the formation of caveolae (Henley et al., 1998, Morén et al., 2012, Senju et al., 2011).

It is commonly thought that the initiation of internalisation via caveolae is induced by ligand engagement with various cell surface receptors. In a model proposed by Kovtun describing carveolar formation, caveolin oligomers are described as inserting into the plasma membrane then clustering with cholesterol and PtdIns(4,5)P_2 (Kovtun et al., 2015). Caveolin-1 is thought not to directly induce membrane curvature but rather to stabilise the membrane once deformed (Nabi and Le, 2003). By working in concert, caveolin and the recruited cavin can, together, nucleate membrane curvature, and subsequently the coordinated assembly of caveolin-cavin coat remodels membrane to shape tubulovesicular structures. Cholesterol is heavily implicated in caveloae formation as cholesterol depletion of the plasma membrane causes the caveolae to flatten (Rothberg et al., 1990). The invagination and budding of caveolae are also highly dependent on the recruitment and the activity of GTPase dynamin (Parton et al., 2006). Although caveolin is a functional and structural component of caveolae, its role in the formation of caveolae-related vesicular intermediates remains controversial. It has been observed that in the absence of caveolin, there is no concomitant inhibition of the invagination and budding of vesicular structures sharing fundamental similarities with caveolae (i.e. structures which, like caveolae, are specialized forms of cholesterol- and sphingolipid-rich lipid raft microdomains and which are dynamin-dependent). This also introduces another argument about whether caveolae and equivalent lipid raft-based vesicular structures mediate a common or distinct endocytic pathway(s). Unlike CME, only a basic understanding of the machinery mediating caveolar endocytosis has been obtained. The precise mechanisms by which caveolae form, the role of caveolin, the lipid composition of caveolae and the functional relevance of other involved proteins all need to be fully explored in the future. This is also the case for caveosomes which are the first internalised structures emanating from caveolae at the plasma membrane.

1.4.2.2.3 Clathrin- and caveolae- independent lipid raft endocytosis

Many years of extensive examinations on CME and caveolar endocytosis also shed light on other types of endocytic pathways. For example caveolae are not essential for clathrin-independent lipid raft endocytosis and few markers have been shown to utilize caveolae alone for uptake (Parton and Richards, 2003). A number of studies have provided evidence for the presence of lipid rafts and the occurrence of lipid raft endocytosis in cells with and without caveolae (Fra et al., 1994, Kirkham et al., 2005). Two forms of non-caveolar lipid raft endocytic pathways will be discussed in this section: flotillin-dependent endocytosis and CLIC/GEEC (clathrin-independent carriers/GPI-enriched early endosomal compartments) - type endocytosis.

Flotillins are integral membrane proteins that can oligomerise to form discrete microdomains in the plasma membrane. Flotillin microdomains have been observed in all mammalian cells studied to date, which implies their importance and conserved functionality in cellular processes, including endocytosis. A large body of evidence has confirmed the involvement of flotillin-rich vesicular structures in the internalisation of diverse endocytic cargos, such as GPI-anchored proteins, cholera toxin B subunit (CTxB) and also an antibody recognizing CD59/protectin on the plasma membrane (Otto and Nichols, 2011). Flotillin -1 and -2 bind each other and colocalise in specific plasma membrane regions i.e. flotillin microdomains (Solis et al., 2007, Frick et al., 2007). The co-assembly of flotillin -1 and -2 may be necessary in the generation of membrane curvature and the vesicle budding at the plasma membrane (Frick et al., 2007).

Flotillin are found to have topological similarities and homology to caveolin, but the two protein families are unrelated in sequence (Bauer and Pelkmans, 2006). Flotillins were once thought to be substitutes for caveolin in cell types lacking detectable caveolin-1. However, some recent studies discovered that, at least in cultured cells, the plasma membrane domains enriched in flotillin are distinct and separate from caveolae (Lang et al., 1998, Frick et al., 2007, Glebov et al., 2006). Therefore, flotillin may define a unique endocytotic pathway or may function upstream other endocytic pathways in the organisation of membrane domains e.g. flotillin was shown to localise intensively in the membranes of early CLIC/GEEC intermediates (Lundmark et al., 2008a).

Studies of the internalisation of GPI-anchored proteins, classical markers of lipid raft membrane fractions, have revealed the existence of a novel clathrin- and dynamin-independent but cholesterol-dependent endotytic pathway. Immediately after internalisation GPI-anchored proteins were detected to localise within specific tubular membrane structures termed GPI-enriched early endosomal compartments (GEEC) (Sabharanjak et al., 2002). This acidic, tubulovesicular membrane structure is seemingly responsible for a considerable proportion of internalisation of fluid phase markers (Kalia et al., 2006). The GEEC pathway appears to be regulated by Rho family GTPase Cdc42, and kinetically separate from the endocytosis of transmembrane proteins (Sabharanjak et al., 2002, Chadda et al., 2007).

In the studies of cholera toxin (CT) cell entry, this protein was found to initially bind a ganglioside and marker of lipid rafts, called GM1. CT internalisation was then shown to be mediated by clathrin-coated pits and by caveolae (Torgersen et al., 2001). However, a remarkable fraction of CT uptake has also been shown to involve a group of novel carriers termed clathrin-independent carriers (CLICs) (Kirkham et al., 2005). These carriers are clathrin- and dynamin- independent and cholesterol-sensitive like caveolae, but have been shown by electron microscopy to be prominently tubular and ring-like in morphology (Kirkham et al., 2005). Colocalisation of CT with both fluid phase markers and GPI-anchored proteins has been demonstrated, linking CLICs to the previously discussed GEEC pathway. This explains why a single CLIC/GEEC pathway is often described. Membrane cholesterol is known to be crucial for actively maintaining the cluster of GPI-linked proteins on the cell surface. However, the molecular mechanisms by which the recruitment of GPI-anchored proteins into these endocytic structures is regulated are still poorly understood (Sharma et al., 2004). It has been reported that when the CLIC/GEEC-type endocytic pathway is inhibited or disrupted, CME acts as a compensatory pathway to take over the endocytosis of GPI-anchored proteins (Sabharanjak et al., 2002). However it is unknown whether the internalised cargos are still transported into appropriate intracellular destinations.

1.4.2.2.4 Macropinocytosis

Macropinocytosis, a cellular endocytic process for the internalisation of large fluid volumes, is characterized by protrusions from the plasma membrane that subsequently fuse with themselves or back with the local plasma membrane, resulting in the formation of large macropinosomes and the indiscriminate uptake of the entrapped extracellular fluid (Jones, 2007, Kerr and Teasdale, 2009). Unlike other pinocytosis vesicles, these resulting macropinosomes are irregular in morphology and inhomogeneous in size (Mercer and Helenius, 2009). This endocytic pathway has been observed in almost all cell types studied to date, usually response to specific stimulation of growth factors or other signals. Some specialized cell types can also utilize macropinocytosis for the constitutive uptake of extracellular fluid in the absence of exogenous stimuli (Jones, 2007, Kerr and Teasdale, 2009). It is difficult to distinguish between constitutive macropinocytosis and a term referred to as fluid phase uptake that for example will also allow entry of components in the extracellular medium without the need for a receptor or binding to the plasma membrane.

The most unique character that distinguishes macropinocytosis from other pinocytic processes is thought to be the formation of membrane ruffles during macropinocytic uptake. In most macropinocytic events, the plasma membrane ruffles usually fall into three distinct subtypes: planar lamellipodia, circular ruffles and blebs (Figure 1.5), depending on the cell type and the ligand. The generation of the lamellipodia-like protrusions and the circular ruffles is initiated by actin polymerisation/remodelling, whereas the formation of blebs is probably resulted from the destabilisation of local actin cortex (Mercer and Helenius, 2009). Actin is critical for macropinocytosis to occur and this process is therefore linked closely to actin binding proteins. This is typifies when growth factors such as Epidermal growth factor (EGF) is added to cells expressing epidermal growth factor receptor (EGFR). Activation of EGFR and other receptor tyrosine kinases (RTKs) in turn activate a signalling cascade, for example, Ras superfamily GTPases-involved pathways, causing the extension of sheet-like membrane ruffles by large-scale localised rearrangement of actin filaments beneath the plasma membrane (Kirkham and Parton, 2005). The autophosphorylation of EGF receptors can be activated by binding of extracellular EGF or signals inside cells, and the phosphorylated receptors then recruit kinases and adaptor proteins which assemble into complex near the plasma membrane. The assembled protein complex stimulates phosphorylation of certain membrane components (lipids and proteins), which results in localised rearrangement of the actin cytoskeleton (Swanson, 2008).

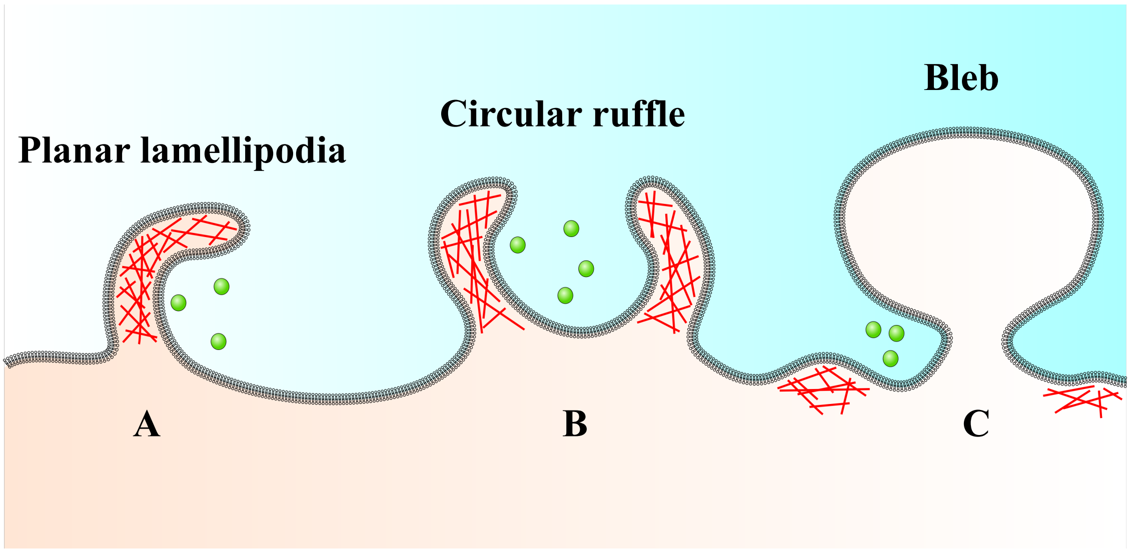

Figure 1.5 Different forms of plasma membrane protrusions involved in macropinocytosis. A) Planar lamellipodia. **B)** Circular ruffle. **C)** Bleb. The red lines represent actin filaments.

Upon activation by RTKs, Ras GTPases trigger three parallel signalling pathways respectively involving Rho GTPase Rac1, Rab GTPase Rab5 and ARF GTPase Arf6. These cell factors work in concert to modulate the formation of membrane ruffles, the maturation of macropinosomes and the subsequent membrane trafficking (Lanzetti et al., 2004). Rac1 is a well-known regulator of macropinocytosis. Once activated, Rac1 in turn switches on the activity of various actin effectors that are involved in actin dynamics and stability, and thus initiates the plasma membrane ruffling of all three types (Ridley et al., 1992, Mercer and Helenius, 2008). Another Rho family member Cdc42 is essentially involved in membrane ruffling during macropinocytic internalisation in immature dendritic cells, where macropinocytosis occurs in a continuous manner and does not require the presence of external stimulus (Garrett et al., 2000, Norbury, 2006). However, it is still no evidence to support the role of Cdc42 in growth factor-induced macropinocytosis. Rab5 is a well-known molecular marker of early endosomes; its increased expression was found to result in increased formation of circular ruffles during macropinocytosis. This protein relocalises along circular ruffles when cells are activated by platelet-derived growth factor (PDGF). This is in association with RN-Tre (related protein N-terminal threonine), a Rab5 effector that interact with actin filaments to promote the crosslinking between F-actin and ruffles (Lanzetti et al., 2004). Another Rab5 effector Rabankyrin-5 was observed to localise to newly formed macropinosomes in epithelial cells and fibroblasts, and its overexpression promoted the formation of macropinosomes and thereby stimulated fluid phase uptake. In the same study, Rabankyrin-5 probably had a role in leading Rab5 to nascent macropinosomes (Schnatwinkel et al., 2004). GTP-binding protein Arf6 is best known for its involvement in endocytic membrane trafficking and plasma membrane remodelling via influence on cortical actin (Radhakrishna et al., 1999, Donaldson, 2005). The activated

Arf6 has been shown to recycle Rac1 to the plasma membrane and thus to promote the formation of macropinosomes (Radhakrishna et al., 1999). A more recent study suggested that Arf6 had a role in stabilising or further facilitating the formation of membrane curvature, which was probably conducive to the biogenesis of macropinocytosis (Lundmark et al., 2008b).

In addition to small GTPases, several kinases are also implicated in macropinocytosis. One of the most vital is the serine/threonine kinase p21-activated kinase-1 (PAK-1) that interacts with and is activated by Rac1 or Cdc42 (Dharmawardhane et al., 2000). Extensive studies have shown that PAK-1 is required for all forms of macropinocytosis and has a role for all stages of macropinocytosis (Dharmawardhane et al., 2000, Parrini et al., 2005, Liberali et al., 2008). After activated, PAK-1 is shuttled to the plasma membrane where it activates a number of actin effectors that participate in the following membrane remodelling events including ruffling/blebbing and macropinosome formation (Mercer and Helenius, 2009). Additionally, some other kinases such as protein kinase C (PKC), another serine/threonine kinase, and c-Src, a non-receptor tyrosine Src-family kinase (SFK) also contribute to macropinocytosis following ligand induced receptor activation. On activation, these kinases are targeted to and associate with the plasma membrane and subsequently stimulate membrane ruffling and macropinocytosis (Miyata et al., 1989, Amyere et al., 2000, Kasahara et al., 2007).

Macropinocytosis is also dependent on several other factors. Like PAK-1, Na^+/H^+ exchangers are another key group that are needed for all forms of macropinocytic processes. Inhibition of the normal functions of Na^+/H^+ exchangers [for example by amiloride or its derivative 5-(N-ethyl-N-isopropyl) amiloride (EIPA)] has been shown to impede the induction of membrane ruffling and thus block the macropinocytic internalisation (West et al., 1989, Veithen et al., 1996, Meier et al., 2002). Membrane cholesterol is also important to macropinocytosis. The localisation of Rac1, Arf6 and other signalling factors to the macropinocytic membrane is dependent on membrane cholesterol (Grimmer et al., 2002, Kwik et al., 2003), and both membrane ruffling and macropinocytosis are inhibited by cholesterol depletion (Grimmer et al., 2002). It should be noted here that experiments using membrane cholesterol depletion are usually designed to examine the role of lipid rafts in cell functions. However, it has been shown that the depletion of cholesterol from the plasma membrane has a global effect on actin organisation through the loss or redistribution of plasma membrane PtdIns(4,5)P_2 (Kwik et al., 2003). Thus care must be taken in optimising methods to inhibit specific endocytic pathways to avoid disrupting the plasma membrane composition and integrity.

Like other membrane microdomain-dependent pathways, it is presumed that concentration/enrichment of specific lipids at heavily activated areas of the plasma membrane induces local intracellular changes that are responsible for the morphological characters of macropinocytosis. Phospholipid phosphatidylinositol (PtdIns) is abundant in the inner leaflet of the plasma membrane. A product of PtdIns phosphorylation PtdIns(4,5)P_2 can bind to a variety of proteins that are involved in modification of membrane chemistry and assembly of actin filaments and enhance their activity. This may explain the increased local concentrations of PtdIns(4,5)P_2 in membrane ruffles during macropinocytosis (Swanson, 2008). Studies have suggested that PtdIns(4,5)P_2 works in concert with activated Rho GTPases including Cdc42 and Rac1 to initiate actin polymerisation for the induction of membrane ruffles (Kerr and Teasdale, 2009). As macropinocytosis is highly dependent on actin dynamics that mediates the formation of actin-based ruffles and blebs, numerous actin effectors controlling/regulating actin assembly/disassembly, actin stabilisation and actin connection with membrane are thought to be necessarily involved in this endocytic process. Actin dynamics is central to this thesis, therefore a separate section on actin is provided later in Section 1.5.

Receptor activation by a ligand is not the only mechanism by which macropinocytosis can be stimulated as several other entities including bacteria and viruses have been observed to induce membrane ruffling and subsequently be internalised together with fluid into macropinosomes (Francis et al., 1993, Watarai et al., 2001). In addition, CPPs, as small molecules, can also initiate this internalisation process, presumably stimulating chemical changes that are otherwise initiated by receptor-ligand interactions (Futaki et al., 2007).

Although substantial efforts have been made to characterize macropinocytosis since the first observation of macropinosomes in 1931 (Lewis, 1931), gaps in our understanding still remain especially in the context of identifying proteins and lipids that are unique in regulating macropinocytosis over other endocytic pathways. These issues in the field of macropinocytosis need to be addressed in the future.

1.4.2.3 Intracellular trafficking after endocytosis

Cellular uptake via direct translocation allows the internalised cargo to be available immediately in the cytosol. If endocytosis is the route of entry then the vector and delivered cargo may be trafficked to a number of cell destinations or recycled out of the cell (Figure 1.4). There is often the case, especially for nucleotide delivery for escape of the cargo into the cytosol and possibly the nucleus.

The intracellular transport of newly formed, plasma membrane derived endocytic vesicles requires the functional participation of a diverse array of membrane-enclosed compartments and organelles. These membrane-based structures include early endosomes (also called sorting endosomes where cargos are sorted and prepared for future transport), late endosomes or multivesicular bodies (MVBs), recycling endosomes, lysosomes, endoplasmic reticulum (ER) and Golgi complex. The basic steps involved in vesicular transport can be generally described as: 1) vesicle budding from donor compartment or organelle, a process during which selected cargos are incorporated into the forming vesicles; 2) vesicle fusion, whereby the entrapped cargos are loaded into a specific acceptor compartment or organelle; 3) retrograde transport, a retrieval process to return transport machinery components and escaped resident proteins from the acceptor back to the corresponding donor compartment (Bonifacino and Glick, 2004). As a consequence of a series of tightly regulated movements, the cargos can reach their destinations within cells or can be recycled.

Depending on the cargo and the endocytic pathway(s) used for internalisation, the materials that are confined in early endosomal compartments can either be sorted into recycling endosomes, or directed into the classical endosome-lysosome pathway, or delivered to the ER via the Golgi complex. The significant contribution of actin cytoskeleton in coordinating the organisation and dynamics of the mentioned intracellular structures will be discussed in Section 1.5. In the classical endosome-lysosome pathway, a cargo is transported from early to late endosomes and then to lysosomes. The cargo may also appear in multivesicular structures that are found within late endosomes and may also be delivered to lysosomes or exocytosed as exosomes (Raposo and Stoorvogel, 2013). As endocytic cargos proceed through the endolysosomal pathway, they experience pH drop from neutral to pH 6.0-6.5 in early endosomes, with further decrease from 6.0 to 4.5 during the transport form late endosomes to lysosomes (Maxfield and McGraw, 2004). This fall in pH within endosomal systems is required for a number of processes including activation of late endosomal and lysosomal hydrolases (e.g. cathepsins) and the disassociation of ligands from their co-internalised cell surface receptors, allowing for their recycling and re-use at the plasma membrane [e.g. Low Density Lipoprotein (LDL) receptor]. For the transferrin receptor (TfR) acidification of endosomes allows for release of iron from transferrin, which in turn allows both receptor and ligand (still as a complex) to recycle back to the plasma membrane (Maxfield and McGraw, 2004). This does not involve the lysosomes but recycling endosomes that coordinate the recycling of both plasma membrane components and resident Golgi enzymes back to their sites of action. Most often, the return of cargo to the outside of cell generally needs to be avoided in the context of drug delivery, thus control of recycling is an important therapeutic consideration.

The classical clathrin-dependent pathway transports most of its contents into late endosomes and lysosomes for degradation, whereas some of the materials can be recycled back to the plasma membrane (Lakadamyali et al., 2006, Conner and Schmid, 2003). Material internalised from caveolae as caveosomes have been proposed to be delivered to the Golgi apparatus or ER by retrograde transport (Le and Nabi, 2003, Nichols, 2002). However, more recent studies suggested that lysosomal delivery could also occur from caveosomes (Parton and Howes, 2010, Hayer et al., 2010).

The cellular destination for macropinosomes is still largely unresolved but is known to be cell type- and induction mode- dependent (Wadia et al., 2004, Jones, 2007). The first organelle formed from the plasma membrane during macropinocytosis is the macropinosome that varies in size from hundreds of nanometers to >2µm diameter. In macrophages, macropinosomes undergo a route similar to endosomes, as characterized by the gain and loss of classical early/late endosomal markers such as TfR and Rab7 before fusion with lysosomes (Racoosin and Swanson, 1993). A similar fate of macropinosomes was also observed in *Dictyostelium discoideum* and in mammalian cells with Src kinase overexpression (Maniak, 2001, Kasahara et al., 2007). In HeLa cells, macropinosomes rarely interact with other endosomal membrane structures and their encapsulated contents appear to return to the extracellular environment through recycling pathways (Meier et al., 2002). Similar to the observations in HeLa cells, the majority of macropinosomes in human carcinoma A431 cells recycle back to the cell surface, although macropinosomes in these cells obtain a number of early endosome proteins that are required for homotypic, i.e. macropinosome-macropinosome fusion (Hewlett et al., 1994, Roberts et al., 2000, Hamasaki et al., 2004). There was little evidence showing the fusion of macropinosomes in A431 cells with other endocytic membrane structures (Hewlett et al., 1994).

1.4.3 CPP uptake via endocytosis

All the known endocytic pathways have been implicated in the cellular entry of CPPs complexed to small cargos such as fluorophores through to large nanoparticles. As suggested earlier the choice of cargo is likely to have a major effect on uptake mechanism(s) (Jones and Sayers, 2012, Cleal et al., 2013). A major limitation of most of the studies on endocytic internalisation of CPPs lies in the fact that they have been confined to *in vitro* analysis using one or several of a range of pharmacological/chemical inhibitors of endocytosis. These inhibitors indeed possess several advantages over some other molecular biological method in terms of targeting endocytic proteins. For instance, the exposure period to inhibitors *in vitro* studies is usually short, which is very likely to preclude the development of side effects and/or mechanism compensation. However, one major issue that may undermine the use of these inhibitors is the lack of specificity. It is often for a particular inhibitor to interfere with not only an endocytic pathway of interest but also alternative entry routes. As these inhibitors are notoriously non-specific and also because of the fact that they are usually cytotoxic, it often difficult to interpret the data and make generalizations (Ivanov, 2008, Vercauteren et al., 2010). Moreover, the poor specificity of these pharmacological/chemical inhibitors makes the specific measurement of the contribution of each endosomal route to the uptake of CPP extremely hard to achieve.

CME has been reported several times to provide for a mean of entry for both CPP alone and CPP-protein complex (Richard et al., 2005, El-Andaloussi et al., 2007). However, CPP uptake events mediated by clathrin-dependent route may be incidental, because the binding of specific ligands to their receptors is thought to be essential for the formation of clathrin-coated invagination at the plasma membrane. Several studies have analysed the uptake of CPPs when co-incubated with endocytic markers for specific pathways such as transferrin for CME. Indeed, in these co-incubation studies, a proportion of CPP-conjugates have been found to be co-internalised with transferrin suggesting they entered the same pathway (Nakase et al., 2004). But the possibility exists that this may be due to extracellular electrostatic interactions between the CPP and the transferrin. When they are separately incubated with cells, i.e. at different time points, co-localisation in endocytic compartments is significantly reduced (Padari et al., 2005). Whether certain CPPs can in fact exploit, as-yet-unidentified receptors and trigger the subsequent uptake via CME is still to be determined.

A major focus of work has concentrated on the possibility that CPPs trigger macropinocytosis and enter via this pathway. This was initially proposed for CPP-protein conjugates and also CPPs attached to fluorophores (Nakase et al., 2004, Wadia et al., 2004, Kaplan et al., 2005). These studies suggested that CPPs were inducing fluid phase uptake similar to growth factor activation and that CPP uptake was dependent on actin. Macropinocytosis was not shown to be required for the cellular delivery of protein cargo using arginine-rich peptides in the presence of pyrenebutyrate, which is a negatively charged counteranion with high hydrophobicity. Here, addition of pyrenebutyrate promoted rapid, direct passage of the CPP-protein cargos and yielded cytosolic cargo distribution (Takeuchi et al., 2006). Later work from the Dowdy laboratory suggested that macropinocytosis was required for the fraction of CPP that escaped into the cytosol over the vast majority that either associated with the plasma membrane or was retained inside endocytic organelles (Gump et al., 2010). This study also challenged the concept that uptake and intracellular fate of cationic CPPs were dependent on the cell surface GAGs.

Work studying CPP uptake and macropinocytosis has largely been dependent on analysing actin dynamics by fluorescence microscopy and flow cytometry. In addition, pharmacological/chemical inhibitors of macropinocytosis (e.g. EIPA) and actin dynamics (e.g. cytochalasin D) have played a major role in assigning macropinocytosis to CPP uptake. Chapter 3 and 4 of this thesis expand on these studies.

A role for caveolae has been proposed in the cellular uptake of the fusion protein Tat-GFP (Ferrari et al., 2003, Fittipaldi et al., 2003), and depletion of caveolin-1 from cells impaired the cellular delivery of CPP-protein complexes (Säälik et al., 2009). The involvement of flotillin-positive endosomes in the cellular delivery of CPP-protein complexes has not been firmly confirmed and in certain cell lines including HeLa cells, the absence of flotillin does not show any substantial influence on the protein delivery by transportans (Säälik et al., 2009). Studies from the Jones laboratory also showed that the cellular uptake of polycationic peptides (R8 and Tat) was not affected in flotillin-1 depleted cells (Al Soraj et al., 2012).

When detached from the plasma membrane, the endocytic vesicles containing CPP cargos move deeper into the cytoplasm and are targeted to different destinations. In a model describing common features of the intracellular transport of these vesicles

(Räägel et al., 2009, Räägel and Pooga, 2011), the initial small vesicular bodies budding from the plasma membrane are usually characterized by low CPP concentrations and varied pH values. During the course of internal fusion, more and more entrapped cargos accumulated in fewer and fewer vesicular structures, resulting in membrane compartments of larger body sizes and higher CPP concentrations. The final destination for the internalised CPP cargos is usually dependent on several parameters such as cargo properties and/or concentrations (Sigismund et al., 2005), and also the vesicle pool in which the cargo reside: in the acidic lysosomes for degradation or in membrane compartments with medium pH values that encourage cargo escape before digestion. The source of these neutral-pH vesicles is not yet known although the non-acidic caveosomal intermediates have been implicated (Pelkmans et al., 2001). Non-acidic vesicles, believed to have been formed during the process of caveolar endocytosis, were observed by Räägel's research group. Moreover, in the same study, arginine-rich peptides appeared to possess high capacity for inhibiting acidification of the membrane-bound structures they were contained in (Räägel et al., 2009).

1.5 Actin cytoskeleton and actin dynamics

1.5.1 Actin filaments as part of the cytoskeleton

As one of the most abundant and highly conserved proteins in all eukaryotes, actin is involved in a myriad of morphological and functional cell roles. Actin's cellular contributions include: complementing the other cytoskeletal polymers microtubules and intermediate filaments (IFs) to establish internal mechanical support, providing actin filament "tracks" for the trafficking of intracellular membrane vesicles and driving cell movement achieved through actin dynamics (Pollard and Cooper, 2009). Additionally, actin is involved in many other important cellular processes including cell division and cytokinesis, muscle contraction, establishment and maintenance of cell shape and cell signalling (Dominguez and Holmes, 2011).

In addition to actin filaments (also known as microfilaments), two other filamentous polymers, microtubules and IFs, are also essential components of the cytoskeletal network in animal cells. Interactions between these three cytoskeletal elements reinforce the cytoskeleton, despite the rapid turnover (on time scales of seconds to minutes) of the polymers. To some extent, the cytoskeleton can sense external mechanical features and force applied to the cell. Microtubules are hollow cylinders that are comprised of polymerised heterodimers of alpha and beta tubulin. The polymerised dimers form protofilaments which associate laterally to generate an imperfect helix, each turn of which is typically made up of 13 protofilaments (Weisenberg, 1972). Microtubules are detectable throughout the cytoplasm and are responsible for the formation of the internal structural support of cilia and flagella. Microtubules also participate in the long-range intracellular transport of certain substances and large vesicles/organelles, and chromosome separation during cell division via the formation of mitotic spindles (Fletcher and Mullins, 2010).

Another cytoskeletal component, intermediate filaments (IFs) are commonly observed as tetramer structures formed by interaction of two anti-parallel helices (Herrmann et al., 2007). The subunits of IFs can be a variety of IF proteins sharing both common amino acid sequences and similar structural characteristics. Some examples of IFs include keratins in epithelial cells, vimentin in mesenchyme and nuclear lamins. IFs are essentially required to maintain the shape of cells and nuclear envelope via the tension borne in the network. Additionally, they also provide organelles with anchoring sites within cytoplasm and transmit signals from cell membrane to nucleus (Lodish et al., 2000).

1.5.2 Monomeric G-actin and polymeric F-actin

In eukaryotic cells, globular actin (G-actin) is a 43 kDa monomeric ATP-binding protein, which is highly evolutionarily conserved due to its essential role in cellular processes and survival (Pantaloni et al., 2001). G-actin can undergo cycles of self-polymerisation into thin filaments in muscle cells or microfilaments in non-muscle cells (Fujita et al., 1996). This assembly process is driven by hydrolysis of the actin-bound ATP, and is reversible i.e. the actin filaments can also undergo depolymerisation to retain the pool of free G-actin. Actin filaments are right-handed, double-chained and single-stranded helix structures that contain highly dynamic barbed ends where new actin subunits incorporate and less active pointed ends where formed filamentous actin disassembles (Figure 1.6). The barbed end and the pointed end of the same actin filament are distinct in structural and biochemical properties (Campellone and Welch, 2010).

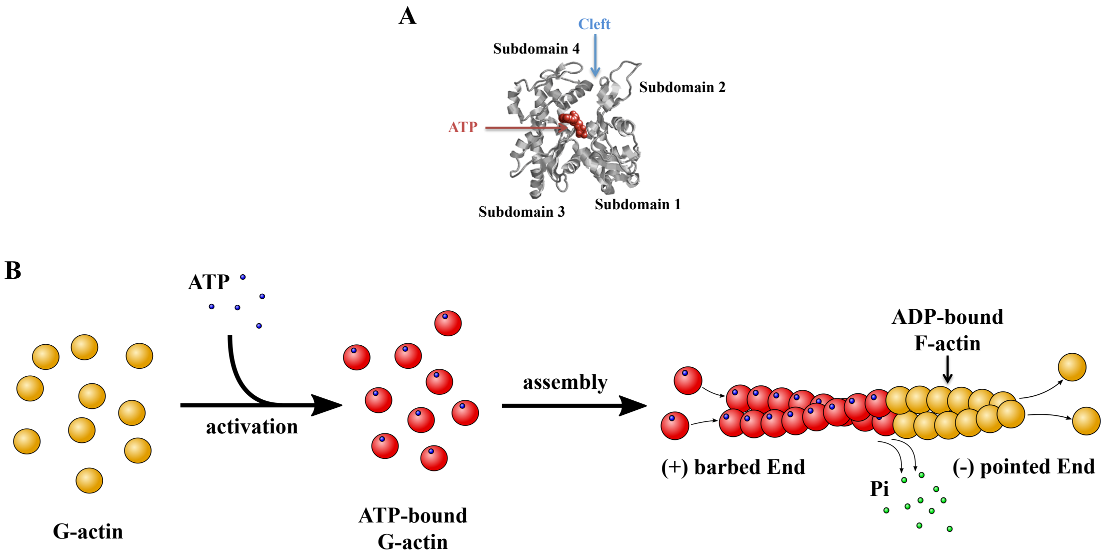

Figure 1.6 Monomeric actin (G-actin) assembly into filamentous actin (F-actin). A) Ribbon diagram of G-actin showing the typical four-domain architecture with the ATP binding site and the target-binding cleft. **B)** After activated by ATP-binding, the ATP-bound monomeric actin can then be polymerised into actin filaments (F-actin) at free barbed ends. This polymerisation process is driven by hydrolysis of the actin-bound ATP to ADP and inorganic phosphate (Pi). Actin filaments can also undergo depolymerisation at pointed ends to retain the pool of free G-actin.

Structural data indicates that G-actin folds into two lobe-like α/β-domains, which are separated by a nucleotide-binding cleft and a target-binding cleft (Figure 1.6A). The two major actin domains are defined by their location within the filaments: the small outer domain (comprised of subdomains 1 and 2), and the large inner domain (composed of subdomains 3 and 4) (Kabsch et al., 1990) (Figure 1.6A). The target-binding cleft of actin provides the interaction site for a wide variety of actin-binding proteins (ABPs) and certain small molecules such as actin disruptors (Dominguez, 2004).

Actin filament turnover is mainly regulated by a diversity of ABPs, some of which importantly participate in filament dynamics that includes nucleation, elongation, capping, severing and disassembly. The nucleotide-binding cleft, as its name implies, acts as the binding target for ATP and Mg^{2+}. Here soon after polymerisation of actin subunits into filaments, ATP is enzymatically hydrolysed to ADP and inorganic phosphate (Pi) (Figure 1.6B). Under physiological conditions, actin monomers can be “activated” by ATP-binding. ATP-bound actin can then be polymerised into actin filaments (F-actin) at free barbed ends, which can be exposed through uncapping, severing pre-existing filaments or ARP2/3 complex and formin-mediated monomer nucleation (Zigmond, 2004, Condeelis, 2001). The incorporated actin subunits are all orientated in the same direction, resulting in a head-to-tail overall arrangement. This gives actin filaments molecular and structural polarity (Pollard and Borisy, 2003).

1.5.3 Actin dynamics

The pool of monomeric actin in the cytoplasm is buffered by the actin binding protein (ABP) profilin, which prevents actin monomers from spontaneous nucleation to form actin dimers and trimeric nuclei (Schlüter et al., 1997). This is thought to partly explain the rarity of spontaneous actin assembly. Upon receiving activation from signalling pathways, nucleation-associated factors will directly nucleate actin. In mammalian cells, the actin-related protein 2/3 complex (ARP2/3), a number of ARP2/3 activators and formin proteins have all been revealed to directly promote actin nucleation (Goley and Welch, 2006, Chesarone et al., 2010, Stradal and Scita, 2006). The first identified actin nucleator was ARP2/3. This 220 kDa complex contains seven stably associated polypeptides including ARP2, ARP3 and five additional subunits ARPC1-ARPC5 (Goley and Welch, 2006). The ARP2/3 complex is unique among the known filament nucleators because of its ability to nucleate branched actin filaments. Based on numerous studies on the ARP2/3 complex, all the seven subunits bind to the side of the parental filament as a whole. However, only ARPC2 and ARPC4 form intimate contacts with the existing filament, whereas ARP2 and ARP3 are presumed to act as the first two subunits of the pointed end of the nascent filament (Rouiller et al., 2008) (Figure 1.7A). The nascent filament can be subsequently elongated at the free barbed end. The primary role of ARP2/3 complex in this event is to join the existing and nascent filaments at an angle to form Y-branches (Figure 1.7B). However, the ARP2/3 complex itself is not sufficient to initiate actin nucleation. Efficient nucleation also relies on ARP2/3 activation, which is achieved through ARP2 phosphorylation and interactions with WCA domain-containing nucleation-promoting factors (NPFs). A WCA domain contains at least one Wiskott-Aldrich syndrome protein (WASP) homology 2 [WH2] domain that can bind monomeric actin, plus a connector sequence and an acidic segment that binds and recruits the ARP2/3 complex to its action site (LeClaire et al., 2008, Hertzog et al., 2004, Chereau et al., 2005) (Figure 1.7B).

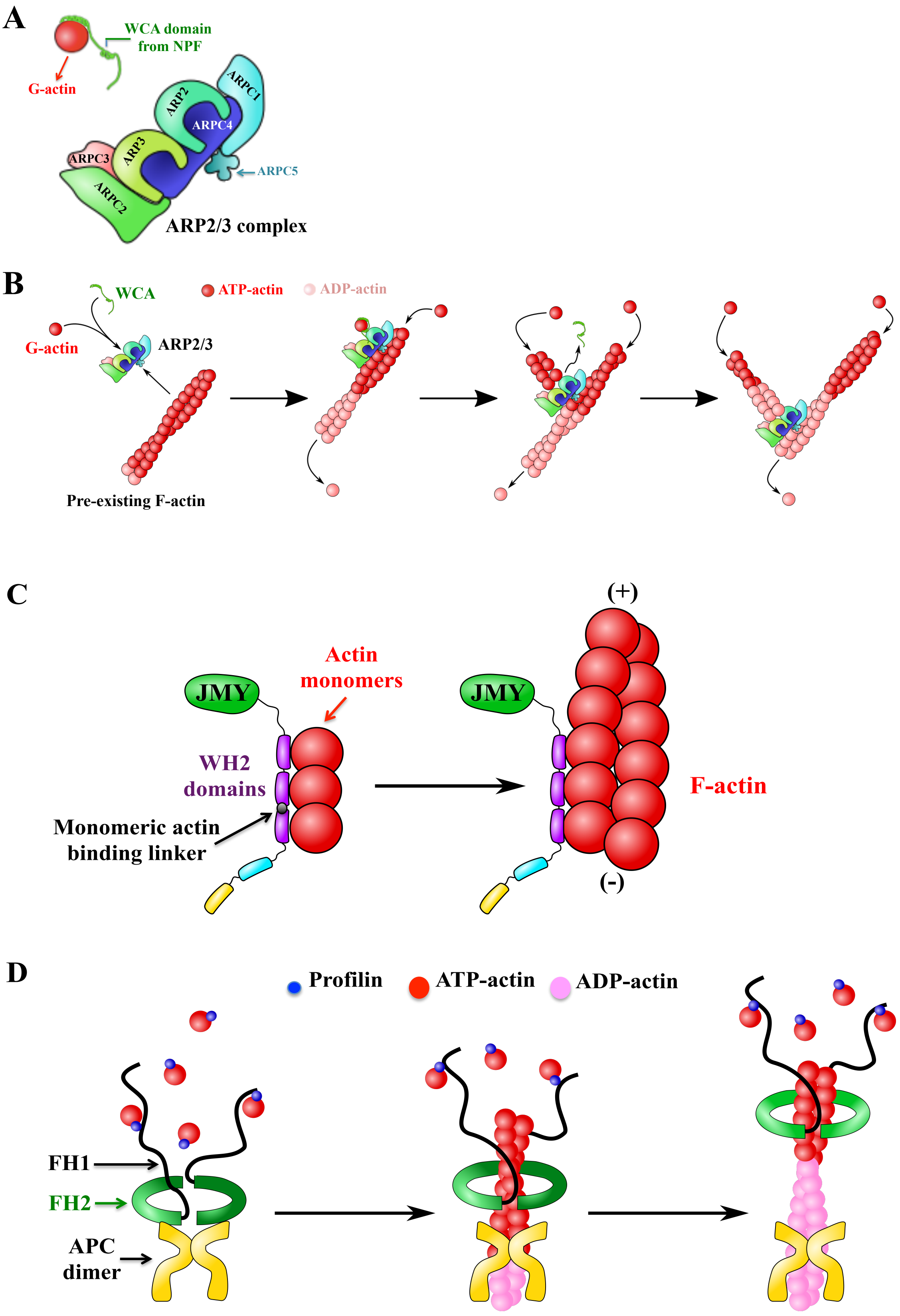

Figure 1.7 The nucleation/assembly of actin filaments mediated by ARP2/3, JMY or formin. A) The ARP2/3 complex is composed of seven subunits (ARP2, ARP3, ARPC1-C5), among which ARPC2 and ARPC4 are responsible for the intimate contacts with the existing filament, whereas ARP2 and ARP3 are presumed to act as the first two subunits of the pointed end of the nascent filament. WCA domain from NPFs bring together the ARP2/3 complex and actin monomers to nucleate new actin branches from

the side of preexisting filaments. **B)** The ARP2/3 complex initially binds to WCA domain from NPFs, inducing a conformational change that primes the complex for activation. This activation occurs upon binding of the WCA–actin–ARP2/3 complex to the preexisting actin filament near the barbed end. ATP is hydrolyzed on ARP2 along with or shortly after nucleation of the nascent filament. The WCA domain dissociates from the action site, while the ARP2/3 complex remains at the pointed end of the filament. The following elongation of the preexisting filaments and the nascent filaments is driven by ATP hydrolysis and phosphate release. **C)** JMY has the ability to nucleate unbranched actin filaments without the presence of ARP2/3 because of its additional WH2 domain and monomeric actin-binding linker. **D)** Two monomeric FH2 domains are joined together by flexible linkers to form an active ring-like FH2 homodimer, which then binds to actin monomers to initiate unbranched actin filament assembly. This process is assisted by additional factors such as APC dimer. The FH1 domains of the formin dimer interact with and bind to profilin, and then deliver the profilin-actin complex to the barbed end for further actin incorporation. During the process of filament elongation, APC dimer remains at the site of nucleation while formin dimer move towards the growing barbed end.

NPFs can be divided into five sub-groups according to their diverse regulatory amino acid terminals: 1) WASP and neuronal WASP, which are the best characterized; 2) WASP-family verprolin homologue isoforms (WAVE1-3); 3) WASP and WAVE homologue (WASH); 4) WASP homologue associated with actin, membranes and microtubules (WHAMM) and 5) junction-mediating regulatory protein (JMY) (Stradal and Scita, 2006). In contrast to mammalian WASP that is specifically expressed in haematopoietic cells, neuronal WASP (N-WASP) can be found in most cell types. Unlike the other identified NPFs, N-WASP itself has very little NPF activity due to its autoinhibitory GTPase-binding domain (GBD) (Miki et al., 1996). Normally, the autoinhibitory portion of the GBD inactivates the connector sequence and acidic segment of the WCA domain via intramolecular interaction. The binding and/or interaction of a wide range of signalling molecules such as the small Rho GTPase Cdc42 with the GBD, causes a conformational change in the GBD and as a consequence, WCA domain is free to recruit ARP2/3 for actin polymerisation. The absence of active N-WASP is suggested to impair many actin-dependent cellular functions including dorsal membrane ruffling, membrane invagination and fission, and endosomal trafficking (Campellone and Welch, 2010). In contrast to N-WASPs, the WAVE family NPFs are not autoinhibited as they do not contain the GBD. These active WAVE isoforms are primarily responsible for ARP2/3 activation during membrane protrusion and cell motility (Suetsugu et al., 2003). NPF WASH has been shown to interact with the barbed end capping protein and protein FAM1 that localises WASH to endosomes (Derivery et al., 2009, Gomez and Billadeau, 2009). Mammalian WASH is associated with early and recycling endosomes: by mediating the local activity of ARP2/3, WASH controls the shape of these membrane compartments and regulates the trafficking to late endosomes or the recycling to the plasma membrane or the *trans*-Golgi (Duleh and Welch, 2010). The recently identified JMY is intensively localised in the nucleus of many cell types, but can also assemble in the lamellipodia of migrating cells. JMY is unique in its ability to nucleate actin even without the presence of ARP2/3 because it has an additional WH2 domain and monomeric actin-binding linker compared with the other NPFs (Zuchero et al., 2009). However, actin filaments polymerised by JMY are unbranched (Figure 1.7C). WHAMM is enriched in the *cis*-Golgi and tubulovesicular membrane influencing the morphology of Golgi and the trafficking of relevant membrane systems (Campellone et al., 2008).

Among all the identified actin nucleators, only ARP2/3 complex is known to produce branched filaments. The best-characterized nucleator facilitating the assembly of unbranched actin is the formin family, which is conserved in all eukaryotes and characterized by the presence of formin homology (FH) domains FH1 and FH2 (Chesarone et al., 2010) (Figure 1.7D). Studies on crystal structures of the formin FH2 domains showed that two monomeric domains are joined together by flexible linkers to form an active ring-like FH2 homodimer (Lu et al., 2007). Unlike the ARP2/3 complex, which caps the pointed end of nascent filament, FH2 dimer localises to the barbed end and initiates processive filament elongation (Pollard, 2007). The elongating barbed end of an actin filament is protected from other capping proteins. Moreover, the competition between the formin and its displacement factors for the growing barbed end is crucial for the determination and regulation of filament length (Chesarone et al., 2009). As proposed, the FH2 dimer controls actin assembly through adopting alternating conformations. Actin incorporation is inhibited in a closed conformation as FH2 dimers binds the two terminal actin subunits; while in an open conformation, the addition of new actin monomers to the filament is enabled. The proline-rich FH1 domain is adjacent to FH2 domain. It binds and delivers profilin-actin complex to the barbed end for further actin incorporation (Vavylonis et al., 2006) (Figure 1.7D).

As previously mentioned, spontaneous actin nucleation and elongation are strongly suppressed by the actin monomer-binding protein profilin and the barbed end-capping protein. Thus, the presence of actin nucleation factors is essentially required in the polymerisation of actin filaments to overcome these barriers. Most of the cellular actin assembly requires the collaboration of two or more such factors to trigger the initial nucleation. For example, the tumor suppressor adenomatous polyposis coli (APC) works with the formin mDia1 to create new actin nucleation sites in cells by forming APC-mDia1 complexes. The two components are then separated in the subsequent process of filament elongation, but still retain their independent contacts with the filament: APC remains at the site of nucleation while mDia1 move towards the growing barbed end (Breitsprecher et al., 2012) (Figure 1.7D).

As a nucleotide exchange factor, the other role of profilin is to promote the exchange of ADP-actin (disassociated from the pointed end of the filament) for ATP-actin, which allows the recycling of actin subunits for future actin assembly at barbed ends (Didry et al., 1998). Another mechanism utilized by cells to maintain a useable pool of unpolymerised actin sufficient to sustain necessary actin assembly is the sequestration of monomeric actin by thymosin-β4. Unlike profilin, the small protein thymosin-β4 prevents both actin nucleation at pointed end and filament growth at barbed end.

However the association of thymosin-β4 with actin monomer is weaker than that of profilin. This allows a competition between profilin and thymosin-β4 for binding to actin monomers. As a result, in the pool of free actin subunits, profilin-actin complexes are ready for incorporation at the barbed end and thymosin-β4 keeps the remaining actin in reserve (Pollard and Borisy, 2003).

The initial stages of actin polymerisation proceed slowly because the small actin oligomers are not sufficiently stable. Once an actin filament reaches a threshold length, the elongation at the barbed end can be very rapid. However, the fast filament elongation is transient, as the capping proteins, such as heterodimeric CapZ in muscle and gelsolin in higher eukaryotes, can bind the barbed end and impede filament growth (Cooper and Schafer, 2000, Sun et al., 1999). The growth of barbed ends blocked by capping proteins may be recovered by local factors such as PtdIns(4,5)P_2, which displace capping proteins from barbed ends (Schafer et al., 1996). Rapid elongation at barbed ends depletes the monomeric actin pool, which may reduce the elongation rate of newly formed actin filaments. By blocking the majority of the barbed ends with high affinity, capping proteins limit the length of the growing actin filaments and compensate for the consumption of the monomer pool. Another mechanism by which the actin monomer pool is replenished utilizes ADF (Actin Depolymerising Factor) /cofilin proteins. These proteins bind to the side of ADP-actin filament and accelerate the rate of actin depolymerisation at the pointed end (Carlier et al., 1997).

1.5.4 Myosin motors in actin-based motility

As a part of the interconnected cytoskeleton, actin filaments not only provide structural support and organisation to cells, but also act as tracks for the movement of protein motors called myosins. The myosin superfamily are ATPases, which convert chemical energy into mechanical energy through ATP hydrolysis and the subsequent conformational changes to generate force and power movements. Thus in addition to actin polymerisation, the interactions between myosin motors and actin filaments are essential for many forms of cellular movements and also contribute to the transport and/or anchoring of organelles, vesicles and other intracellular components (Woolner and Bement, 2009).

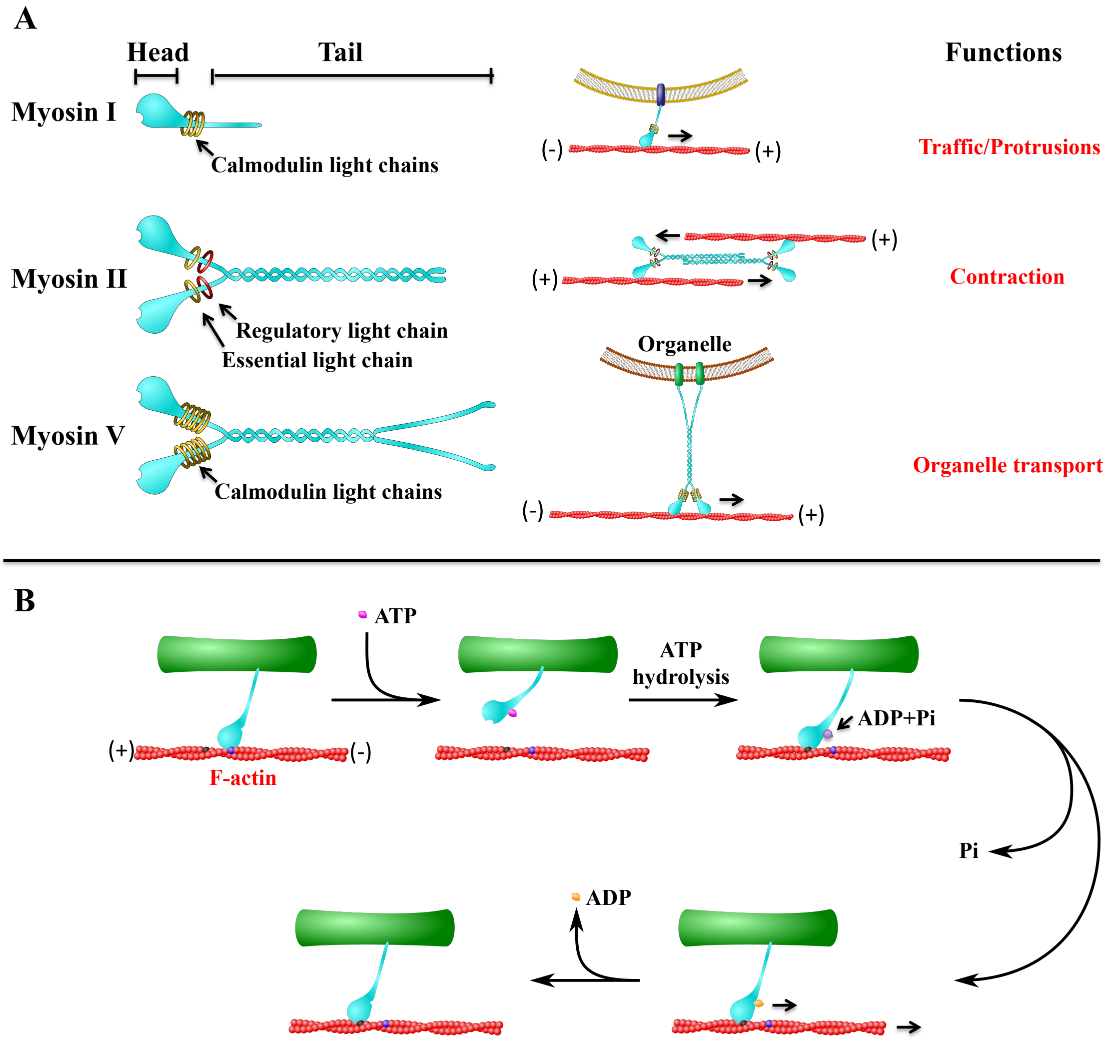

Figure 1.8 Molecular organisation of three types of myosin molecules and their interactions with actin filaments. A) Myosin I, II and V share a motor domain on their heavy chains at the amino-terminus (the 'head' domain), but differ considerably at the carboxy-terminus (the 'tail' domain). Myosin II is composed of two heavy chains that homodimerize via an extended coiled-coil tail. Each heavy chain binds a pair of essential and regulatory light chains. These rodlike tail sequences of multiple myosin II dimers self-associate in an anti-parallel fashion to assemble into bipolar thick filaments, serving as an essential part of the contractile apparatus. The heavy chains of myosin V are bound by identical calmodulin light chains and the tail domains only form coiled-coil structure in the region adjacent to the neck and leave two tail ends untwisted to provide cargo binding domains. Myosin V can interact with different organelles and walk on an actin filament towards the barbed end. Myosin I is a monomer only containing a globular head domain and a comparatively short tail. It usually interacts with calmodulin light chain to form complex. The tails of myosin I molecules also provide binding domains for some adaptor proteins or other binding proteins. Myosin I can either associate with membranes or bind to an actin filament, thus mediating actin-based movement – traffic and protrusions. **B)** In the current model describing how myosin molecules power movements along actin, myosin initially binds to actin in the absence of ATP. The binding of ATP to myosin causes a rapid disassociation of the myosin head domain from actin filament. The subsequent hydrolysis of the bound ATP results in a conformational change in the mysoin head and re-anchors myosin on the actin filament at a new position. The release of ADP and Pi makes the myosin head regain its original conformation and it is this movement that moves the actin for one step.

Myosins are the only known molecular motors involved in actin–based motility (Hartman and Spudich, 2012). The first myosin (myosin II) was discovered by Kühne in 1864 in muscle, where in association with actin filaments, it fuels muscle contraction (a special form of movement). During 1960s, the presence of myosins (including the conventional myosin II) in other nonmuscle cells was confirmed (Hatano and Oosawa, 1966, Adelman and Taylor, 1969), and their role in a variety of other eukaryotic motility processes such as cell movement and vesicle transport has been revealed by the subsequent research (Ross et al., 2008). Although all the discovered myosins function as motor proteins, a particular myosin, conventional myosin II, is thought to carry out specific activities. This protein is mainly responsible for muscle contraction whereas myosin I and V primarily participate in the transport of membrane vesicles along actin filaments in nonmuscle cells (Krendel et al., 2007, Salas-Cortes et al., 2005, Wang et al., 2008). All myosins consist of one or two identical heavy chains and several light chains. Moreover the heavy chains are usually arranged into different domains, which display distinct structures and functions. For example, myosin II is composed of two identical heavy chains and two pairs of essential and regulatory light chains (Figure 1.8A). Each heavy chain is functionally made up of three major subdomains. The globular head domain provides binding sites for actin and ATP. An adjacent α-helical neck region is bound by a pair of light chains, and also amplifies head rotations through lever arm swinging during energy conversion. Following the neck domain it is a long α-helical tail sequence that twists around the other one to form the complete myosin II dimer (Vicente-Manzanares et al., 2009). These rodlike tail sequences of multiple myosin II dimers self-associate to assemble into bipolar thick filaments, which are anti-parallel arrays of myosin II serving as an essential part of the contractile apparatus in muscle cells (Niederman and Pollard, 1975, Svitkina et al., 1995). By contrast, the neck domains of myosin V dimer are bound by two identical calmodulin light chains and also its tail domains only form coiled-coil structure in the region adjacent to the neck and leave two tail ends untwisted to provide cargo binding domains (Tóth et al., 2005) (Figure 1.8A). Unlike myosin II and V dimers, myosin I is a monomer containing a globular head domain and a comparatively short tail (Figure 1.8A). Light chains, usually calmodulin molecules interact with the α-helical junction of myosin I to form complex (Barylko et al., 2000). Like the untwisted ends of myosin V, the tail regions of myosin I also possess specific domains that bind to some adaptor proteins or other binding proteins. As a result, these unconventional myosins are recruited to their specific cellular targets such as membranes of vesicles and organelles and the plasma membrane, and then operate movement – traffic and protrusions (Akhmanova and Hammer Iii, 2010).

All the known myosins are thought to use the same basic working model to power movements along actin, however the precise molecular mechanisms underlying this are still not fully understood. Their highly conserved globular head acts as a specialized ATPase whose activity is actin-activated. It means that without the association with actin, myosins convert ATP to ADP slowly, and only when the head binds to actin, the myosin ATPase works at a much faster rate. Described in a well-accepted model (Figure 1.8B), the cycle starts with the binding of ATP to myosin, which causes rapid disassociation of the tightly bound myosin-actin complex. The subsequent hydrolysis of the bound ATP then initiates a change in myosin conformation. The myosin neck domain is consequently affected and acts as a lever arm to displace the myosin head domain, which then re-anchored on the actin filament at a new position. This action induces the release of ADP and Pi and an event called power stroke, in which the head domain regains its original conformation and draws a full stop of one step of movement

(De La Cruz and Ostap, 2004). These cyclic interactions fuel myosins to walk along the actin filaments toward the barbed end, with the exception of myosin VI (Wells et al., 1999).

1.5.5 Roles of actin dynamics in endocytosis

It is generally accepted that each endocytic pathway is equipped with distinct internalisation machinery, despite the overlaps in some of the involved proteins. Dynamin, a GTPase, is a good example of a protein that is involved in numerous endocytic pathways. However, almost all the known endosomal routes induce cell cortex remodelling during internalisation, either via membrane invagination (for clathrin/caveolae-dependent routes) or by membrane protrusion (for macropinocytosis and phagocytosis). As an important constituent of the cell cortex, there is extensive research demonstrating the role of the actin cytoskeleton in these uptake processes. There is a growing body of evidence that indicates the actin involvement in downstream endocytic pathway events including budding, fission and intracellular movements of endocytic vesicles (Mooren et al., 2012).

1.5.5.1 Actin in Clathrin-Mediated Endocytosis

It appears that in mammalian cells, actin is not always essential for CME. However, in certain settings, such as the internalisation of large cargos or endocytosis at sites rich in actin filaments, the involvement of actin becomes necessary. Clathrin and adaptors are initially recruited to the plasma membrane, generating the membrane curvature (~80-100 nm) required for CME to proceed. The accumulated evidence supports the functional importance of interactions between many of the endocytic adaptors and the actin cytoskeleton. The implication is that the regulation of actin assembly may take place in response to endocytosis (Le Clainche et al., 2007). Actin polymerisation in the curved membrane region may be inhibited by certain endocytic proteins such as Syp1 during early stages of CME (Suetsugu, 2009, Saffarian et al., 2009). As invagination proceeds, certain endocytic proteins and ARP2/3 regulators can sense the changes in membrane curvature, and gather around the invagination. Following the activation of ARP2/3, an actin network is nucleated and established along invagination. During this process, the barbed ends of actin filaments point toward the plasma membrane, leading to a filament flow-away from the cortex. As the actin filaments are anchored to the clathrin-coat of the invagination membrane, the flowing of the network provides the force to push the endocytic pit further extruding into the cytoplasm. The dendritic actin network remains attached to endocytic membrane to assist vesicle scission and to drive the formed vesicle away from the plasma membrane. Our understanding on the involvement of actin in CME is still limited as investigations are commonly conducted by treating cells with chemical inhibitors, such as cytochalasin D to disrupt actin filaments. The results obtained by such methods, have frequently been conflicting and so many attempts have been made to explain this clearly very complicated process. Kirchhausen and co-workers reported the existence of other clathrin-coated structures, distinct from clathrin pits, which were termed as clathrin plaques. These plaques were found at the adherent surface of certain cell types (Saffarian et al., 2009). The two subgroups of clathrin-coated structures may be responsible for the discrepancies for the role of actin in CME.

1.5.5.2 Actin in Caveolae-Mediated Endocytosis

Caveolae are flask-shaped plasma membrane invaginations with a width range of 50-80 nm (See Section 1.4.2.2.2). To facilitate the caveolae fission step, dynamin is recruited and concentrated at the neck of membrane invagination. In the internalisation of SV40 via caveolae, actin filaments were observed to interact transiently with cargo-containing caveolae at the stage when dynamin localises to the invagination. Treatment with actin-disrupting drugs such as latrunculin A or jasplakinolide, has been shown to reduce the translocation of SV40 by ~60%, implying the importance of actin in caveolar pathways (Pelkmans and Helenius, 2002). Significant changes in the actin cytoskeleton were also demonstrated during virus internalisation in the same study: the depolymerisation of actin stress fibres occurred together with the recruitment of actin filament structures to virus-containing caveolar invagination (Pelkmans and Helenius, 2002). This indicates that like clathrin-mediated internalisation, caveolae-dependent uptake also appears to require actin in later endocytotic stages including vesicle fission and/or transport into cytoplasm. However, many important questions remain to be answered e.g. those concerning which proteins involved in recruiting F-actin to caveolae or/and regulation of actin polymerisation/depolymerisation, and whether/how actin functions in the uptake of other types of cargos mediated by caveolae.

1.5.5.3 Actin in macropinocytosis

In macropinocytosis, the plasma membrane protrudes outwards and engulfs extracellular fluid inwards to form large vesicles called macropinosomes. Our knowledge about this type of endocytosis in mammalian cells is limited, mainly due to the lack of appropriate molecular markers to specifically identify macropinosomes. To date, the most commonly used fluid-phase marker is fluorophore-labelled dextrans of various molecular weights. Experiments using diverse cell types or even different growth conditions may reveal the existence of different macropinosome types and macropinocytic pathways. Among the proteins with identified roles in macropinocytosis, a number of factors are also necessary in actin regulation, e.g. profilin (Engqvist-Goldstein and Drubin, 2003). Actin has a crucial role in the formation of macropinosomes by driving membrane protrusion and its subsequent closure. In 1999, Merrifield et al. described how the actin associated with pinocytic vesicles in leukemia cells. This study showed that actin could polymerise transiently on these endocytic vesicles providing a propulsive force that appeared to push the vesicles through cytoplasm (Merrifield et al., 1999). In mouse macrophages, actinin-4, an actin-binding protein that cross-links actin filaments into thick bundles or links filamentous actin to the plasma membrane, were found by immunofluorescence analysis to be associated with dextran-labelled macropinosomes, and this linkage was diminished during the course of macropinosome maturation (Araki et al., 2000). Additionally, a large number of the components of signalling pathways acting as bridge between receptor stimulation and actin reorganisation have been reported to regulate macropinocytosis. Studies in dendritic cells have showed that small GTPase Cdc42 can activate WASP-related proteins and in turn promotes actin assembly for macropinocytosis (Rohatgi et al., 1999). In another study, the impaired activity of Cdc42 and Rac1 and consequently of their downstream effectors caused by cytosolic acidification was suggested to account for the inhibited macropinocytosis (Koivusalo et al., 2010). Active phosphatidylinositol-3 (PI-3) kinase that is responsible for the production of phosphatidylinositol (3,4,5)-trisphosphate (PtdIns(3,4,5)P_3) and phosphatidylinositol (3,4)-bisphosphate (PtdIns(3,4)P_2) at the plasma membrane, has also been reported to make contribution to the actin cytoskeleton remodelling required for macropinocytosis (Amyere et al., 2000, Rupper et al., 2001). The activation of PI-3 kinase was found to induce the kinase activity of PAK-1 via a Cdc42/Rac1-independent mechanism and thus to promote actin phosphorylation and cytoskeletal reorganisation (Papakonstanti and Stournaras, 2002). A downstream signalling pathway upon EGFR activation involves the increased levels of PtdIns(3,4,5)P_3 and PtdIns(3,4)P_2 that are possibly mediated by PI-3 kinase. PtdIns(3,4)P_2 in turn recruits sorting nexin 5 (SNX5) to the plasma membrane, and the BAR domain of SNX5 was suggested to have a direct role in the generation of membrane curvature and thereby the formation of macropinocytic pits (Peter et al., 2004, Carlton et al., 2004, Lim et al., 2008). Evidence of the importance of actin in macropinocytosis is growing though the mechanism employed by actin to recruit to newly forming pinocytic vesicles has yet to be elucidated.

1.6 Hypothesis and Aims of the thesis

CPPs as vectors have the capacity to deliver a variety of macromolecules including nucleic acids, peptides and proteins into cells. Endocytic pathways are thought to be of significant importance for providing CPP-based vector systems with routes for cellular entry. All these at some point in time will involve cell-cortex remodelling, a process shown to be regulated by reorganisation of the actin cytoskeleton. Tentative links between actin remodelling and CPP uptake have been shown but more information is required to determine the extent of this association and how it could influence further research into improving the delivery capacity of these entities. Therefore this PhD project will investigate the hypothesis that actin organisation and disorganisation differentially influences the cellular uptake of the CPP octaarginine (R8) when attached to a model small molecule fluorophore (Alexa 488) or a much larger biological entity in the from of Enhanced Green Fluorescent Protein (EGFP). Overall a deeper understanding of the relationship between CPPs and the actin cytoskeleton during the process of cell penetration will be achieved by addressing the following major aims: 1) optimise a protocol to obtain a high yield of pure EGFP-R8 from *E.coli* cultures; 2) investigate in detail using laser scanning confocal microscopy the effects of a variety of actin inhibitors on the actin cytoskeleton; 3) examine the influence of actin disruption/reorganisation on cellular uptake levels of the two R8 conjugates.

Chapter 2: Materials and Methods

2.1 General materials

Listed here are details of the general experimental materials used in this project. Other more specific materials including CPP conjugates, cell lines, protein expression vector, plasmid, antibodies and single siRNAs are indicated in the text, along with their sources.

2.1.1 General chemicals

Acetic acid: #A/0400/PB17, Fisher Scientific, Loughborough, UK

Calcium chloride ($CaCl_2$): #C5080, Sigma-Aldrich, Poole, UK

Citric acid: #C/6160/53, Fisher Scientific, Loughborough, UK

Dimethyl sulphoxide (DMSO): #D2650, Sigma-Aldrich, Poole, UK

Ethanol: #E/0650/17, Fisher Scientific, Loughborough, UK

Glycerol: #G/0600/08, Fisher Scientific, Loughborough, UK

Methanol: #M/4056/17, Fisher Scientific, Loughborough, UK

Magnesium chloride ($MgCl_2$): #M8266, Sigma-Aldrich, Poole, UK

Sodium chloride (NaCl): #S/3120/53, Fisher Scientific, Loughborough, UK

Sodium hydroxide (NaOH): #S/4880/53, Fisher Scientific, Loughborough, UK

Tris-base: #BPE152-1, Fisher Scientific, Loughborough, UK

Tris-HCl: #BPE153-1, Fisher Scientific, Loughborough, UK

2.1.2 Protein expression, purification and analysis

Ampicillin: #A1593, Sigma-Aldrich, Poole, UK

Benzonase nuclease: #70746, Merck Millipore, Feltham, UK

Bicinchoninic acid solution: #B9643, Sigma-Aldrich, Poole, UK

Broad range protein molecular weight markers: #V8491, Promega, Loughborough, UK

Bovine serum albumin (BSA): #A7906, Sigma-Aldrich, Poole, UK

Complete protease inhibitor cocktail tablets:

#11836153001, Roche Diagnostics, Burgess Hill, UK

Copper (II) sulphate solution: #C2284, Sigma-Aldrich, Poole, UK

Imidazole: #I5513, Sigma-Aldrich, Poole, UK

Isopropyl β-D-1-thiogalactopyranoside (IPTG): #I6758, Sigma-Aldrich, Poole, UK

LB Agar: #A5306, Sigma-Aldrich, Poole, UK

LB Broth: #L3022, Sigma-Aldrich, Poole, UK

Lysozyme (hen egg white): #62970, Sigma-Aldrich, Poole, UK

Ni-NTA Agarose: #30210, Qiagen, Manchester, UK

Slide-A-Lyzer dialysis cassette: #87736, Life Technologies, Paisley, UK

S.O.C. (Super Optimal broth with Catabolite repression) medium:

#15544-034, Life Technologies, Paisley, UK

Phenol red-free Dulbecco’s Modified Eagle’s medium (D-MEM):

#31053, Life Technologies, Paisley, UK

2.1.3 SDS-PAGE

40% acrylamide/Bis: #10376643, Fisher Scientific, Loughborough, UK

Ammonium persulphate (APS): #A3678, Sigma-Aldrich, Poole, UK

Bromophenol blue: #161-0404, Biorad, Hemel Hempstead, UK

Dithiothreitol (DTT): #D9163, Sigma-Aldrich, Poole, UK

Glycine: #G/0800/60, Fisher Scientific, Loughborough, UK

Isopropanol: #10215331, Fisher Scientific, Loughborough, UK

Sodium dodecyl sulfate (SDS): #161-0301, Biorad, Hemel Hempstead, UK

Tetramethylethylenediamine (TEMED): #T9281, Sigma-Aldrich, Poole, UK

2.1.4 Electrophoresis gel staining reagents

Ammonia solution: #A/3240/PB15, Fisher Scientific, Loughborough, UK

Coomassie brilliant blue G-250: #161-0406, Biorad, Hemel Hempstead, UK

Formaldehyde: #BP531-500, Fisher Scientific, Loughborough, UK

Glutaraldehyde: #BP2547-1, Fisher Scientific, Loughborough, UK

Potassium ferricyanide: #702587, Sigma-Aldrich, Poole, UK

Silver nitrate: #209139, Sigma-Aldrich, Poole, UK

Sodium carbonate: #S/2880/53, Fisher Scientific, Loughborough, UK

Sodium thiosulphate: #15219656, Fisher Scientific, Loughborough, UK

2.1.5 Cell culture

Tissue culture flasks (25 cm^2 or 75 cm^2):

#430641U or #430639, Corning, Fisher Scientific, Loughborough, UK

6-well tissue culture plates: #3516, Corning, Fisher Scientific, Loughborough, UK

Coverslips 16 mm diameter: #12313138, Fisher Scientific, Loughborough, UK

Dulbecco's Modified Eagle's medium (D-MEM):

#21885, Life Technologies, Paisley, UK

Fetal bovine serum (FBS): #16000-044, Life Technologies, Paisley, UK

MatTek glass-bottom imaging dishes (35mm diameter):

#P35G-1.5-10-C, MatTek Corporation, Ashland, USA

Penicillin/streptomycin: #15070, Sigma-Aldrich, Poole, UK

0.05% Trypsin-Ethylenediaminetetraacetic acid (Trypsin-EDTA):

#25300062, Life Technologies, Paisley, UK

Epidermal growth factor (EGF): #E9644, Sigma-Aldrich, Poole, UK

2.1.6 Endocytic probes

Dextran (10kDa)-Alexa 488: #D22910, Life Technologies, Paisley, UK

Dextran (10kDa)-Alexa 647: #D22914, Life Technologies, Paisley, UK

Transferrin-Alexa 647: #T-23366, Life Technologies, Paisley, UK

2.1.7 Actin inhibitors

In this thesis the term actin inhibitor or disruptor refers to agent that either directly or indirectly interfere with actin functions in cells.

Cytochalasin D (Cyt D): #C8273, Sigma-Aldrich, Poole, UK

Jasplakinolide (JAS): #J7473, Life Technologies, Paisley, UK

Latrunculin B (Lat B): #428020, Merck Millipore, Feltham, UK

PP2: #529576, Merck Millipore, Feltham, UK

Y-27632: #688001, Merck Millipore, Feltham, UK

2.1.8 siRNA transfection

Oligofectamine transfection reagent: #12252-011, Life Technologies, Paisley, UK

Opti-MEM (Minimal Essential medium): #51985, Life Technologies, Paisley, UK

2.1.9 Cell washing and imaging for confocal microscopy

Heparin sodium salt: #H3149, Sigma-Aldrich, Poole, UK

HEPES sodium salt: #H3784, Sigma-Aldrich, Poole, UK

Roswell Park Memorial Institute (RPMI) 1640 medium:

#21875, Life Technologies, Paisley, UK

2.1.10 Cell fixation, permeablisation and staining

Fluorescence mounting medium Dako oil: #S3023, DAKO, Ely, UK

Hoechst 33342: #H3570, Life Technologies, Paisley, UK

Paraformaldehyde (PFA): #P/0840/53, Fisher Scientific, Loughborough, UK

Rhodamine Phalloidin (Rh-P): #R415, Life Technologies, Paisley, UK

Triton-X 100: #X100, Sigma-Aldrich, Poole, UK

2.1.11 Immunoblotting

Clarity, Western ECL substrate: #170-5060, Biorad, Hemel Hempstead, UK

Ponceau S solution: #P7170, Sigma-Aldrich, Poole, UK

Polyvinylidene difluoride (PVDF) membrane:

#10344661, Fisher Scientific, Loughborough, UK

Tween 20: #P1379, Sigma-Aldrich, Poole, UK

2.2 Expression of histidine tagged (His_6) proteins (EGFP-R8 or EGFP alone)

Histidine tagged (His_6) CPP-Enhanced Green Fluorescent Protein conjugate, referred to here as His_6-EGFP-R8 was produced in BL21 (DE3) *E.coli*, which was transformed with a pEV3b plasmid carrying sequences for His_6-EGFP-R8 and Ampicillin resistance (Figure 2.1). Both non-competent BL21 (DE3) *E.coli* and pEV3b plasmid were provided by Dr Peter Watson, School of Biosciences, Cardiff University following their manufacture for a separate project. The harvested recombinant protein His_6-EGFP-R8 was then purified under native conditions exploiting the high affinity of the His tag to Ni-NTA (nickel-nitrilotriacetic acid) resin. The same protein expression method was used for the expression of His_6-EGFP, except for that the competent BL21 (DE3) *E.coli* was transformed with a distinct pEV3b plasmid carrying sequences for His_6-EGFP and Ampicillin resistance (provided by Dr Peter Watson, School of Biosciences, Cardiff University). The obtained protein sample containing His_6-EGFP was then purified using the same protocol as that used for His_6-EGFP-R8. The purity of the expressed protein was analysed using SDS-PAGE. Protein concentration was determined by Bicinchoninic Protein Assay (BCA). Full experimental details are provided below.

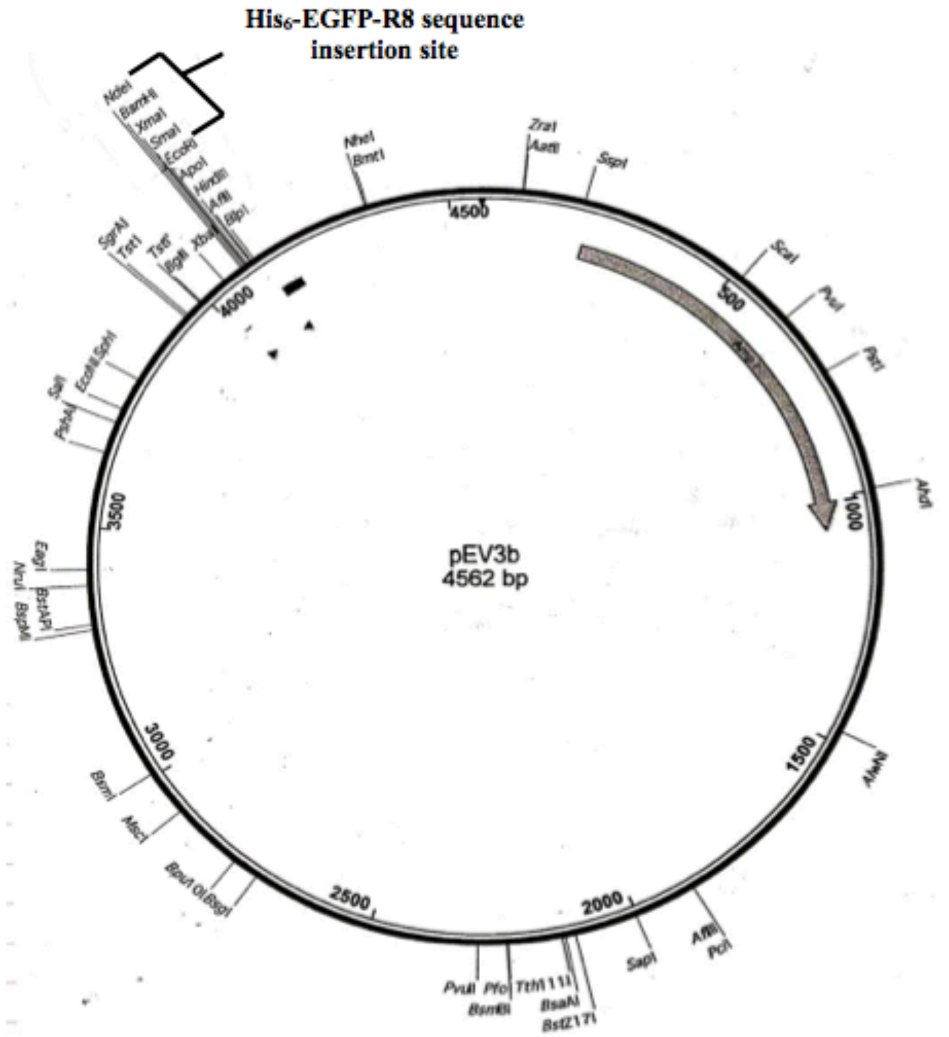

Figure 2.1 His$_6$-EGFP-R8 plasmid map.

2.2.1 Preparation of LB agar plates for bacterial growth

LB agar powder (17.5 g) was dissolved in 500 mL of dH_2O and autoclaved at 120°C/250°F for 50 min. The liquid LB agar was cooled down to ~ 50°C before plate setting. For ampicillin LB agar plates, 100 mg/ml ampicillin stock in dH_2O was added into LB agar liquid to achieve a final concentration of 100 µg/ml. Ampicillin negative plates were also prepared. All the LB agar plates were prepared in a biological safety cabinet and were stored upside down at 4°C (in the fridge or cold room) until required.

2.2.2 Preparation of chemically competent BL21 (DE3) *E.coli*

Non-competent BL21 (DE3) *E. coli* were originally stored in 25% glycerol in a 2 mL screw top cryovial at -80°C. To recover bacteria from stock, a sterile loop was used to scrape some of the frozen bacteria off of the top and this was then used to streak LB agar plates in a safety cabinet. The inoculated plates were then incubated overnight (16-20 hr) upside down at 37°C, until single colonies (~2 mm in diameter) could be visualised. Bacteria on these plates could be immediately used or the plates were sealed with parafilm and stored upside down at 4°C until required. To grow competent cells, a single bacteria colony was scraped with a sterile loop and used to inoculate a 2 ml solution of sterile LB broth (40 mg of LB broth powder dissolved in 2 ml dH_2O and autoclaved). After overnight (16-18 hr) incubation at 37°C with constant agitation of 150 RPM, 1 ml of this starter culture was diluted into 100 ml of fresh LB broth and this was incubated at 37°C/150 RPM until the OD_{600} reached ~0.4. The *E.coli* cells were then immediately chilled on ice for 20-30 min and harvested by centrifugation at 2700 x *g* for 10 min at 4°C. The cells were maintained at 4°C for the reminder of the procedure, and any containers or solutions that came in contact with the cells needed to be pre-chilled to 4°C. The supernatant was discarded and the cell pellets were washed by vortexing in 60 ml of ice-cold $MgCl_2$-$CaCl_2$ solution (80 mM $MgCl_2$ and 20 mM $CaCl_2$ in dH_2O). The cells were then fully resuspended in 4 ml of ice-cold 0.1 M $CaCl_2$ in dH_2O. At this point, the $CaCl_2$-treated competent cells can be directly used for transformation or be aliquoted into 200 µl and then stored at 4°C in the $CaCl_2$ solution for up to 48 hr. For long-term storage, the competent cells prepared in 0.1 M $CaCl_2$ and 15% glycerol were aliquoted into 50 µl, snap-frozen in liquid nitrogen and stored in a -80°C freezer.

2.2.3 Transformation of competent BL21 (DE3) *E.coli*

Competent BL21 (DE3) *E. coli* cells prepared as above were thawed on ice before starting transformation. Plasmid vector pEV3b (15 ng in 10 µl) carrying the sequences encoding His$_6$-EGFP-R8 and ampicillin resistance was added to the competent *E.coli* cells and the contents were mixed by pipetting up and down very gently. Negative controls containing the competent *E.coli* cells only and lacking the vector were also prepared. All the tubes were incubated on ice for 30 min and then heat-shocked at 42°C in water bath for exactly 90 seconds. The tubes were rapidly returned on to ice and the cells were chilled for 1-2 min. S.O.C. medium (800 µl) containing 2% tryptone, 0.5% yeast extract, 10 mM NaCl, 2.5 mM KCl, 10 mM $MgCl_2$, 10 mM $MgSO_4$, 20 mM glucose, was added to each tube and the contents were gently mixed before incubation at 37°C/150 RPM for 45 min. The transformed competent cells (20/50/100/200 µl) or the non-transformed competent cells (200 µl) were respectively pipetted on to ampicillin plates and spread over the surface. The plates were then cultured overnight in a 37°C incubator. Additionally, 30 µl of the transformed competent cells or the non-transformed competent cells were also pipetted onto LB agar plates lacking ampicillin. Single transformed colonies growing on ampicillin LB agar plates were then used as the source of the recombinant His$_6$-EGFP-R8 protein.

2.2.4 Expression of His$_6$-EGFP-R8 protein

Fresh LB broth medium were prepared in 5 L conical flasks and the solution was autoclaved. Single transformed *E.coli* colonies were picked from the selection plate and added into a 80 ml of LB broth containing 100 µg/mL ampicillin for overnight culture at 37°C with constant agitation of 200 RPM. The following day, 2 L of ampicillin-containing LB broth medium was inoculated with 40 ml of this *E.coli* starter culture. The diluted culture was then cultured at 37°C/200 RPM to an OD_{600} of approximately

0.6. It usually took ~4 hr to reach this OD if adding 40 ml starter culture to 2 L fresh LB medium; the OD_{600} was carefully monitored after 2 hr incubation and checked every half an hour through measuring the culture absorbance using a spectrophotometer - LB broth alone was set as reference. Before induction of protein expression, 1 ml of bacteria culture was collected from conical flask as non-induction sample and stored at -20°C. Expression of His_6-EGFP-R8 protein was induced by the addition of 1 ml of 1 M isopropyl β-D-1-thiogalactopyranoside (IPTG) stock to 2 L LB medium (working concentration of IPTG=0.5 mM). The culture was incubated under the same conditions for an additional 3 hr, during which 1 ml of bacteria culture was collected every 1 hr and stored at -20°C for subsequent analysis of IPTG induction/protein expression. At the end of the induction, the *E.coli* cells were harvested by 4°C centrifugation at 4000 x *g* for 20 min. The cell pallets were snap-frozen in liquid nitrogen and then thawed on ice for 5-10 min before resuspending in 40 ml of pre-chilled lysis buffer (20 mM Tris-HCl (pH7.5), 20 mM NaCl, 20 mM imidazole, protease inhibitor cocktail, 1 mg/ml lysozyme and 25 U/ml Benzonase nuclease. The cell debris was then removed by 4°C centrifugation at 10,000 x *g* for 30 min, and the clear green strongly fluorescent supernatant termed crude *E.coli* extract was then used for the next purification step.

2.2.5 Purification of His_6-EGFP-R8 protein by affinity chromatography

The Ni-NTA protein purification system was set up as shown in Figure 2.2 and the purification protocol used in this study was according to manufacturers (Qiagen) instructions with modifications that were introduced to increase protein purity. It should be noted that volumes are not always specified here, as this was dependent on the volume of the original *E.coli* culture. The Ni-NTA resin placed in column was equilibrated with 20 ml of equilibration buffer (20 mM Tris-HCl (pH7.5), 400 mM NaCl, 20 mM imidazole and protease inhibitor cocktail), pH 8.0. Before loading the cell lysate slowly into the column, the NaCl concentration of the extract was increased from 20 mM in the original protocol to 400 mM in the optimised protocol and each time the pH was adjusted to 8.0. Once the entire sample was passed down the column, the Ni-NTA resin was washed in order with 10 mL of four different pH 6.3 buffers containing 20 mM Tris-HCl (pH7.5), 400 mM NaCl and either 20, 30, 40 or 50 mM imidazole as part of the optimisation procedure. After the four washing steps, 6×his-tagged EGFP-R8 protein was eventually eluted with appropriate volume of elution buffer (20 mM Tris-HCl (pH7.5), 20 mM NaCl, 250 mM imidazole and protease inhibitor cocktail). To remove the imidazole and other low molecular weight contaminants, the eluted protein fraction was dialysed overnight at 4°C in dialysis buffer (20 mM Tris-HCl (pH7.5) and 150 mM NaCl) in a 20 kDa molecular weight cut off dialysis cassette. The Ni-NTA resin was finally washed with 0.5 M NaOH and stored at 4°C with 30% ethanol to inhibit microbial growth.

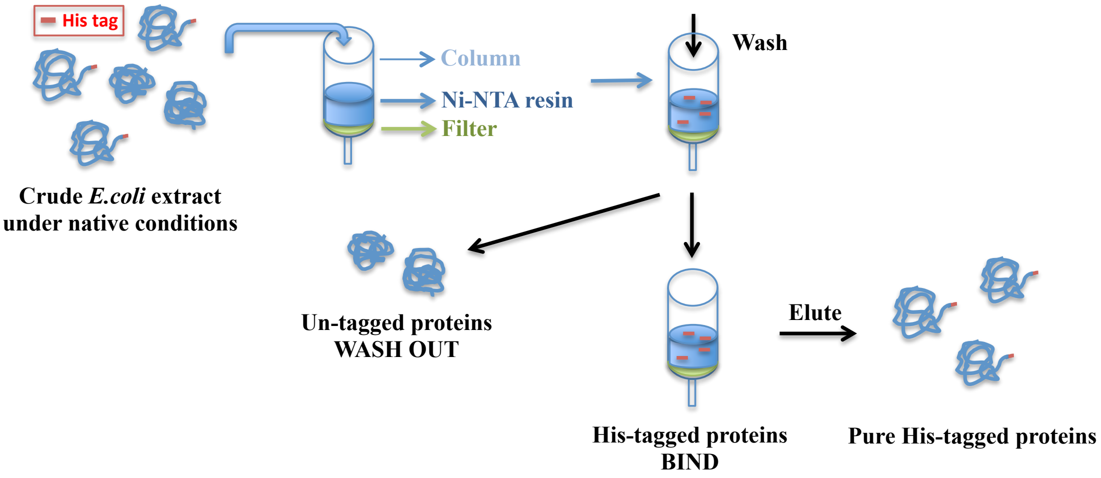

Figure 2.2 Purification of His$_6$-EGFP-R8 with the Ni-NTA protein purification system.

2.2.6 Bicinchoninic acid assay (BCA)

Bicinchoninic acid assay (BCA) was used in this study to determine protein concentrations of samples. Bovine serum albumin (BSA) was used as a protein standard and prepared by dissolving a concentration range of 0-1.0 mg/ml in 1× SDS sample buffer. In order to make the absorbance measurements of each sample fit in the linear range of the assay, the cell lysates were diluted 1:10, 1:20 or 1:50 in the same buffer. The BCA working solution was prepared by adding 1 volume copper sulphate pentahydrate to 49 volumes bicinchoninic acid. BCA working solution (200 µl) was then pipetted into each wells of a 96 well measurement plate containing 10 µl of the BSA standards or protein samples. Triplicate measurements for the standards or samples were prepared and after incubation at 37°C for 30 min, the absorbance at 562 nm was measured on a plate reader (Sunrise 96-well Microplate Reader, Tecan) and the protein concentration of each sample was extrapolated from the BSA calibration curve.

2.2.7 Examination of IPTG induction efficacy

The *E.coli* cell samples collected before and after IPTG addition were stored at -20°C and analysed for protein expression using SDS-PAGE. To prepare cell lysates for this procedure, the bacteria samples were thawed on ice and mixed well, and their absorbance at 600 nm was measured. The cells were then harvested by centrifugation of 13,000 x *g* for 5 min at room temperature. The supernatant was decanted and each cell pellet was re-suspended by vortexing in 100 µl of 1×SDS sample buffer (pH 6.8; 20 mM Tris-HCl; 0.75% (w/v) SDS; 2.75% glycerol; 0.125% (w/v) bromophenol blue and 0.25 M DTT). These suspensions were then denatured by heating at 95°C for 5 min and then centrifuged at 13,000 x *g* for 5 min. Samples were stored at -20°C or appropriate volume of each supernatant (usually 40 µg for crude proteins and 2 µg for purified proteins; see section 2.2.6 for protein concentration determination) were loaded onto a

12% resolving SDS-PAGE gel (see section 2.3.8 for SDS-PAGE gel preparation). Protein standard molecular weight markers (10 µL) were loaded on to one lane. The proteins were separated by SDS-PAGE at 100 V for ~ 90 min.

2.2.8 Preparation of standard denaturing SDS-PAGE gel

BioRad Mini-Protean II SDS-PAGE kit was used to cast and run the gels. A front and a back plate in the clamp frame were assembled, which was then secured into a casting stand. The recipes for the stacking (4% acrylamide) and resolving (10% or 12% acrylamide) gels are shown in tables 2.1 and 2.2 respectively.

Table 2.1 Recipe for 10% or 12% resolving gel.

	10% Gel		**12% Gel**	
Total volume of gel (mL)	10	20	10	20
40% acrylamide/Bis (mL)	2.5	5	3	6
3M Tris pH 8.8 (mL)	1.25	2.5	1.25	2.5
10% SDS (µL)	100	200	100	200
dH_2O (mL)	6.10	12.2	5.6	11.2
10% freshly made APS (µL)	75	150	75	150
TEMED (µL)	7.5	15	7.5	15

The TEMED should be the last ingredient added into the liquid gel preparation, and once added, the liquid mixture was quickly mixed by inversion and poured into the casting assembly, leaving a 2-3 cm gap at the top that was immediately filled with isopropanol. The resolving gel was left to set for 45 min until solidified. Then the isopropanol was descanted and the gap at the top of the resolving gel was washed with dH_2O ten times and the stacking gel was prepared the same way as the resolving gel.

Table 2.2 Recipe for 4% stacking gel.

	4% Gel	
Total volume of gel (mL)	10	15
40% acrylamide/Bis (mL)	1	1.5
1M Tris pH 6.8 (mL)	1.3	1.95
10% SDS (µL)	100	150
dH_2O (mL)	7.22	10.82
10% freshly made APS (µL)	75	112.5
0.1% Bromophenol blue (µL)	300	450
TEMED (µL)	10	15

The liquid stacking gel was immediately poured on top of the resolving gel. Then the 10 (or 15)-well comb was inserted into the stacking gel and after 30 min this was removed and the gel was transferred into running tank and incubated in running buffer (385 mM glycine, 250 mM Tris base and 0.5% SDS).

2.2.9 Concentrating His_6-EGFP-R8

This was performed using an anisotropic ultrafiltration membrane of centriplus concentrator. For this the His_6-EGFP-R8 protein sample was centrifuged at 15,000 x *g* for 10 min at 4°C. The green supernatant was saved and transferred to a sterile falcon tube and the cell debris in the sample if there was any was discarded. This step was included as debris caused blockage of the concentrator. A small amount of dH_2O was added into the upper centriplus reservoir (~0.6 cm height). The concentrator was then centrifuged at 3000 x *g* for 10 min in order to wash the membrane with water. After the water in the filtrate vial was discarded, the protein sample to be concentrated was pipetted into the upper reservoir. The sample-containing concentrator was centrifuged at 3000 x *g*/4°C until a desired volume of clear liquid (solvents and low-molecular-weight solutes) had accumulated in the filtrate vial. Solutes larger than membrane pore size such as His_6-EGFP-R8 were retained in the sample reservoir. The final protein retained at the top of the concentrator was collected and the protein concentration determined via the BCA assay.

This concentration procedure was problematic due to blockage of the membrane and it was very difficult to obtain protein at concentrations >200 μM. This was not of sufficient concentration to be used as a stock solution for subsequent cellular uptake assays using confocal microscopy. Therefore larger *E.coli* volumes were used (5 L total) keeping all purification volumes described above the same. This resulted in much higher concentration of His_6-EGFP-R8 that following purification from the Ni matrix. The eluted protein solution was firstly dialysed overnight at 4°C in dialysis buffer and then dialysed against phenol red-free D-MEM in 20 kDa molecular weight cut off dialysis cassette and this could then be incubated directly with cells after adjusting the concentration with more D-MEM.

2.2.10 Staining SDS-PAGE gels with Coomassie blue

Gels following SDS-PAGE were incubated and stained in Coomassie blue stain (0.25% Coomassie blue G-250, 50% methanol and 10% acetic acid) for 2-4 hr, until the gel was a uniform blue colour. The staining solution was then decanted and the protein gel was de-stained overnight in 5% methanol and 7.5% acetic acid until the background was clear. Gels were then imaged on a BioRad ChemiDoc system.

2.2.11 Silver staining SDS-PAGE gels

In some cases, following Coomassie blue staining, protein gels were subjected to a silver staining procedure. All required solutions needed to be freshly prepared prior to use. The gel was rehydrated by washing twice in dH_2O for 20 min and incubated in 10% glutaraldehyde solution for 30 min, followed by three 20-min washes in dH_2O. Staining was performed with silver diamine solution prepared by adding 21 ml of 0.36% (w/v)

NaOH, 1.4 ml of 35% ammonia to 73.6 ml of dH_2O and then adding 4 ml of 20% (w/v) silver nitrate drop by drop with constant stirring. Gels were stained for 30 min and then washed three times in dH_2O for 5 min. To visualise protein bands, the gel was soaked in developing solution containing 2.5 ml of 1% (w/v) citric acid and 0.26 ml of 36% formaldehyde in 500 ml of dH_2O for 1-10 min. Stopping solution (40% ethanol and 10% acetic acid in dH_2O) was added onto the gel to terminate further development. To reduce background staining, Farmer's reducing agent (0.3% w/v potassium ferricyanide, 0.6% w/v sodium thiosulphate and 0.1% w/v sodium carbonate) was added onto gels for 7-10 min, after which it was removed and replaced with stopping solution.

2.3 Labelling of CPP octaarginine (R8) with Alexa488

Peptide octaarginine (R8), extended with GC at its C-terminal (RRRRRRRR-GC), was synthesized by American Peptide Company (California, USA). Alexa Fluro® 488 C5 maleimide salt was purchased from Invitrogen (Paisley, UK).

The extended GC at the C-terminal of R8 allows conjugation to Alexa Fluro® 488 C5 maleimide salt. The labelling reaction was performed by Dr Edward Sayers in the laboratory and production of the fluorescent peptide was monitored by HPLC. Fractions corresponding to R8-GC-Alexa488 were freeze dried and resuspended in dH_2O and characterized by mass spectrometry. All peptides analysed in this thesis were labelled, purified and characterized by Dr Edward Sayers.

2.4 Cell culture

2.4.1 Cell lines and growth medium

HeLa (cervical carcinoma, epithelial) cells: ATCC Code CCL-2.

A431 (skin epidermal) cells: ATCC Code CRL-1555.

Dulbecco's Modified Eagle's medium (D-MEM) supplemented with fetal bovine serum (FBS, 10% final volume) and penicillin/streptomycin (100 units/ml and 100 µg/ ml respectively)

The two cell lines used in this project were chosen due to the fact that they had already been particularly characterised with respects to cellular uptake of R8-Alexa 488 and had shown major differences in both the organisation of their actin network and internalisation of dextran and R8-Alexa488 in the presence of the actin inhibitor cytochalasin D (Al Soraj et al., 2012).

2.4.2 Cell recovery from liquid nitrogen storage

The frozen cell vials were removed from liquid nitrogen and thawed in a 37°C water bath for ~1-2 min. Cells (1 ml) were then transferred into a 15 ml falcon tube that contained 9 ml of growth medium and centrifuged at 1000 x g for 5 min. The supernatant was discarded and the cell pallet was resuspended in 5 ml of growth medium and transferred into a 25 cm^2 tissue culture flask prior to incubation at tissue culture conditions (37°C/5% CO_2). The growth medium was changed every 2-3 days until the cells were confluent. Cells were then washed twice with PBS and trypsinised with 1 ml of 0.05% Trypsin-EDTA at 37°C/5% CO_2 (usually 3-4 min for HeLa cells and 7-8 min for A431 cells). Then growth medium (4 ml) was added into flask to stop trypsinisation and the detached cells (5 ml) were transferred into a 75 cm^2 tissue culture flask containing 15 ml growth medium for routine maintenance.

2.4.3 Cell maintenance

HeLa or A431 cells were maintained in growth D-MEM at 37°C/5% CO_2. Medium was regularly changed every 2-3 days and cell passaging was done as previously described in section 2.4.2 when cells reached 80-90% confluency. Passage numbers between 5-25 were used for all cell assays in this study to avoid high passage number-related effects such as cellular morphology changes and genomic instability.

2.5 Cell transfection with siRNA

Three autoclaved coverslips were placed into each well of 6-well tissue culture plate. HeLa (0.1 × 10^6 cells/well) or A431 (0.3 ×10^6 cells/well) cells were then seeded in 2.5 ml D-MEM containing 10 % FBS and allowed to adhere for 24 hr at 37°C/5 % CO_2 and then grown to a confluence of ~50-60%. Single siRNA sequences targeting different endocytic proteins are shown in Table 2.3.

Table 2.3 siRNA sequences and stock concentrations.

siRNA target	Concentration	Sequence
Non-targeting control (GFP)	100 µM	5'-GGCUACGUCCAGGAGCGCAdTdT-3'
AP2µ2	50 µM	5'-GUGGAUGCCUUUCGGGUCAdTdT-3'
Caveolin-1	100 µM	5'-AGACGAGCUGAGCGAGAAGdTdT-3'
Flotillin-1	100 µM	5'-AGAUGCACGGAUUGGAGAAdTdT-3'
PAK-1	100 µM	5'-AUAACGGCCUAGACAUUCAdTdT-3'
Cdc42	100 µM	5'-GACUCCUUUCUUGCUUGUUdTdT-3'

The siRNA sequences listed here were dissolved in 6 mM HEPES, 20 mM KCl and 0.2 mM $MgCl_2$ (pH 7.4).

On the day of cell transfection, the transfection reagent was prepared by mixing 2 µl of oligofectamine in 13 µl of Opti-MEM to a final volume of 15 µl. Diluted siRNA solution was prepared by adding 1 µl of 100 µM siRNA stock (or 2 µl of 50 µM siRNA stock) into 184 µl (or 183 µl) of Opti-MEM to a final volume of 185 µl. The diluted siRNA and oligofectamine solutions were gently mixed and incubated at room temperature for 30 min. During this incubation period, the cells were washed three times with serum free D-MEM and then the medium was replaced with 800 µl of fresh serum-free D-MEM. The siRNA:oligofectamine complex was added to each well and incubated with cells for 4 hr at 37°C/5 % CO_2. Using this method a final siRNA concentration of 100 nM in the transfection mixture has been previously shown to silence expression of flotillin-1 and caveolin-1 in both HeLa and A431 cells (Al Soraj et al., 2012). Then 500 µl of D-MEM containing 30% FBS was added to each well without removing the transfection mixture and the cells were further incubated 37°C/5 % CO_2 for 48 hr. Cell lysate collection or live cell assays could be then conducted.

For live cell imaging experiments the same transfection procedure was employed on cells plated on 35mm MatTek dishes. See section 2.8.5.

2.6 Cell lysate collection and preparation for Western blotting

Culture plates (6 well) prepared as above but without coverslips were placed on ice and the medium in each well was aspirated. The cells were then washed three times with ice-cold PBS before addition of 100 µl of lysis buffer (150 mM NaCl, 50 mM Tris base (pH 8.0) and 1% Triton-X 100 including protease inhibitors) to each well. The cell plates were kept on ice and placed on a lateral, circular shaker for 5 min before cells were scraped and the cell lysate were transferred to pre-cooled eppendorfs. Samples were then centrifuged at 4°C/13,800 x g for 10 min. The supernatants (crude protein samples) were finally transferred to fresh, pre-cooled eppendorfs.

The concentrations of the collected crude protein samples were determined by BCA as described in section 2.2.6, and then were equalised by addition of appropriate volumes of lysis buffer. The samples were mixed with appropriate volumes of 4× loading buffer (8% sodium dodecyl sulphate [SDS], 40% glycerol, 0.08% bromophenol blue, 250 mM Tris-HCl and 2 M freshly-made DTT) at a ratio of 3:1 and denatured by heating at 95°C for 5 min, followed by centrifugation at 13,000 x *g* for 5 min. Samples were stored overnight at -20°C before analysis by SDS-PAGE.

2.7 Protein detection by Western blotting

Collected cell lysates from each experiment (15 µg) were loaded onto a 12% SDS-

PAGE gel alongside 10 µl of protein molecular weight markers. SDS-PAGE gel was prepared as described in section 2.2.8. The proteins in each sample were separated by SDS-PAGE at 100V for ~ 90 min, and then transferred to a polyvinylidene fluoride (PVDF) membrane at 100V for ~ 60 min at 4°C.

The membrane with transferred proteins was then washed briefly in dH_2O, placed in Ponceau S solution for ~1 min and then returned to dH_2O for a confirmation of protein transfer. The unwanted membrane regions were cut out and the membrane strips containing proteins of interest were retained. The Ponceau solution was recycled and the membrane strips were washed thoroughly in PBS to remove all traces of stain.

For immunoblotting, the membrane strips were blocked in 5% milk in PBS containing 0.025% Tween20 (PBST) for 1 hr at room temperature. Then the blocking solution was discarded and the membrane was incubated with relevant primary antibodies diluted in 2% milk in PBST for 1 hr at room temperature. Primary mouse anti-β-tubulin antibody purchased as a HRP conjugate was diluted in 5% milk in PBST and no secondary antibody was required for it. The primary antibodies and the corresponding secondary antibodies are listed in Table 2.4.

Table 2.4 Primary and secondary antibodies and dilutions for immunoblotting.

Primary antibody	**Dilution**	**Secondary antibody**	**Dilution**
Mouse anti-AP50 (#611351, BD Biosciences)	1:200	Goat anti-mouse HRP	1:2000
Rabbit anti-Caveolin-1 (#3238S, Cell Signaling)	1:1000	Goat anti-rabbit HRP	1:2000
Mouse anti-Flotillin-1 (#610820, BD Biosciences)	1:500	Goat anti-mouse HRP	1:2000
Rabbit anti-PAK-1 (#2602S, Cell Signaling)	1:200	Goat anti-rabbit HRP	1:2000
Rabbit anti-Cdc42 (#2462S, Cell Signaling)	1:200	Goat anti-rabbit HRP	1:2000
Mouse anti-β-tubulin HRP conjugated (#AB21058, Abcam)	1:50,000	-	
Rabbit anti-GAPDH (#2118S, Cell Signaling)	1:1000	Goat anti-rabbit HRP	1:2000

The membrane was then washed three times with PBST for 15 min prior to incubation with appropriate secondary antibody diluted in 2% milk in PBST at room temperature for 1 hr.

The membrane was washed three times in PBST for 5 min before development. Equal volumes of Clarity^{TM} Western enhanced chemiluminescence (ECL) reagents were mixed, applied to the PVDF membrane and left for 5 min. After incubation with the ECL mixture, excess solution was removed from the membrane. Subsequently the membrane was wrapped in cling film and then imaged on a BioRad ChemiDoc system. Band intensities were quantified using ImageJ software. The values were exported to excel where they were normalised against the loading control. For full quantification method see Wymant, Ph.D thesis 2014. Accessible from orca.cf.ac.uk/72275.

2.8 Confocal fluorescence microscopy

Fluorescence images shown in Chapter 3 and 4 are representatives of at least 2 independent experiments. For fluorescence quantification and the following statistical analysis some experiments in Chapter 5 were performed three times.

2.8.1 Cellular uptake of CPP conjugates

HeLa or A431 were seeded on MatTek dishes at respective densities of 0.5×10^6 cells/dish and 1.0×10^6 cells/dish and maintained in 2.5 ml D-MEM containing 10 % FBS. Cells were then allowed to adhere for 24 hr at 37°C/5% CO_2 to reach a confluence of ~80 %. Alternatively cells on MatTek dishes had been transfected for 48 hr with siRNA as described in Section 2.5. On the day of experiment cells were washed twice with PBS and then either 2 μM CPP conjugate R8-Alexa488 or EGFP-R8 or EGFP alone prepared in 100 μl serum-free D-MEM was carefully added on to the central glass-bottom microwell drop by drop. This volume (100 μl) was used for all microscopy experiments employing MatTek dishes. The cells were then incubated for 1 hr at 37°C/5% CO_2. Cells were washed three times with 0.5 mg/ml heparin in PBS to reduce the plasma membrane-associated R8 conjugates and then once with PBS, prior to the addition of 2 ml of imaging medium [RPMI with 20 mM HEPES (pH 7.4)]. Cells were then subjected to analysis by confocal microscopy.

2.8.2 Uptake of CPP conjugates in Cyt D-treated cells

HeLa or A431 cells were seeded on MatTek dishes as described in section 2.8.1 and cultured for 24 hr. Cells were washed with PBS before addition of diluent control (DMSO) or 10 µM Cyt D for 15 min in serum-free D-MEM at 37°C/5% CO_2. Then CPP conjugates at 2 µM concentration in serum-free D-MEM were added to the cells in the absence (control) or presence of 10 µM Cyt D for 1 hr at 37°C/5% CO_2. The cells were then washed three times with 0.5 mg/ml heparin and once with PBS, and incubated in 2 ml imaging medium prior to analysis by confocal microscopy.

2.8.3 Uptake of EGFP-R8 in control or Cyt D-treated cells at 4°C or 37°C

A431 cells were seeded on MatTek dishes as described in section 2.8.1 and cultured for 24 hr. Cells were washed with PBS before addition of diluent control (DMSO) or 10 µM Cyt D for 15 min in serum-free D-MEM at 37°C/5% CO_2. For control cells, EGFP-R8 (2 µM) was added to the cells for 1 hr at 4°C/5 % CO_2 or at 37°C/5% CO_2. For Cyt D-treated cells, 2 µM of EGFP-R8 in serum-free D-MEM was incubated with the cells in presence of 10 µM Cyt D for 1 hr at 4°C/5% CO_2 or at 37°C/5% CO_2. Then cells were washed three times with 0.5 mg/ml heparin and once with PBS, and incubated in 2 ml imaging medium prior to analysis by confocal microscopy.

2.8.4 Uptake of CPP conjugate EGFP-R8 in cells treated with other actin inhibitors

A431 cells were seeded on MatTek dishes as described in section 2.8.1 and cultured for 24 hr. Cells were washed with PBS before incubation with diluent control (DMSO or dH_2O) or actin inhibitor prepared in serum-free D-MEM at 37°C/5% CO_2. Table 2.5 lists the inhibitors used along with working concentrations and cell incubation time used in this study. Then 2 µM of CPP conjugate EGFP-R8 prepared in serum-free D-MEM was added to the cells in the absence (control) or presence of relevant actin drug for 1 hr at 37°C/5% CO_2. Cells were washed three times with 0.5 mg/ml heparin and once with PBS, and incubated in 2 ml imaging medium prior to analysis by confocal microscopy.

Table 2.5 Actin inhibitors, concentrations and cell incubation period used to disrupt/modify the actin cytoskeleton in section 2.8.

Actin inhibitor	Concentration(s)	Incubation
Lat B	0.5 µM	30 min
JAS	2 µM, 4 µM, 8 µM	45 min
***Y-27632**	1 µM, 10 µM, 50 µM, 100 µM	4 hr
PP2	1 µM for HeLa cells; 10 µM for A431 cells	48 hr

*The diluent control was dH_2O

2.8.5 Uptake of EGFP-R8 in siRNA-transfected cells

HeLa (0.1 × 10^6 cells/well) or A431 (0.3 × 10^6 cells/well) cells were seeded on MatTek dishes in 2.5 ml D-MEM containing 10 % FBS and allowed to adhere for 24 h at 37°C/5 % CO_2 and then grown to a confluence of ~50-60%, before transfection with siRNA for 48 hr as described in section 2.5. Cells were then washed with PBS before incubation with 2 µM of EGFP-R8 in serum-free D-MEM for 1 hr at 37°C/5% CO_2. Cells were washed three times with 0.5 mg/ml heparin and once with PBS, incubated in 2 ml of imaging medium prior to analysis by confocal microscopy. Untransfected cells were also investigated.

2.8.6 Cyt D effects on EGFP-R8 uptake in cells transfected with si-Cdc42

A431 cells seeded and cultured as described in section 2.8.5 were transfected with control si-GFP or si-Cdc42 for 48 hr as described in section 2.5. After washing with PBS, they were incubated with either diluent control (DMSO) or 10 µM Cyt D at 37°C/5% CO_2 for 15 min prior to a further incubation with 2 µM EGFP-R8 in serum-free D-MEM for 1 hr at the same conditions in the presence or absence of Cyt D. Cells were then washed three times with 0.5 mg/ml heparin and once with PBS, and incubated in 2 ml of imaging medium prior to analysis by confocal microscopy. Untransfected cells were also investigated.

2.8.7 Uptake of transferrin-Alexa 647 in Cyt D-treated cells

HeLa or A431 cells were seeded on MatTek dishes as described in section 2.8.1 and cultured for 24 hr. Cells were washed with PBS before addition of diluent control (DMSO) or 10 µM Cyt D for 15 min in serum-free D-MEM at 37°C/5% CO_2. Then 5 µg/ml transferrin-Alexa 647 (TF-647) prepared in serum-free D-MEM was added to the cells in the absence (control) or presence of 10 µM Cyt D for 30 min at 37°C/5% CO_2. The cells were washed three times with PBS before addition of 2 ml imaging medium and a further incubation at 37°C/5% CO_2 for 10 min to deplete the plasma membrane labelling by TF-647.

2.8.8 Uptake of dextran (10kDa)-Alexa 647 in Cyt D-treated cells

HeLa or A431 cells were seeded on MatTek dishes as described in section 2.8.1 and cultured for 24 hr. Cells were washed with PBS before addition of diluent control (DMSO) or 10 µM Cyt D for 15 min in serum-free D-MEM at 37°C/5% CO_2. Then 0.1 mg/ml dextran (10kDa)-Alexa 647 (dextran10-647) prepared in serum-free D-MEM was added to the cells in the absence (control) or presence of 10 µM Cyt D for 1 hr at

37°C/5% CO_2. Then cells were washed three times with PBS and incubated in 2 ml imaging medium prior to analysis by confocal microscopy.

2.8.9 Endosomal co-localisation of EGFP-R8 and dextran

2.8.9.1 Co-localisation of dextran (10kDa)-Alexa 488 and dextran (10kDa)-Alexa 647

A431 cells were grown on MatTek dishes, as described in section 2.8.1, for 24 hr. They were then washed twice with PBS before addition of diluent control (DMSO) or 10 µM Cyt D for 15 min in serum-free D-MEM at 37°C/5% CO_2. Dextran (10kDa) labelled with different fluorophores Alexa 488 (dextran10-488; 0.2 mg/ml) and Alexa 647 (dextran10-647; 0.1 mg/ml) prepared in serum-free D-MEM were co-incubated with the cells in the absence (control) or presence of 10 µM Cyt D for 1 hr at 37°C/5% CO_2. Then the cells were washed three times with PBS and incubated in 2 ml imaging medium prior to analysis by confocal microscopy.

2.8.9.2 Co-localisation of EGFP-R8 and dextran10-647

HeLa or A431 cells were cultured on MatTek dishes, as described in section 2.8.1, for 24 hr. They were then washed twice with PBS before addition of diluent control (DMSO) or 10 µM Cyt D for 15 min in serum-free D-MEM at 37°C/5% CO_2. EGFP-R8 (2 µM) and dextran10-647 (0.1 mg/ml) prepared in serum-free D-MEM were co-incubated with the cells in the absence (control) or presence of 10 µM Cyt D for 1 hr at 37°C/5% CO_2. Then cells were washed three times with 0.5 mg/ml heparin and once with PBS, and incubated in 2 ml imaging medium prior to analysis by confocal microscopy.

2.8.9.3 Co-localisation of EGFP-R8 and lysosome-located dextran10-647

HeLa or A431 cells were seeded on MatTek dishes, as described in section 2.8.1, and cultured for 24 hr. They were then washed with PBS before incubation with 0.1 mg/ml dextran10-647 for 2 hr (pulse) in serum-free D-MEM at 37°C/5% CO_2. Dextran containing medium was removed and the cells were washed again with PBS prior to a further 4 hr chase in growth medium at 37°C/5% CO_2. Then cells were treated with diluent control (DMSO) or 10 μM Cyt D for 15 min in serum-free D-MEM at 37°C/5% CO_2. EGFP-R8 (2 μM) in serum-free D-MEM was added to the cells in the absence (control) or presence of 10 μM Cyt D for 1 hr at 37°C/5% CO_2. Then cells were washed three times with 0.5 mg/ml heparin and once with PBS, and incubated in 2 ml imaging medium prior to analysis by confocal microscopy.

2.8.10 Confocal fluorescence microscopy

Confocal fluorescence microscopy analysis was performed on a Leica SP5 confocal laser scanning microscope, equipped with laser lines 405 Blue Diode (Excitation wavelength 405 nm) for visualisation of Hoechst 33342, Argon (Excitation wavelength 488 nm) for visualisation of fluorophore Alexa 488 and fluorescent protein EGFP, Helium Neon 1 (Excitation wavelength 543 nm) for visualisation of Rhodamine Phalloidin (Rh-P) and Helium Neon 3 (Excitation wavelength 633 nm) for visualisation of fluorophore Alexa 647. All images presented in this study were obtained using a HCX PL APO 63× 1.4 NA oil immersion objective with Leica Type F immersion oil. Parameters “Gain” and “Off-set” of the individual photomultiplier tubes need to be adjusted within an experiment in order to obtain optimal image acquisition avoiding saturation. For multi-channel image acquisition, the channels were scanned in a sequential recording mode to avoid spectral cross-talk caused by overlapping excitation and/or emission spectra of fluorophores. The acquisition mode “XYZ” and the image resolution (pixels/image) of 1024×1024 were selected to use. Pinhole size was set to 1 Airy Unit, and scan speed was set as 700 Hz. For single section images, the same optical section is scanned three times to generate a line average image. Captured images were then analysed using ImageJ.

2.9 Actin cytoskeleton visualisation

2.9.1 Cell culture for actin labelling

Three autoclaved coverslips were placed into each well of 6-well tissue culture plate. HeLa (0.5×10^6 cells/well) or A431 (1.0×10^6 cells/well) cells were then seeded in 2.5 ml D-MEM containing 10 % FBS and allowed to adhere for 24 hr at 37°C/5% CO_2 and to reach a confluence of ~80–90 %.

2.9.2 Actin cytoskeleton labelling

HeLa or A431 cells were prepared on coverslips as described in section 2.9.1. Then cells were washed three times with PBS and fixed with 3 % PFA in PBS at room temperature for 15 min. Cells were washed three times again with PBS and permeabilised with 0.2 % Triton-X 100 in PBS at room temperature for 5 min. After three washing with PBS, cells were stained for cell nuclei with 1.0 µg/ml Hoescht 33342 in PBS and for polymerised actin with 1.0 µg/ml Rhodamine-conjugated phalloidin (Rh-P) in PBS through incubation at room temperature for 15 min. The cells were finally washed three times with PBS and once with distilled water (to remove salt from the coverslip), and the coverslips with cells were mounted onto a clean glass microscope slide containing 12 µl of DAKO mounting medium.

2.9.3 Actin cytoskeleton visualisation in actin inhibitor-treated cells

HeLa or A431 cells were seeded on coverslips as described in section 2.9.1, and cultured for 24 hr. Cells were then washed three times with PBS before addition of diluent control (DMSO or dH_2O) or actin inhibitor prepared in serum-free D-MEM at 37°C/5% CO_2. Table 2.6 contains a list of various actin inhibitors used in this study and their incubation time with cells. Following incubation with actin drug, cells were washed with PBS, fixed with 3% PFA, permeabilised with Triton-X 100 and stained for cell nuclei and for F-actin as described in section 2.9.2. Finally the coverslips with cells were mounted onto a clean glass microscope slide containing 12 µl of DAKO mounting medium, prior to actin visualisation on confocal microscopy as described in section 4.2.1.

Table 2.6 Actin inhibitors, concentrations and cell incubation period used to disrupt/modify the actin cytoskeleton for visualisation in section 2.9.

Actin inhibitor	Concentrations	Incubation
Cyt D	20 nM, 200 nM, 2 µM	15 min
Lat B	0.1 µM, 0.5 µM, 1.0 µM	30 min
JAS	0.2 µM, 0.8 µM, 2 µM, 4 µM	45 min
***Y-27632**	1 µM, 10 µM, 50 µM, 100 µM	4 hr
PP2	1 µM for HeLa cells; 1 or 10 µM for A431 cells	48 hr

* The diluent control was dH_2O

* For each actin inhibitor, a wide range of concentrations, selected on the basis of published literature, were tested. Based on this information, the appropriate concentration(s) of compound to use was determined by its visual effects on actin and acceptable cytotoxicity.

2.9.4 Actin cytoskeleton visualisation in serum-starved cells treated with R8 or EGF

HeLa and A431 cells were seeded at respective densities of 0.25×10^6 and 0.5×10^6 cells/well as described in section 2.9.1, and cultured for 24 hr at 37°C/5% CO_2. For serum starvation, the cells were washed three times with PBS and placed in fresh D-MEM lacking serum. For control cells the medium was replaced with fresh D-MEM supplemented with 10 % FBS. After a further culture at 37°C/5% CO_2 for 16 hr, the cells were washed three times in PBS and then incubated with serum-free DMEM containing 10 or 20 µM R8 (HeLa cells) or 20 µM R8 or 50 nM EGF (A431 cells) at 37°C/5% CO_2 for 2.5 min only. The cells were then quickly washed, fixed, labelled for the nucleus and actin, and finally imaged by confocal microscopy as described in section 2.9.2 and 4.2.1.

2.9.5 EGFP-R8 effects on the actin cytoskeleton in cells treated with actin inhibitors

A431 cells were seeded on coverslips as described in section 2.9.1, and cultured for 24 hr. They were washed three times with PBS before pre-treatment of either diluent control (DMSO or dH_2O), 10 μM Cyt D for 15 min, 0.5 μM Lat B for 30 min, 0.8 μM JAS for 45 min or 50 μM Y27632 for 4 hr at 37°C/5% CO_2. All actin inhibitors used here were prepared in serum-free D-MEM. Cells were then incubated with 2 μM EGFP-R8 in the absence (control) or presence of relevant actin inhibitor for 1 hr and washed three times with 0.5 mg/ml heparin and once with PBS. Following several wash steps, cells were fixed with 3% PFA, permeabilised with Triton-X 100 and stained for cell nuclei and for F-actin as described in section 2.9.2. Finally the coverslips were mounted onto a clean glass microscope slide containing 12 μl of DAKO mounting medium, prior to actin visualisation by confocal microscopy as described in section 4.2.1.

2.9.6 Actin cytoskeleton visualisation in si-Cdc42-treated cells

A431 cells were seeded on coverslips as described in section 2.5 and cultured for 24 hr before being transfected with si-GFP (control) or si-Cdc42 for 72 hr as described in 2.5. Following siRNA transfection, cells were washed with PBS, fixed with 3% PFA, permeabilised with Triton-X 100 and stained for cell nuclei and for F-actin as described in section 2.9.2. Finally the coverslips with cells were mounted onto a clean glass microscope slide containing 12 μl of DAKO mounting medium, prior to actin visualisation on confocal microscopy as described in section 4.2.1. Untransfected cells were also investigated.

Chapter 3: Examination of the effect of Cytochalasin D on the uptake of CPP conjugates and endocytic probes

3.1 Introduction

As discussed in the general introduction, the actin cytoskeleton is believed to play a role in different endocytic pathways, and most especially in macropinocytosis. The subsequent intracellular trafficking of endosomal vesicles has also to a certain extent been shown to be dependent on actin. Widely used tools to examine the roles of the actin cytoskeleton in various cellular processes including endocytosis are pharmacological/chemical inhibitors such as cytochalasin D (Cyt D) that influence actin dynamics through different mechanisms. Cyt D is a member of a class of fungal metabolites known as cytochalasins, which were discovered in 1967 and have been shown to affect a variety of motile functions of eukaryotic cells (Carter, 1967, Casella et al., 1981, Wessells et al., 1971). Cyt D disrupts actin cytoskeleton *in vitro* by binding to the fast-growing ends of actin nuclei and filaments with high affinity. Consequently, the addition of monomeric actin to these sites is prevented. Therefore, Cyt D has become a popular reagent in research of actin-dependent cellular uptake mechanisms.

In the previous studies performed in the Jones' laboratory (Al Soraj et al., 2012), Cyt D inhibited the uptake of cell penetrating peptides R8 and Tat in two different cell models: HeLa and A431 cells. But interestingly, the effect of actin disruption with Cyt D on the uptake of the fluid phase marker dextran was highly dependent on the choice of cell line as it was found to reduce uptake in HeLa cells and stimulate uptake in A431 cells. This indicated that in A431 cells, these CPPs utilized a different pathway from that used by dextran. This novel finding in A431 cells (enhanced dextran uptake by Cyt D) has been described before in opossum kidney cells (Gekle et al., 1997) and inspired us to ask more questions on the role of actin in endocytosis. Normally macropinocytosis requires functional actin rearrangement close to the plasma membrane to facilitate the formation of membrane protrusions that mediate the engulfment of fluid. Less is known about the un-stimulated fluid phase uptake processes that also allow dextran to be internalised into cells (Al Soraj et al., 2012). Cyt D has been extensively used to study macropinocytosis and is a powerful inhibitor of this process. The effect of this drug on fluid phase uptake is less characterized and merits further study.

Several CPPs have demonstrated an ability to deliver intact proteins into cells either as fusion proteins or as non-covalent complexes [reviewed in (Kristensen et al., 2016)]. Most importantly the biofunctionality of specific proteins has been shown to be maintained to influence intracellular processes (Futaki et al., 2004, Wadia and Dowdy, 2003). This is one reason why these peptides are interesting candidates for delivery of therapeutic proteins. Efforts have been focused on understanding the internalisation mechanisms of these CPP-protein conjugates, as it is fundamental for improving their therapeutic potential. Among the different subtypes of endocytosis, macropinocytosis is one of the most frequently suggested pathways to be involved in the cellular entry of these CPP-protein conjugates (Wadia et al., 2004a, Liu et al., 2002) and much of this is due to studies using Cyt D.

Green fluorescent protein (GFP) traditionally refers to the ~ 27 kDa bioluminescent protein that was first isolated from *Aequorea* jellyfish by Shimomura et al (Shimomura et al., 1962, Johnson et al., 1962). GFP has become one of the most widely exploited proteins in cell and molecular biology due to its ability to generate green fluorescence when it absorbs light in the blue to ultraviolet range (maximally excited at 395 nm and emitting with a peak at 509 nm) (Tsien, 1998). In order to gain greater potential for widespread usage, a variety of mutants of GFP including enhanced GFP (EGFP), which is a popular humanized version of GFP and color mutants such as yellow fluorescent protein (YFP) derivatives have been engineered.

GFP has also been attached to CPPs to monitor how the peptides are able to deliver a protein cargo to the inside of cells (Nischan et al., 2015, Jo et al., 2014). The first study showing artifacts on the cellular location of CPPs due to fixation was in fact performed using a variety of GFP-attached CPPs (Lundberg and Johansson, 2002). Typically GFP extended with CPPs are first purified from *E.coli* lysates after the bacteria have been transfected with plasmids encoding the fluorescent protein in frame at the N- or C-terminus of the CPP. These fusion proteins can then be added to cells in medium and using live cell imaging confocal microscopy the fate of the fluorophore in cells can be monitored under different conditions. A variety of CPP-GFP constructs have been used to evaluate the translocation efficiency and intracellular protein uptake of these CPP delivery systems in a wide range of cell lines including stem cells and primary cells (Jo et al., 2014, Simon et al., 2009, Jones, 2010). GFP has also incorporated into more complex delivery systems such as Tat mediated cell delivery of DNA complexed with a second protein called p50. Here p50 was expressed in frame with Tat and GFP that acted as a reporter for cell entry into mammalian PC12 (a clonal cell line derived from a transplantable rat pheochromocytoma) cells (Gao et al., 2009). The delivery of large cargos such as full-length proteins mediated by arginine-rich CPPs (for example Tat) usually shows that they are effectively internalised but entrapped in endocytic vesicles, which quite possibly also deliver the cargo to lysosomes for degradation. In a recent study, the internalisation efficiency of Tat-GFP conjugate into live cells was significantly increased by peptide cyclization, and the internalised conjugates were rapidly visible in the cytosol and the nucleus. Meanwhile the linear Tat analogue did not confer evident GFP escape into the cytosol (Nischan et al., 2015). The fusion of pH-sensitive E(1)GFP to the HIV-Tat protein enabled the monitoring of pH changes during endocytosis and allowed for real-time tracking of multiple steps in endocytosis from initial cell surface binding (Serresi et al., 2009). As previously discussed the internalisation modes of CPPs include direct entry across cell membranes and a variety of endocytic pathways. Arginine-rich peptides such as R8 may utilize either or both mechanisms to gain the cell entry, depending on physicochemical properties of the peptides and/or the attached cargo and the administration conditions. However, when attached with cargo of high molecular weight such as GFP (27 kDa), the fusion protein R8-GFP employed endocytosis to transduce through the plasma membrane, usually followed by confinement in punctate membrane vesicles (Futaki et al., 2004). The addition of pyrenebutyrate prior to the loading of R8-EGFP led to direct membrane translocation of the R8 conjugate into the cytosol within a few minutes (Takeuchi et al., 2006). Although numerous cell uptake studies have been published using a range of CPP-GFP fusion proteins, there is almost no general agreement regarding the exact mechanisms of their uptake and the details remain unclear.

Aims

A major focus of this thesis was to perform comparative analysis of the cellular uptake of R8 attached to a fluorophore (Alexa 488) or a small protein (EGFP) in different cell lines. The aims of this chapter were to 1) optimise a protocol to obtain a high yield of pure EGFP-R8 from *E.coli* cultures and 2) investigate and compare the cellular uptake mechanism(s) of R8-Alexa 488 and EGFP-R8 in HeLa and A431 cells using actin disruptor Cyt D. This may shed new light on the role of actin in endocytic pathways and gain a better understanding of how protein attached CPPs enter into cells.

3.2 Results

3.2.1 Expression and purification of His$_6$-EGFP-R8

The initial objective of this chapter was to purify His$_6$-EGFP-R8 from BL21 (DE3) *E.coli* to allow subsequent cell uptake studies. BL21 (DE3) *E.coli* is a widely used expression vector and suitable for expression of many non-toxic and soluble proteins. This strain contains the lambda DE3 lysogen, which carries the gene for T7 RNA polymerase under the control of the modified lacUV5 promoter and a lac operator. In the absence of lactose, the lac repressor binds in a sequence-specific manner to the lac operator sequence of DNA in the host chromosome and prevents *E.coli* RNA polymerase from binding the lacUV5 promoter, which consequently blocks the expression of T7 RNA polymerase. As soon as the lac repressor disassociates from the lac operator, T7 RNA polymerase will be transcribed and translated. Therefore it is ideal for use with T7 promoter-based expression systems such as pEV3b plasmid, encoding His$_6$-EGFP-R8 and conferring ampicillin resistance.

Without lactose, the lac repressor also binds to the lac operator sequence on the plasmid DNA and thus blocks the access of T7 RNA polymerase to the T7 promoter. IPTG, a molecular mimic of allolactose can bind to lac repressor and release the repressor from lac operator, allowing the gene transcription in the lac operon. The T7 RNA polymerase will be first expressed and binds to the T7 promoter sequence upstream of the gene of interest on the plasmid to trigger the subsequent transcription of the target gene His$_6$-EGFP-R8. Unlike lactose, IPTG is not involved in any metabolic pathways and thus unlikely to be broken down or used by cells. This makes IPTG a more useful inducer of lac operon than lactose itself as the concentration of IPTG added could remain constant during the induction period.

E.coli was successfully transfected with the plasmid that then allowed growth on ampicillin LB plates. As expected no growth was observed from *E.coli* controls lacking the pEV3b vector (data not shown). As written in the Materials and Methods (section 2.2.4), samples were removed from cultures following inoculation of LB media with the starter culture. This allowed for analysis of protein expression before and after adding IPTG.

Following culture the *E.coli* cells were lysed and efficacy of IPTG induction on expression of His_6-EGFP-R8 was estimated by SDS-PAGE and visualised with Coomassie blue staining (Figure 3.1). Before IPTG addition, some basal level expression of His_6-EGFP-R8 in *E.coli* cell culture was seen to occur showing as a weak band at ~30 kDa. In BL21(DE3) cell lines, binding of the lac repressor with operator sites is never 100% efficient, and thus gene transcription from the *lac* operon promoter can not be completely shut off. This always leads to some basal expression of T7 RNA polymerase from the *E.coli* genome (often termed leaky expression) in the absence of inducer such as IPTG and the subsequent basal expression of target gene located downstream of the lac operator on the plasmid. With the addition of IPTG, EGFP-R8 expression was significantly boosted, as indicated by the detection of the more intense bands at ~30 kDa in +IPTG samples.

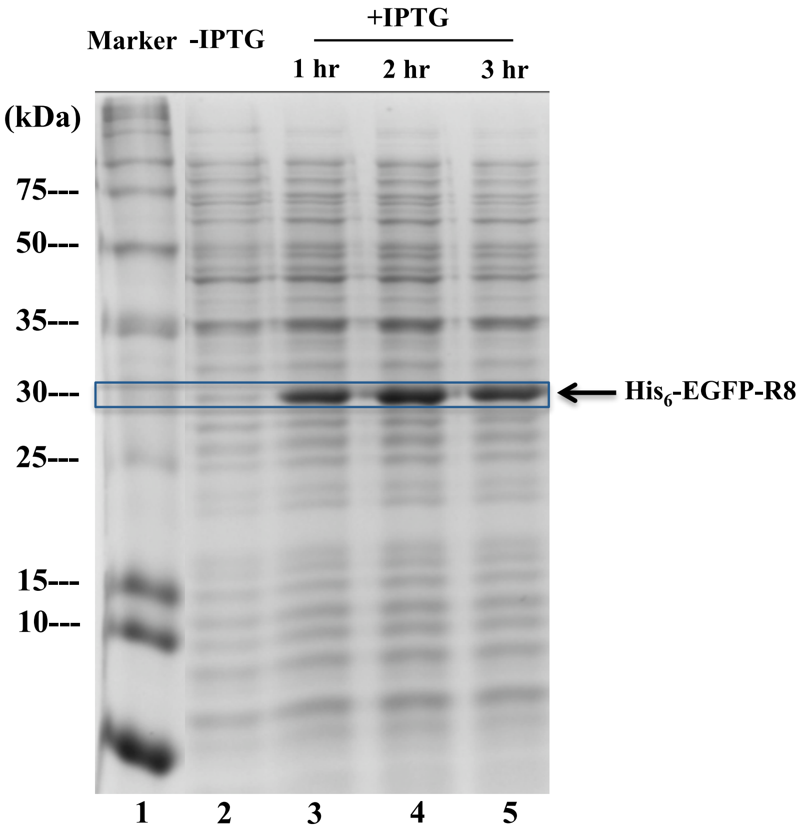

Figure 3.1 Expression of His$_6$-EGFP-R8 in BL21 (DE3) *E.coli* cell cultures before and after IPTG induction. Crude *E.coli* extracts (40 µg) from non-IPTG induced sample (-IPTG; lane 2) and samples induced with 0.5 mM IPTG for 1-3 hr (+IPTG; lane 3-5) were loaded onto a 12% SDS-PAGE gel and electrophoresis was performed at 100V for 90 min. Gel was then stained using Coomassie blue. His$_6$-EGFP-R8 is highlighted with a blue frame. Marker (lane 1): protein molecular weight markers.

EGFP-R8 was tagged with six consecutive histidine residues (6×His) at its C-terminal, and the purification of the target protein was performed on Ni-NTA resin. NTA (nitrilotriacetic acid) has four metal-chelating sites and can tightly bind metal ions. In the purification resin used here, four of the six ligand binding sites in the coordination sphere of the nickel ion are occupied by NTA, leaving two sites free to interact with two imidazole rings of the 6×His tag respectively. Therefore, Ni-NTA matrices have high selectivity and affinity for biomolecules that have been tagged with six histidine residues.

The purification of His$_6$-EGFP-R8 is composed of four main steps: cell lysis, protein binding, resin washing and protein elution. When passing the crude cell lysate slowly through the resin column, proteins lacking this His affinity tag will be eluted but the 6×His tagged EGFP-R8 will strongly bind to the nickel ions immobilised by the NTA groups on the resin. However, under native conditions there is still potential for binding background contaminants. To reduce nonspecific, low affinity binding of untagged proteins, low concentration of imidazole (20 mM) was added into crude cell lysate and column equilibration buffer. The imidazole ring is part of the histidine structure; therefore imidazole itself can also bind to the nickel ions and consequently shield the matrix in the first place and disrupt the binding of dispersed histidine residues in background proteins. Although Ni-NTA resin offers high binding capacity to the tag, a small fraction of the target protein was observed to pass through the column (lane 3 in Figure 3.2). This loss might be partly due to the presence of imidazole (20 mM) in cell lysate. Imidazole rings of different sources including imidazole itself compete for the binding sites, which may interfere with the binding of the 6×His tag to column.

By adding imidazole in the washing buffer at 20 mM, a large number of unrelated endogenous proteins that interacted with the Ni-NTA groups were eluted and appeared in the washes (lane 4-7 in Figure 3.2). However, at the same time, the interaction of the target protein with the Ni-NTA matrix also seems to be disturbed by washing steps, which could be reflected by appearance of the weak bands around 30 kDa in lane 4-7 (Figure 3.2).

Imidazole of a much higher concentration (250 mM) was utilized to elute the his-tagged protein from the matrix. Apart from His$_6$-EGFP-R8, a number of other proteins especially the one(s) at ≤10 kDa, were observed in the final preparation (lane 8 in Figure 3.2). To remove imidazole in the purified protein preparation, dialysis was performed using a 20 kDa MWCO (molecular weight cut off) membrane cassette. Most of the contaminating proteins including the ones under 10 kDa were still remained in the purified protein sample (lane 9 in Figure 3.2). It should be noted that truncated products of the original full-length fusion protein are common contaminants as they may have His tag attached to them. The source of these contaminants could be premature translation termination or protein degradation during protein expression or purification steps. On the other hand, proteins that are linked to or non-specifically associate with the tagged protein can also appear as unwanted contaminants in the final product. R8 is known to bind non-specifically to proteins such as BSA (MW=66.5 kDa) (Kosuge et al., 2008).

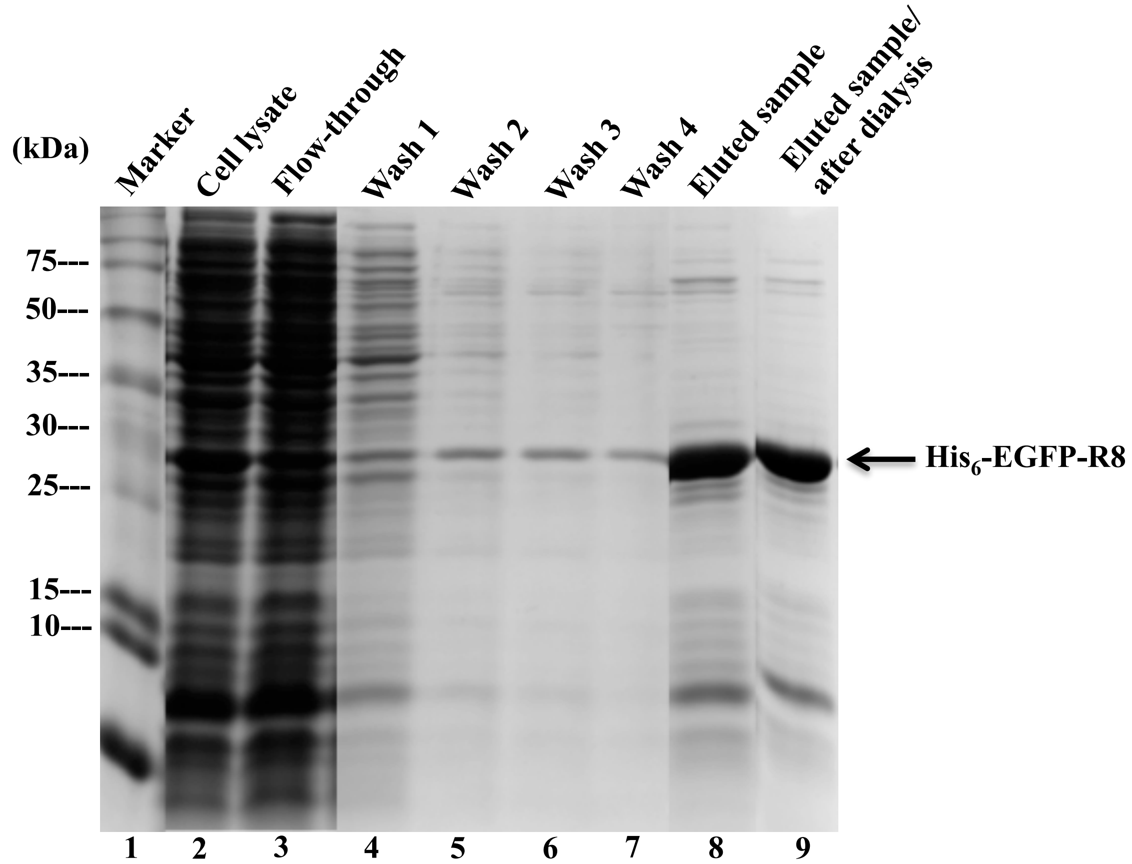

Figure 3.2 Purification of His$_6$-EGFP-R8 from BL21 (DE3) *E.coli* lysate using Ni-NTA resin. All the protein samples from crude cell lysate (lane 2), flow-through (lane 3), four washes (lane 4-7) and purified products before and after dialysis (lane 8 or 9) were loaded onto a 12% SDS-PAGE gel and electrophoresis was performed at 100V for 90 min. Gel was then stained using Coomassie blue. The band of His$_6$-EGFP-R8 is pointed out with a black arrow. Marker (lane 1): protein molecular weight markers. For experiments more than one lane were run for each protein sample and shown are specific lanes from these merged together omitting a number of duplicate lanes. The original gel is presented as Appendix 1.

Though a high purity product was obtained it was decided to further optimise the protocol in an attempt to remove some of these contaminants. Optimisation was based on using the product obtained from the first large (2L *E.coli* culture) preparation and after dialysis subjecting it to "repurification". Optimisation was performed on the basis of three different strategies.

Strategy 1: The concentration of NaCl in the crude cell lysate, column equilibration buffer and washing solutions was increased from 20 mM to 400 mM (recommended by Qiagen on www.qiagen.com). The higher ionic strength has been shown to prevent nonspecific ionic interactions between proteins and the Ni-NTA resin during binding and washing steps. Another benefit using NaCl of higher concentration is to reduce hydrophobic interactions between the target protein and the other background contaminants. Additionally, the concentration of imidazole in washing solutions was set as a gradient (20-50 mM) to gradually disturb the binding of dispersed histidine residues in non-tagged background proteins.

Strategy 2: The pH in washing buffers was lowered to 6.3 to disturb the interaction between histidine residues of endogenous proteins and the Ni-NTA matrix. Here the imidazole concentration in washing buffers was also prepared as a gradient of 20-50 mM, but the NaCl concentration in all the working buffers was kept as 20 mM as described in the original protocol.

Strategy 3: Heparin was utilized here to shield the R8 tail. Heparin is highly negative and will interact with cationic R8 thus reducing its tendency to bind to negative charges on other background proteins. Here 1 mg/ml heparin dissolved in dH_2O was added to the protein sample prior to column loading and the column equilibration buffer respectively. Imidazole (20-50 mM) was also present in the washing buffers used in this heparin–based strategy.

Increasing the concentration of NaCl (Strategy 1; Figure 3.3) in the purification process (except for the elution buffer) improved the purity of the sample especially with respects to the band at ~5 kDa. This was observed on both Coomassie blue (Figure 3.3A) and Silver stained gels (Figure 3.3B) that were included in the experimental set up as a more sensitive method to detect proteins on gels. However, NaCl of increased concentration caused the loss of the target protein during washing steps (shown in lane 4-7 of Figure 3.3). This protein loss became more striking when the imidazole concentration reached 50 mM (lane 7 in Figure 3.3). Lowering the pH (Strategy 2; Figure 3.4) was also an effective method to gain purity of the final product. The addition of heparin (Strategy 3; Figure 3.5) into the column equilibration buffer and the protein sample before passing through the Ni-NTA resin also resulted in significant loss of His_6-EGFP-R8 into the elute (lane 4-7 in Figure 3.5A and B). Moreover, low molecular weight proteins were still retained on the column and only eluted upon high imidazole elution.

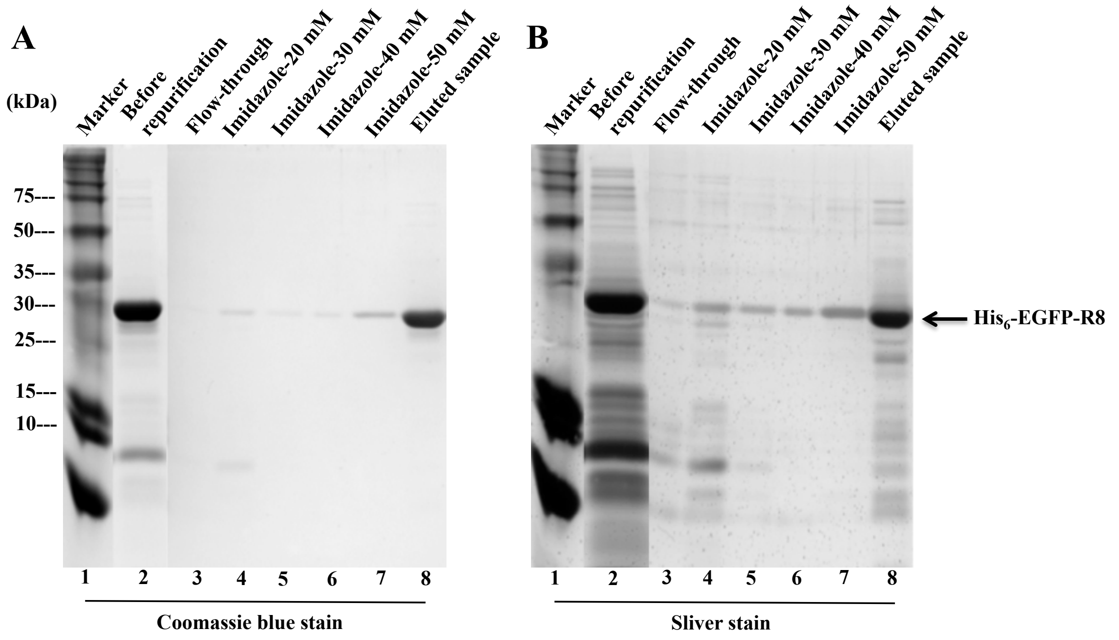

Figure 3.3 Strategy 1. Optimisation of the purification of His_6-EGFP-R8 by increasing NaCl concentration. Previously prepared EGFP-R8 (1.0 ml of 2.5 mg/ml) was applied to an equilibrated Ni-NTA resin column, followed by four washes (1 ml washing buffer for each) containing 20-50 mM imidazole respectively and then elution with 1 ml elution buffer. Sample (10 µl) from each fraction was loaded on to 12% SDS-PAGE gel. Electrophoresis was performed at 100V for 90 min. Proteins were visualised initially by Coomassie blue staining (A) and further by Silver staining (B). Protein bands corresponding to His_6-EGFP-R8 are highlighted with black arrow.

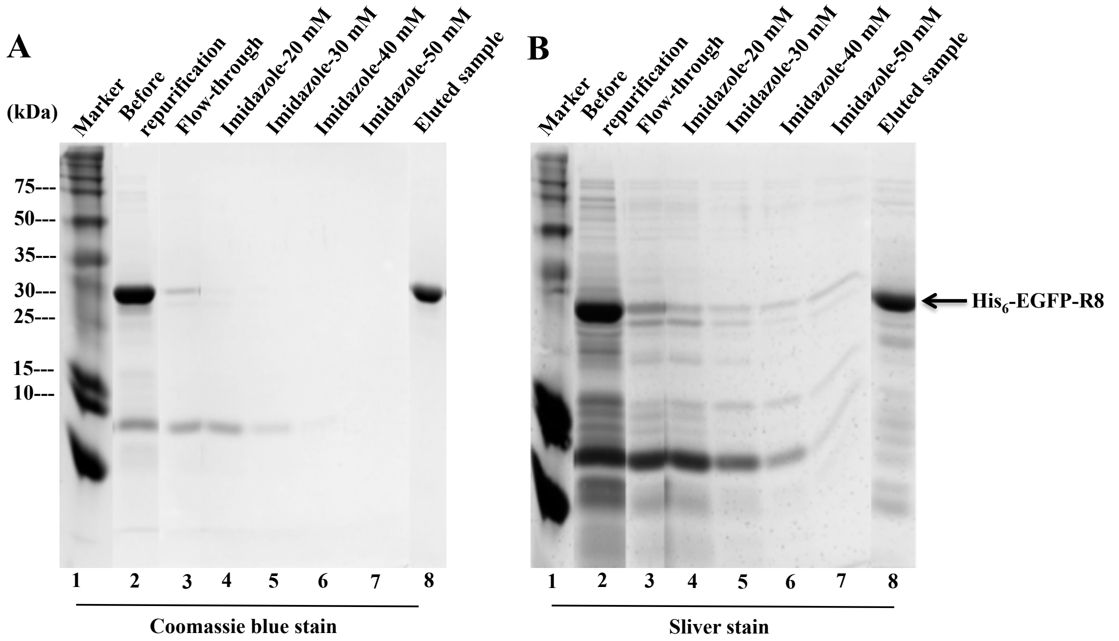

Figure 3.4 Strategy 2. Optimisation of the purification of His_6-EGFP-R8 by lowering pH. Previously prepared EGFP-R8 (1.0 ml of 2.5 mg/ml) was applied to an equilibrated Ni-NTA resin column, followed by four washes (1 ml washing buffer for each) containing 20-50 mM imidazole respectively and then elution with 1 ml elution buffer. Sample (10 µl) from each fraction was loaded on to 12% SDS-PAGE gel. Electrophoresis was performed at 100V for 90 min. Proteins were visualised initially by Coomassie blue staining (A) and further by Silver staining (B). Protein bands corresponding to His_6-EGFP-R8 are highlighted with black arrow.

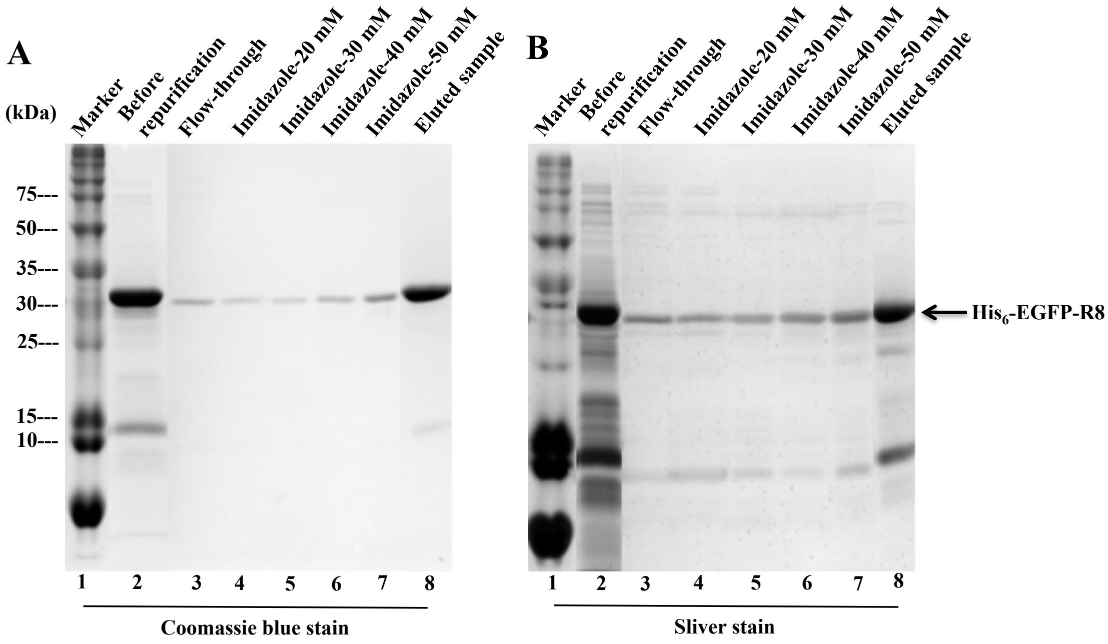

Figure 3.5 Strategy 3. Optimisation of the purification of His$_6$-EGFP-R8 by adding heparin. Previously prepared EGFP-R8 (1.0 ml of 2.5 mg/ml) was applied to an equilibrated Ni-NTA resin column, followed by four washes (1 ml washing buffer for each) containing 20-50 mM imidazole respectively and then elution with 1 ml elution buffer. Sample (10 µl) from each fraction was loaded on to 12% SDS-PAGE gel. Electrophoresis was performed at 100V for 90 min. Proteins were visualised initially by Coomassie blue staining (A) and further by Silver staining (B). Protein bands corresponding to His$_6$-EGFP-R8 are highlighted with black arrow.

For all further protein purification, low pH (6.3) and imidazole gradients were employed. Additionally NaCl concentration of the column equilibration buffer and the protein sample to be purified was also increased to 400 mM, in order to prevent hydrophobic association between the target protein and the other unrelated background proteins. Figure 3.6 shows a representative gel using this final amended protocol and here the final eluate (lane 8) was also dialysed against phenol red-free D-MEM through a 20 kDa MWCO cassette. This then allowed the protein sample to be directly loaded on to HeLa and A431 cells for endocytosis studies. Analysis of this gel using the BioRad chemidoc system showed a purity of >99% for the main protein band from Coomassie blue stained gel. The purified protein following D-MEM dialysis was aliquoted (20 µl each) and snap frozen in liquid nitrogen and stored at -80°C. With this procedure a 5 L *E.coli* preparation resulted in obtaining ~21 ml of a 50 µM solution of

His$_6$-EGFP-R8. This same procedure was also used to purify protein His$_6$-EGFP lacking the R8, and a preparation of ~98% purity was obtained (Figure 3.7 for final product).

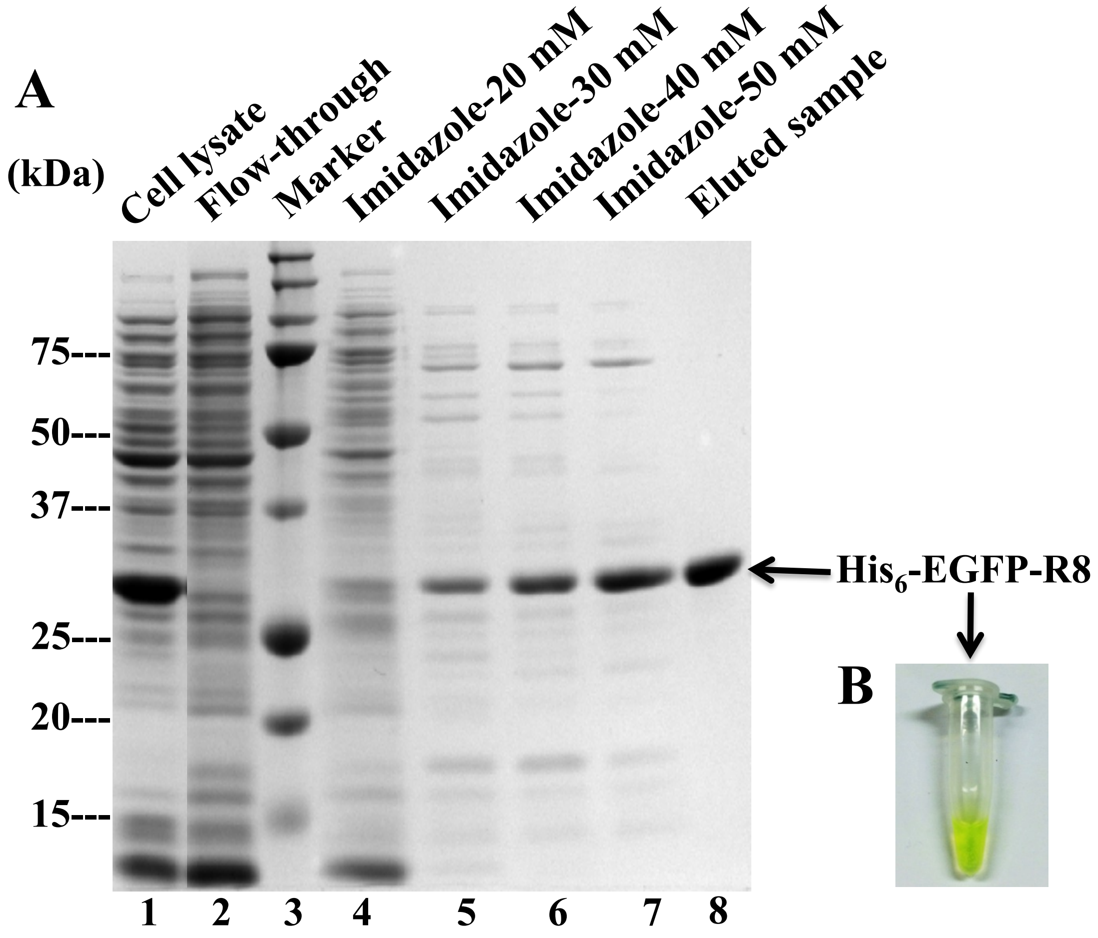

Figure 3.6 Optimised protocol for His$_6$-EGFP-R8 purification. Optimisation was performed on the basis of three different strategies that were higher NaCl concentration, stringent lower pH and imidazole gradients. Crude cell lysate (40 µg; lane 1) obtained from a 5 L *E.coli* preparation was applied to an equilibrated Ni-NTA resin column, followed by four washes (25 ml washing buffer for each) containing 20-50 mM imidazole respectively and then elution with buffer of 250 mM imidazole. Sample (20 µl) from each wash (lane 4-7) and 2 µg of the eluted His$_6$-EGFP-R8 protein sample (lane 8) were loaded on to 12% SDS-PAGE gel. Electrophoresis was performed at 100V for 90 min. Proteins were visualised by Coomassie blue staining (A). Marker (lane 3): protein molecular weight markers. Protein bands corresponding to His$_6$-EGFP-R8 are highlighted with black arrow. Insert (B) shows the final purified product.

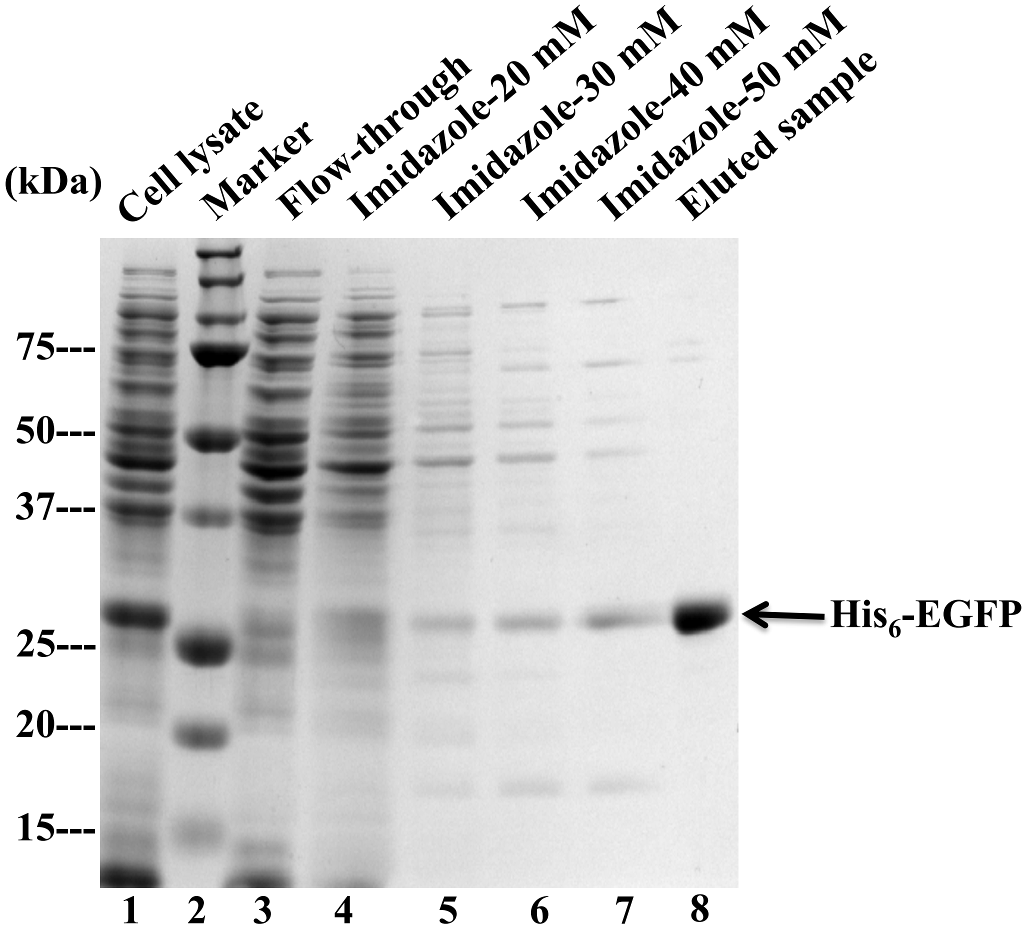

Figure 3.7 His$_6$-EGFP purification. The same optimised purification protocol including higher NaCl concentration, stringent lower pH and imidazole gradients was used to purify His$_6$-EGFP. Crude cell lysate (40 µg; lane 1) obtained from a 1.5 L *E.coli* preparation was applied to an equilibrated Ni-NTA resin column, followed by four washes (10 ml washing buffer for each) containing 20-50 mM imidazole respectively and then elution with buffer of 250 mM imidazole. Sample (20 µl) from each wash (lane 4-7) and 2 µg of the eluted His$_6$-EGFP protein sample (lane 8) were loaded on to 12% SDS-PAGE gel. Electrophoresis was performed at 100V for 90 min. Proteins were visualised by Coomassie blue staining (A). Marker (lane 2): protein molecular weight markers. Protein bands corresponding to His$_6$-EGFP are highlighted with black arrow.

3.2.2 Studying the role of actin in the uptake of R8-Alexa 488 and EGFP-R8 in HeLa and A431 cells

Due to quite extensive differences in endocytosis of dextran and to a lesser extent of CPPs like R8- and Tat-Alexa 488 between HeLa and A431 cells (Al Soraj et al., 2012), it was decided to focus on these two cell lines for analysing the cellular uptake of both EGFP-R8, EGFP alone and also R8-Alexa 488 as model for a CPP conjugate with a low molecular weight (720 Da) cargo. This fluorescent peptide was prepared by Dr Edward

Sayers in the laboratory (See Section 2.3 for more details). In the absence of R8, work from our laboratory has shown that the fluorophore alone (as Alexa488-Cysteine) exhibits no cell penetrating capacity (Fretz et al., 2007). The cells were plated into 35 mm MatTek dishes and cultured overnight before washing in PBS and adding 100 µl serum-free D-MEM containing 2 µM of either R8 conjugates (R8-Alexa 488 or EGFP-R8) or EGFP alone. It should be noted that cell confluency has been shown to be important in endocytic uptake of CPPs in epithelial MDCK cells (Foerg et al., 2007). In that study, higher cell confluency led to reduced uptake and this was attributed to down-regulation of endocytosis by Rho GTPases. The cells were then incubated under tissue culture conditions (37°C/5% CO_2) for 1 hr before performing live cell confocal microscopy. In HeLa cells, fluorescent vesicular structures were clearly observed scattered in the cytoplasm for both R8 conjugates but not for EGFP alone (Figure 3.8). This conformed the vital role of R8 in mediating cellular uptake. Similarly, EGFP alone did not show the capacity to enter A431 cells but again the R8 conjugates were internalised (Figure 3.9). These representative images were collected at the same day using identical microscopy setting and A431 cells appeared to be more efficient at internalising both R8 cargos.

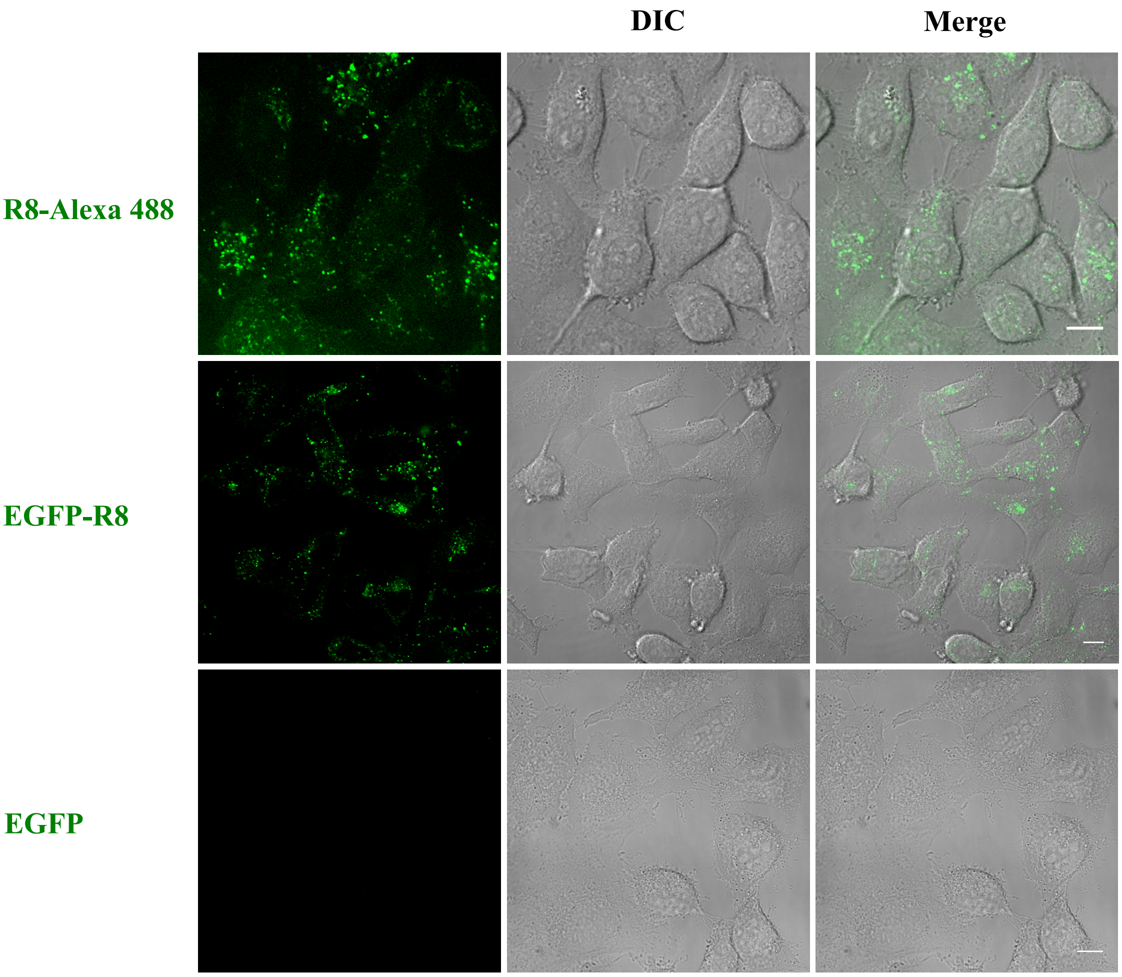

Figure 3.8 Verification of the importance of R8 in cellular uptake in HeLa cells. Cells were washed and incubated with 2 µM of either R8 conjugates (R8-Alexa 488 or EGFP-R8) or EGFP alone in serum free D-MEM for 1 hr, and analysed by confocal microscopy. Images were taken as single sections and shown with green fluorescence, DIC or merge. Scale bars 10 µm.

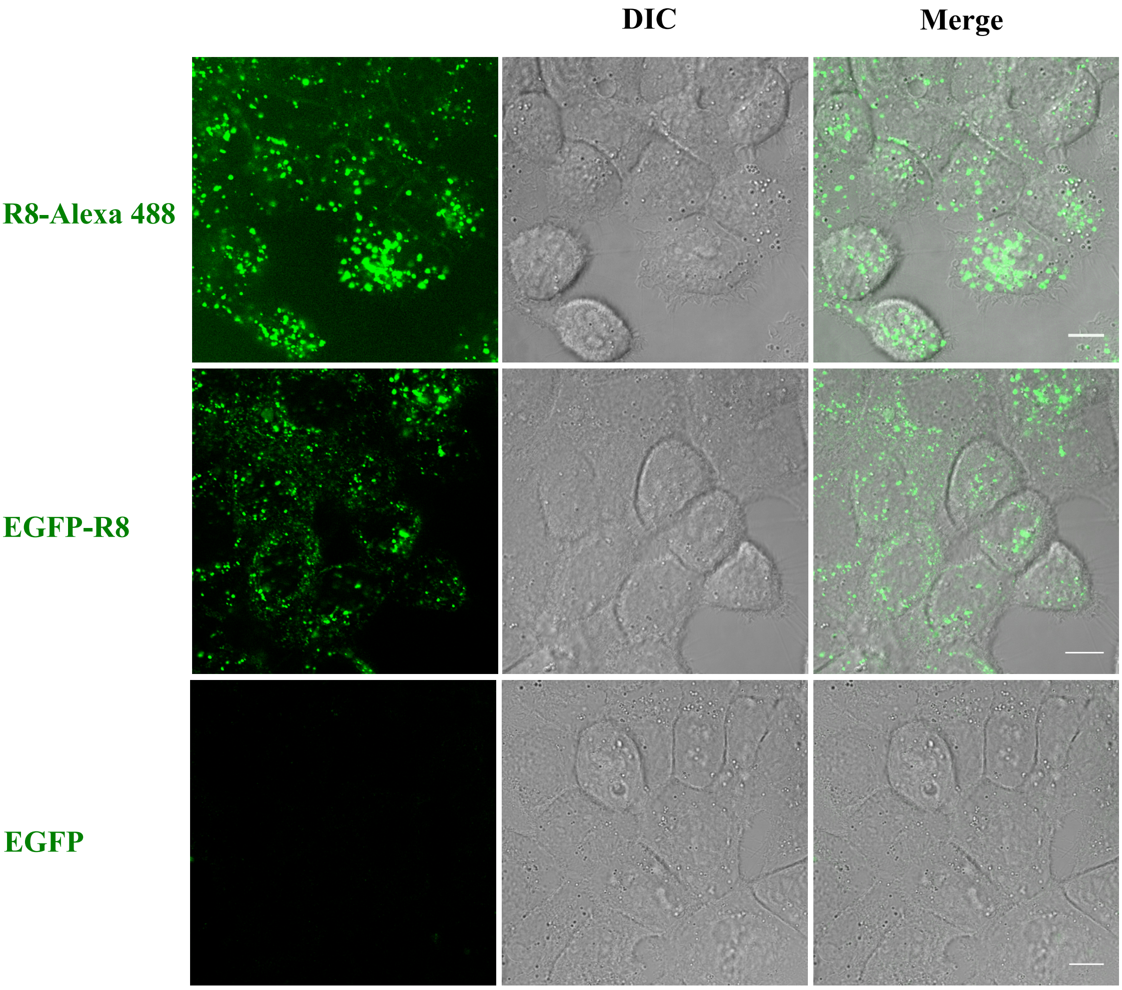

Figure 3.9 Verification of the importance of R8 in cellular uptake in A431 cells. Cells were washed and incubated with 2 µM of either R8 conjugates (R8-Alexa 488 or EGFP-R8) or EGFP alone in serum free D-MEM for 1 hr, and analysed by confocal microscopy. Images were taken as single sections and shown with green fluorescence, DIC or merge. Scale bars 10 µm.

To examine the effect of Cyt D on the cellular uptake of R8-Alexa 488 and EGFP-R8 in the two chosen cell lines, cells were washed with PBS and pre-treated with or without 10 µM Cyt D for 15 min. Then 2 µM of R8-Alexa 488 or EGFP-R8 was loaded onto the cells in presence or absence of 10 µM Cyt D for 1 hr. The cells were then washed three times with 0.5 mg/ml heparin in PBS to reduce the plasma membrane-associated fluorescence (Lundberg et al., 2003) and analysed by confocal microscopy.

As shown by DIC microscopy, 10 µM Cyt D had dramatic morphological effects on both HeLa and A431 cells (Figure 3.10-3.13). There was also clear evidence of membrane blebbing following Cyt D treatment. This drug strongly inhibited the internalisation of R8-Alexa 488 in HeLa cells (Figure 3.10) to the point that only very low cell associated fluorescence was observed. There was no clear evidence of Cyt D mediated inhibition of EGFP-R8 uptake but treatment with this drug caused a scattering of punctate fluorescence compared to untreated cells that displayed strong perinuclear labelling (Figure 3.11).

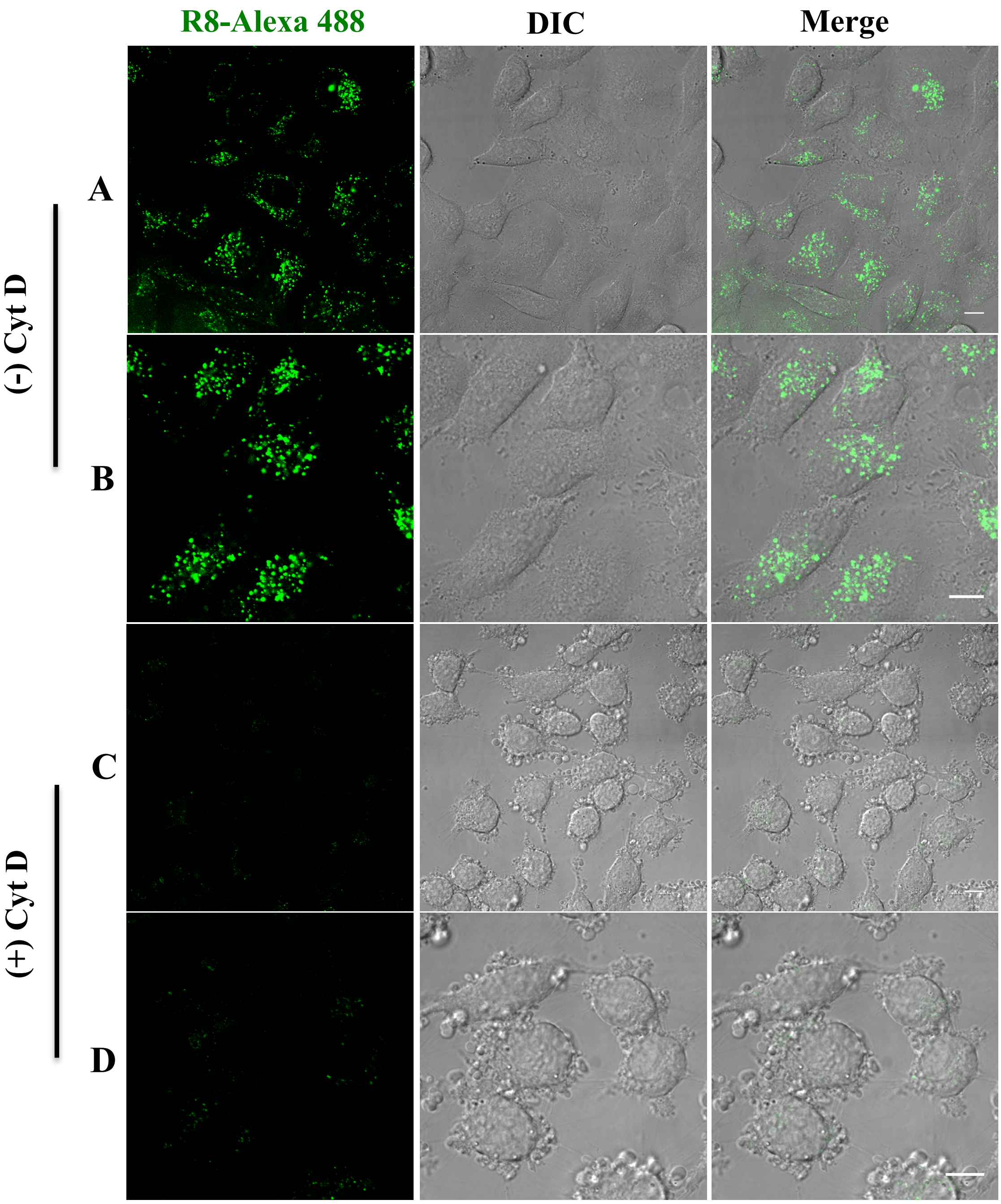

Figure 3.10 Cyt D effects on the cellular uptake of R8-Alexa 488 in HeLa cells. Cells were incubated with 2 µM R8-Alexa 488 in the absence (A, B) or presence (C, D) of 10 µM Cyt D for 1 hr before heparin washes and analysis on confocal microscopy. Shown are single projection images of fluorescence only (R8-Alexa 488), DIC and merges of fluorescence and DIC of the same cells. B and D represent zoomed images from different fields of view of A and C respectively in order to provide more information on the heterogeneity of fluorescence labelling. Scale bars 10 µm.

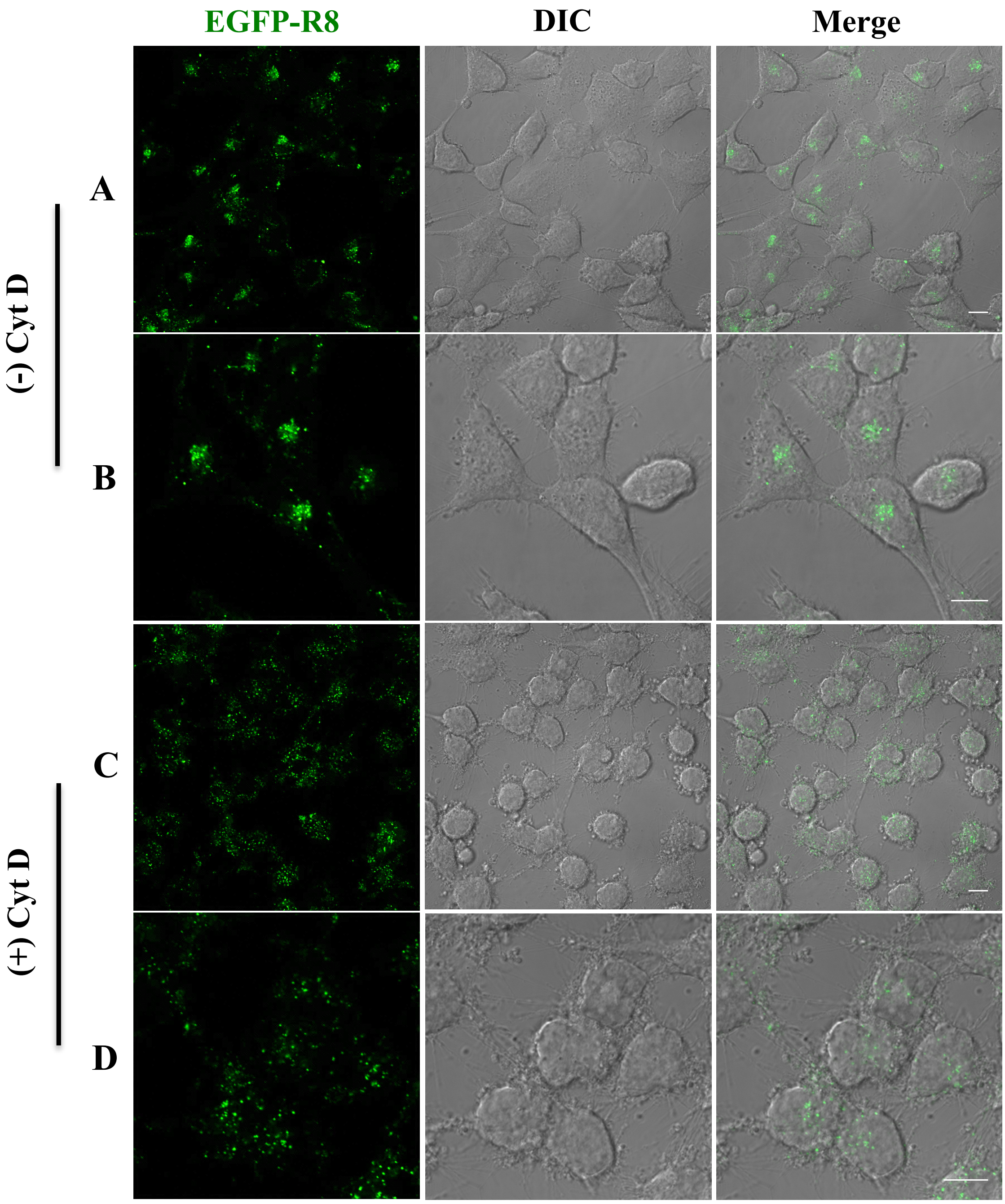

Figure 3.11 Cyt D effects on the cellular uptake of EGFP-R8 in HeLa cells. Cells were incubated with 2 µM EGFP-R8 in the absence (A, B) or presence (C, D) of 10 µM Cyt D for 1 hr and washed thoroughly using heparin. Cell associated fluorescence was analysed on confocal microscopy. Shown are single projection images of fluorescence only (EGFP-R8), DIC and merges of fluorescence and DIC of the same cells. B and D represent zoomed images from different fields of view of A and C respectively in order to provide more information on the heterogeneity of fluorescence labelling. Scale bars 10 µm.

In contrast to HeLa cells, the Cyt D treatment did not evidently reduce the internalisation of R8-Alexa 488 by A431 cells (Figure 3.12). But the drug indeed altered the distribution pattern of the cargo significantly. The green vesicular structures observed in normal untreated A431 cells were relatively evenly scattered throughout the cytoplasm (Figure 3.12A and B), whereas most of the punctate structures found in the drug-treated A431 cells were largely clustered (Figure 3.12C and D). The insensitivity of R8 uptake to Cyt D treatment may imply that R8 has at least one alternative endocytic pathway to utilize to enter into A431 cells, when its routine actin-dependent pathway is blocked. Therefore, by following different uptake route(s), the intracellular location or destination of the delivered cargo may also be changed. Surprisingly, the same experiment but adding EGFP-R8 onto A431 cells revealed that Cyt D dramatically enhanced the internalisation of this cargo into vesicular structures and affected their distribution throughout the cell (Figure 3.13) as previously had been observed in HeLa cells. Instead of scattered in cytoplasm (Figure 3.13A and B), a large number of the observed green fluorescent punctae were aggregated and enriched in small “islands” or U-like structures mainly surrounding the nucleus (Figure 3.13C and D). A major difference in the behaviour of these two cell lines to actin disruption was also previously noted by us for uptake of the fluid phase endocytic probe dextran (Al Soraj et al., 2012). The actin cytoskeleton in A431 cells interestingly appears to act as a hindrance to the cellular uptake of protein attached R8, which challenges our previous thoughts about the positive role of actin in endocytic pathways.

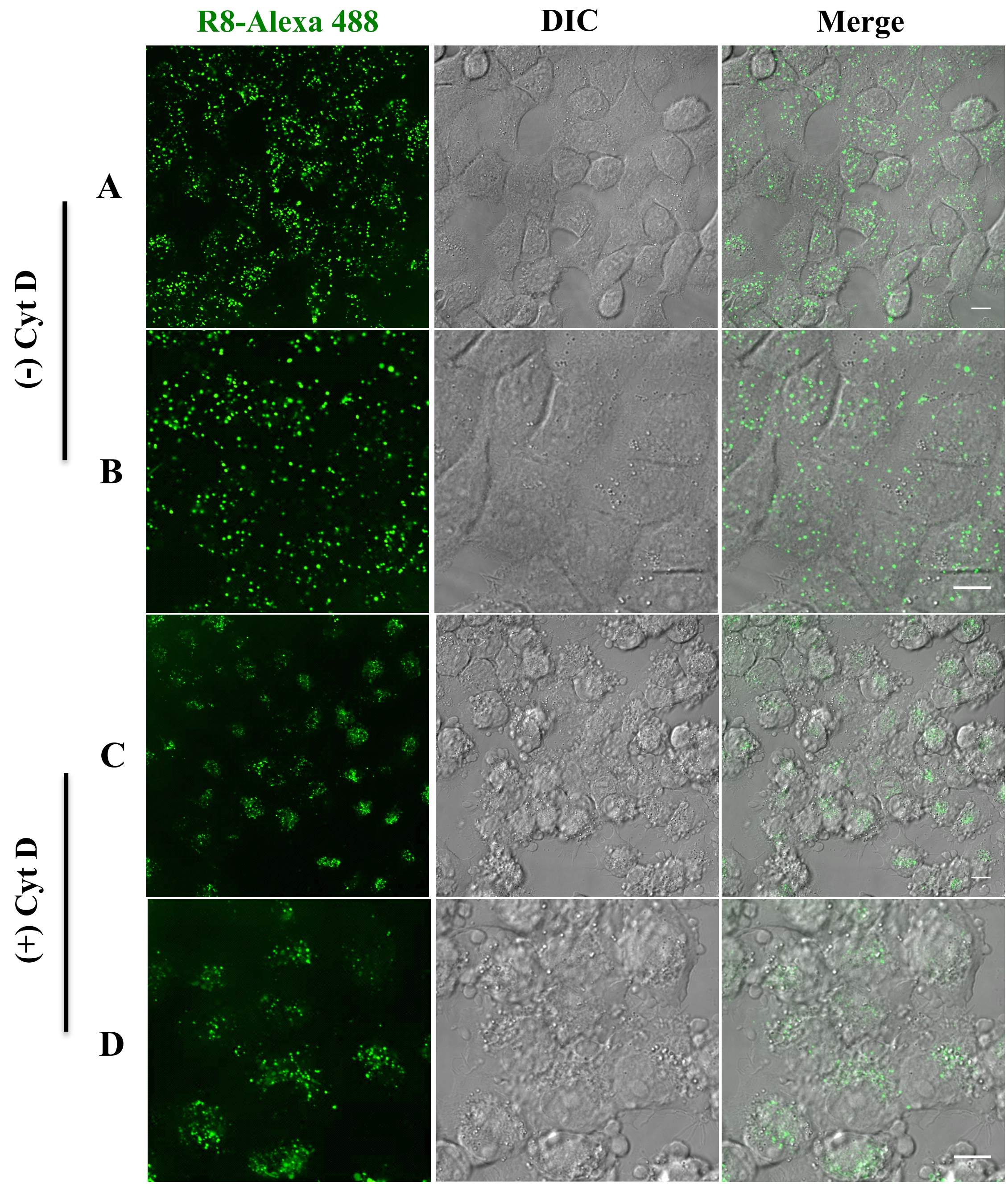

Figure 3.12 Cyt D effects on the cellular uptake of R8-Alexa 488 in A431 cells. Cells were incubated with 2 µM R8-Alexa 488 in the absence (A, B) or presence (C, D) of 10 µM Cyt D for 1 hr before heparin washes and analysis on confocal microscopy. Shown are single projection images of fluorescence only (R8-Alexa 488), DIC and merges of fluorescence and DIC of the same cells. B and D represent zoomed images from different fields of view of A and C respectively. Scale bars 10 µm.

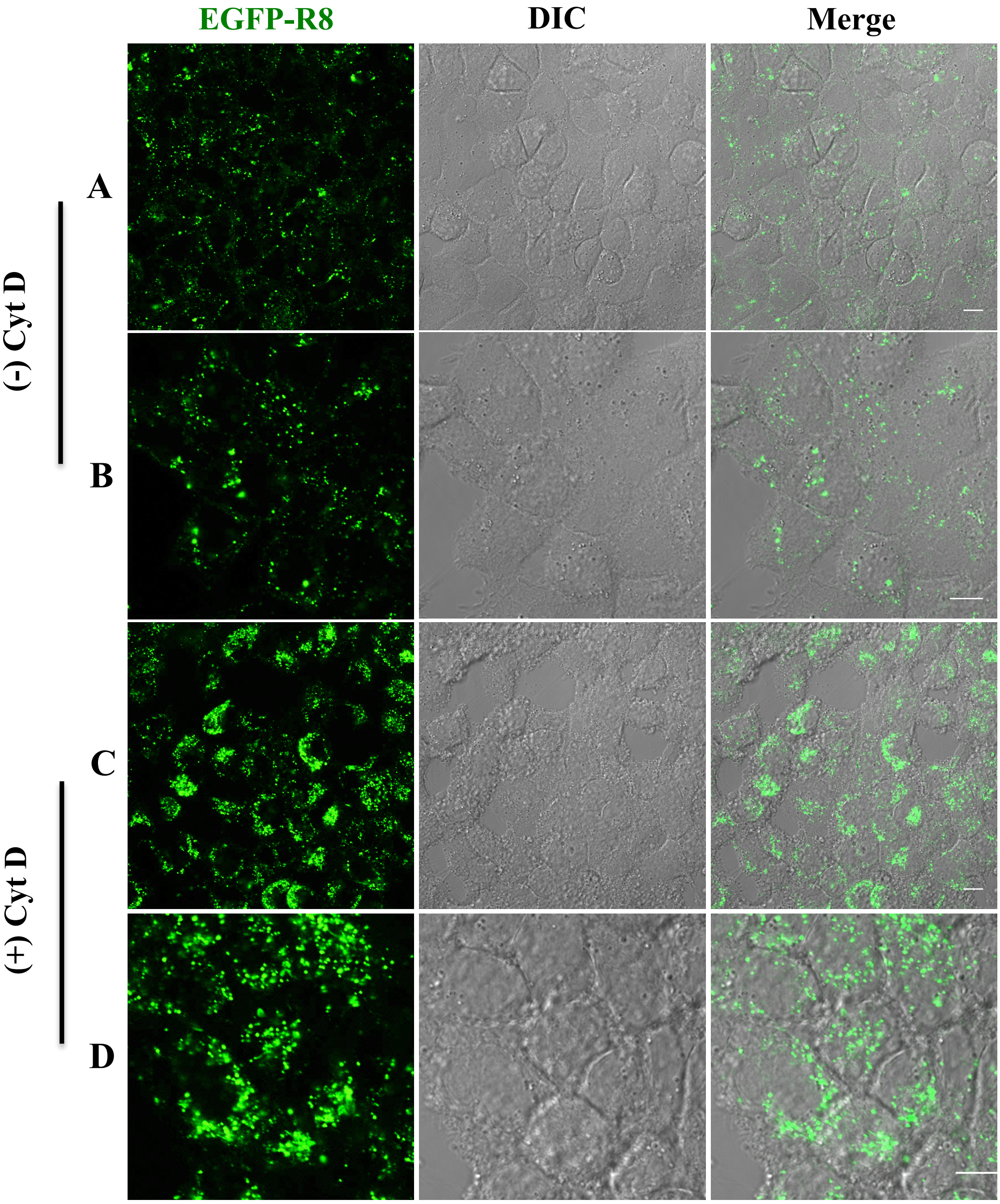

Figure 3.13 Cyt D effects on the cellular uptake of EGFP-R8 in A431 cells. Cells were incubated with 2 µM EGFP-R8 in the absence (A, B) or presence (C, D) of 10 µM Cyt D for 1 hr and washed thoroughly using heparin. Cell associated fluorescence was analysed using confocal microscopy. Shown are single projection images of fluorescence only (EGFP-R8), DIC and merges of fluorescence and DIC of the same cells. B and D represent zoomed images from different fields of view of A and C respectively. Scale bars 10 µm.

3.2.3 Studying the role of actin in the uptake of transferrin and dextran in HeLa and A431 cells

To further explore the role of actin in endocytosis in these two cell lines the effects of Cyt D was similarly assessed on the clathrin-mediated endocytosis marker transferrin (transferrin-Alexa 647) and the fluid phase/macropinocytosis probe 10 kDa dextran (dextran10-Alexa 647). HeLa or A431 cells were pre-incubated in the absence or presence of 10 μM Cyt D for 15 min, and then further incubated with 5 μg/ml transferrin-Alexa 647 (TF-647) for 30 min or 0.1 mg/ml dextran10-Alexa 647 (Dex-647) for 1 hr in the absence or presence of 10 μM Cyt D. Cells were then washed with PBS and the cell-associated fluorescence was analysed by confocal microscopy as previously described.

As shown in Figure 3.14, Cyt D treatment did not seem to result in noticeable inhibition or enhancement of TF-647 internalisation in either A431 (Figure 3.14A and B) or HeLa (Figure 3.14C and D) cells. In Cyt D treated HeLa cells, the transferrin appeared to be more prominent on the plasma membrane (Figure 3.14D).

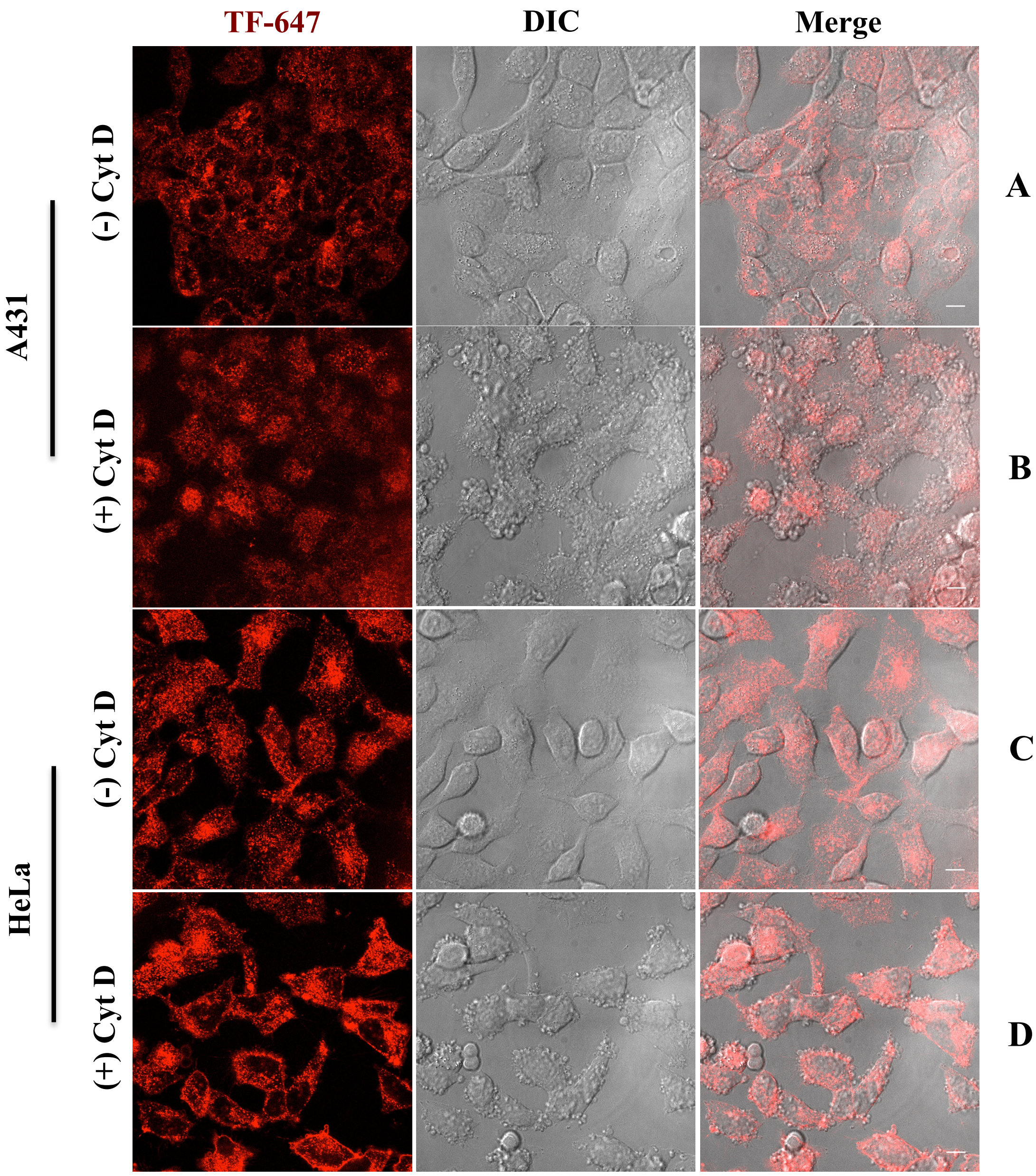

Figure 3.14 Cyt D effects on the internalisation of transferrin-Alexa 647 (TF-647) in A431 (A, B) and HeLa (C, D) cells. Control cells or cells pre-treated with Cyt D were incubated with 5 µg/ml TF-647 in the absence (A or C) or presence (B or D) of 10 µM Cyt D for 30 min and washed with PBS. Cell associated fluorescence was analysed using confocal microscopy. Shown are single section images of fluorescence only (TF-647), DIC and merges of fluorescence and DIC of the same cells. Scale bars 10 µm.

Our previous work demonstrated that whereas dextran uptake was inhibited in Cyt D treated HeLa cells it was increased in A431 cells treated with the same drug (Al Soraj et al., 2012). This was confirmed using flow cytometry and data in Figure 8F of the manuscript was generated as part of this thesis. Experimental details and results are shown in Appendix 2. In this thesis the same experiments were performed but confocal microscopy was used to visualise the fluorescence. Figure 3.15 and 3.16 clearly demonstrate the marked difference in Cyt D effects on dextran uptake between these two cell lines. In Hela cells (Figure 3.15) there was evidence of inhibition of uptake as previously described (Al Soraj et al., 2012) but in A431 cells a very large increase in fluorescence was noted and here again it was aggregated in the cells (Figure 3.16). The images here were taken as single sections inside the cells and these fluorescent structures were not clusters on the plasma membrane.

These results suggested that EGFP-R8 and dextran use the same endocytic route(s), especially macropinocytosis, for their uptake in A431 cells. Interfering with actin-dependent pathway(s) could stimulate the activity of other pathways leading to increased uptake levels.

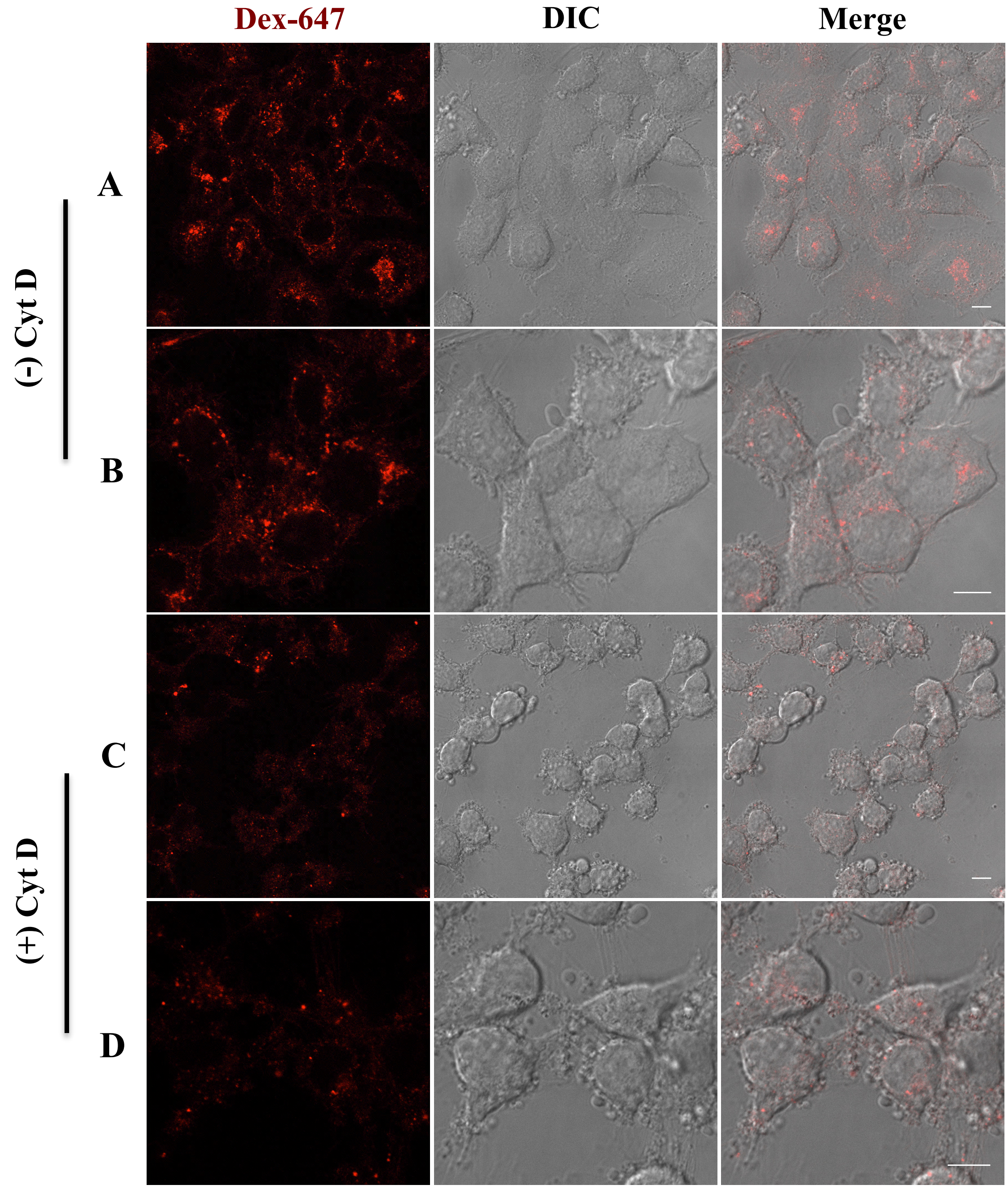

Figure 3.15 Cyt D effects on the internalisation of dextran10-Alexa 647 (Dex-647) in HeLa cells. Control cells or cells pre-treated with 10 µM Cyt D were further incubated with 0.1 mg/ml dextran10-Alexa 647 in the absence (A, B) or presence (C, D) of 10 µM Cyt D for 1 hr and washed with PBS. Cell associated fluorescence was analysed using confocal microscopy. Shown are single section images of fluorescence only (Dex-647), DIC and merges of fluorescence and DIC of the same cells. B and D represent zoomed images from different fields of view of A and C respectively. Scale bars 10 µm.

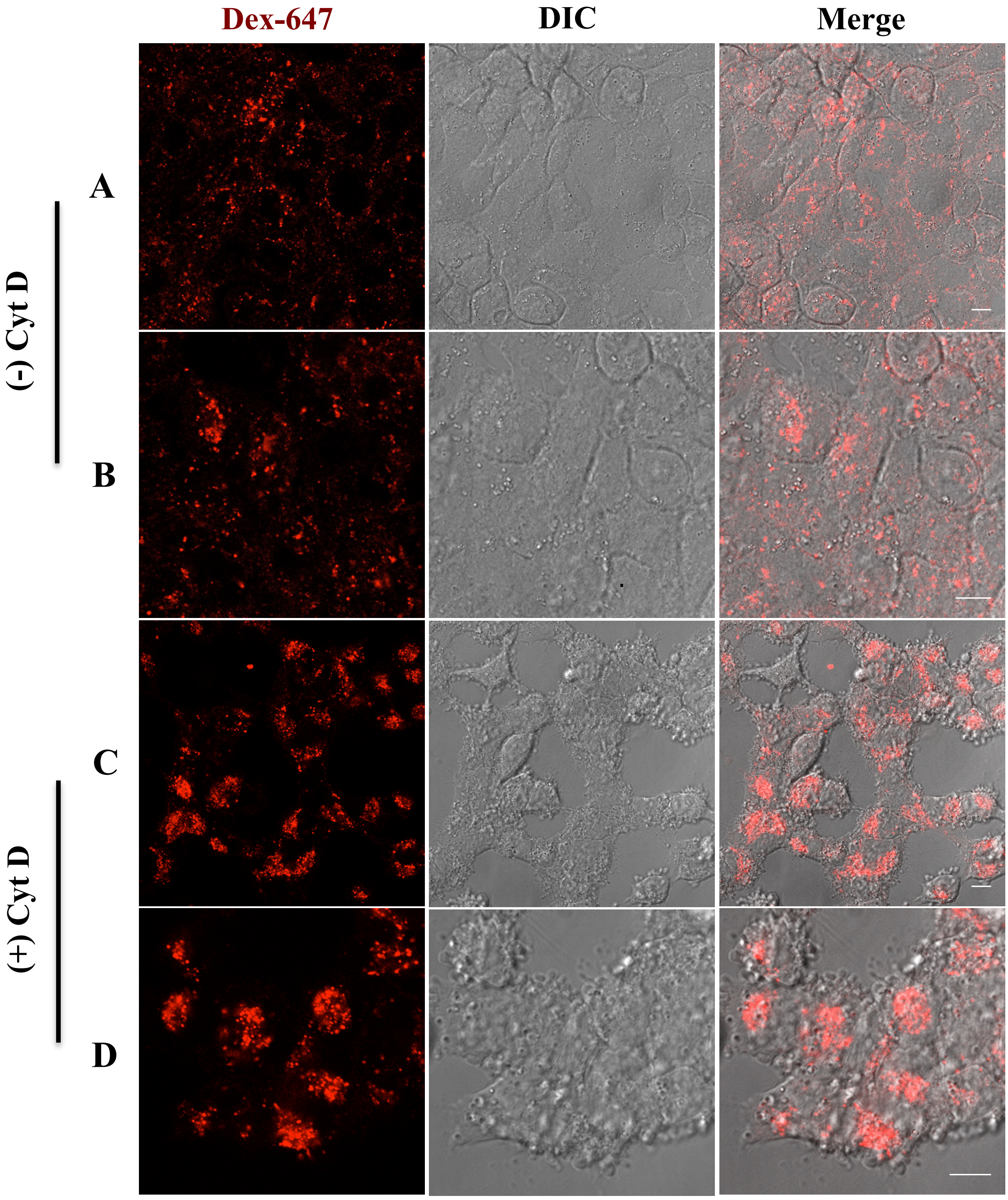

Figure 3.16 Cyt D effects on the internalisation of dextran10-Alexa 647 (Dex-647) in A431 cells. Control cells or cells pre-treated with 10 µM Cyt D were further incubated with 0.1 mg/ml dextran10-Alexa 647 in the absence (A, B) or presence (C, D) of 10 µM Cyt D for 1 hr and washed with PBS. Cell associated fluorescence was analysed using confocal microscopy. Shown are single section images of fluorescence only (Dex-647), DIC and merges of fluorescence and DIC of the same cells. B and D represent zoomed images from different fields of view of A and C respectively. Scale bars 10 µm.

3.2.4 Endosomal co-localisation of EGFP-R8 and dextran

The data presented above with Cyt D suggested that dextran and EGFP-R8 utilize the same endocytic pathway(s), to enter into A431 cells. Experiments were then performed to compare the subcellular distribution of these two molecules in the two cell lines. Initially co-localisation of dextran (10 kDa) labelled with fluorophores Alexa 488 and Alexa 647 respectively was examined in A431 cells only to provide a good model for co-localisation using this technique. Cells were co-incubated with 0.1 mg/ml dextran10-Alexa 488 (Dex-488) and dextran10-Alexa 647 (Dex-647) in medium containing or lacking 10 μM Cyt D for 1 hr, washed and then analysed as live cells by confocal microscopy. As expected, in control cells these two dextran probes were located in the same endocytic organelles, revealed as yellow structures somewhat concentrated in a perinuclear region (Figure 3.17A and B). The uptake of both probes was dramatically increased in Cyt D treated cells confirming that this effect is not due to any specific characteristic associated with Dex-647 (Figure 3.17C and D). Again in Cyt D-treated cells there was extensive co-localisation between the two probes in a perinuclear region.

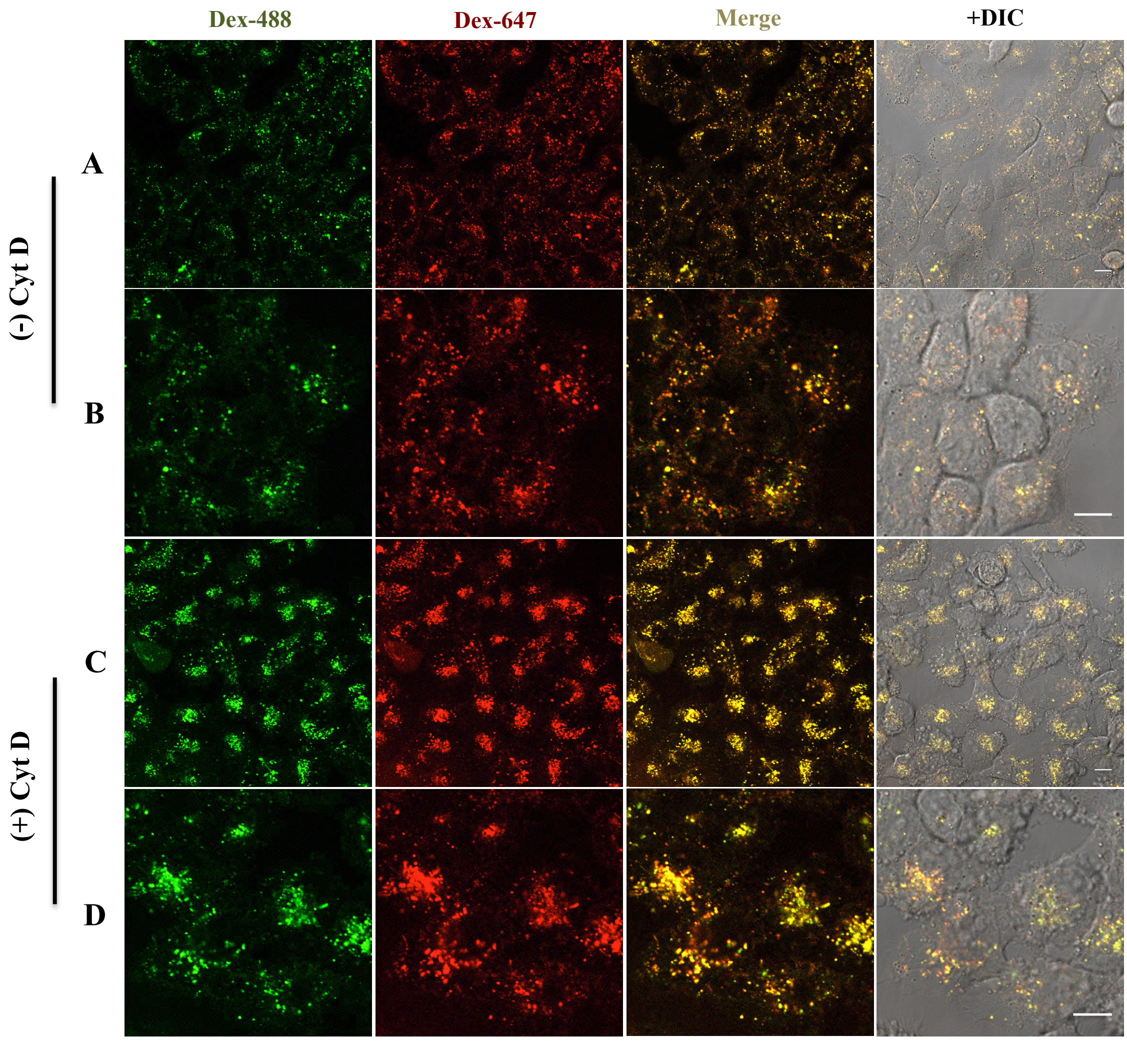

Figure 3.17 Endosomal co-localisation of dextran10-Alexa 647 (Dex-647) and -Alexa 488 (Dex-488) in A431 cells. Control cells or cells pre-treated with 10 µM Cyt D were incubated with 0.1 mg/ml Dex-647 and Dex-488 in the absence (A, B) or presence (C, D) of 10 µM Cyt D for 1 hr and washed with PBS. Cell associated fluorescence was analysed using confocal microscopy. Shown are single section images of fluorescence only (Dex-488 or Dex-647) and merges of fluorescence with or without DIC of the same cells. B and D represent zoomed images from different fields of view of A and C respectively. Scale bars 10 µm.

A431 or HeLa cells were then first incubated with Dex-647 for 2 hr (pulse) to label endosomes and lysosomes. Following this dextran pulse, the medium was replaced with fresh dextran-free medium and the cells were further incubated for a 4 hr chase period. At the end of chase period, the internalised dextran would empty from the early and late endosomes and accumulate in lysosomes (Al-Taei et al., 2006). EGFP-R8 was then added to these cells that were further incubated for 1 hr before confocal microscopy. In both A431 (Figure 3.18A and B) and HeLa (Figure 3.18C and D) cells, a low extent of co-localisation of the conjugates was observed. This suggested that in the 1 hr incubation very little EGFP-R8 had travelled to lysosomes or that any fraction that had reached the lysosomes had been degraded and was no longer fluorescent. The same experiment was then performed in cells incubated with 10 μM Cyt D after the chase period and immediately prior to the addition of EGFP-R8. As shown in Figure 3.19, Cyt D had no visible effects on the level of co-localisation of dextran and EGFP-R8 in either A431 (Figure 3.19A and B) or HeLa (Figure 3.19C and D) cells. This suggested but did not prove that Cyt D was not altering the intracellular traffic of EGFP-R8 in these cells to drive it into lysosomes.

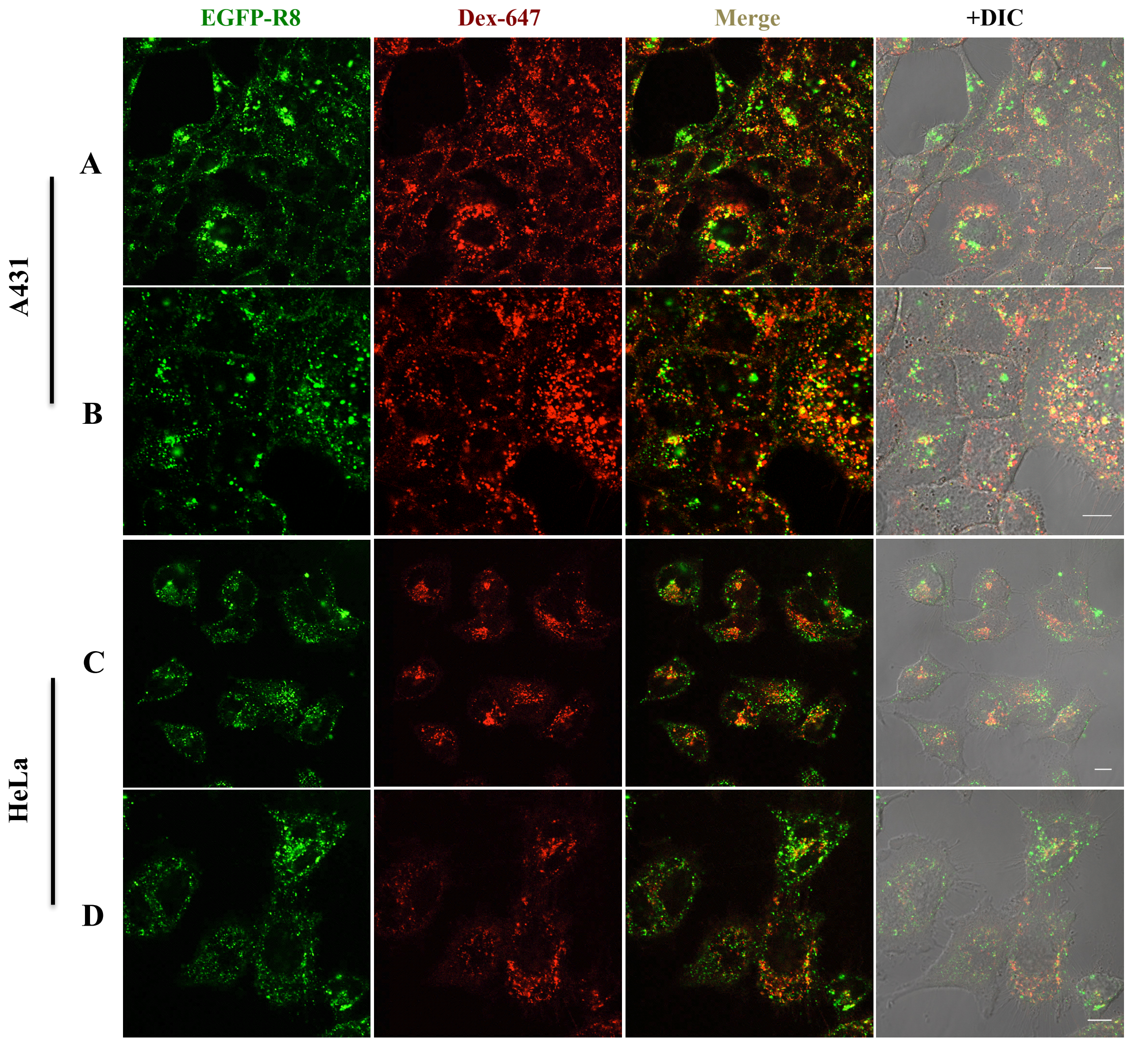

Figure 3.18 Endosomal co-localisation of EGFP-R8 and dextran10-Alexa 647 (Dex-647) in A431 or HeLa cells. Cells were incubated with 0.1 mg/ml Dex-647 for 2 hr followed by 4 hr chase in fresh growth medium. EGFP-R8 (2 μM) was then added to A431 (A, B) or HeLa (C, D) cells for 1 hr. Cell associated fluorescence was analysed using confocal microscopy. Shown are single section images of fluorescence only (EGFP-R8 or Dex-647) and merges of fluorescence with or without DIC of the same cells. B and D represent zoomed images from different fields of view of A and C respectively. Scale bars 10 μm.

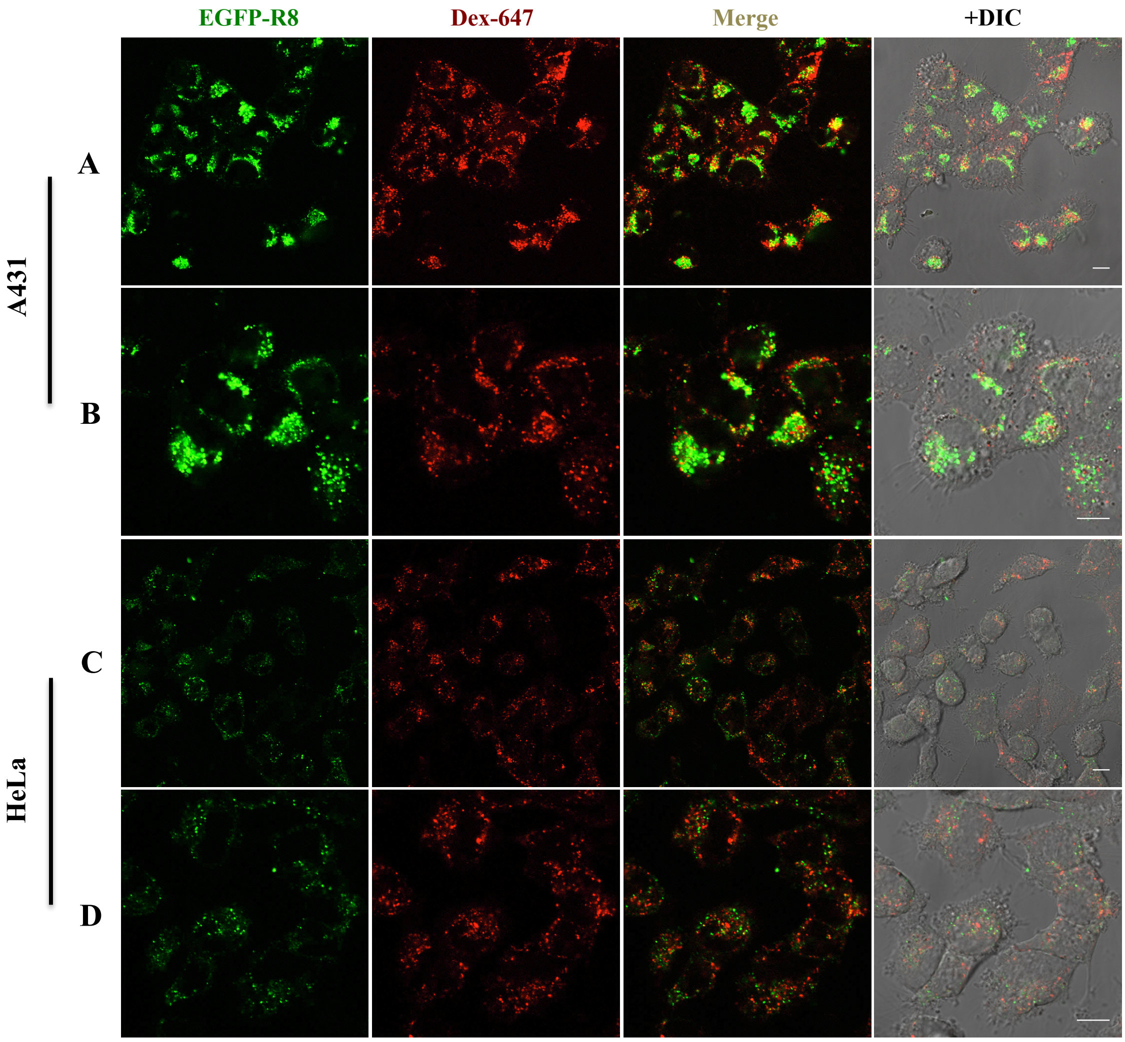

Figure 3.19 Endosomal co-localisation of EGFP-R8 and dextran10-Alexa 647 (Dex-647) in Cyt D treated A431 or HeLa cells. Cells were incubated with 0.1 mg/ml Dex-647 for 2 hr followed by a 4 hr chase in fresh growth medium. EGFP-R8 (2 µM) was then added to Cyt D-treated A431 (A, B) or HeLa (C, D) cells for 1 hr. Cell associated fluorescence was analysed using confocal microscopy. Shown are single section images of fluorescence only (EGFP-R8 or Dex-647) and merges of fluorescence with or without DIC of the same cells. B and D represent zoomed images from different fields of view of A and C respectively. Scale bars 10 µm.

Control or Cyt D-treated A431 or HeLa cells were then simultaneously incubated with Dex-647 and EGFP-R8 for 1 hr before confocal microscopy. Co-incubation of the probes in control cells showed some co-localisation in both A431 (Figure 3.20A and B) and HeLa cells (Figure 3.20C and D). There were in both cell types, however, clear examples of structures containing only one probe. In Cyt D treated A431 cells there was as expected an extensive increase in fluorescence and this time co-localisation in punctate structures and large clusters were more clearly evident (Figure 3.21A and B).

Very faint signal of both EGFP-R8 and dextran was observed in Cyt D treated HeLa cells due to the inhibitory effects of Cyt D on the uptake of these cargos in this cell line (Figure 3.21C and D), which is consistent with the data previously shown in section 3.2.3.

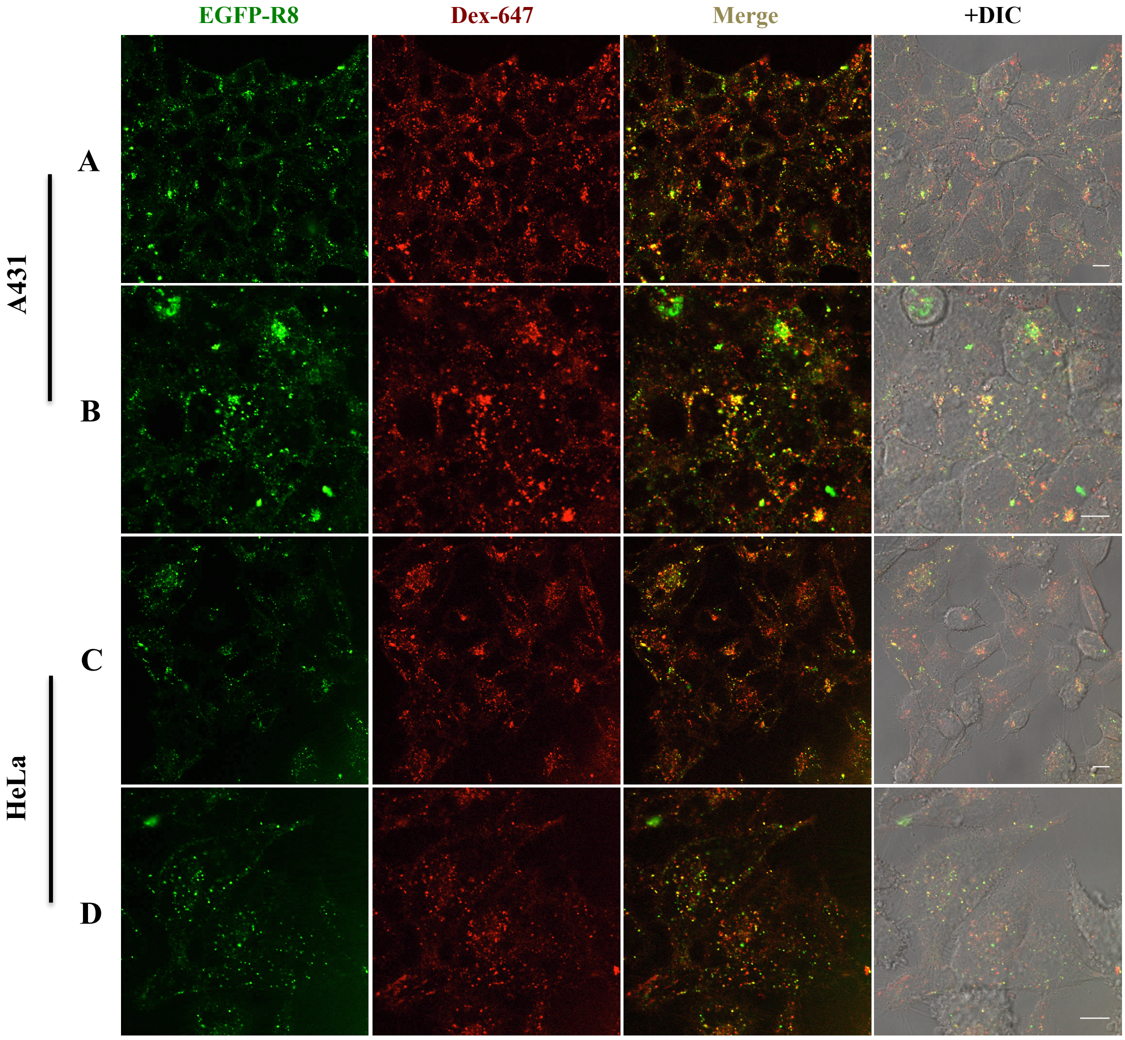

Figure 3.20 Endosomal co-localisation of EGFP-R8 and dextran10-Alexa 647 (Dex-647) in A431 or HeLa cells. A431 (A, B) or HeLa (C, D) cells were co-incubated with 0.1 mg/ml Dex-647 and 2 µM EGFP-R8 in serum-free D-MEM for 1 hr. Cell associated fluorescence was analysed using confocal microscopy. Shown are single section images of fluorescence only (EGFP-R8 or Dex-647) and merges of fluorescence with or without DIC of the same cells. B and D represent zoomed images from different fields of view of A and C respectively. Scale bars 10 µm.

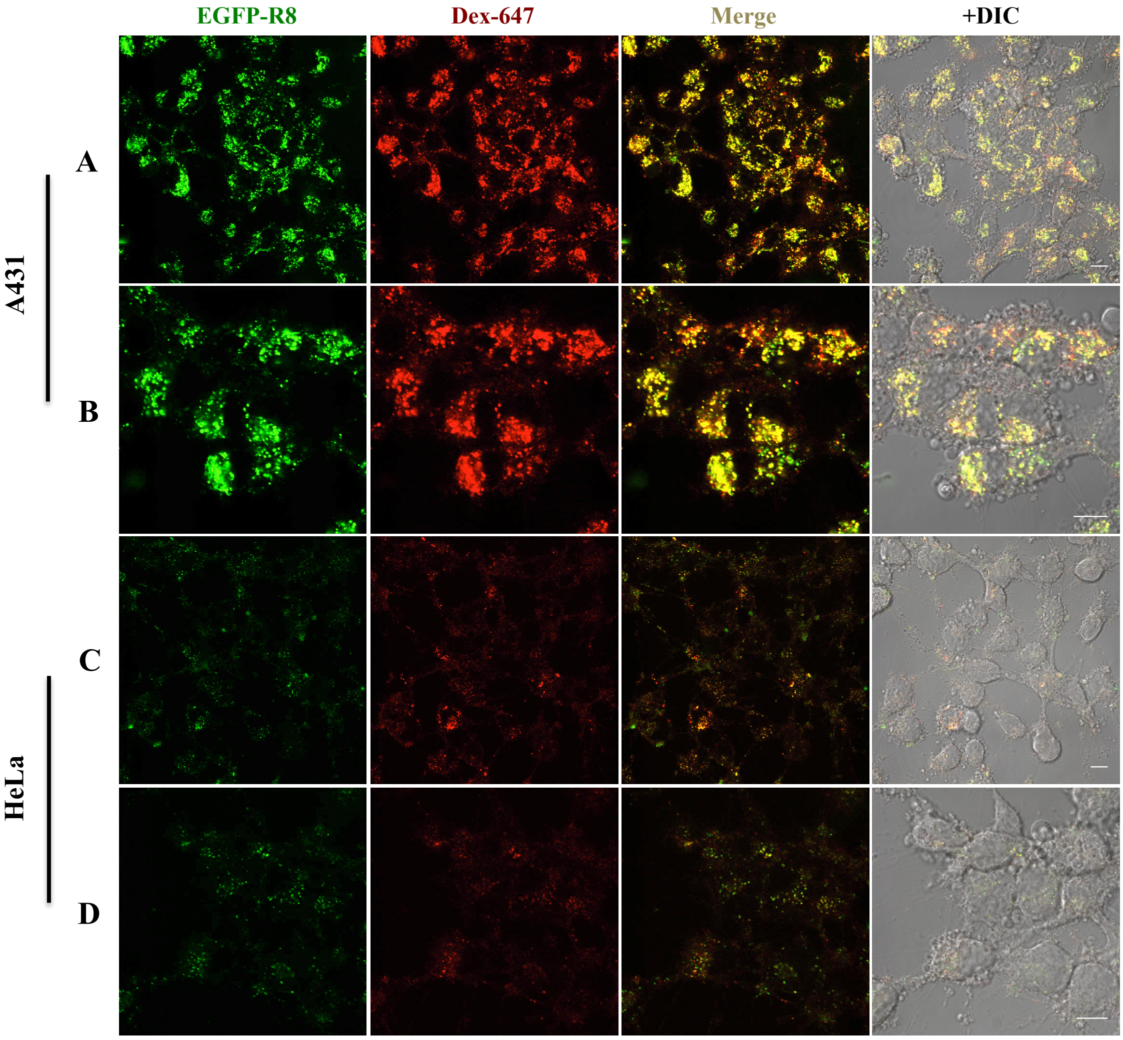

Figure 3.21 Endosomal co-localisation of EGFP-R8 and dextran10-Alexa 647 (Dex-647) in Cyt D treated A431 or HeLa cells. A431 (A, B) or HeLa (C, D) cells that pre-treated with 10 µM Cyt D for 15 min, were co-incubated with 0.1 mg/ml Dex-647 and 2 µM EGFP-R8 in serum-free D-MEM for 1 hr. Cell associated fluorescence was analysed using confocal microscopy. Shown are single section images of fluorescence only (EGFP-R8 or Dex-647) and merges of fluorescence with or without DIC of the same cells. B and D represent zoomed images from different fields of view of A and C respectively. Scale bars 10 µm.

3.3 Discussion

Since the coining of the term CPPs almost twenty years ago, considerable efforts have been made to clarify their internalisation mechanisms. The majority of the early microscopy and flow cytometry studies on these peptides were conducted using fixation techniques and their internalisation appeared to be unaffected by low-temperature incubation or non-sensitive to endocytosis inhibitors. Therefore, the entry routes of CPPs were described as energy- and endocytosis- independent (Vivès et al., 1997). However, fixation was later found to cause artefact translocation of these peptides that were found to be strongly associated with the plasma membrane and upon fixation were accumulating in the nucleus (Lundberg and Johansson, 2002, Richard et al., 2003). Since then investigations on their mechanisms of membrane penetration and cell uptake were performed using live cell confocal microscopy or flow cytometry, in the absence of fixation and also including trypsinisation and washing with heparin. Flow cytometry is unlikely to provide information regarding the cellular location of fluorescent CPPs in individual cells and heterogeneity across the cell population. For these reasons almost all the studies here were performed by live cell confocal microscopy. It would however have been very interesting to compare the confocal data with flow cytometry analysis. Unfortunately time did not allow for this.

Previously, the laboratory has predominantly focused on analysing the cellular uptake of CPP-fluorophore conjugates, but the availability of the plasmid encoding EGFP-R8 allowed us to study uptake of this CPP fused to a much larger cargo. The conjugation of cargo to CPP makes the linkage between the two elements more stable and has been employed in a large number of studies in the field of drug delivery although non-covalently complexed CPP-based delivery systems are more easily prepared and capable of bearing cargos at higher cargo/CPP ratios. BL21 (DE3) *E.coli* was selected for this project to express EGFP-R8, and unsurprisingly leaky expression of this fusion protein in *E.coli* cell culture was observed prior to IPTG addition. To reduce basal level expression of the gene of interest, some *E.coli* strains such as BL21(DE3)pLysS have been designed to contain an additional gene encoding T7 lysozyme which inactivates the T7 promoter. This prevents background expression of T7 RNA polymerase from expressing the target gene prior to IPTG induction. This class of expression systems are suitable for expression of toxic proteins, but not ideal for non-toxic proteins like EGFP. The existence of the additional plasmid pLysS carrying gene sequence for T7 lysozyme may interfere with the level of expression achieved following IPTG induction. Following protein expression, methods were developed to optimise the purification of this CPP-protein conjugate from *E. coli*. This was initially achieved using a previously established protocol that resulted in high expression of the protein but there were concerns regarding some impurities that were eluted from the purification column and appearing on the gels. An optimisation approach was then initiated changing a number of purification variables such as salt, pH and imidazole concentration. Eventually a preparation of >99% purity was obtained and dialysed into cell culture medium. This EGFP-R8 preparation could then be directly applied to cells. Silver staining is rarely used to show purification of CPP-protein conjugates. We could not find a single paper in the literature showing silver stained gel that reveals impurities that are not apparent on Coomassie stained gels. The product obtained was deemed to be of sufficient purity to continue with cell uptake assays. One approach often used for further purification of proteins is size exclusion chromatography (Wang et al., 2010), but it was felt that purity was high from the optimised assay and that further purification was not necessary. The availability of this reagent allowed us to study its uptake in cell lines that were of particular interest in the laboratory due to the fact that they had major differences with respects to actin organisation and also CPP uptake (Al Soraj et al., 2012). Additionally the uptake of the CPP-protein allowed us to study any differences in cell association and uptake of the same CPP attached to small (Alexa 488) and large cargo (EGFP). It should be noted that for this work we observed the fluorescence of the cargo without having information on the possibility that it is no longer attached to an intact CPP. It is possible that the peptide itself may get degraded after cell entry or even in the extracellular medium especially in the presence of serum proteases (Saar et al., 2005). The same is not true for EGFP as any degradation of the cargo would abolish the fluorescence.

Macropinocytosis has been proposed to be a major contributing pathway in the internalisation of arginine-rich peptides such as R8 with or without the attachment to small molecular weight fluorophores or large protein cargo (El-Sayed et al., 2008, Nakase et al., 2004, Wadia et al., 2004a). The involvement of macropinocytosis in mediating CPP uptake was linked to the reorganisation of the actin cytoskeleton, a required process for this pathway to proceed. It should however be noted that actin activity has been shown for several other endocytic pathways such as clathrin-mediated endocytosis (CME) in mammalian cells in certain settings (Fujimoto et al., 2000, Mooren et al., 2012). In comparison with CME, the role of actin in clathrin-independent pathways including caveolae and flotillin-mediated pathways still remains less certain and less well-defined (Doherty and McMahon, 2009).

The actin depolymerisation reagent Cyt D was the main tool used in this chapter to evaluate the role of actin cytoskeleton in the internalisation of R8 conjugates in two different cell lines HeLa and A431 cells. This reagent has been used to study actin assembly, endocytosis and most importantly phagocytosis, for over 40 years.

Initially we investigated the role of actin on R8 conjugate uptake using live cell confocal microscopy focusing on both the effects of the actin reagent was having on cell morphology, conjugate uptake and also subcellular distribution. The early studies confirmed previous flow cytometry data showing differential effects of Cyt D on cellular uptake of R8 and dextran, and extended these studies to look at EGFP-R8. Inhibition on R8 uptake by Cyt D in HeLa cells was previously observed by Futaki and co-workers (Nakase et al., 2004). They also suggested in the same study that the dramatic morphological changes induced by Cyt D in the cells were reversible and the decrease in R8-Texas Red internalisation was caused by actin disruption rather than necrosis, porosity and cell death (Nakase et al., 2004). In our studies, the EGFP-R8 internalisation into HeLa cells was also suppressed by Cyt D. This observation was consistent with a previous report proposing the inhibitory effects of Cyt D on the uptake of Tat-protein conjugate in C2C12 mouse myoblasts (Tünnemann et al., 2006). Tat fusion proteins have been suggested to use macropinocytosis to enter into living cells (Wadia et al., 2004a). Therefore, actin disruption by Cyt D was expected to delay or impair the internalisation of Tat-protein cargo. As shown in studies performed by Tünnemann et al., Cyt D pre-incubation completely blocked the vesicular uptake of Tat-protein, and the majority of the cargo was only plasma membrane-associated (Tünnemann et al., 2006).

In contrast to R8, Cyt D did not show any effects on the uptake of the CME marker transferrin. To further investigate whether R8 was utilizing a pathway that was also used by dextran we performed the same Cyt D experiments using dextran10-Alexa 647, and inhibition was again observed in HeLa cells. This kind of Cyt D data using different endocytic probes has raised the profile of macropinocytosis as a potential uptake mechanism for different CPPs associated with many different types of cargos. It is however worth noting that dextran is not solely a probe for macropinocytosis and can in fact enter cells via several different pathways including fluid phase uptake. The fact that fluid phase uptake has been difficult to analyse as a distinct process and that macropinocytosis can be constitutive and induced makes data interpretation very difficult when looking at uptake of probes such as dextran.

Cyt D had little effect on the internalisation of R8 by A431 cells, and flow cytometry confirmed that this difference was apparent during time points 0-60 min but only statistically significant at 80 min (Al Soraj et al., 2012). Interestingly transferrin uptake was inhibited in suspension A431 cells incubated with another actin inhibitor jasplakinolide (see Chapter 4) but not in those grown on plates as we performed here (Fujimoto et al., 2000). Similarly, in this thesis transferrin uptake was unaffected by Cyt D in A431 and also HeLa cells. Uptake of EGFP-R8 and dextran10-Alexa 647 was inhibited by Cyt D in HeLa cells. However it was very surprised to see that their uptake in A431 cells was increased following actin disruption. The very different effects of actin disruption on R8 and EGFP-R8 uptake in A431 cells suggest their internalisation mechanisms are, at least, partially distinct. It may be the case that EGFP-R8 employs a pathway that is more similar to that used by dextran as both behaved similarly to the effects of Cyt D.

From these data it appears that actin in A431 cells is acting as a hindrance to EGFP-R8 and dextran endocytosis. There is some evidence to suggest that endocytosis in other cell types can be enhanced by actin disruption (Shurety et al., 1998, Lewis et al., 1998). These were all performed in different *in vitro* systems and some also employed other fluid phase markers such as horseradish peroxidase. The cellular uptake of other CPPs TP10 or pVec in HeLa cells was found to be evidently increased by Cyt D but generally it is regarded as an inhibitor of cationic-CPP uptake (Mäger et al., 2010, Wadia et al., 2004b). Such observations may suggest that the endocytic pathways involved in the uptake of a particular CPP conjugate are competing simultaneously with each other at different efficacies rather than being the involvement of only one specific pathway.

In addition, a hypothesis on the compensation of different endocytic mechanisms was also proposed: when the rate-limiting pathway is dampened e.g. by inhibitors, another pathway(s) might be induced to a higher level. This hypothesis was also supported by data obtained from Säälik et al. They studied different endocytic pathways in uptake of transportan-protein conjugates and noted the involvement of the flotillin-1, caveolar/caveosomal routes. Unexpectedly, flotillin-1 depletion using siRNA transfection resulted in a notable increase rather than decrease in the uptake of these transportan conjugates (Säälik et al., 2009). Those results imply the simultaneous involvement of more than one endocytic pathway in this process. It may be the case that when one rate-limiting pathway(s) is inhibited, uptake compensation by other routes might be stimulated. Of note here is that siRNA transfection is not a rapid process to shut down an endocytic pathway and when one endocytic protein is depleted and one endocytic pathway is inhibited other proteins can be upregulated to stimulate other pathway(s) before the uptake experiment is performed. The use of pharmacological inhibitors that are only placed on the cells for short periods of time does not allow for this compensation to occur. But the major problem with these agents is their lack of specificity. One recent study investigated the uptake of 22 different CPPs including R7 and R9 in a wide range of cell lines and here they employed three different endocytosis inhibitors - chrorpromazine, nystatin, wortmannin and also chloroquine and heparin (Mueller et al., 2008). Unfortunately they did not include one that inhibited actin and based on the data presented in this thesis it would have been interesting to perform similar studies with Cyt D.

We then examined whether the EGFP-R8 and dextran (10 kDa) localised to the same vesicular compartments, in an attempt to obtain further information on the cellular uptake of both probes. Noted here is the fact that dextran is also a commonly used carrier for the uptake of drugs (Varshosaz, 2012) and it's clear that more needs to be determined regarding its uptake into cells. Both HeLa and A431 cells (control and Cyt D-treated cells) showed very little co-localisation between dextran10-Alexa 647 and EGFP-R8 when they were separately incubated with cells. However the possibility exists that a fraction of EGFP-R8 reaches lysosomes within the incubation period. EGFP could therefore have been degraded and/or its fluorescence could have been pH-quenched (Tsien, 1998). Alternatively they may be trafficked to different compartments inside the cells. There were however clear examples of the probes being located in the same organelle.

Interestingly, these two probes (EGFP-R8 and dextran) showed a strikingly high level of co-localisation in Cyt D treated A431 cells after 1 hr co-incubation. This strongly suggests that these two cargos enter the same pathways when actin cytoskeleton is disrupted. However, the dextran probe used here was anionic, it may electrostatically associate with the highly positively charged R8 resulting in dimers, polymers or even aggregates that were too small to be observed using the microscopy techniques used here. The fact that Cyt D increased the uptake of both probes into punctate structures inside the cells highlighted this co-localisation even further.

These studies provided very interesting data on the role rather than the dependence of actin for the uptake of two different R8 conjugates. This led to the design of experiments to further explore actin organisation in these two cell types and how this can be perturbed by inhibitors that interfere with actin in different ways. These data from these experiments are presented in the next results chapter.

Chapter 4: Examination of the effects of different actin inhibitors on actin architecture and the uptake of EGFP-R8

4.1 Introduction

As previously discussed in detail in the Introduction (Section 1.5), the health of all eukaryotic cells is absolutely dependent on a functional cytoskeleton as numerous cellular events rely on the duties of actin, microtubules, and intermediate filaments. Membrane traffic involves the packaging of materials into vesicular-like compartments that bud from and fuse with each other and travel along defined pathways to a variety of cellular destinations. These vesicles associate with the cytoskeleton that provide the necessary directionality to allow them to reach their final destination. Microtubules, often working in association with actin, are most often thought to regulate downstream traffic from the very early stages of endocytosis (Anitei and Hoflack, 2012), and comparatively little is known about the role of intermediate filaments. The starting point for endocytosis is the plasma membrane that undergoes reorganisation to form invaginations or protrusions that eventually results in the formation of a vesicular compartment containing a portion of the plasma membrane and accompanying extracellular medium. These starting steps of endocytosis, especially the formation of membrane protrusions for macropinocytosis/phagocytosis requires reorganisation of the actin network. Although the role of the actin cytoskeleton has been widely studied within the endocytosis remit, there is, to date, still little consensus as to exactly how, spatially and temporally actin filaments control endocytic processes (Fujimoto et al., 2000, Mooren et al., 2012, Robertson et al., 2009).

Two independent studies published 10 years ago brought attention to the actin cytoskeleton in the uptake of cationic CPPs, and the possibility that they may in fact be promoting their own uptake by influencing the actin cytoskeleton (Nakase et al., 2004, Wadia et al., 2004). One endocytic pathway that is absolutely reliant on actin is macropinocytosis that when activated has the capacity to form large intracellular vesicles termed macropinosomes (Falcone et al., 2006, Jones, 2007, Kerr and Teasdale, 2009, Lim and Gleeson, 2011). Classically this process is induced in response to growth factor activation such as epidermal growth factor (EGF) binding to the EGF receptor, initially leading to extensive actin-dependent ruffling on the plasma membrane. This induces a “gulping effect” manifest as an increased uptake of extracellular fluid (Haigler et al., 1979, Jones, 2007, Kerr and Teasdale, 2009). To what extent this occurs in the absence of growth factor activation - constitutive macropinocytosis - or indeed after the addition of artificial entities such as CPPs remains to be determined. Of interest are observations that some CPPs may induce plasma membrane effects similar to that seen upon growth factor activation (Nakase et al., 2004, Nakase et al., 2007), and that they also promote the uptake of 70 kDa Rhodamine-labelled dextran, a marker of fluid phase endocytosis (Wadia et al., 2004, Al Soraj et al., 2012, Åmand et al., 2008).

4.1.1 Actin organising proteins and actin inhibitors

As previously described in chapter 3, Cyt D induces the depolymerisation of filamentous actin by capping its barbed end that therefore blocks the incorporation of more monomeric actin at this site (Figure 4.1). In contrast to Cyt D, latrunculin B (Lat B), obtained from the marine sponge *Latruncula magnifica* binds to and complexes with actin monomers (Figure 4.1) at a molecular ratio of 1:1 and thereby prevents actin polymerisation (Spector et al., 1989). Jasplakinolide (JAS) is a natural cyclic peptide that was originally isolated from the marine sponge *Jaspis johnstoni* (Braekman et al., 1987), and has become another convenient and potent method for altering intracellular actin organisation. Unlike Cyt D and Lat B, JAS binds directly to filamentous actin (Figure 4.1) and induces stabilisation of the existing actin filaments to inhibit actin disassembly (Bubb et al., 1994, Visegrády et al., 2005, Bubb et al., 2000, Henquin et al., 2012). However data obtained from *in vivo* experiments suggested that actin filaments were also disrupted by JAS (Senderowicz et al., 1995, Spector et al., 1999). The possible explanations for these *in vivo* effects have been described based on observations that this compound enhanced the rate of nucleation of filament assembly and then stimulated the polymerisation of actin filaments, and as a result decreased the cellular level of G-actin. Consequently, cellular monomeric actin was suggested to polymerise into amorphous masses and also the available G-actin was insufficient for actin remodelling into fibres (Krendel and Bonder, 1999, McGrath et al., 1998, Bubb et al., 2000).

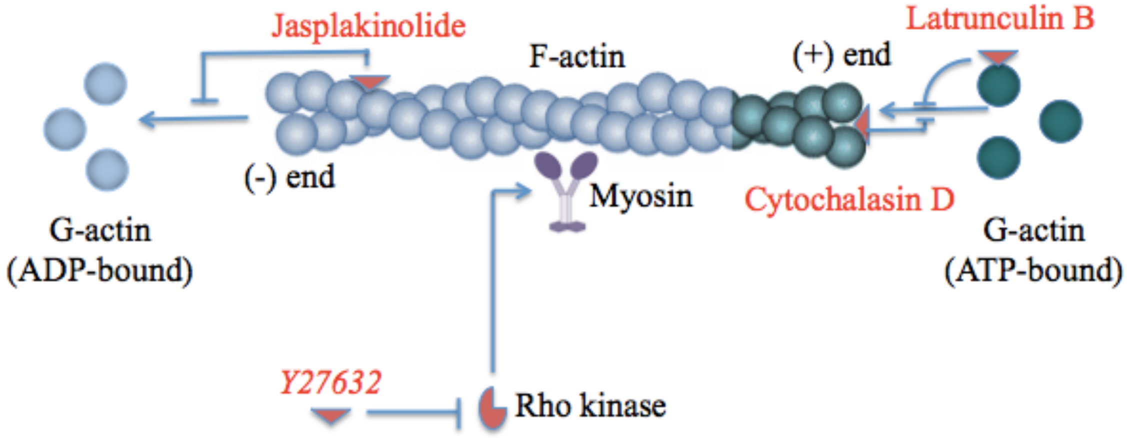

Figure 4.1 Actin inhibitors and their mechanism of action. Only those utilized in this chapter are shown. Cytochalasin D caps the barbed end of filamentous actin, thereby blocking further polymerization. Latrunculin B binds to and complexes with monomeric actin and inhibit its incorporation into actin filament. Jasplakinolide binds directly to the side of filamentous actin and prevents polymer disassembly. Y27632 inhibits the kinase activity of ROCKs and the Rho-ROCK signalling pathway that drives phosphorylation and activation of myosin.

Members of the Ras-related small GTP-binding protein family Rho are known to act as molecular switches for a wide range of cellular processes. All these transform between inactive, GDP-bound and active, GTP-bound forms (Figure 4.2). In mammals, 22 Rho GTPase variants have been identified, and most of these can be sub-grouped into Rac, Cdc42 and RhoA subfamilies (Ridley, 2006). Among these, Rac1, Cdc42 and RhoA are the best-studied members. Rho family members have been widely reported to participate in the regulation of actin polymerisation/depolymerisation and the formation of focal adhesions and stress fibres in response to extracellular signals (Ridley and Hall, 1992, Tapon and Hall, 1997, Thumkeo et al., 2013). They are also critically involved in other cellular processes such as cytokinesis and nuclear transcription (reviewed in (Chircop, 2014, Rajakylä and Vartiainen, 2014).

As previously mentioned, actin assembly and disassembly needs to be very tightly regulated and highly coordinated. The dynamics and regulation of actin is usually achieved through the concerted action of actin regulatory proteins whose activities are finely modulated by protein kinases. These include Rho-associated coiled-coil forming serine/threonine kinases ROCK I and II (Figure 4.2) that have been identified as important downstream effectors of RhoA through their interaction with its GTP-bound form (Ishizaki et al., 1996, Leung et al., 1995); ROCK I and II exhibit 90% identity in their kinase domain. A number of pharmacological inhibitors of the Rho-ROCK signalling cascade have been developed for research in the field of cell motility and adhesion. Among these inhibitors, the synthetic compound Y27632 [(+) -(R) - trans - 4 - (1-aminoethyl) - N - (4-pyridyl) cyclohexanecarboxamide dihydrochloride] (Figure 4.1) has been shown to inhibit the kinase activity of ROCKs by binding to their catalytic sites (Uehata et al., 1997, Ishizaki et al., 2000). Inhibition by Y27632 could be reversed by ATP binding to the same site in a competitive manner (Ishizaki et al., 2000). In addition to ROCK I and ROCK II, Y27632 also has inhibition effects on some other kinases including protein kinase C-related protein kinase 2 (PRK2) (Vincent and

Settleman, 1997). However, the inhibition by this compound on the ROCK family was suggested to be 100 times more potent than that on other kinases including protein kinase C and myosin light chain kinase (Ishizaki et al., 2000). Therefore Y27632 at low μM concentrations has been considered as a useful tool to assess the involvement and roles of the ROCKs in various cellular processes including actin organisation (Duess et al., 2016).

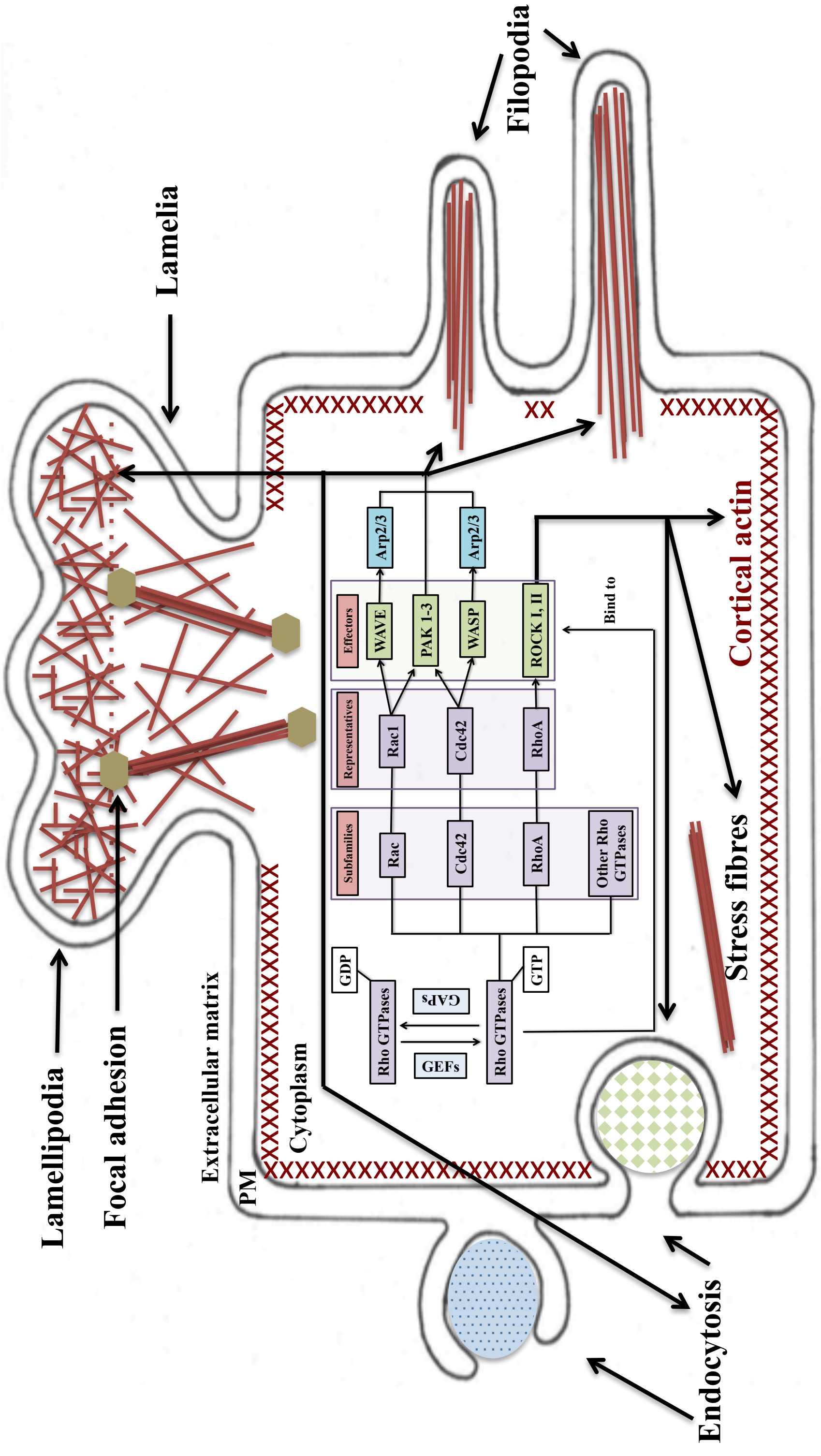

Figure 4.2 The roles of Rho family GTPases and their downstream effectors in the organisation of the actin cytoskeleton. The Rho GTPases are usually activated by guanine nucleotide exchange factors (GEFs), which release GDP and therefore allow for GTP binding. Their activity is down regulated by GTPase activated proteins (GAPs), which hydrolyse the bound GTP to GDP. The activated forms of Rho family members bind to and activate their downstream effectors including WASP/WAVE, which stimulate actin polymerisation via ARP2/3 complex, PAK1-3 and ROCK I and II, which have been shown to have indirect effects on actin dynamics/organisation, and consequently influence actin-involved membrane protrusions including filopodia and lamellipodia and also endocytosis (Ridley, 2006, Sit and Manser, 2011). PM: plasma membrane.

In addition to the Rho family and their downstream effectors mentioned in Figure 4.2, Src-family kinases (SFKs), a group of non-receptor tyrosine kinases also regulate the activity of a variety of actin regulatory proteins including nucleation promoting factor WASP (Torres and Rosen, 2006), the severing factor cofilin (Yoo et al., 2009) and the polymerisation promoting factor cortactin (Tehrani et al., 2007). The Src kinase family comprises nine closely related members including c-Src (Parsons and Parsons, 2004) that share a common domain structure including SH1-4. PP2 [4-amino-5-(4-chloro-phenyl)-7-(*t*-butyl)pyrazolo [3,4-*d*] pyrimidine)] is a molecule that has been frequently used as a selective inhibitor for SFKs (Hanke et al., 1996, Frauenstein et al., 2015). It has been shown to have inhibitory effects on several Src members including c-Src, Lck, Hck and Fyn (Hanke et al., 1996). In contrast to those previous reports and despite its popular usage as a selective inhibition tool, PP2 has been recently shown to also inhibit many other kinases with similar binding affinities; these include Fyn-related kinase FRK and STE7 kinase family member MEK1 (Brandvold et al., 2012). The inhibition of Src kinase activity with PP2 has been shown to have similar effects on actin polymerisation as those produced by Cyt D, but not to disturb the organisation of cortical actin (Olivares et al., 2014).

Aims

For studies involving actin and CPPs it is useful to gain an initial insight into how actin is arranged within cell models that are under scrutiny. Our studies and other highlighted how this differs between different cell lines. This initial analysis for example could provide much needed supporting information on the effects of actin-modifying agents on cellular uptake of CPPs using both microscopy and flow cytometry as analytical tools. As previously discussed in Chapter 3, the cellular uptake of the CPP-protein conjugate EGFP-R8 and the fluid phase probe dextran in different cell models, HeLa and A431, showed very different responses as a result when actin was disrupted with Cyt D. To study in more detail how actin is distributed in different cells (HeLa and A431 cells) with and without Cyt D, we attempted to optimise the existing confocal microscopy methods. Once in place it was hoped that these methods would shed further light on the putative effects of cationic CPPs on actin and how actin disruption by different chemical actin inhibitors influence the actin cytoskeleton to modify cellular levels of CPPs.

The selected actin inhibitors were cytochalasin D (Cyt D), latrunculin B (Lat B), jasplakinolide (JAS), Y27632 and PP2 and based on data presented in Chapter 3 EGFP-R8 was used as the CPP conjugate and for these analysis A431 cells were utilized as the *in vitro* model. It should be noted here that only Cyt D and JAS had previously been investigated in the laboratory and to our knowledge no CPP studies had been performed on Y27632 and PP2.

4.2 Results

4.2.1 Optimising microscopy based methods for analysing the actin architecture in HeLa and A431 cells

To visualise the actin arrangement in these two cell lines the cells were seeded on coverslips as previously described in section 2.9.1 and cultured for 24 hr to reach a confluence of ~80–90 %. After removal of incubation medium, cells were fixed, stained for cell nuclei and polymerised actin and finally imaged by the confocal microscopy. Described below is the final method based on iterative analysis and discussion, and other details of experimental procedure have been described in section 2.9.2.

All analysis was performed on the Leica SP5 confocal laser scanning microscope equipped with laser lines 405 Blue Diode (Excitation wavelength 405 nm) and Helium

Neon laser (Excitation wavelength 543 nm) for visualisation of Hoechst 33342 and Rh-P respectively. All images presented here were obtained using a HCX PL APO 63× 1.4 NA oil immersion objective with Leica Type F immersion oil. For multi-channel image acquisition, the channels were scanned in a sequential recording mode (two channels separately), which avoids spectral cross-talk caused by overlapping excitation and/or emission spectra of fluorophores. Although the scan time increases two fold, this ensures spectral separation of the two cell stains.

The percentage of laser output was initially set quite low to avoid bleaching and saturation of the fluorescent signal. The signal-to-noise level was assessed on the basis of the image acquired, and the laser output intensity was adjusted accordingly. Emission (capture) bands ~420–500 nm (Hoechst 33342) and ~560–680 nm (Rh-P) were finally selected. Parameters "Gain" and "Off-set" of the individual photomultiplier tubes needed to be adjusted for each experiment in order to obtain optimal image acquisition avoiding saturation. "XYZ" was selected as the acquisition mode with image resolution (pixels/image) of 512×512. Pinhole size was set to 1 Airy Unit, and scan speed was set at 200 Hz. For both single sections and multiple projection images, the same optical section is scanned three times to generate a frame average image. To obtain a three-dimensional actin distribution (Z-stack) the scanning was initiated at the glass–cell interface. Imaging through the cell body with a step size of 0.3 μm would ensure coverage of the whole cell volume. In HeLa cells this typically required approximately 25–30 sections, as fixing causes the cells to flatten thus reducing the *Z*-axis depth and the number of optical sections that need to be imaged. Step size must be calculated according to the axial resolution of the microscope. Actin protrusions such as filopodia may extend above the obvious cell outline so ensure the imaging volume extends beyond the cell surface to capture these structures.

The obtained confocal images were analysed using Fiji, the open source platform for biological image analysis (Schindelin et al., 2012). Classically, images are shown as a maximum intensity projection through the entire stack and highlight the location of the nucleus (Figure 4.4 Max Proj). However, depth information regarding the localisation of the actin cytoskeleton is lost. Here, the data is presented in an alternative format to highlight differences in the actin cytoskeleton across the entire depth of the cell. The images shown in Figure 4.4 represent the following four cell profiles: 1. *Max Proj* representing maximum intensity projections through the entire cell volume of both Hoechst (blue) and Rh-P (red); 2. *Basal*, representing the three sections closest to the coverslip as a maximum intensity projection of Rh-P corresponding to the lower surface of the cell approximately 1.0 µm from the glass surface; 3. *Cell Body and Apex* (*CBA*), representing maximum *Z*-projection through the rest of the cell; 4. *Merge*, representing false colour merge of basal and CBA images highlighting in a single image the different actin structures found at the different sections of the cell. These cell regions 1-4 are illustrated in Figure 4.3.

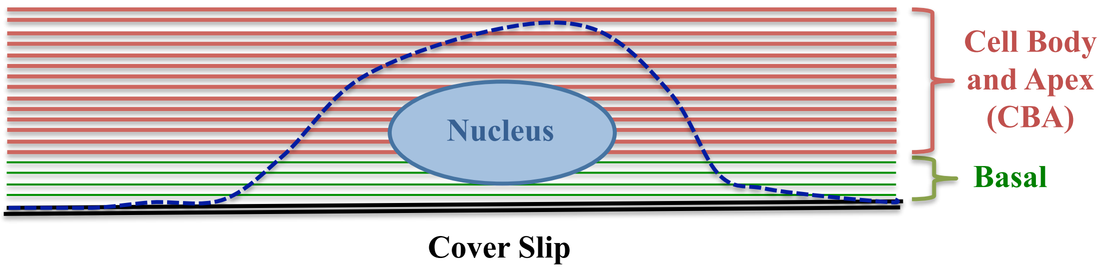

Figure 4.3 Illustrations of Cell Body and Apex (CBA) and Basal used in the confocal microscopy-based analysis of this chapter. Basal represents the three sections closest to the coverslip as a maximum intensity projection of Rh-P corresponding to the lower surface of the cell approximately 1.0 µm from the glass surface. CBA represents maximum *Z*-projection through the rest of the cell. The dotted blue line represents the plasma membrane of the imaged cells.

HeLa cells displayed classical filamentous actin (stress fibres) that was very apparent in the basal sections (Figure 4.4), whereas the CBA image displayed a more granulated appearance highlighting actin structures near the top surface of the cells. However, in A431 cells generally very few stress fibres were observed (Figure 4.4) and the fluorescence was concentrated at the cell periphery especially at cell–cell contacts. This is where cortical actin is found and it remains to be determined what role it has, whether positive or negative, on endocytosis (Al Soraj et al., 2012, Ridley, 2011). The A431 cells shown are confluent but clear projections are seen emanating from the plasma membrane, especially in the grey scale CBA image.

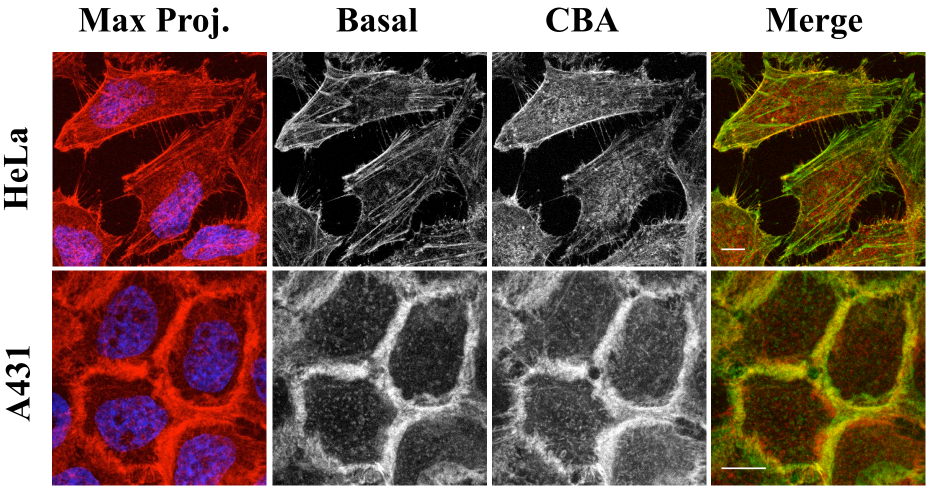

Figure 4.4 The actin architecture in HeLa and A431 cells. HeLa and A431 cells fixed and stained with Rh-P and Hoechst 33342 were imaged by confocal microscopy as described in Section 4.2.1. The images shown represent: Maximum intensity projection (Max Proj.), Basal, Cell Body and Apex (CBA) and Merge images as defined in section 4.2.1. Scale bars 10 µm.

4.2.2 Visualisation of the actin architecture in Cyt D-treated HeLa cells

Here the cells were seeded on coverslips as previously described and cultured for 24 hr prior to analysis using the new imaging method described above. Cells were then washed with PBS and incubated with or without 1 or 10 µM Cyt D for 15 min in serum-free D-MEM under tissue culture conditions (37˚C/5% CO_2). After removal of incubation medium, cells were fixed, stained for cell nuclei and polymerised actin and finally imaged by confocal microscopy.

The selected control cells in Figure 4.5 had very well defined stress fibres but also long filopodia that are commonly observed in this cell line at <100% confluency. Actin labelling this way showed the dramatic effect that short Cyt D treatment had on the cells. Basal sections showed that actin stress fibres were almost completely disassembled with 1 µM Cyt D; less effect was observed on filopodia (Figure 4.5). In these cells, actin aggregated especially at the cell periphery and apical surface sections; this was particularly apparent at 10 µM Cyt D (Figure 4.5). The Cyt D effects on the actin cytoskeleton of A431 cells are shown and discussed in detail in section 4.2.6.

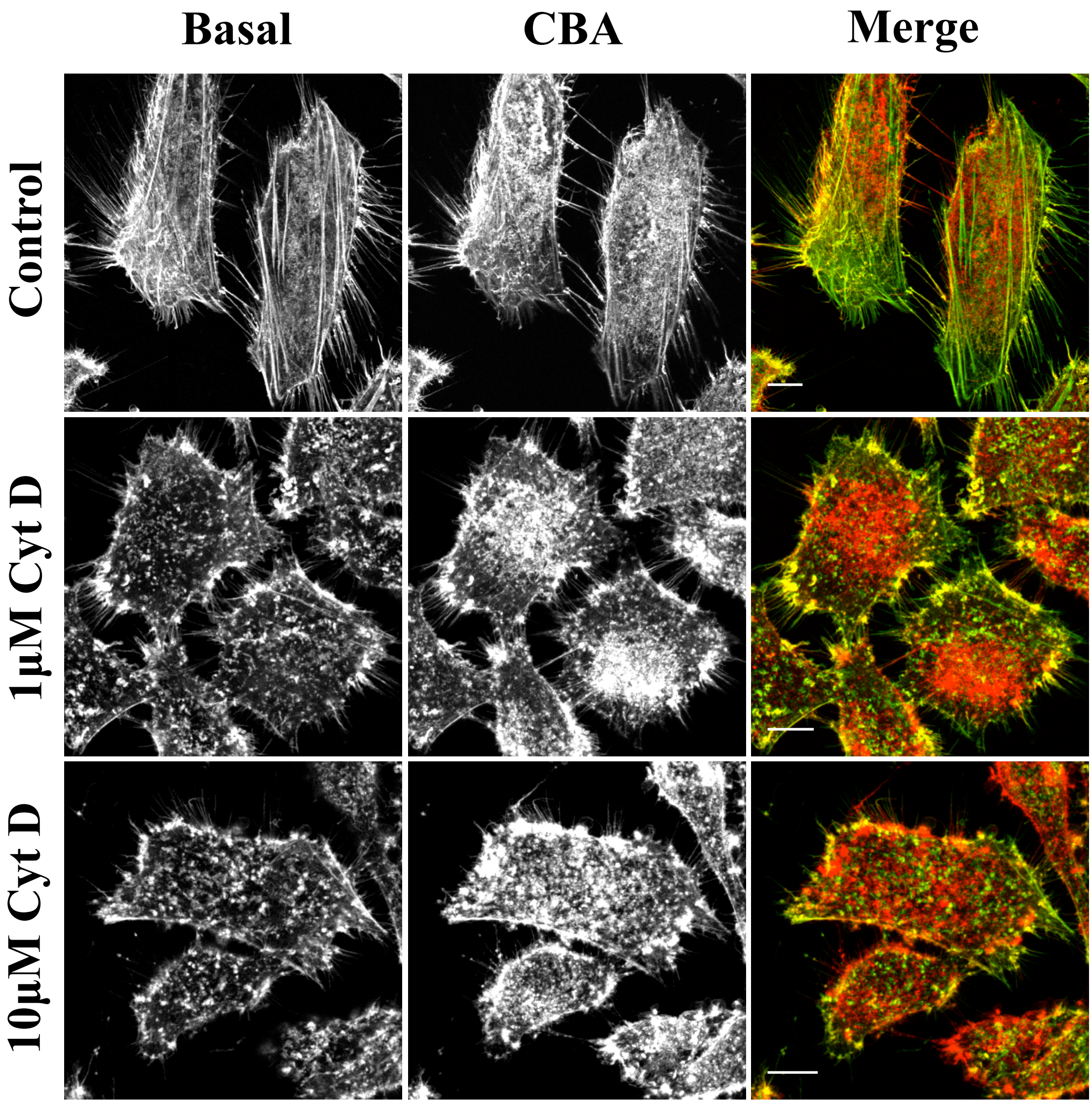

Figure 4.5 Visualisation of the actin architecture in Cyt D-treated HeLa cells. HeLa cells on coverslips were treated either with diluent control, 1 or 10 µM Cyt D for 15 min before fixing and staining with Rh-P and Hoechst. Images were acquired as described in section 4.2.1. Scale bars 10 µm.

4.2.3 Visualisation of R8 effects on plasma membrane ruffling of serum-starved or non-starved HeLa cells

To analyse plasma membrane dynamics in control or serum-starved cells treated with R8, HeLa cells were seeded and cultured for 24 hr under tissue culture conditions. For serum starvation the cells were washed with PBS and replaced with fresh D-MEM lacking serum. For control cells the old medium was replaced with fresh D-MEM supplemented with 10% FBS. Cells were then cultured under tissue culture conditions for 16 hr. Cells were washed again in PBS and then incubated with serum-free D-MEM containing 10 or 20 μM unlabelled R8 (Ac-RRRRRRRR-NH_2) under tissue culture conditions for 2.5 min. After quickly washing the cells were fixed, labelled for the nucleus and actin and imaged by confocal microscopy as previously described in section 4.2.1.

Analysis of these non-starved HeLa cells demonstrated that there was no clear effects on actin staining in cells treated with 10 μM R8. Membrane ruffling was, however, apparent in some cells treated with 20 μM R8 (Figure 4.6 right hand side). The arrow denotes the thin sheet-like lamellipodium at the leading edge of the cell that is clearly defined in the basal image. When the same experiment was performed in serum-starved HeLa cells (Figure 4.6 left hand side), there was a dramatic effect at both concentrations with single cells displaying very prominent splayed membrane sheets often covering several micrometres and also long filopodia emanating from them. At 20 μM the cells had severely altered morphologies, were spiculated and quite possibly in retraction. Incubating HeLa cells with 20 μM R8 in serum-containing medium is non-toxic but the data here suggests that adding the peptide at this concentration in serum-free medium to serum-starved cells could result in cytotoxicity. This could be confirmed by performing viability assays in non-treated and serum-starved cells incubated with different concentrations of R8.

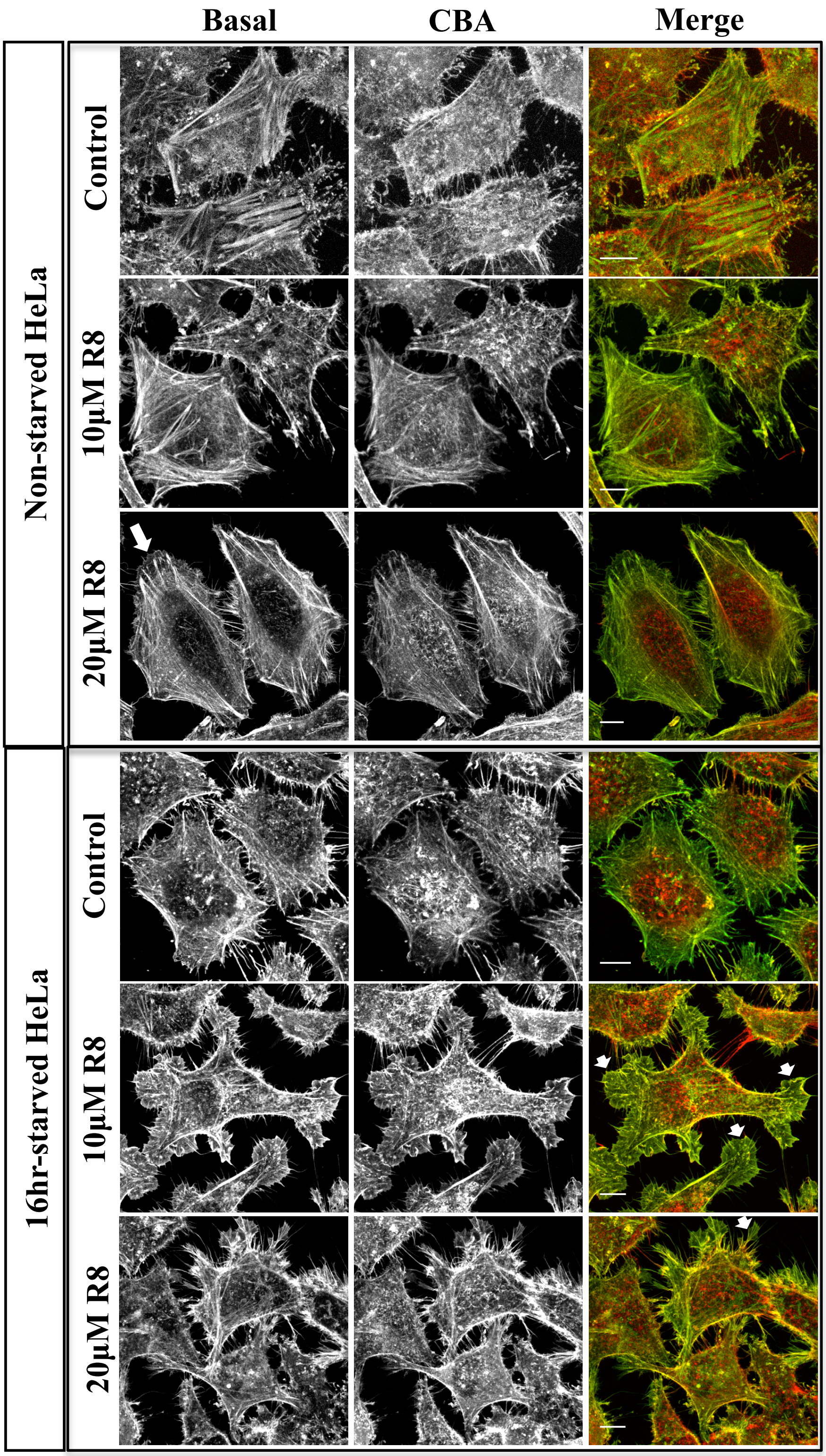

Figure 4.6 R8 effects on plasma membrane ruffling of serum-starved or non-starved HeLa cells. Non-starved or serum-starved HeLa cells were incubated for 2.5 min with diluent control, 10 or 20 μM R8 before fixing and staining with Rh-P and Hoechst. Images were acquired as described in in section 4.2.1. *Large arrow* denotes R8-induced lamellipodia structure on the leading edge of the cell. *Small arrows* in Merge image show R8-induced membrane protrusions/extensions in serum-starved cells. Scale bars 10 μm.

4.2.4 Visualisation of R8 or EGF effects on plasma membrane dynamics of serum-starved A431 cells

A431 cells express very high levels of the EGF receptor (EGFR) and it is well documented that addition of EGF to these cells causes extensive membrane ruffling and macropinocytosis (Jones, 2007, Al Soraj et al., 2012, Hewlett et al., 1994, Swanson and Watts, 1995). Serum-starved A431 cells, prepared as previously described in section 2.9.5, were incubated for 2.5 min with EGF (50 nM) or R8 (20 μM) before fixation and staining for actin and the nucleus and then performing confocal microscopy. Extensive membrane reorganisation at the cell edges was observed in response to these short R8 incubations (Figure 4.7) with clear display of the formation of lamellipodia (arrow) on the basal portion of the cells. EGF treatment, compared with R8, however, had a very different effect and seen in this figure were confluent cells with interdigitated ruffles that were most apparent on the apical portion of the cells. This data set clearly highlighted the different effects on cell morphology, and actin organisation caused by R8 vs EGF activation of EGFR.

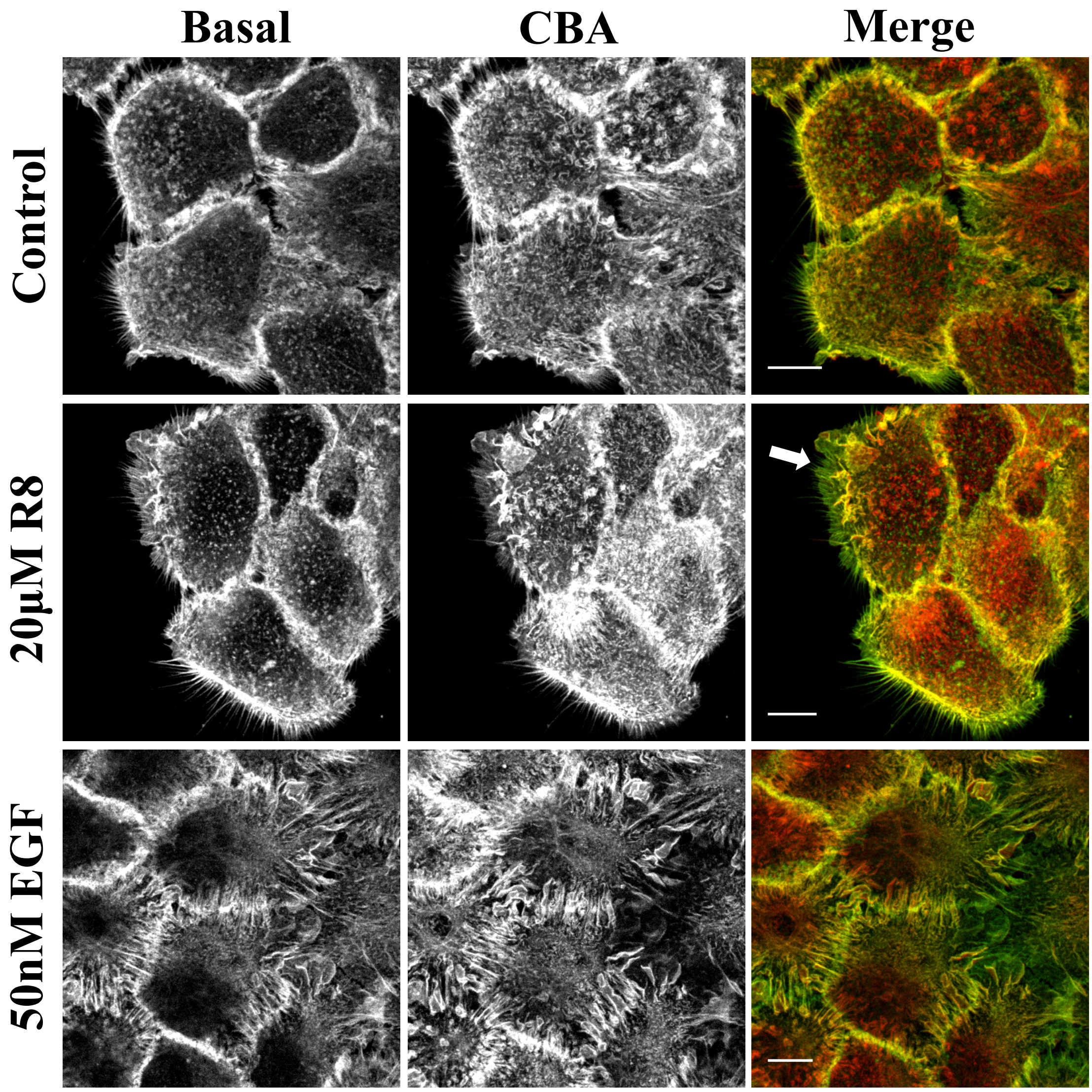

Figure 4.7 Effects of R8 or EGF on plasma membrane dynamics of serum-starved A431 cells. Serum-starved A431 cells were incubated for 2.5 min with diluent control, 20 µM R8 or 50 nM EGF before fixing and staining with Rh-P and Hoechst. Images were acquired as described in section 4.2.1. *Arrow* denotes R8-induced lamellipodia structure on the cell periphery. Scale bars 10 µm.

4.2.5 Discussion: actin visualisation based on optimised confocal analysis

Defining the exact role of the actin cytoskeleton in mediating endocytosis through different pathways is a significant challenge. The general consensus is that actin has an important role in organising the early stages of endocytosis but there is still much to learn. Actin has also been implicated in cell internalisation of CPPs. It is suggested that CPP variants such as octaarginine (R8) and the HIV Tat peptide induce actin-dependent plasma membrane perturbation and enter via macropinocytosis (Nakase et al., 2004, Nakase et al., 2007). In this chapter a confocal microscopy technique was developed that allowed for high-resolution spatial characterisation of the actin cytoskeleton in untreated mammalian cells and those incubated with actin-disrupting agents and CPPs.

Phalloidin binds to polymeric and oligomeric actin but not the monomeric form known as G-actin. Thus in contrast to observing total cellular actin, only organised structures were visualised in these studies using fluorescent phalloidin. The difference in actin organisation between these two cells lines (HeLa and A431 cells) was noted in this chapter (Figure 4.4) and further analysed in attempts to explain differences between these cells lines that we obtained when analysing the role of actin in cell uptake of CPPs R8 and HIV Tat, and especially the fluid phase marker dextran (Al Soraj et al., 2012). Between different cell lines, extensive differences in organisation/localisation pattern of actin, including a cortical actin ring close to the plasma membrane, thick actin bundles/stress fibres, small actin punctates and large actin aggregations have been noted (McKayed and Simpson, 2013). There are also differences between the way HeLa and A431 cells expand during tissue culture. A431 cells tend to grow in clusters and this is clearly reflected in the way the actin is organised especially at the cell periphery. As described these two cell lines also display very different endocytic characteristics when incubated with CPPs and endocytic probes (Al Soraj et al., 2012).

Cyt D, as discussed in chapter 3, binds to actin filaments and prevents further filament assembly by monomeric actin. Other actin inhibitors are also available working directly or indirectly at different processes of assembly and disassembly. They can often provide supporting information to Cyt D experiments and may be used together as a cocktail (Peng et al., 2011). As shown in chapter 3, live cells were imaged then the effects of Cyt D on cell morphology could be clearly observed using bright field or Differential

Interference Contrast (DIC) microscopy. Endocytosis studies, including those analysing CPP uptake typically use Cyt D at 10 μM for longer pre-incubation times, but data in Figure 4.5 showed that the actin cytoskeleton in HeLa cells was significantly affected at 1 μM with the appearance of large actin aggregates becoming more pronounced. Using these microscopy methods, visible effects on the actin cytoskeleton of A431 cells can be visualised at a Cyt D concentration of only 200 nM (data shown in section 4.2.6).

Activation of epidermal growth factor receptor (EGFR) by EGF stimulates a number of signalling pathways including those involving GTPase Ras and kinase Src, and thereby induces the recruitment and activation of a variety of protein factors controlling and regulating actin dynamics at the plasma membrane (Krause and Gautreau, 2014). The first pathway is triggered by the activation of PI3K (phosphoinositide 3-kinase) by EGFR binding, which then results in the generation of PtdIns(3,4,5)P_3. The produced PtdIns(3,4,5)P_3 in turn activates GTPase Rac through GEFs and thus promotes the activity of their downstream effectors including WAVE and hence ARP2/3, leading to the actin-mediated membrane remodelling (Rossman et al., 2005). PtdIns(3,4,5)P_3 can also directly bind to WAVE and relocate it to the plasma membrane (Oikawa et al., 2004). The second activated cascade involves the activation of GTPase Ras, which activates certain kinases including the Ser/Thr kinase ERK that phosphorylate actin regulatory proteins such as WAVE (Mendoza et al., 2011). The third pathway is dependent on the kinase Src that activates a number of actin factors and enables them to initiate actin rearrangement (Olivares et al., 2014). Studies have shown that some CPPs cause membrane ruffling in cells akin to that observed upon growth factor stimulation. Noted in these studies is that the cells were previously starved of serum for periods 18-24 hr (Nakase et al., 2004, Nakase et al., 2007). To investigate whether serum starvation is required to observe CPP-induced membrane ruffling, HeLa cells were incubated with

R8 (20 μM) as untreated cells or those starved of serum for 16 hr. The concentration of R8 used in this experiment was much higher than is usually used to demonstrate endocytic uptake of a fluorescent R8 conjugate and at these levels the peptide freely diffuses through the plasma membrane and into the cytosol (Watkins et al., 2009). Most notably in serum-starved cells lamellipodia were formed in response to this peptide highlighting that serum starvation sensitised the cells to the effects of this peptide. As lamellipodia are linked with cell motility it would be interesting to determine whether incubation with R8 influences cell migration. However, it is questionable as to whether these structures (Figure 4.6) are true lamellipodia or blebs or structures unique to cells incubated with this CPP. It is also unknown as to whether actin is actually required for them to form; they may simply be a product of the direct effects of the peptides on the membranes. Membrane blebs are formed when there is loss of actin interaction with the plasma membrane, often due to excess membrane, but that actin–membrane interaction is essential for lamellipodia to form (Ridley, 2011).

These lamellipodia-like structures shown in Figure 4.6 can only clearly be observed in A431 cells that are not in contact with each other and it is documented that cell–cell contact inhibits the formation of these structures (Ridley, 2011). It remains to be determined exactly how much cell confluency influences the effects of CPPs on the plasma membrane of the cells studied here and others. We observed very little actin rearrangement in non-starved A431 cells similarly treated with R8 but extensive ruffling of the type observed in Figure 4.7 when they were incubated with EGF. As little as 1 hr serum starvation is sufficient for EGF to mediate macropinocytosis, measured as an increase in fluid phase endocytosis (Al Soraj et al., 2012). It remains to be determined as to whether this short starvation period also sensitises the plasma membrane of the cells to CPPs. The optimised microscopy technique allowing for separate analysis of basal and apical profiles provided new information regarding the differential effects of R8 vs EGF on cells and can be used to analyse other CPPs but also other drug delivery vectors who may have similar effects - noted is that many of these including polyplexes and lipoplexes are cationic in nature.

Cellular actin can now be microscopically visualised in tissue culture cells using a number of techniques and discovery of GFP allowed for live cell imaging analysis of this protein as a monomer and in organised structures (Ballestrem et al., 1998). Additionally a recent study revealing how microscopy development and new actin probes allows us to image actin action in live cells (Chen et al., 2014). The future clearly lies in supporting fixed cell analysis highlighted in this chapter with the capacity to monitor actin in live cells. The advent of super-resolution technology and new probes for visualisation of actin structures (Lukinavicius et al., 2014) will undoubtedly provide much needed new information on exactly why this protein is of such fundamental importance in cell physiology and how it impacts on the cellular uptake of CPPs.

4.2.6 Effects of low Cyt D concentrations on the actin architecture and EGFP-R8 uptake in A431 cells

As shown by DIC/confocal microscopy in chapter 3, treatment with 10 μM Cyt D induced significant morphological alterations in both HeLa and A431 cells and also increased the cellular uptake of both EGFP-R8 and dextran in A431 cells. A previous report suggested that similar morphological changes observed by phase-contrast microscopy in HeLa cells were not due to cell death (Nakase et al., 2004). Cyt D of lower concentrations (20 nM-2 μM) were employed in this section in an attempt to minimise gross morphological effects on cells but to retain disruption of actin filaments.

Cells were seeded on coverslips and cultured for 24 hr under tissue culture conditions prior to treatment with or without 20 nM-2 μM Cyt D for 30 min. Then cells were fixed and labelled for the nucleus and actin and imaged by the optimised confocal microscopy method as previously described. Shown in Figure 4.8 are single sections through 6-10 cells showing the overall distribution of the actin relative to the nucleus and images of 2-3 cells from different z-regions. The figure clearly shows that Cyt D disrupts the organisation of the actin cytoskeleton in A431 cells in a concentration-dependent manner. The selected control cells showed diffused actin meshwork at both CBA and basal sections. Additionally a number of scattered F-actin specks in the cytoplasm were observed especially at basal section. Similar actin organisation was also exhibited in cells treated with 20 nM CytD, suggesting this concentration had little effects on the A431 actin architecture. When Cyt D concentration was increased to 200 nM, more actin specks started to appear in both CBA and basal sections and large patch of actin aggregates was present at the cell edges, which could be clearly seen in the CBA section. This large-scale actin disorganisation and intensive actin aggregation became more striking in cells treated with 2 μM Cyt D and were usually observed at the perinuclear region. These results suggested that by using this phalloidin labelling method, the concentration for Cyt D to have visible effects on actin organisation could be as low as 200 nM.

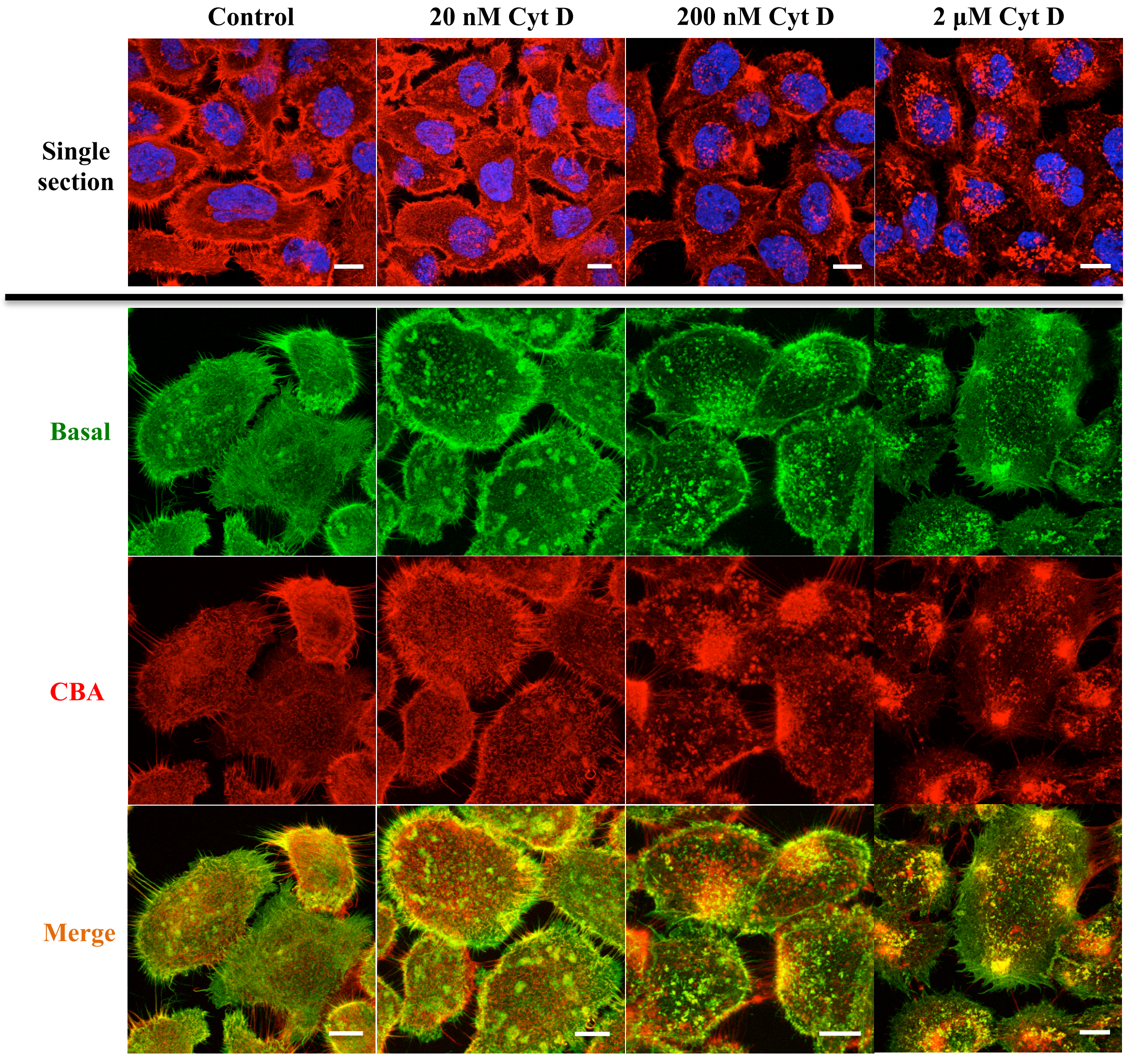

Figure 4.8 Cyt D effects on the actin architecture in A431 cells. Cells on coverslips were treated either with diluent control (0.1% DMSO), or with 20 nM to 2 µM Cyt D for 30 min before fixing and staining with Rh-P and Hoechst. Images were acquired as described in section 4.2.1. Single sections show the overall distribution of the actin relative to the nucleus and highlight the effects of the compound on 6-10 cells to give a better overview of the compound effects. Images below the black line show the actin arrangement of 2-3 cells (from other fields of view of single sections) from different z-regions. Scale bars 10 µm.

In the following experiments, the effect of Cyt D of the same concentrations as that used above was investigated with respects to the cellular uptake of EGFP-R8 in A431 cells. Cells were cultured on 35 mm MatTek dishes and pre-treated with or without Cyt D of 20 nM-2 µM for 30 min. Then 2 µM of EGFP-R8 was loaded onto the cells in the continued presence or absence of Cyt D of relevant concentration for 1 hr. The cells were then washed three times with 0.5 mg/ml heparin in PBS to reduce plasma membrane associated fluorescence and analysed by live cell imaging confocal microscopy. As demonstrated in Figure 4.9, Cyt D of 20 nM did not show any evident effects on EGFP-R8 uptake in terms of the internalisation level or the distribution of fluorescence throughout the cell. Although in the previous actin labelling experiments, Cyt D of 200 nM brought obvious alterations to the actin architecture in cells, here by live cell microscopy, its effects on EGFP-R8 uptake was hard to define. Unsurprisingly Cyt D at the higher concentration 2 μM dramatically enhanced the internalisation of this cargo into vesicular structures and affected the subcellular distribution of fluorescence. Instead of scattered cytoplasmic structures as shown in control cells, a large number of the observed green fluorescence was aggregated in small "island" structures, which were also found with 10 μM Cyt D (Figure 4.10). Using DIC microscopy (Figure 4.9; Merge), Cyt D of 2 μM caused very minor morphological changes in these cells and overall these results indicated that the increase of cargo uptake in A431 cells was due to the more subtle effects of this compound on the actin cytoskeleton rather than being due to gross morphological changes.

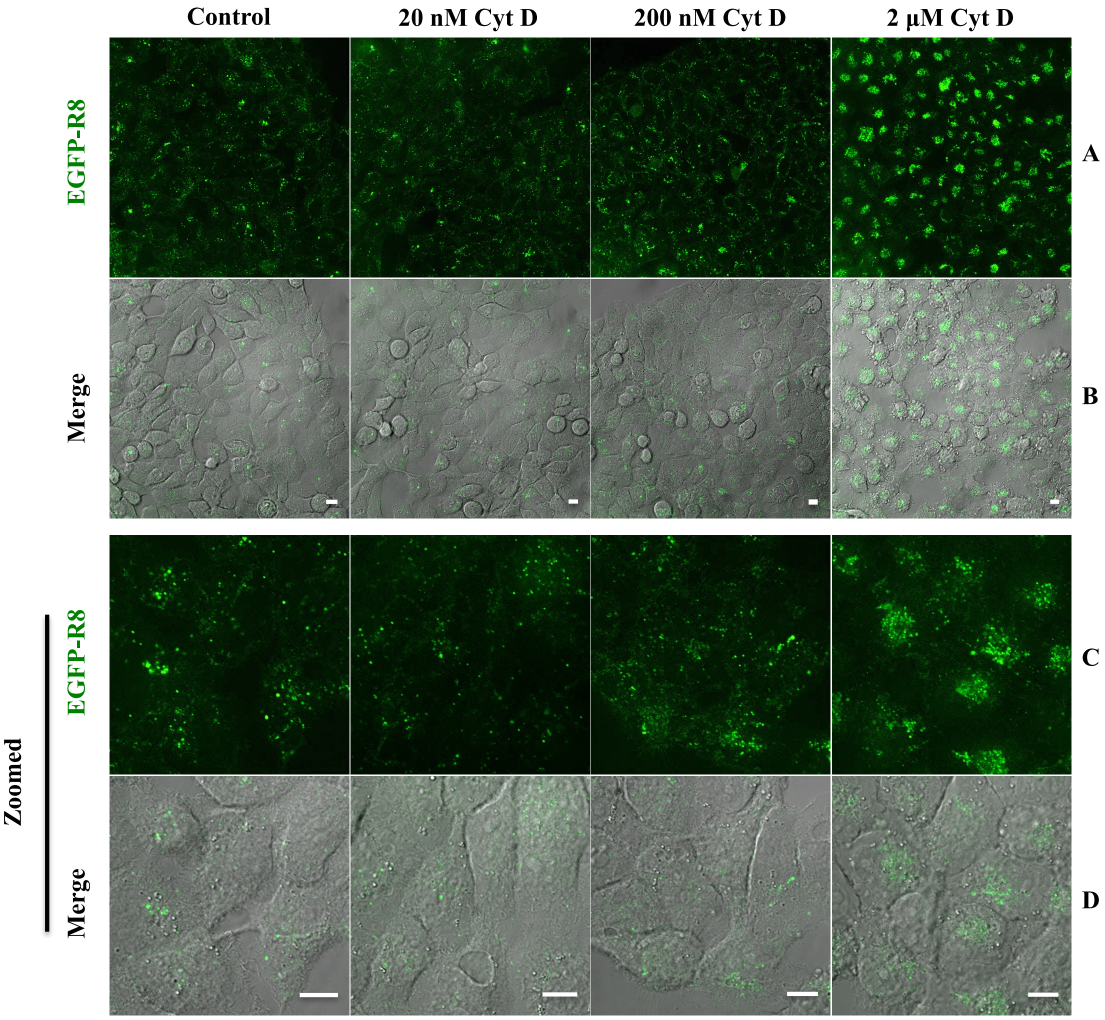

Figure 4.9 Effects of different concentration Cyt D on cell morphology and the cellular uptake of EGFP-R8 in A431 cells. Cells were incubated with 2 µM EGFP-R8 in the absence (control) or presence of 20 nM-2 µM Cyt D for 1 hr and washed with heparin. Cell associated fluorescence was analysed using confocal microscopy and shown are single projection images of fluorescence only (top rows) and merges of fluorescence and DIC of the same cells. C and D represent zoomed images from different fields of view of A and B. Scale bars 10 µm.

To further confirm that the enhanced cellular uptake of EGFP-R8 in A431 cells by Cyt D treatment was mediated by endocytosis, rather than energy- and receptor-independent direct uptake through plasma membrane translocation, the same live-cell experiments were performed at 4°C and 37°C respectively. Cells plated on 35 mm MatTek dishes were pre-treated in the absence (Figure 4.10B and D) or presence (Figure 4.10A and C) of 10 µM Cyt D for 15 min. For control cells, 2 µM of EGFP-R8 was then incubated with the cells for 1 hr at 4°C or 37°C. For Cyt D-treated cells, 2 µM of EGFP-R8 was incubated with the cells in presence of 10 µM Cyt D for 1 hr at 4°C or 37°C. The cells were then washed with heparin and analysed by live cell imaging confocal microscopy.

Fluorescent vesicular structures were observed scattered in the cytoplasm of the control cells incubated with cargo at 37°C (Figure 4.10C) but not of that at 4°C (Figure 4.10A). This confirmed that the EGFP-R8 uptake by A431 cells was primarily mediated by endocytosis. Similarly in Cyt D-treated cells, there was very little evidence of EGFP fluorescence in cells treated at 4°C (Figure 4.10B), but clear vesicular labelling in cells incubated at 37°C (Figure 4.10D). Again the uptake of EGFP-R8 in Cyt D treated cells was dramatically enhanced (Figure 4.10D) compared with control cells (Figure 4.10C). This confirmed the absolute requirement for endocytosis in mediating the cellular entry of EGFP-R8 in this cell line in the absence of Cyt D and in the presence of Cyt D to cause this cell accumulation phenomenon.

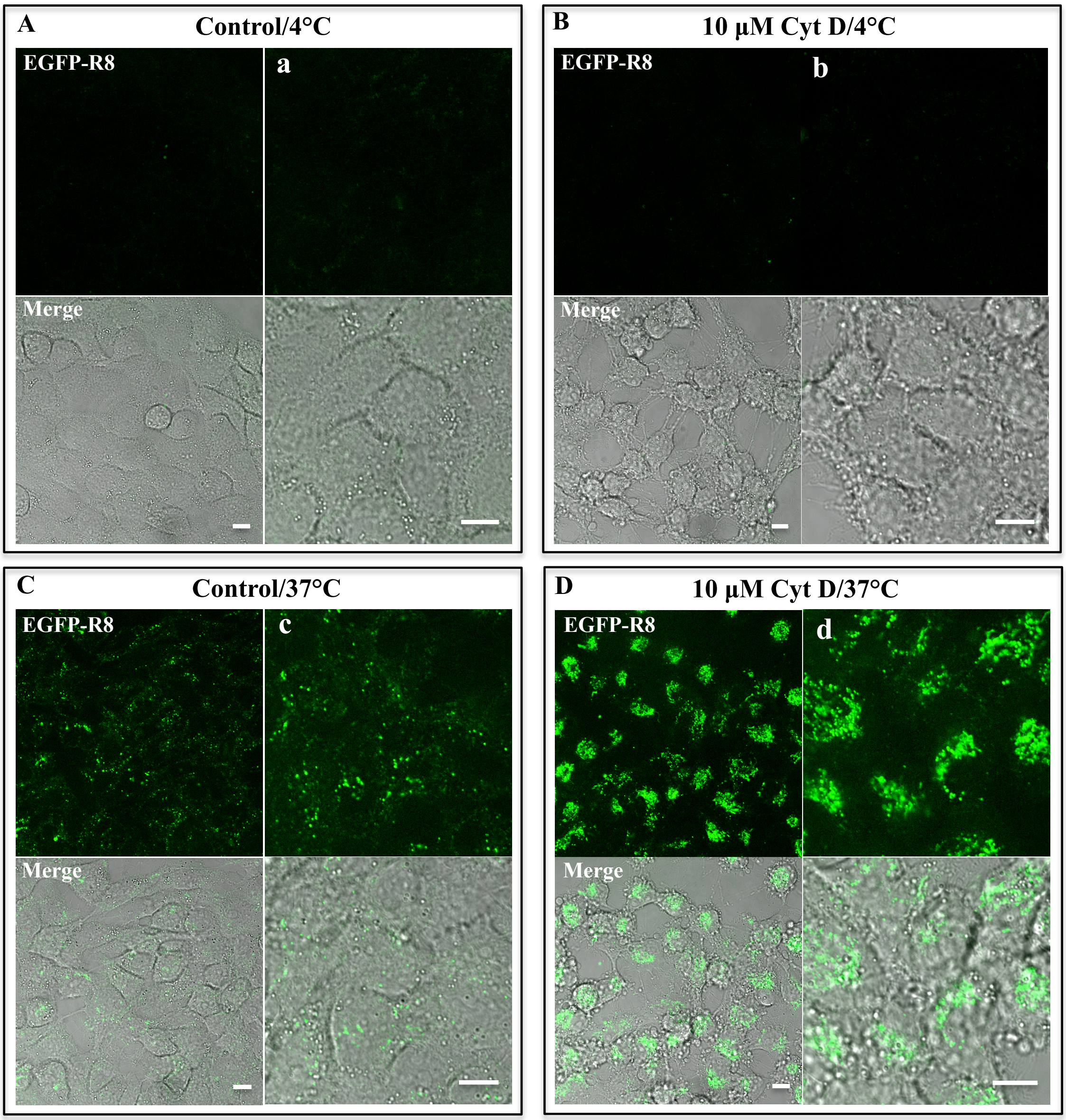

Figure 4.10 Cellular uptake of EGFP-R8 in control or Cyt D-treated A431 cells at 4°C or 37°C. Cells were incubated with 2 μM EGFP-R8 in the absence (control) or presence of 10 μM Cyt D for 1 hr at 4°C or 37°C, washed with heparin and analysed using confocal microscopy and shown are single projection images of fluorescence only (top rows) and merges of fluorescence and DIC of the same cells. Columns a-d represent zoomed images from different fields of view. Scale bars 10 μm.

4.2.7 Effects of latrunculin B (Lat B) on the actin architecture and EGFP-R8 uptake in A431 cells

To identify the effects of Lat B on actin structures in A431 cells, cells were seeded on coverslips and cultured for 24 hr under tissue culture conditions, and then treated with 0-1.0 μM Lat B for 30 min. Then cells were fixed and labelled for the nucleus and actin and imaged by the optimised confocal microscopy method as previously described. Visible alterations in the actin organisation were detectable even at the lowest Lat B concentration of 0.1 μM (Figure 4.11). At this concentration, compared with control a larger number of small actin specks appeared at both the basal and CBA sections of the cells. At a Lat B concentration of 0.5 μM (Figure 4.11), actin specks/aggregations were extremely prominent especially at basal section, and also the cells started to round up and this was most noticeable in the CBA section. Figure 4.11 also shows that 1 μM Lat B caused a major disruption of the actin organisation and resulted in visualisation of large amorphous actin masses throughout the cells. Experiments were then performed in cells pre-incubated with 0.5 μM Lat B or 10 μM Cyt D that were then incubated with EGFP-R8. As expected, Cyt D treated cells had higher fluorescence compared with control cells and the same effects were also seen in Lat B treated cells that similarly accumulated the fluorescence in a perinuclear region (Figure 4.12). Thus the overall effects of these two agents was the same suggesting they influence the uptake of this CPP conjugate via a very similar if not identical mechanism of action.

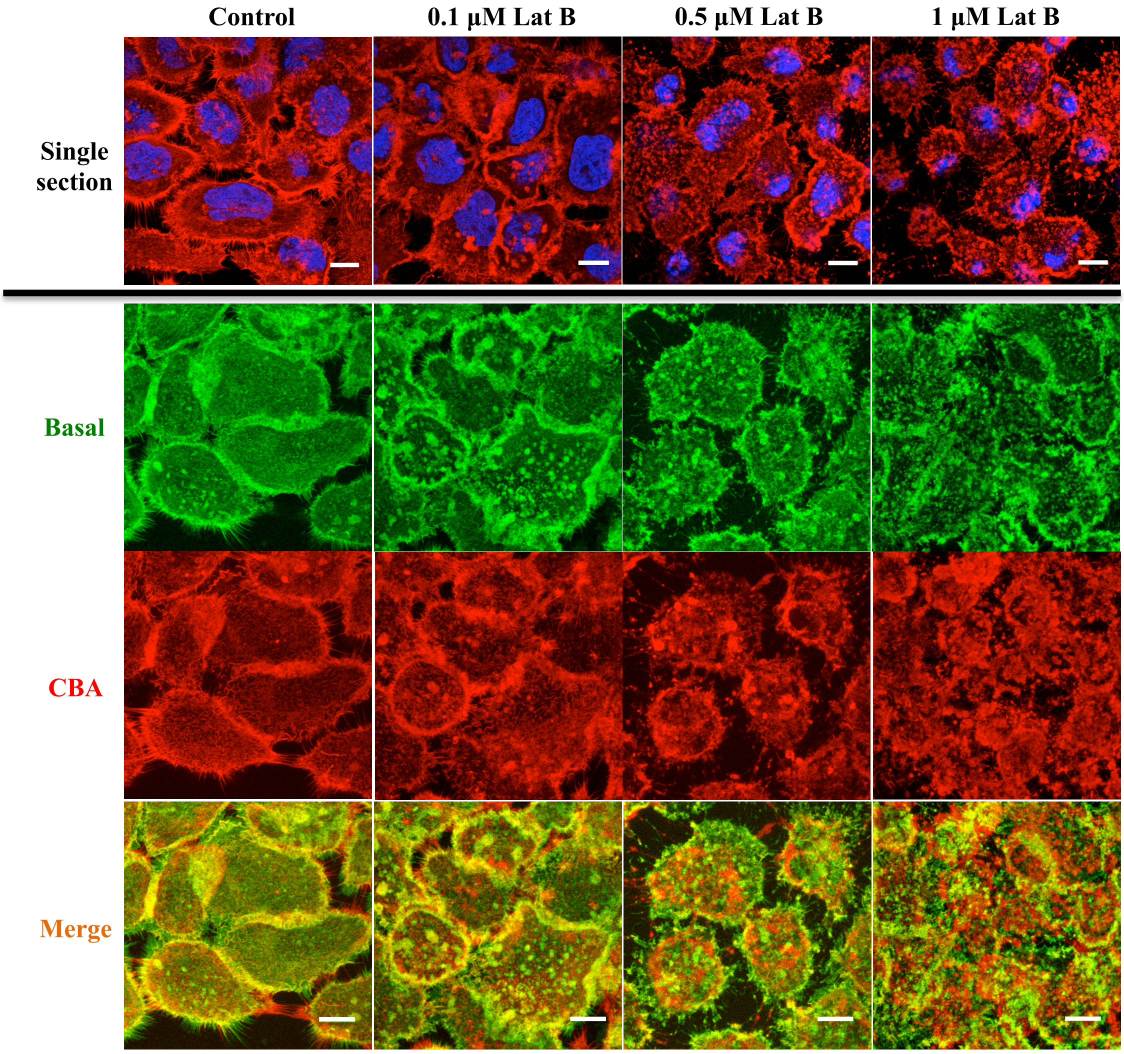

Figure 4.11 Effects of Lat B on the actin architecture in A431 cells. Cells on coverslips were treated either with diluent control (0.1% DMSO) or 0.1-1.0 µM Lat B for 30 min before fixing and staining with Rh-P and Hoechst. Images were acquired as described in section 4.2.1. Single sections show the overall distribution of the actin relative to the nucleus and highlight the effects of the compound on 6-10 cells to give a better overview of the compound effects. Images below the black line show the actin arrangement of 4-5 cells (from other fields of view of single sections) from different z-regions. Scale bars 10 µm.

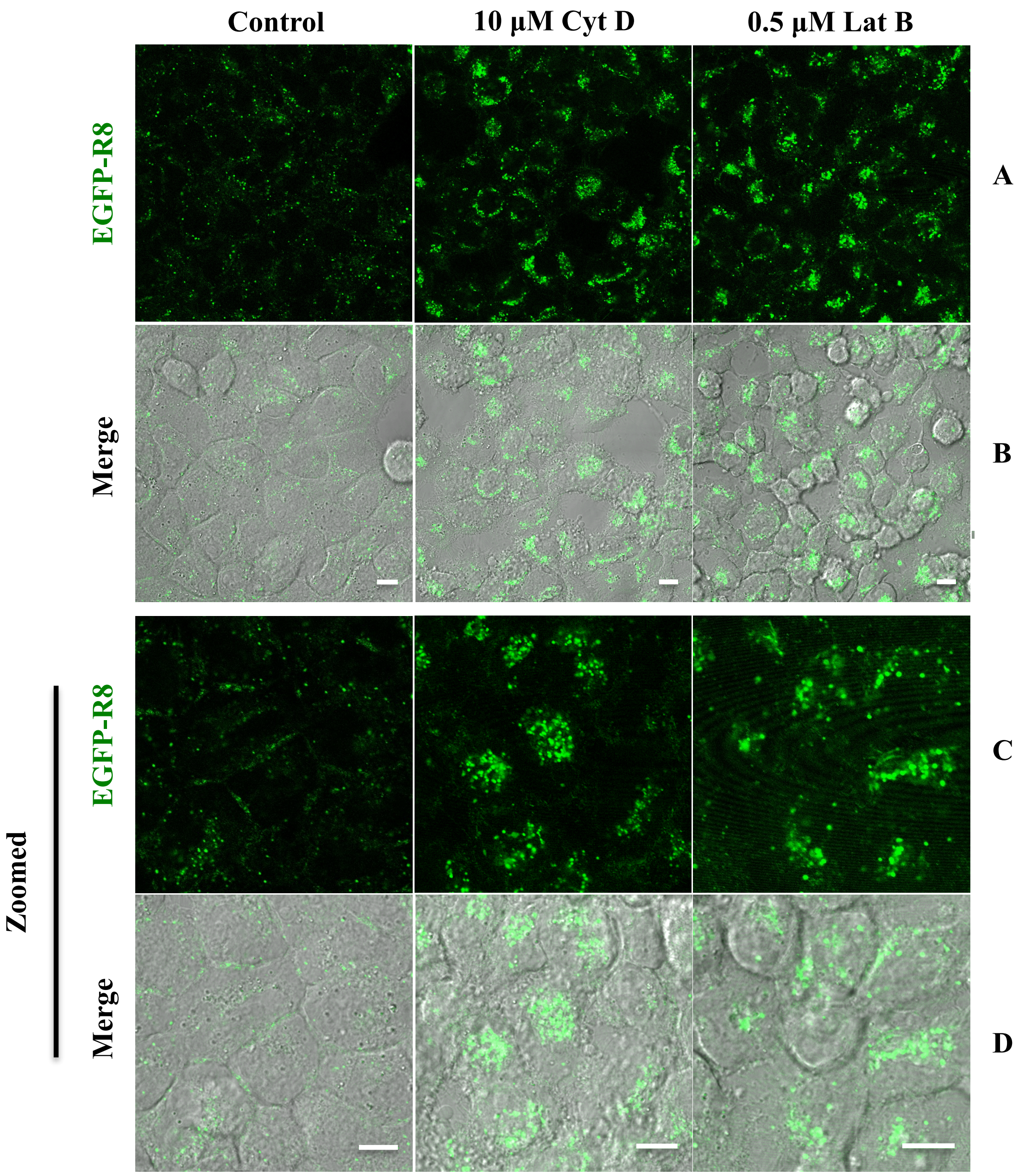

Figure 4.12 Effects of Lat B and Cyt D on the cellular uptake of EGFP-R8 in A431 cells. Cells were incubated with 2 µM EGFP-R8 in the absence (control) or presence of 0.5 µM Lat B or 10 µM Cyt D for 1 hr and washed in heparin. Cell associated fluorescence was analysed using confocal microscopy and shown are single projection images of fluorescence only (top rows) and merges of fluorescence and DIC of the same cells. C/D represent zoomed images from different fields of view of A/B. Scale bars 10 µm.

4.2.8 Effects of jasplakinolide (JAS) on the actin architecture and EGFP-R8 uptake in A431 cells

As described in Section 4.1.1 JAS is thought to stabilise actin fibres but has also been shown to affect actin assembly. Based on the similar effects of Cyt D and Lat B on actin and EGFP-R8 uptake it was interesting to investigate whether similar effects would be observed with this agent. A431 cells grown on coverslips were treated with concentrations of JAS ranging from 0.2 to 4 µM for 45 min. Then cells were fixed with formaldehyde and labelled for the nucleus and actin and imaged by confocal microscopy as previously described for Cyt D and Lat B. Compared with control cells, no visible changes in actin organisation were observed in both basal and CBA sections of cells (Figure 4.13A) until the concentration of JAS reached 2 µM (Figure 4.13B). At this concentration, filamentous actin staining almost completely disappeared and only some small actin aggregates and large actin patches could be detected in a number of cells. At higher JAS concentration (4 µM) cellular F-actin staining was no longer visible (Figure 4.13C).

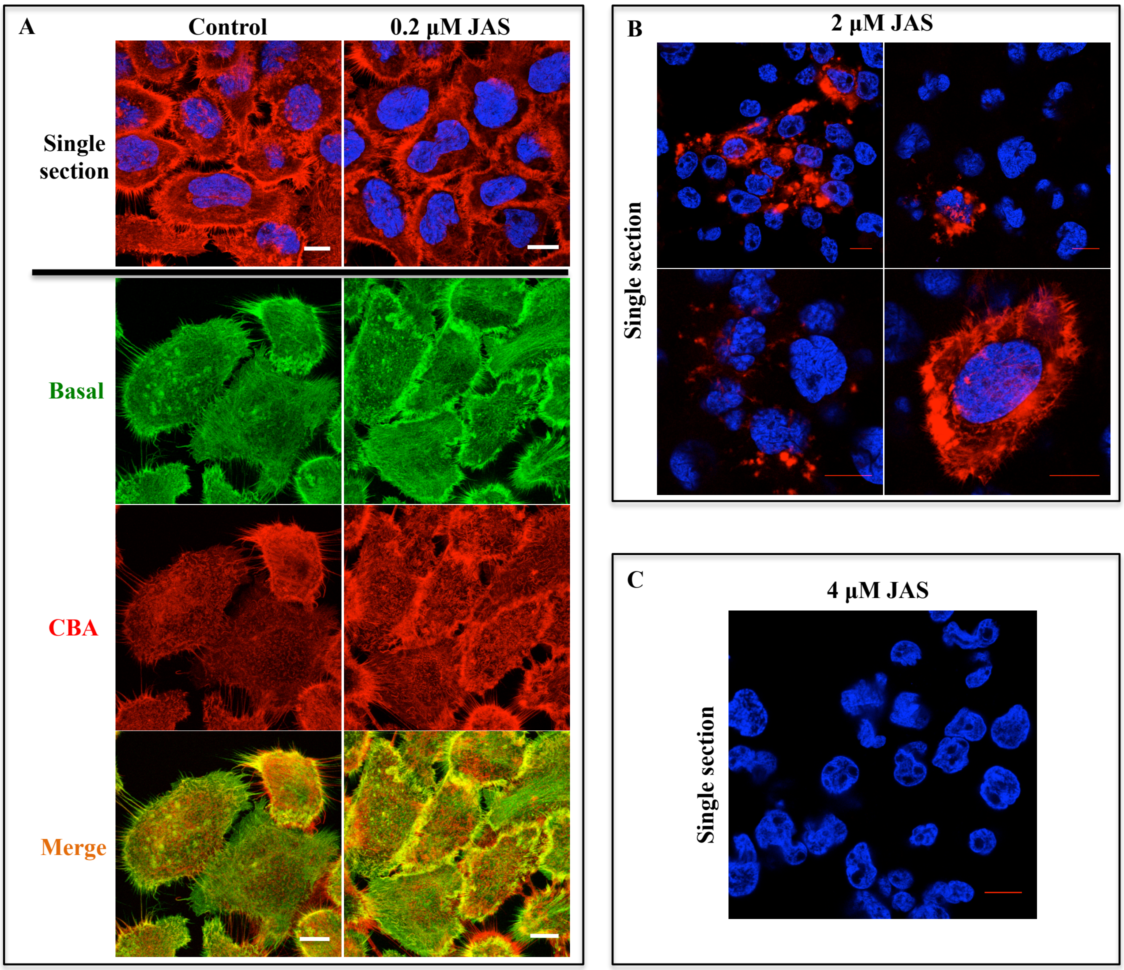

Figure 4.13 Effects of JAS on the actin architecture in A431 cells. Cells on coverslips were treated either with diluent control (0.1% DMSO) or 0.2-4.0 µM JAS for 45 min before fixing and staining with Rh-P and Hoechst. Images were acquired as described in section 4.2.1. Single sections in (A) show the overall distribution of the actin relative to the nucleus and highlight the effects of the compound on 6-8 cells to give a better overview of the compound effects and images below the black line show the actin arrangement of 3-4 cells (from other fields of view of single sections) from different z-regions. Scale bars 10 µm.

EGFP-R8 uptake in JAS treated cells was studies as previously described. Cells were seeded on 35 mm MatTek dishes and pre-treated with or without 2-8 µM JAS for 45 min. Then the cells were incubated for 1 hr with 2 µM of EGFP-R8 in the continued presence or absence of the appropriate concentration of the compound. The cells were then washed and analysed by live cell imaging confocal microscopy. The influence of JAS on the uptake of EGFP-R8 was evident at 2 µM, a concentration that, as previously shown, strongly disrupted the actin cytoskeleton. At this concentration, JAS increased cell fluorescence in vesicular structures and also altered their distribution in cytoplasm from scattered to clustered. The same uptake experiment was also performed with a lower JAS concentration (0.8 µM) that showed little effects on cell morphology and the cellular uptake of EGFP-R8 (Appendix 3). As the JAS concentration was increased to 4 or 8 µM, the enhancement in cargo uptake by this compound became more pronounced and strongly fluorescent clustered structures could be observed in most of the imaged cells (Figure 4.14). Thus though the effects of JAS on actin distribution was very different to that observed by Cyt D and Lat B, the overall effects of the three compounds on the uptake of EGFP-R8 was the same.

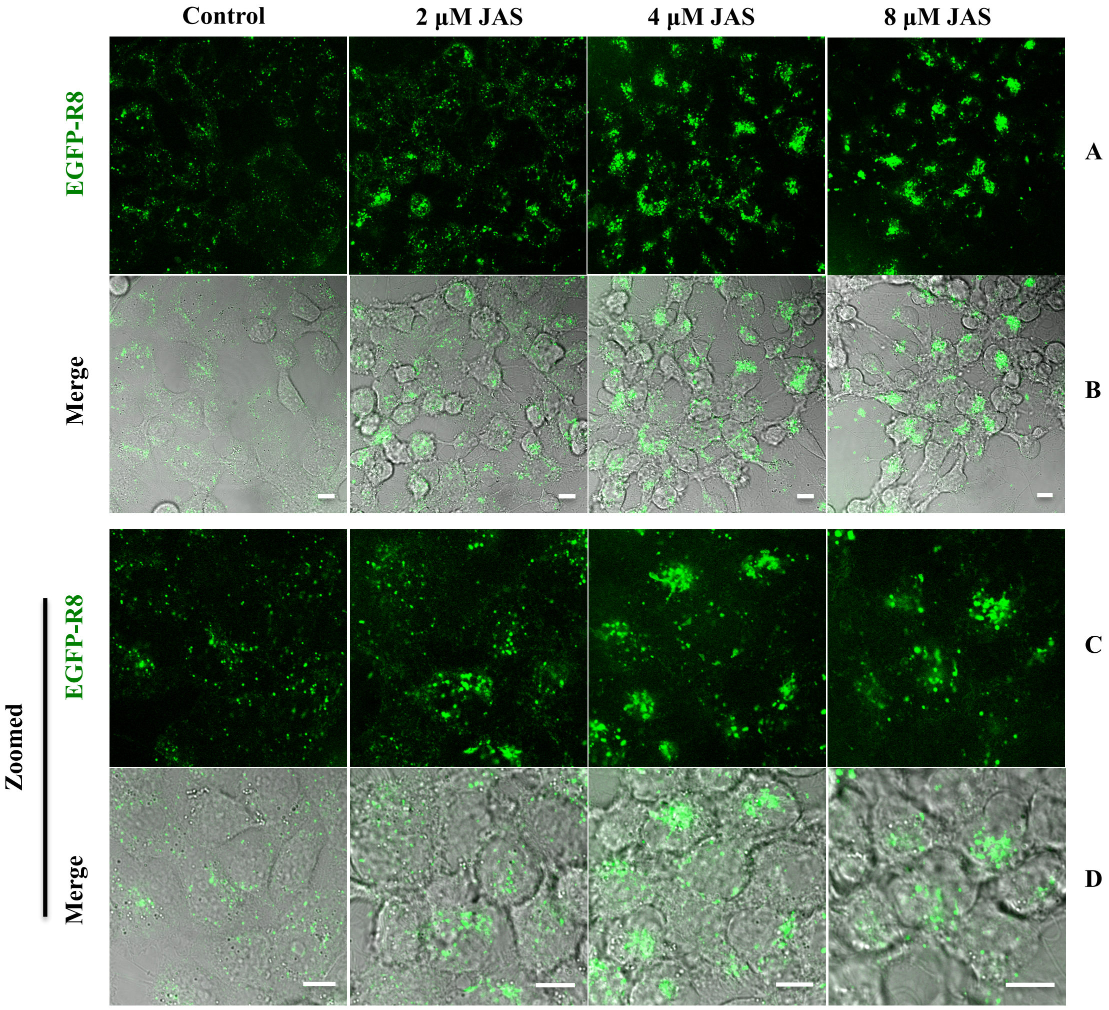

Figure 4.14 Effects of JAS on the cellular uptake of EGFP-R8 in A431 cells. Cells were incubated with 2 µM EGFP-R8 in the absence (control) or presence of 2-8 JAS µM for 1 hr and washed thoroughly using heparin. Cell associated fluorescence was analysed using confocal microscopy and shown are single projection images of fluorescence only (top rows) and merges of fluorescence and DIC of the same cells. C/D represent zoomed images from different fields of view of A/B. Scale bars 10 µm.

4.2.9 Effects of Y27632 on the actin architecture and EGFP-R8 uptake in A431 cells

Y27632 is known to influence actin dynamics through its direct effects on ROCK proteins and thus indirectly through myosin (Figure 4.1). No studies had been previously been performed on this agent in the laboratory and initially different concentrations were tested for their putative effects on the actin structures in A431 cells using the methods described for the other actin inhibitors. Initially, concentrations 1 and 10 µM were examined based on published observations (Ishizaki et al., 2000, Hoang et al., 2004). Figure 4.15 demonstrates that no visible changes in the organisation of the actin cytoskeleton were detected even at 10 µM. This concentration was used in previous studies showing effects on actin morphology (Darenfed et al., 2007). Higher concentrations of Y27632 (50 and 100 µM) (Figure 4.16) induced the formation of a large number of actin needles that were mostly running perpendicular to the plasma membrane (Figure 4.16Z). It should be noted that the cortical actin network was still evident in cells treated with these concentrations of Y27632. In contrast, upon treatment with Cyt D of lower concentrations the cortical actin in A431 cells was thinned out or even disappeared (Figure 4.8).

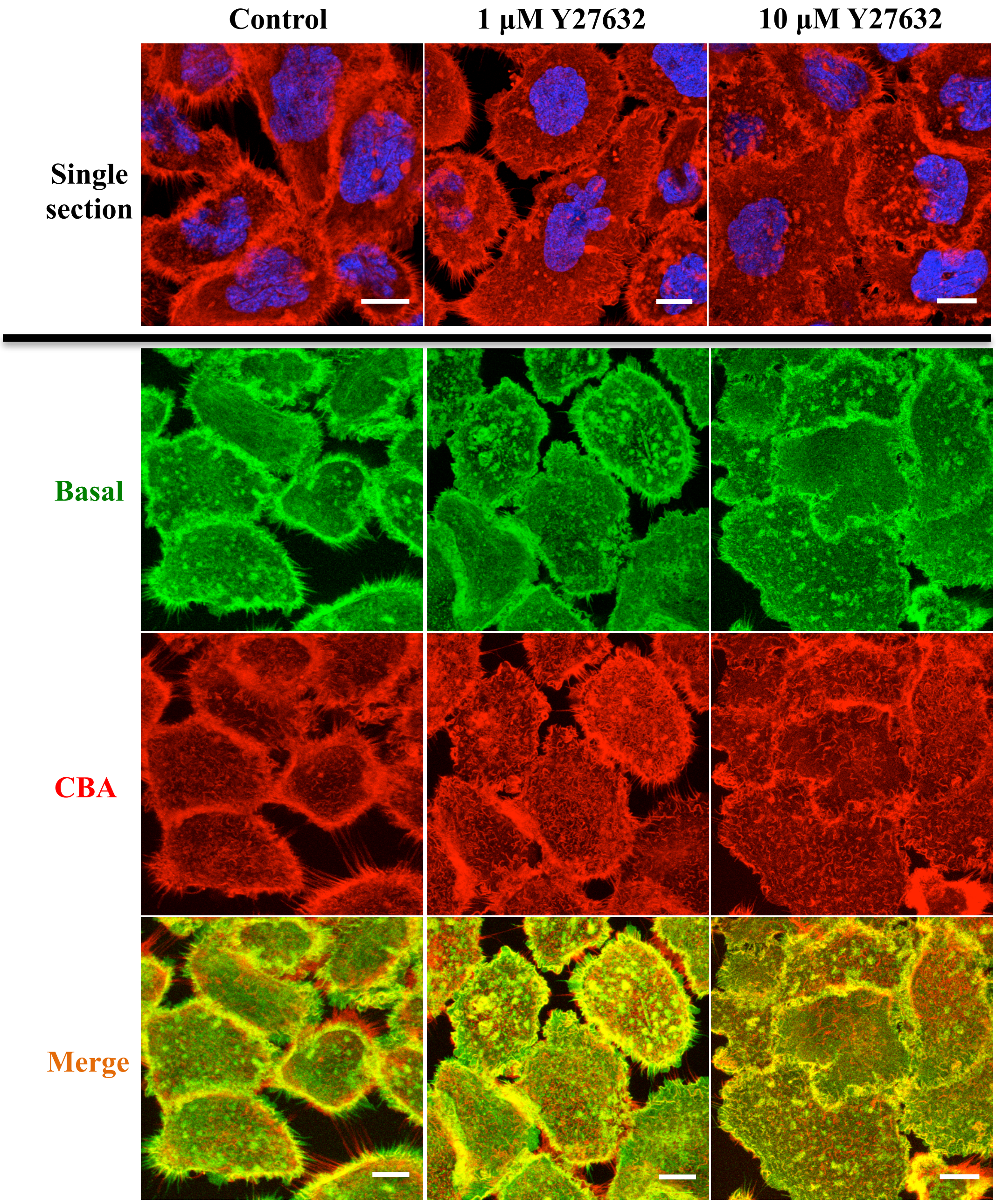

Figure 4.15 Effects of Y27632 (low concentrations) on the actin architecture in A431 cells. Cells on coverslips were treated either with diluent control (D-MEM) or Y27632 of 1 or 10 µM for 4 hr before fixing and staining with Rh-P and Hoechst. Images were acquired as described in section 4.2.1. Single sections show the overall distribution of the actin relative to the nucleus and images shown below the black line provide information on the actin arrangement of cells (from other fields of view of single sections) from different z-regions. Scale bars 10 µm.

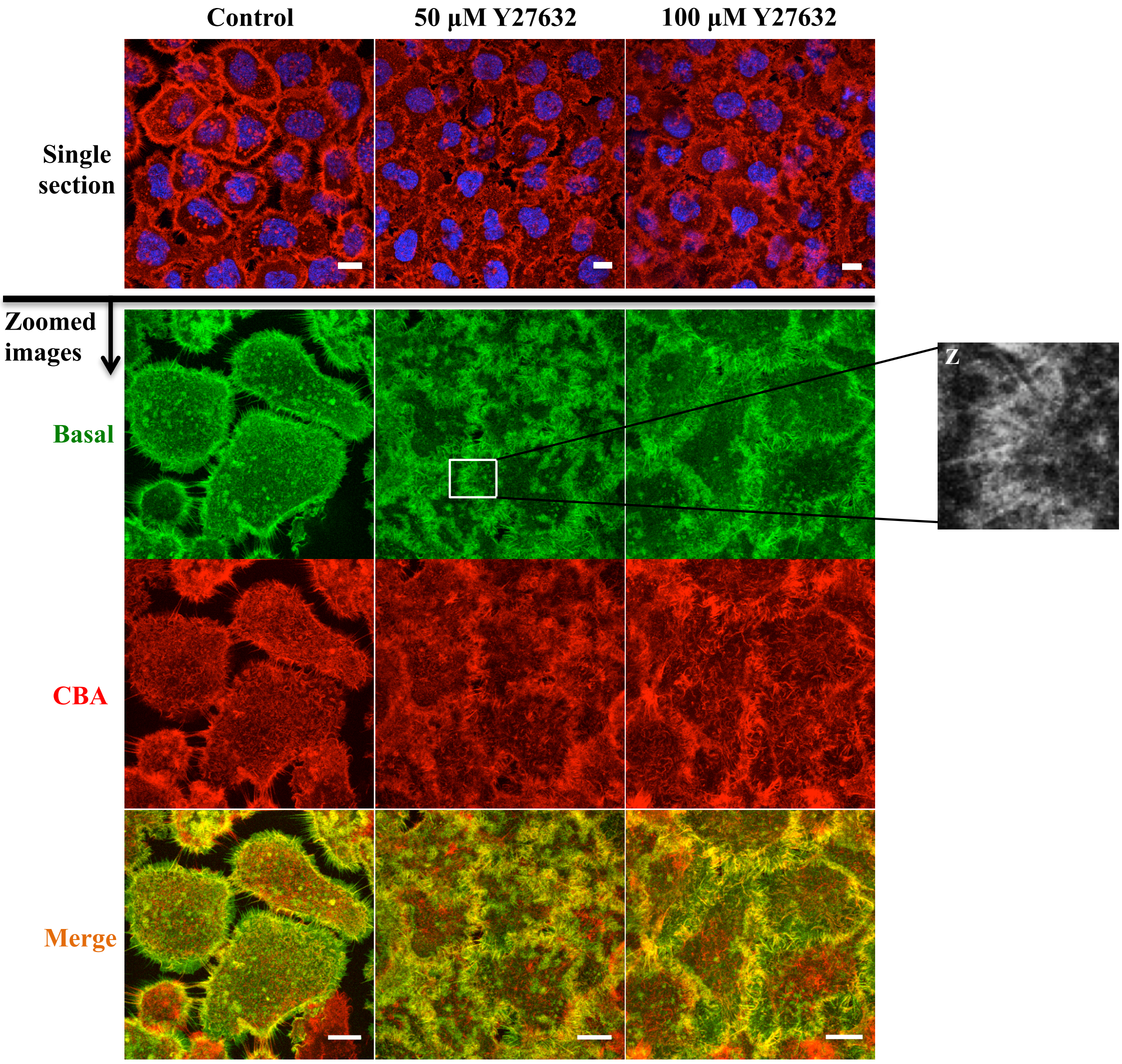

Figure 4.16 Effects of Y27632 (high concentrations) on the actin architecture in A431 cells. Cells on coverslips were treated either with diluent control (D-MEM) or 50, 100 µM of Y27632 for 4 hr before fixing and staining with Rh-P and Hoechst. Images were acquired as described in section 4.2.1. Single sections show the overall distribution of the actin relative to the nucleus and highlight the effects of the compound on more cells to give a better overview of the compound effects and zoomed images show the actin arrangement of 3-4 cells from different z-regions. Scale bars 10 µm.

The effects of Y27632 on the cellular uptake of EGFP-R8 was then investigated at various concentrations 1-100 µM. A431 cells seeded in 35mm MatTek dishes were pre-treated with or without 1-100 µM Y27632 for 4 hr. EGFP-R8 (2 µM) was then incubated with the cells in the presence or absence of the appropriate concentration of Y27632 for 1 hr. The cells were then washed and analysed by live cell imaging confocal microscopy. Only minimal effects were observed in cells treated with low concentrations (1 and 10 µM) of this compound (Figure 4.17) and in comparison with control cells, EGFP-R8 uptake was increased slightly in cells treated with 50 μM Y27632 but this increase was more apparent in cells exposed to 100 μM of this agent (Figure 4.18). Interestingly in contrast to the Cyt D treatment, the observed fluorescent vesicular structures in Y27632 treated cells distributed in a scattered manner, which was similar to the pattern in control cells. Moreover, unlike Cyt D and other actin disruptors previously used, Y27632 treatment did not show any significant morphological changes (Figure 4.17 and 4.18; Merge).

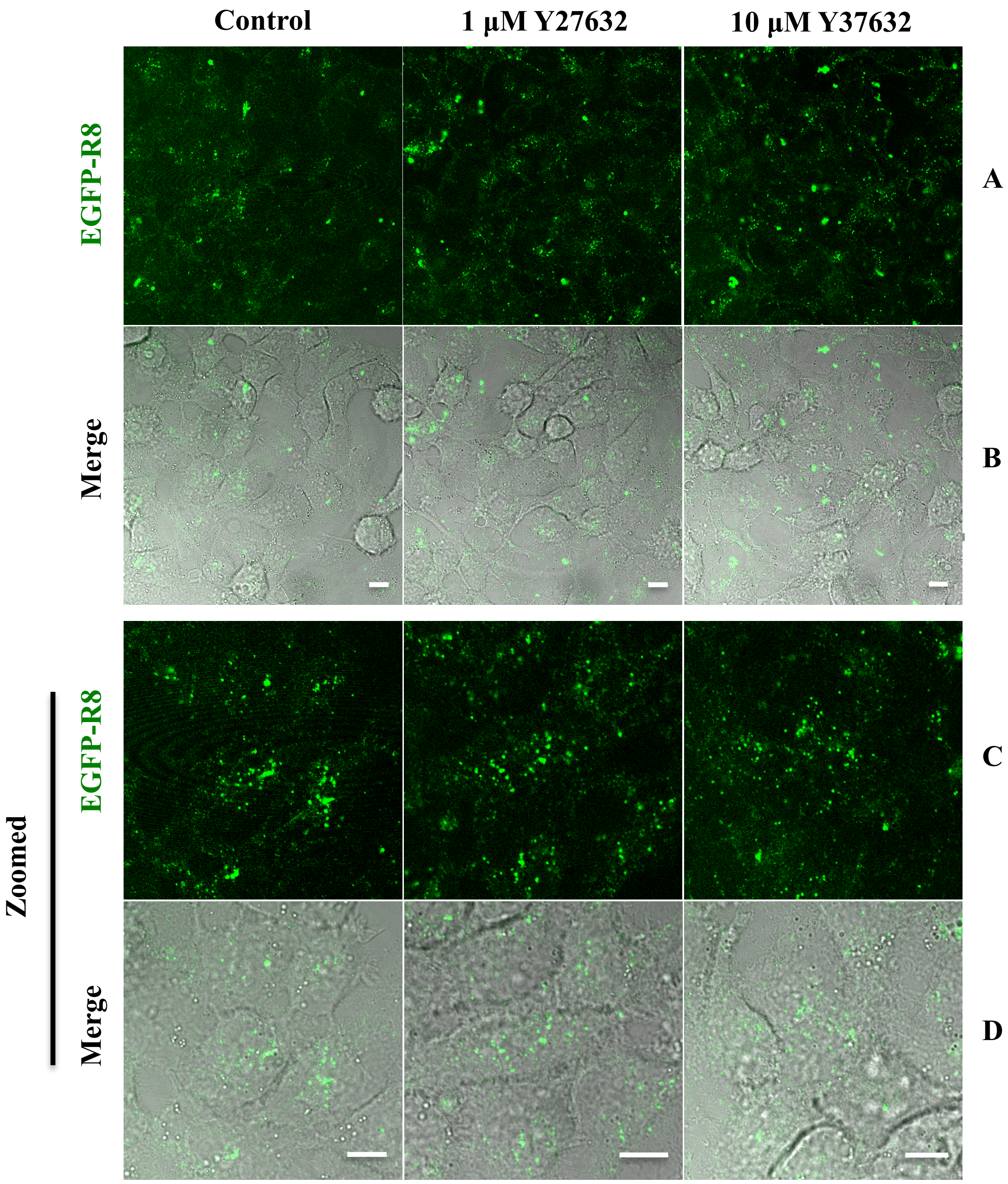

Figure 4.17 Effects of Y27632 (low concentrations) on the cellular uptake of EGFP-R8 in A431 cells. Cells were incubated with 2 µM EGFP-R8 in the absence (control) or presence of 1 or 10 µM Y27632 for 4 hr and washed with heparin. Cell associated fluorescence was analysed using confocal microscopy and shown are single projection images of fluorescence only (top rows) and merges of fluorescence and DIC of the same cells. C/D represent zoomed images from different fields of view of A/B. Scale bars 10 µm.

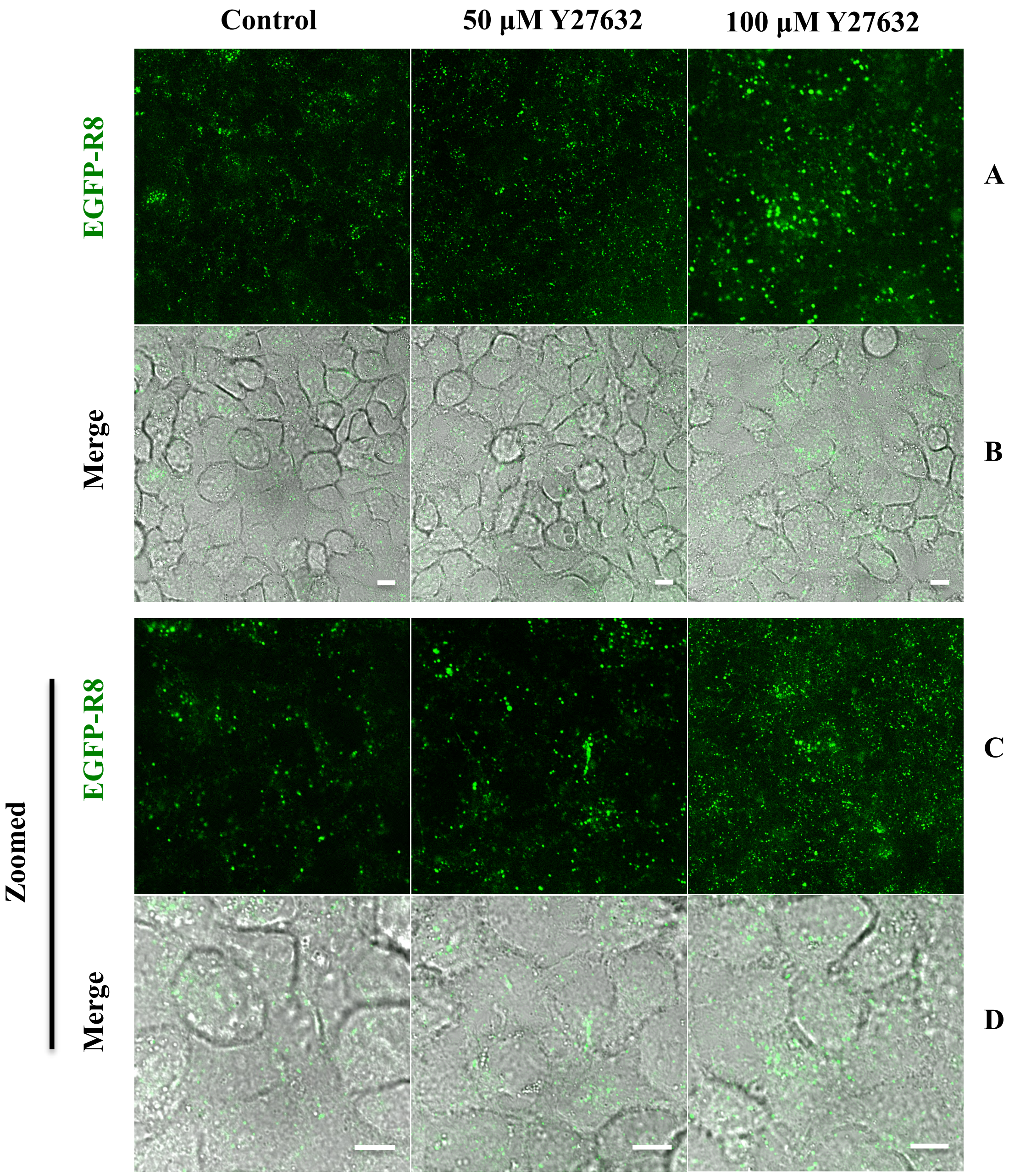

Figure 4.18 Effects of Y27632 (high concentrations) on the cellular uptake of EGFP-R8 in A431 cells. Cells were incubated with 2 µM EGFP-R8 in the absence (control) or presence of 50 or 100 µM Y27632 for 4 hr and washed with heparin. Cell associated fluorescence was analysed using confocal microscopy and shown are single projection images of fluorescence only (top rows) and merges of fluorescence and DIC of the same cells. C/D represent zoomed images from different fields of view of A/B. Scale bars 10 µm.

4.2.10 Visualisation of EGFP-R8 effects on the actin dynamics of control or A431 cells treated with actin inhibitors

In the previous sections, the changes made by a range of actin inhibitors on actin arrangement in A431 cells were examined individually and concentrations showing clear effects on actin and EGFP-R8 uptake were also identified. In this section further experiments were performed to investigate possible effects of EGFP-R8 on actin organisation in both control and compound-treated A431 cells. This was to determine whether EGFP-R8 influenced the actin cytoskeleton further to what was observed with the actin inhibitors. For these experiments cells on coverslips were pre-treated either with diluent control (0.1% DMSO or D-MEM) or the following concentrations of the actin inhibitors for the following times: 10 μM Cyt D for 15 min; 0.5 μM Lat B for 30 min; 0.8 μM JAS for 45 min or 50 μM Y27632 for 4 hr. Control or compound treated cells were then incubated with 2 μM EGFP-R8 for 1 hr. Cells were then washed with heparin before fixing and staining with Rh-P and Hoechst and imaging by the optimised confocal microscopy method. EGFP-R8 at this concentration did not induce any visible changes to the actin arrangement in control cells (Figure 4.19A and B); both the cortical actin running beneath the plasma membrane observed in basal sections and the reticular actin network shown in CBA sections appeared in normal order. This CPP-conjugate also had minimal effects on the actin reorganisation in Cyt D treated cells identified by disruption of actin meshwork, loss of cortical actin and the presence of patchy actin aggregations at the perinuclear regions (Figure 4.19C and D). The same was true of Lat B and Y27632 treated cells (Figure 4.19E and F and Figure 4.20E and F) where EGFP-R8 failed to have any notable effects.

In order to visualise the F-actin staining by Rh-P in JAS treated cells, the concentration of JAS was reduced from 2 μM to 0.8 μM, this was due to the fact that at 2 μM JAS either significantly reduced actin staining or removed it altogether (Figure 4.13). The cortical actin network and the actin meshwork throughout the cell body were completed disrupted by 0.8 μM JAS and replaced by extensive actin aggregation (Figure 4.20 C and D). Again addition of EGFP-R8 had no visible contribution to this actin disruption.

These results indicated that the internalisation of EGFP-R8 did not evidently stimulate the reorganisation of the actin network in either control or compound-treated A431 cells.

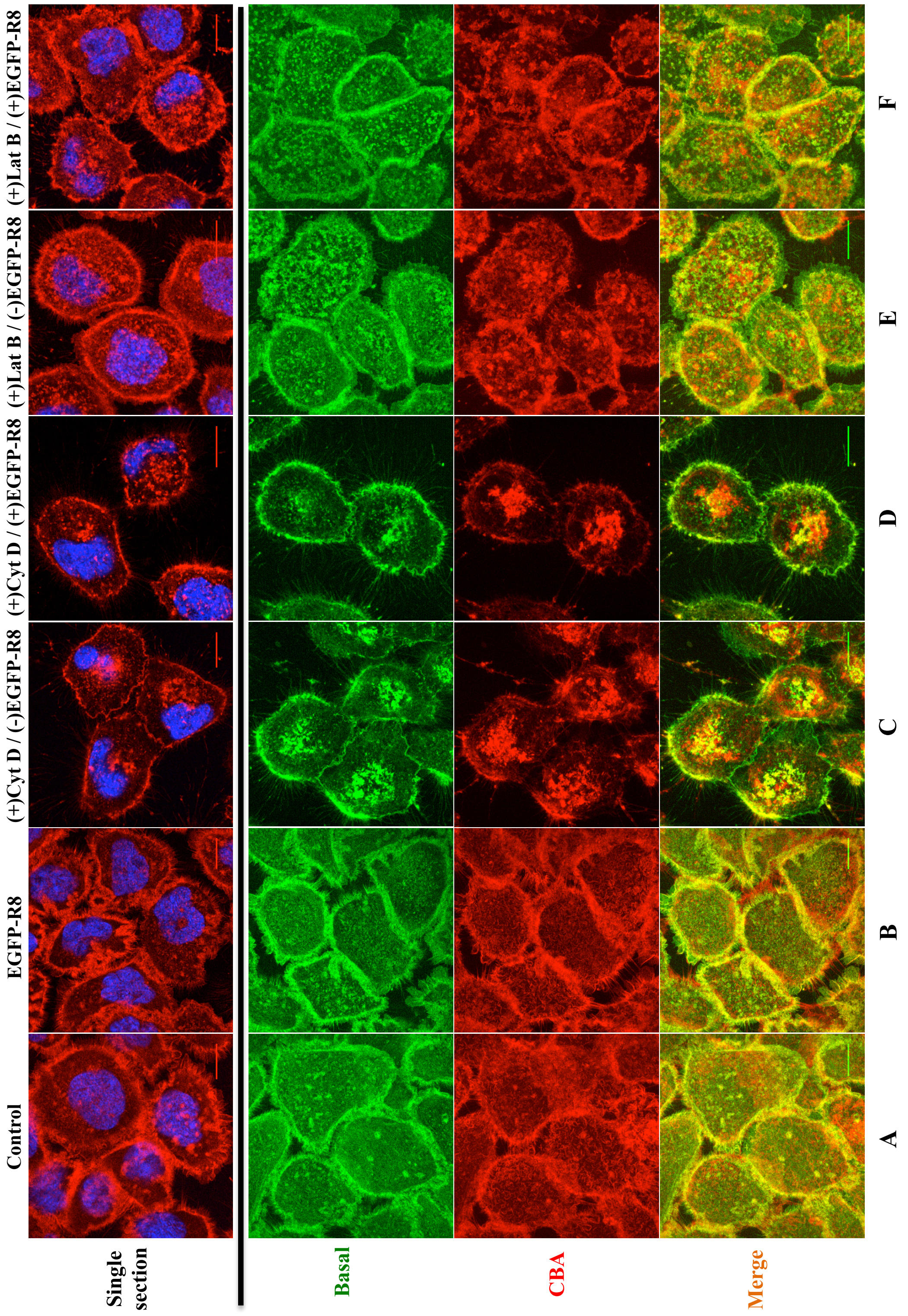

Figure 4.19 EGFP-R8 effects on the organisation of the actin architecture in control and A431 cells treated with Cyt D or Lat B. Cells on coverslips were pre-treated either with diluent control (0.1% DMSO), 10 µM Cyt D for 15 min or 0.5 µM Lat B for 30 min. Cells were then incubated with 2 µM EGFP-R8 in the continued absence (control) or presence of Cyt D or Lat B for 1 hr and washed with heparin before fixing and staining with Rh-P and Hoechst. Images were acquired as described in section 4.2.1. Single sections show the overall distribution of the actin relative to the nucleus and images shown below the black line provide information on the actin arrangement of cells (from other fields of view of single sections) from different z-regions. Scale bars 10 µm.

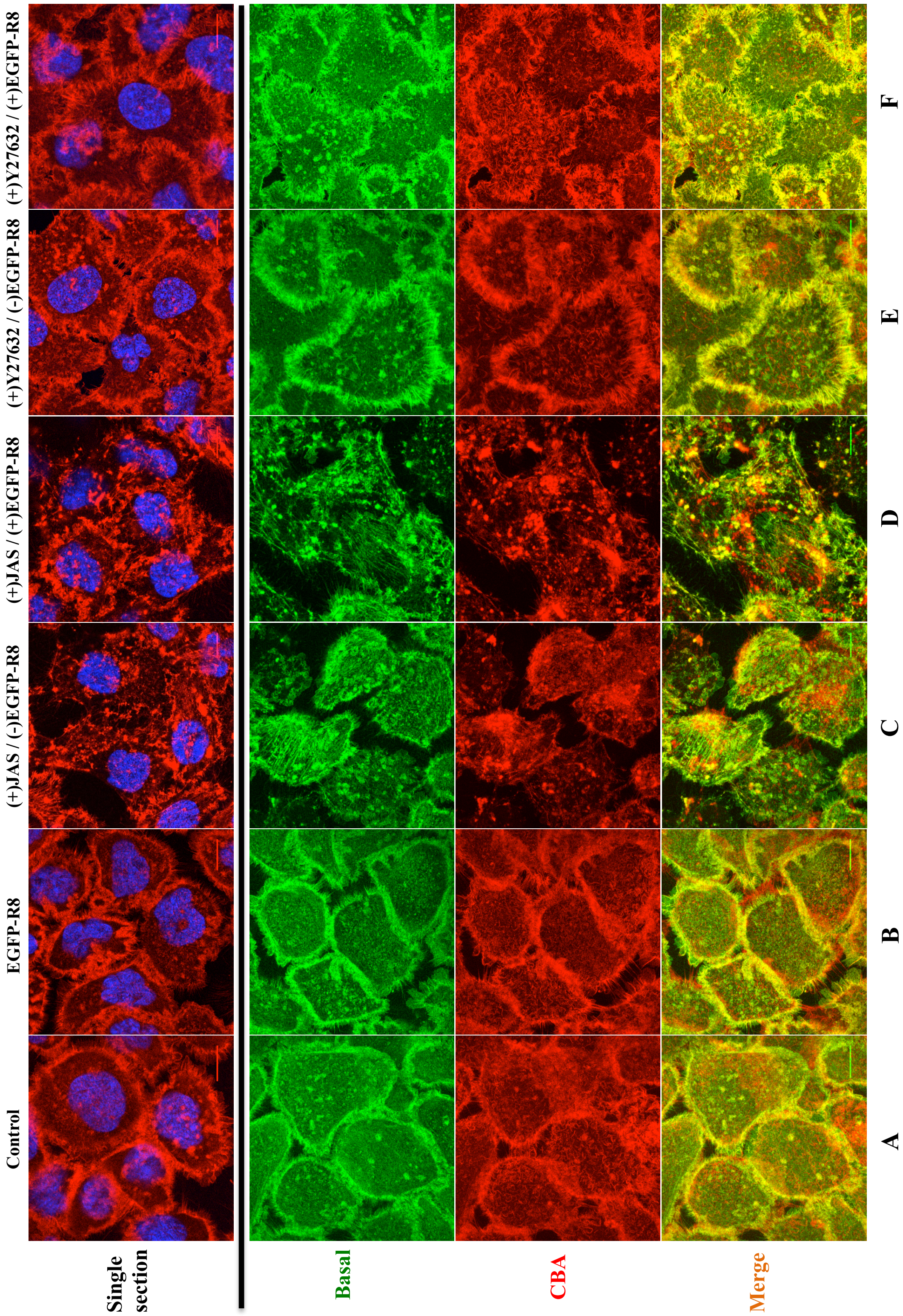

Figure 4.20 EGFP-R8 effects on the organisation of the actin architecture in control and A431 cells treated with JAS or Y27632. Cells on coverslips were pre-treated either with diluent control (0.1% DMSO for JAS or D-MEM for Y27632), 0.8 μM JAS for 45 min or 50 μM Y27632 for 4 hr. Cells were then incubated with 2 μM EGFP-R8 in the absence (control) or presence of JAS or Y27632 for 1 hr and washed with heparin before fixing and staining with Rh-P and Hoechst. Images were acquired as described in section 4.2.1. Single sections show the overall distribution of the actin relative to the nucleus and images shown below the black line provide information on the actin arrangement of cells (from other fields of view of single sections) from different z-regions. Scale bars 10 μm.

4.2.11 Effects of PP2 on the actin architecture and EGFP-R8 uptake in HeLa or A431 cells

In view of the described link between actin dynamics and SFKs (Section 4.1.1) new investigations were performed investigating the actin cytoskeleton and EGFP-R8 uptake in HeLa and A431 cells incubated with the SFK inhibitor PP2. Here, cells were seeded on coverslips and cultured for 24 hr under tissue culture conditions, and treated with or without 1, 10 or 25 μM PP2 for 48 hr. Then cells were then fixed and labelled for the nucleus and actin and imaged by confocal microscopy as previously described. The higher concentrations of PP2 (10 and 25 μM) resulted in significant toxicity in HeLa cells and most of the cells had lifted either before the fixing procedure or did so during this process (data not shown). A431 cells were less sensitive to PP2 but at 25 μM, toxicity again became a major factor (data not shown). Inhibition of cell growth by PP2 treatment at these concentrations was previously reported in a variety of cancer cell lines (Nam et al., 2002).

As shown in Figure 4.21, 1 μM PP2 had no visible effects on the actin architecture of HeLa cells and long actin stress fibres or bundles were well maintained. However in A431 cells, at of 1 or 10 μM, the agent PP2 stimulated actin polymerisation into long filamentous bundles (Figure 4.22), observed predominantly in CBA sections. The effects of PP2 alone or in combination of PP2 and Cyt D (an actin depolymeriser) on the cellular uptake of EGFP-R8 in both HeLa and A431 cells was then investigated. Cells in 35mm MatTek dishes were pre-treated with or without PP2 (1 μM only for HeLa cells and 1 or 10 μM for A431 cells) for 48 hr. Some of the non-treated and PP2 treated cells were further incubated with 10 μM Cyt D for an extra 15 min. Then EGFP-R8 (2 μM) was added to the cells in the continued presence or absence of 10 μM Cyt D for 1 hr. The cells were then washed and analysed by live cell imaging confocal microscopy.

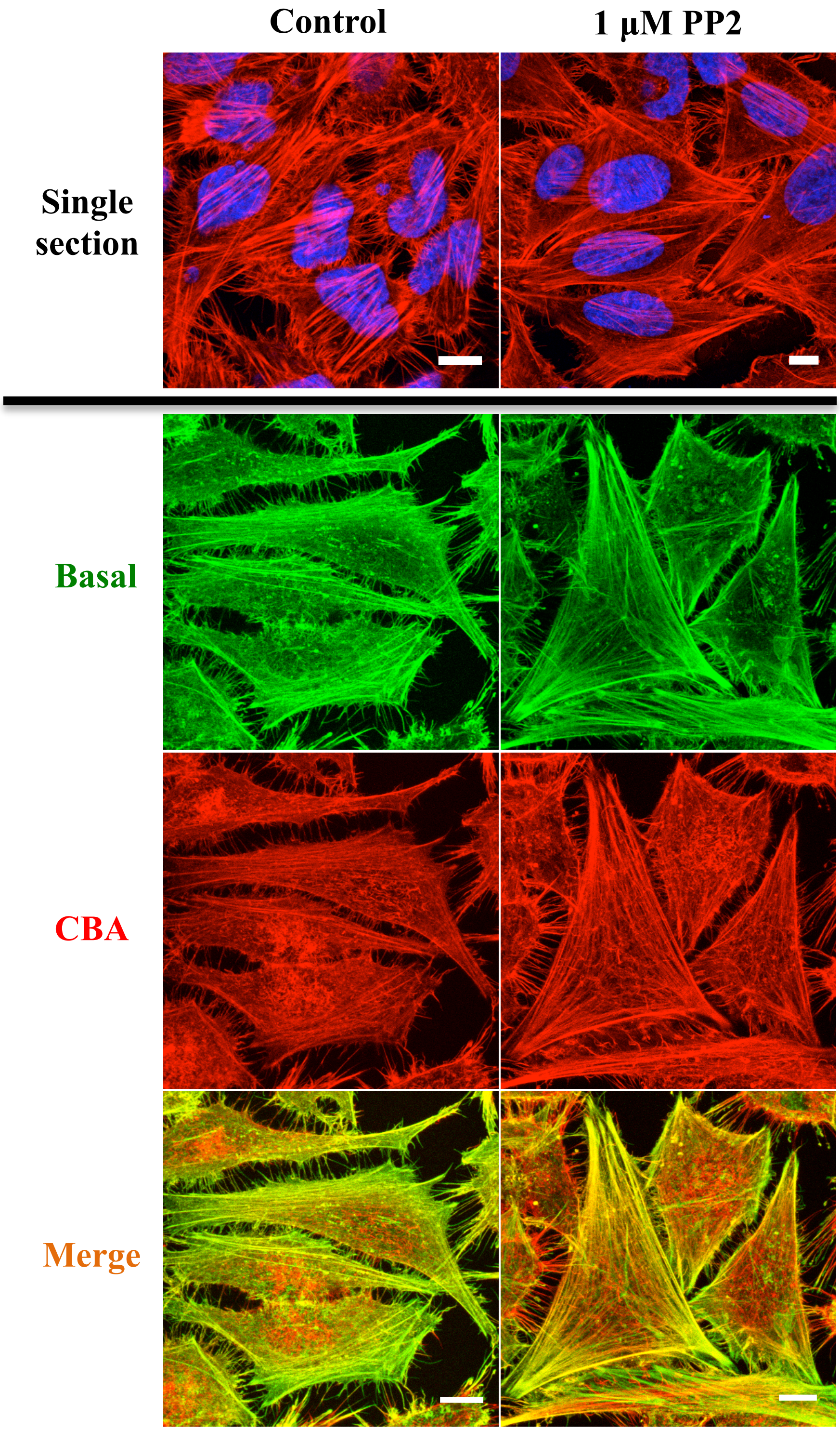

Figure 4.21 Effects of PP2 on the actin architecture in HeLa cells. Cells on coverslips were treated either with diluent control (0.1% DMSO) or PP2 of 1 µM for 48 hr before fixing and staining with Rh-P and Hoechst. Images were acquired as described in section 4.2.1. Single sections show the overall distribution of the actin relative to the nucleus and highlight the effects of the compound on more cells to give a better overview of the compound effects and images shown below the black line provide information on the actin arrangement of 2-3 cells (from other fields of view of single sections) from different z-regions. Scale bars 10 µm.

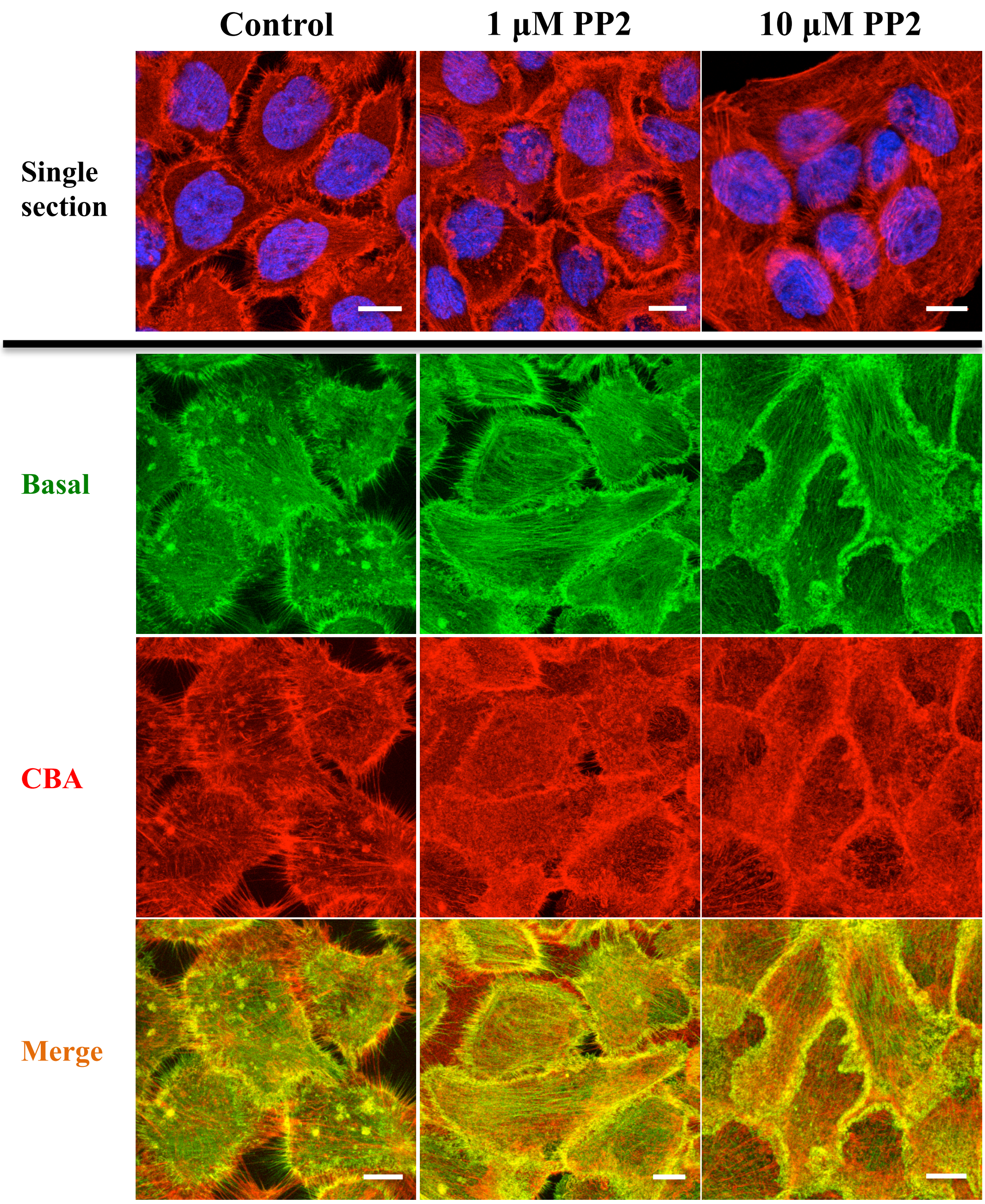

Figure 4.22 Effects of PP2 on the actin architecture in A431 cells. Cells on coverslips were treated either with diluent control (0.1% DMSO) or PP2 (1 or 10 µM) for 48 hr before fixing and staining with Rh-P and Hoechst. Images were acquired as described in section 4.2.1. Single sections show the overall distribution of the actin relative to the nucleus and images shown below the black line provide information on the actin arrangement of cells (from other fields of view of single sections) from different z-regions. Scale bars 10 µm.

PP2 at 1 µM had no visible effects on the delivery of EGFP-R8 into HeLa cells regarding the efficiency of uptake and the distribution of internalised cargo (Figure 4.23E-F). This was consistent with the observation on its effects on the actin cytoskeleton at this concentration (Figure 4.21). As already described in chapter 3, 10 μM Cyt D inhibited the uptake of EGFP-R8 by HeLa cells, however, this inhibition was prevented by the pre-treatment of the cells with 1 μM PP2 (Figure 4.23G-H). DIC also revealed clear morphological effects on the cells treated with Cyt D. A similar phenomenon was observed in A431 cells. In contrast to the striking increase of EGFP-R8 uptake by Cyt D, PP2 at 10 μM did not noticeably influence EGFP-R8 uptake by A431 cells (Figure 4.24E-F). But again the pre-treatment of PP2 eliminated the Cyt D mediated enhancement of cargo uptake (Figure 4.24G-H). Thus the effects of Cyt D on EGFP-R8 uptake could be reversed in these two cell lines by prior incubation with PP2.

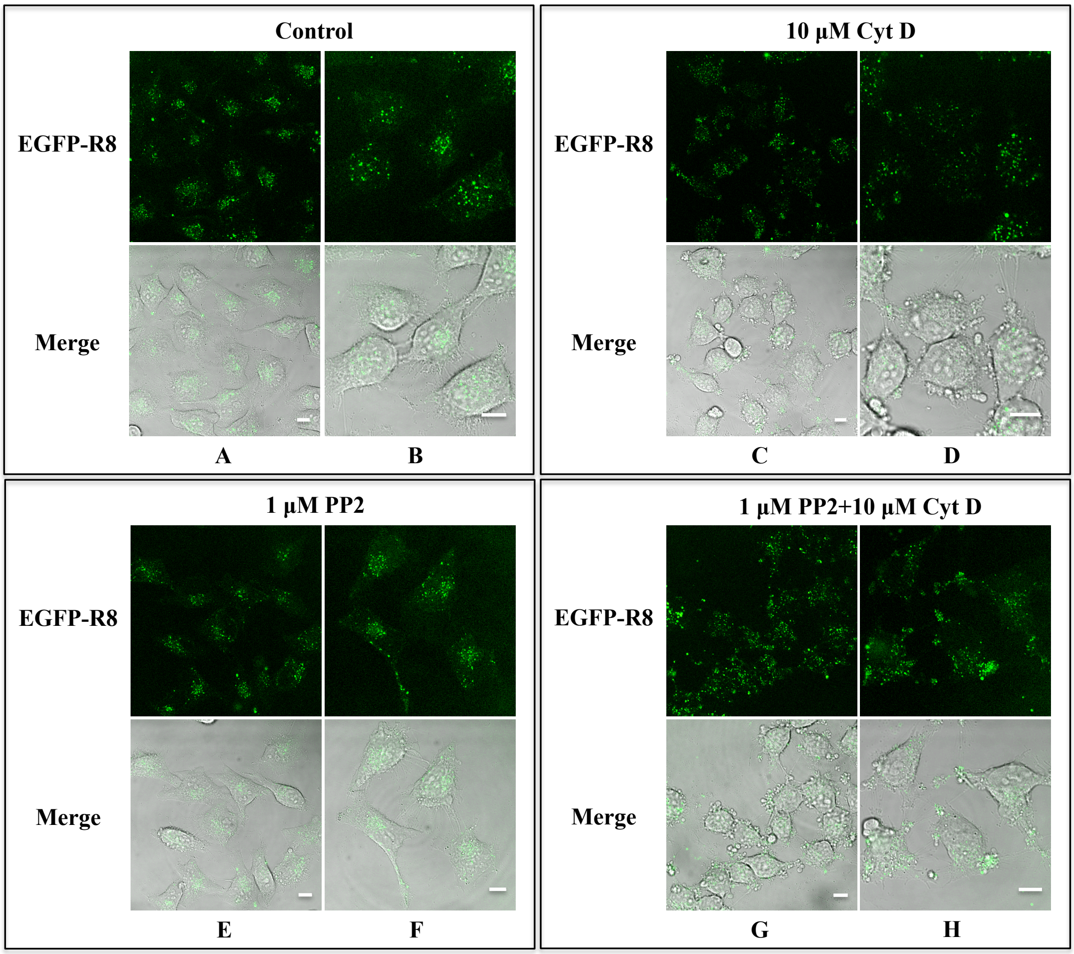

Figure 4.23 Effects of PP2 alone and the combination of PP2 and Cyt D on the cellular uptake of EGFP-R8 in HeLa cells. Cells were cultured and pre-treated either with diluent control (0.01% DMSO) or 1 μM PP2 for 48 hr at 37°C/5% CO_2. Cells were then incubated with or without 10 μM Cyt D for 15 min prior to a further incubation with 2 μM EGFP-R8 for 1 hr in the continued presence or absence of Cyt D. Cells were then washed with heparin, and cell-associated fluorescence was analysed by confocal microscopy. Shown are representative single projection images of fluorescence only (top rows) and merges of fluorescence and DIC of the same cells. Shown in column B, D, F and H are zoomed images obtained from different fields of view of A, C, E and G respectively. Scale bars 10 μm.

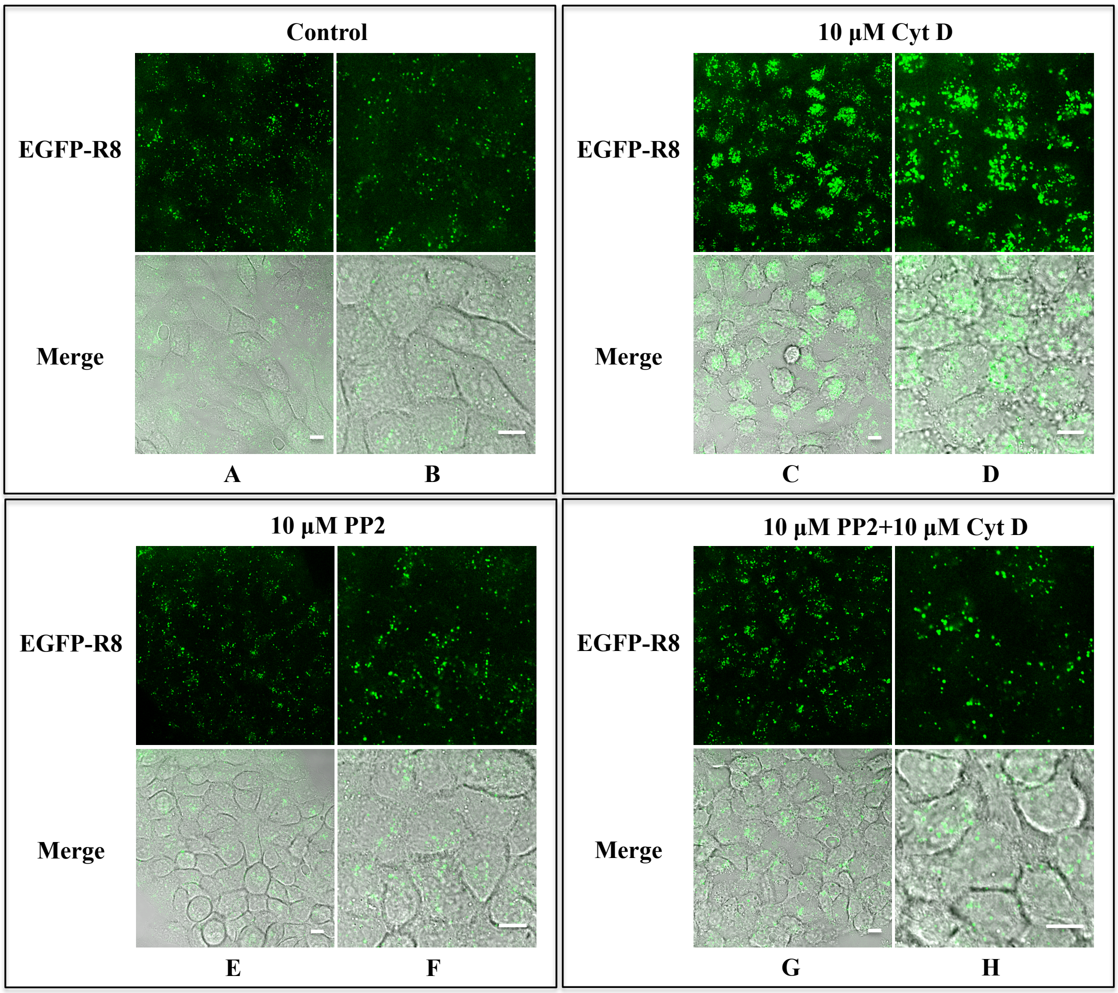

Figure 4.24 Effects of PP2 alone and the combination of PP2 and Cyt D on the cellular uptake of EGFP-R8 in A431 cells. Cells were cultured and pre-treated either with diluent control (0.1% DMSO) or 10 µM PP2 for 48 hr at 37°C/5% CO_2. Cells were then incubated with or without 10 µM Cyt D for 15 min prior to a further incubation with 2 µM EGFP-R8 for 1 hr in the continued presence or absence of Cyt D. Cells were then washed with heparin, and cell-associated fluorescence was analysed by confocal microscopy. Shown are representative single projection images of fluorescence only (top rows) and merges of fluorescence and DIC of the same cells. Shown in column B, D, F and H represent zoomed images obtained from different fields of view of A, C, E and G respectively. Scale bars 10 µm.

Further investigations into the effects of the combination of PP2 and Cyt D on the actin cytoskeleton in A431 cells were performed. For this, cells seeded on coverslips were cultured for 24 hr under tissue culture conditions and were pre-treated with or without 10 µM PP2 for 48 hr. At the very end of the experiment, some of the non-treated and PP2 treated cells were further incubated with 10 µM Cyt D for 15 min. The cells were then washed, fixed and labelled for the nucleus and actin, and then imaged by confocal microscopy as previously described. As expected, Cyt D alone induced a dramatic disruption of the actin organisation, while PP2 alone stimulated actin assembly into filament bundles and these structures were clearly observed in the CBA section (Figure 4.25). Interestingly, the pre-incubation with PP2 failed to prevent Cyt D-mediated actin disruption, although, as previously shown, this compound abrogated the Cyt D-mediated increase in EGFP-R8 uptake (Figure 4.25).

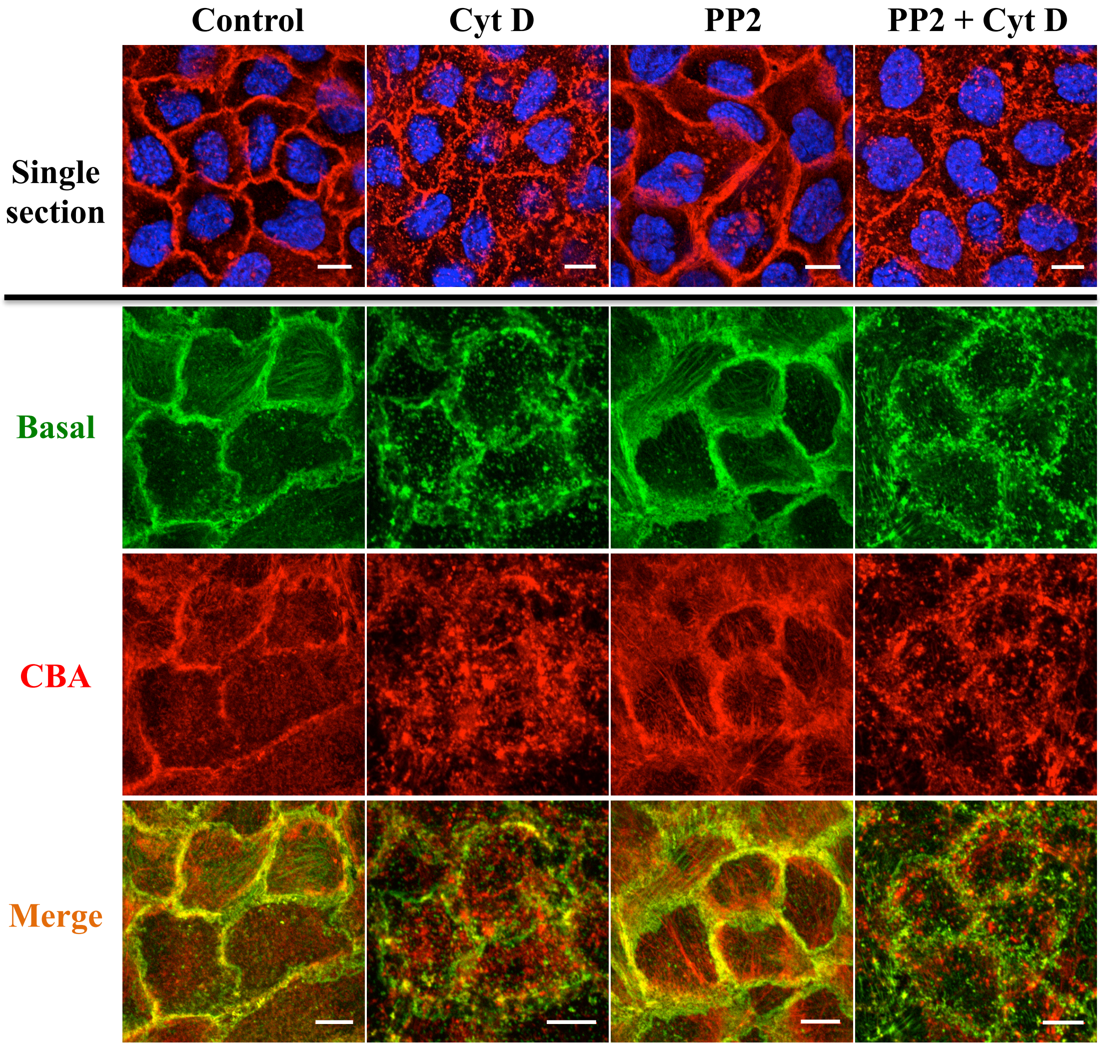

Figure 4.25 Effects of the combination of PP2 and Cyt D on the actin cytoskeleton in A431 cells. Cells seeded on coverslips were cultured and pre-treated either with diluent control (0.1% DMSO) or 10 µM PP2 for 48 hr at 37°C/5% CO_2. They were then incubated with or without 10 µM Cyt D for 15 min prior to fixing and staining with Rh-P and Hoechst. Images were acquired as described in section 4.2.1. Single sections show the overall distribution of actin relative to the nucleus and images below the black line provide information on the actin arrangement of cells (from other fields of view of single sections) from different z-regions. Scale bars 10 µm.

4.2.12 Discussion on Section 4.2.6 to 4.2.11

At present, one of the most commonly utilized approaches to study the role of actin organisation and dynamics in a range of cellular functions including endocytosis is via perturbation of actin architecture using pharmacological inhibitors. A number of natural compounds and synthetic products have been identified or developed to target the actin cytoskeleton directly or indirectly and to disrupt its arrangement and thus function. The most commonly used by a long margin are Cyt D, Lat B and JAS. But of interest to this thesis is the fact that they also have unique mechanisms of action and also that previously no comparative studies had been performed on their individual and combined effects on CPP uptake.

Cyt D of high concentration (10 μM) was initially used in cultured cells to induce complete depolymerisation of actin cytoskeleton, although concentrations of 1-2 μM have also used for this purpose (Kolodney and Wysolmerski, 1992, Pelham and Wang, 1999, Kasas et al., 2005, Pesen and Hoh, 2005). In this chapter it was identified the Cyt D induced increased uptake of EGFP-R8 in A431 cells was due to the effects of severe actin disorganisation on endocytosis rather than a general increase in plasma membrane permeability that could be caused by toxicity/necrosis. Lower concentrations of Cyt D were then tested and its disruption effects on actin could only be seen when the concentration reached 200 nM. However, visualisation of Cyt D effects on cellular uptake of EGFP-R8 required a higher concentration of 2 μM. The resulting actin visualisation experiments revealed that actin in HeLa cells was prominent in long filaments extending over several micro meters while cortical actin, associated with the plasma membrane is much more abundant in A431 cells. These major differences in actin organisation of these two cell lines has been previously reported by our group (Al Soraj et al., 2012). We therefore postulated that the observed difference in organisation of the actin cytoskeleton between these two cell lines has significant influence on their sensitivity to Cyt D with respects to uptake of both dextran and EGFP-R8. Previously the group usually relied on acquiring single section images (wide field or confocal) of actin dynamics in fixed cells. In this thesis a significant effort was invested in optimising confocal microscopy based methods to visualise and highlight actin profiles at different sections of the cells. An optimised method was developed and published as He et al in *Methods in Molecular Biology* and the ruffling cell shown in Figure 4.6 at 10 μM R8 was selected as the cover image for the 2015 volume of Cell Penetrating Peptides Methods and Protocols that also contains this publication (Figure 4.26).

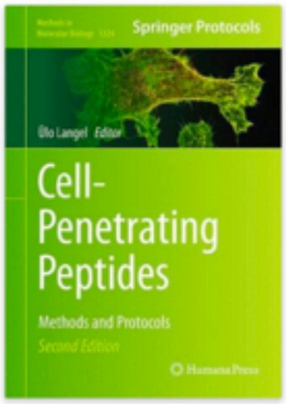

Figure 4.26 Cell Penetrating Peptides Methods and Protocols Volume showing a cell image presented in He et al 2015 (He et al., 2015).

To further investigate the role of actin and especially cortical actin for endocytic EGFP-R8 uptake in A431 cells, four other actin inhibitors, Lat B, JAS, Y27632 and PP2 were studied. Initially experiments were performed to assess their effects on actin using confocal fluorescence microscopy in fixed cells labelled with Rhodamine-Phalloidin. Similar to Cyt D, Lat B at 0.5 μM destroyed actin organisation, and a large number of amorphous actin aggregates were observed in treated cells. It should be noted that in Lat B treatment, the cortical actin network in a majority of the imaged cells was also disturbed. Based on results with Cyt D here and in Al Soraj et al (Al Soraj et al., 2012) it was expected that treatment with this agent would increase EGFP-R8 uptake and indeed this is what happened. Time did not allow for similar analysis to be performed with this agent and others using dextran as an endocytic probe; but this data would further substantiate the similarities that we have observed with this probe and R8 conjugates with respects to actin breakdown. JAS- and Y27632- treated cells also had increased levels of EGFP-R8 when the concentration was high enough to reveal clear evidence of actin breakdown. It should be noted here that high drug concentrations may also lead to cell death, which might in turn result in actin rearrangement. To minimise the possibility of cell death-induced actin reorganisation, viability assays might help determine the correct drug concentration to use. JAS is usually employed to stabilise pre-existing actin filaments and also to promote actin polymerisation (Bubb et al., 1994). However in this chapter the effects of JAS were quite striking as it completely obliterated the actin architecture and at the higher levels actin staining altogether. It is known that after prolonged JAS treatment (1-24 hr), actin arrangement is significantly modified manifest as the formation of actin specks/patches and the disruption of filamentous actin (Braet et al., 1998, Senderowicz et al., 1995, Bubb et al., 2000, Sawitzky et al., 1999). Binding of JAS to F-actin is competitive with phalloidin (Bubb et al., 1994) and this is the likely reason for the disappearance of actin labelling at the higher concentrations. A decrease in actin labelling was also reported in JAS (1 μM) treated MDCK cells stained with FITC-phalloidin (Shurety et al., 1998). In order to avoid these visualisation difficulties, electron microscopy has been used as an alternative technique for observation of the effects of JAS on actin (Shaw and Tilney, 1999).

Rho signalling pathways critically participate in the regulation of actin reorganisation in a variety of systems, and downstream Rho effectors including ROCKs have been reported to play a critical role in regulating actin dynamics (Sit and Manser, 2011, Riento and Ridley, 2003). Y27632 has been widely used as an inhibitor of ROCKs by competing with the ATP binding site (Ishizaki et al., 2000). After Y27632 treatment an altered distribution of filamentous actin has been reported in a variety of cell lines such as Swiss 3T3 cells, characterised by various phenotypes including the decrease or abolishment of the filamentous actin system (Ishizaki et al., 2000, Rao et al., 2001, Tee et al., 2015), the induction of long spiculate protrusions (Ishizaki et al., 2000) and the appearance of small circular actin structures (Svoboda et al., 2004). Intriguingly, at similar low micro molar concentrations that were commonly used in the studies mentioned above, Y27632 induced the reorganisation of actin into thick filament bundles underneath the plasma membrane of A431 cells; these interesting spiculated actin structures were found to be perpendicular with the membrane and oriented toward extracellular regions. The optimised methodology for visualising actin was a major factor in observing this phenomenon and these structures.

Recent studies have confirmed the critical role of the SFK family in actin cytoskeleton dynamics/reorganisation via their phosphorylation and activation of a wide range of actin regulatory factors such as the actin polymerisation promoter cortactin that usually occurs in response to extracellular stimulation (Tehrani et al., 2007, Koivusalo et al., 2009). Growth factor activated receptor tyrosine kinases (RTKs) such as EGFR and Platelet Derived Growth Factor Receptor (PDGFR) mediate extensive signalling to locally induce the formation of actin-rich dorsal membrane ruffles and globally promote cell migration and cell proliferation (Shah and Vincent, 2005, Reinecke and Caplan, 2014). Src kinase family is a group of non-receptor tyrosine kinases (NRTKs) and acts directly downstream of RTKs and thus is involved in these cellular activities. Src family members have also been shown to regulate endocytosis via phosphorylating and interaction with various components of the endocytic machinery including dynamin and actin-related cortactin (reviewed in (Lavoie et al., 2010).

The Src kinases inhibitor PP2 was previously observed to significantly inhibit the invasion and proliferation of brain tumour cells (malignant glial cells) and induce a rapid disappearance of peripheral membrane ruffles and loss of lamellipodia at a concentration of 10 µM (Angers-Loustau et al., 2004). In our studies, the addition of 10 µM PP2 stimulated the appearance of long actin fibres in A431 cells, but this agent was very toxic to HeLa cells at the same concentration. It should be noted that in contrast to the other actin influencing compounds used in the chapter, Src inhibition by PP2 did not disturb the cortical actin in A431 cells. Therefore it was somewhat unsurprising that the increase of EGFP-R8 uptake that was observed in A431 cells treated with the other actin inhibitors did not occur in cells incubated with PP2. Of particular interest was that the striking increase in EGFP-R8 uptake induced by Cyt D in the same cell line was diminished or even prevented by PP2 pre-treatment; this is interesting as the inhibition of Src kinase activity has previously been shown by other research group to prevent the Cyt D effects (Olivares et al., 2014). As reported in this study, inhibition of the SH3 domain-dependent Src kinase association with other proteins by the microinjection of isolated cSrc-SH3 domain diminished both the disruption of the actin network and the increased neurotransmitter release in neuroendocrine chromaffin cells by Cyt D treatment, but the underlying reason for this was not mentioned and is still unknown. However, it should be noted that the link between these PP2 effects on actin arrangement/peptide uptake shown in this thesis and Src inhibition needs further characterisation. As noted in the introduction to this chapter, PP2 also inhibits other kinases such as FRK. The kinase activity of Src within a cell sample treated with PP2 in our cell model could be measured by Western blotting using Src phospho-specific antibodies. Alternatively Src expression could be silenced using siRNA transfection and then Src depleted cells could be treated with Cyt D to assess whether the same effects are observed.

Based on the results obtained from different actin inhibitors, the actin cytoskeleton and most probably the cortical network in A431 cells acts as a hindrance to the cellular uptake of EGFP-R8 and even endocytosis as a whole. This now needs to be further explored as classically the actin is deemed to support and promote endocytosis rather than hinder the process. Further attempts to separate the differential roles of cortical actin from the remaining actin cytoskeleton in mediating the uptake of CPP-protein cargo such as EGFP-R8 may further help us in defining their internalisation mechanisms. This may for example be achieved by using actin reagents in a different way. Studies have reported that low doses of Cyt D (50-100 nM) selectively destabilised the fine-mesh cortical filaments in endothelial cells while the larger filament bundles and stress fibres were unaffected by this treatment (Fels et al., 2012, Kronlage et al., 2015). Lower concentrations of Cyt D could thus be tested with EGFP-R8, R8-Alexa 488 and indeed other CPP conjugates that are thought to enter cells via the involvement of actin. Indeed other probes that enter cells via endocytosis, such as dextran, could be similarly investigated.

Further analysis will highlight how these agents alone can give additional clues regarding the role of actin in endocytosis of CPP conjugates and their eventual intracellular fate. This is especially pertinent to the possibility that the CPP themselves, such as cationic R8, may either induce actin rearrangement to promote uptake via macropinocytosis or influence actin rearrangement in a manner similar to the chemical inhibitors that clearly induced endocytosis of EGFP-R8. As some of these actin-disrupting agents have reverse effects on actin (polymerisation vs depolymerisation), they might be used together as a cocktail to disrupt actin function but maintain cell morphology, thus causes less overall effects on cell architecture and integrity. In this chapter a major finding was that pre-treatment of HeLa and A431 cells with PP2 desensitised them to the effects of Cyt D on EGFP-R8. Whatever the true mechanism of PP2 it is able to inhibit both the negative (HeLa) and positive effects (A431) of Cyt D on EGFP-R8 uptake. It is hypothesized that the same would be true for Lat B and JAS but this remains to be tested. A combination of JAS, Lat B and Y27632 as a pharmacological cocktail was reported to rapidly arresting actin dynamics within seconds and also preserve the existing actin architectures in a range of cell models. However, the responses to extracellular stimuli of the tested cells were retained (Peng et al., 2011). Unfortunately we failed to reproduce the preservation of actin cytoskeleton in either HeLa or A431 cells by loading these three dugs as a cocktail onto cells (data not shown). Future studies focusing on the potential tools/methods that can selectively disrupt the newly formed actin structures but preserve the pre-existing actin architecture would shed new light on the role of actin in mediating the endocytosis of CPPs or CPP conjugates.

Chapter 5: siRNA inhibition of endocytic pathways to investigate the cellular uptake mechanisms of the CPP-protein conjugate EGFP-R8

5.1 Introduction

The studies performed in the previous two results chapters primarily used pharmacological inhibitors of the actin cytoskeleton to assess the role of actin in internalisation of CPP conjugates and well characterised endocytic probes in two different cell lines. However, as highlighted in this thesis and previously noted, the chemical actin inhibitors used here have their own limitations. They for example can cause severe and rapid morphological effects on cells and can induce cytotoxicity (Vercauteren et al., 2010, Ivanov, 2008). An alternative to chemical inhibition of endocytosis is that based on siRNA depletion of key endocytic proteins to selectively inhibit different endocytic pathways. This approach was used in our laboratory to investigate the roles of individual endocytic pathways and actin in the uptake of Alexa 488 conjugates of HIV-Tat peptide and R8 (Al Soraj et al., 2012). This was the study that set the template for this PhD thesis with a view to further understanding how actin regulated CPP uptake when the peptide is attached to large protein cargo.

Below, some of the identified endocytic pathways are described, as these were targets for studies performed in this chapter. It is important to note that other pathways have been described such as the CLIC-GEEC pathway that is thought to be involved in fluid phase uptake and endocytosis of GPI-linked proteins. This is a poorly described pathway as are others and these will not be described further in any great detail.

5.1.1 Clathrin-mediated endocytosis (CME)

To date, the best-characterised endocytic pathway is CME (Figure 1.4) (McMahon and Boucrot, 2011). During this process, the highly conserved protein complex AP2 plays crucial roles especially in the formation and maturing of clathrin-coated vesicles on intracellular membranes. AP2 components are recruited to the plasma membrane, following the initiation of membrane invagination at the sites where the clathrin-coated vesicles will bud. It was previously thought that AP2 contributes to the initial generation of membrane curvature through binding to membrane-specific phosphatidylinositol-4,5-bisphosphate (PtdIns(4,5)P_2) and the cytoplasmic tails of transmembrane receptors (Ohno et al., 1995, Höning et al., 2005). However this concept on AP2 has been challenged by more recent research that suggested the essential requirement of a putative membrane nucleation complex for membrane curvature initiation (Stimpson et al., 2009, Henne et al., 2010). Upon arrival at the plasma membrane, the AP2 complexes directly recruit several types of receptors including EGFR (Huang et al., 2004) and TfR (Boucrot et al., 2010) through their α-subunit and μ2-subunit, and also bind to a number of cargo-specific adaptor proteins (using appendage domains), which then recruit other specific receptors to the AP2 hub (Collins et al., Kelly et al., 2008). Another crucial role for AP2 is to recruit clathrin from the cytosol to the plasma membrane to mediate the formation of coated vesicles; the depletion or absence of AP2 from cells has been suggested to abrogate the recruitment of clathrin and the consequent clathrin coat assembly and vesicle formation (Motley et al., 2003, Boucrot et al., 2010). Given the fact that AP2 acts as core component of the protein interaction network required for the formation of clathrin-coated vesicles, silencing expression of AP2 subunits such as the μ2 subunit and clathrin heavy and light chain through siRNA transfection has been often used as a tool to perturb the clathrin-mediated endocytic pathway (Ravikumar et al., 2010, Motley et al., 2003, Kolokoltsov et al., 2007).

5.1.2 Caveolae-mediated endocytosis

Caveolae are flask-shape membrane invaginations that bud from specialised glycosphingolipid- and cholesterol- enriched microdomains (rafts) and are defined by membrane proteins caveolins (caveolin-1 and muscle-specific caveolin-3) (Parton and del Pozo, 2013) and also cavins (Kovtun et al., 2015). Caveolae have been detected with high density in endothelial cells, adipocytes and skeletal muscle cells, whereas there is still no evidence for their presence in other cells types including commonly used cancer cell lines e.g. breast cancer MCF7 cells (reviewed in (Rewatkar et al., 2015). Caveolin-1 (or caveolin-3 in muscle cells) are essential structural components for caveolae formation and form oligomers, which are suggested to drive membrane curvature (Pelkmans and Zerial, 2005). From in vitro studies with cell lines, depletion of caveolin-1 via siRNA targeting results in the absence of caveolae (Hill et al., 2008, Rewatkar et al., 2015) and hematopoietic cell lines do not express caveolin-1 and thus do not make caveolae (Van Deurs et al., 2006). As caveolae gained prominence as mediators of endocytosis, drug delivery researchers have attempted to inhibit uptake through this route either by depleting caveolin-1 expression with siRNA or using chemical agents such as nystatin and cyclodextrins that disrupt lipid rafts. These studies have suggested caveolae may play a role in uptake of spherical nucleic acid-conjugated gold nanoparticles (Choi et al., 2013), recombinant Tat-M13 phages (Kim et al., 2012) and other non-viral delivery vectors such as polyethylinimine (PEI) (Gabrielson and Pack, 2009).

5.1.3 Flotillin-mediated endocytosis

Flotillins (1 and 2) are also found on lipid rafts and in 2006 flotillin-1 was proposed to regulate a distinct endocytic pathway (Glebov et al., 2006, Hansen and Nichols, 2009). To date, the flotillin-1-mediated endocytosis has been reported to provide cell entry for a variety of cargo molecules such as the GPI-anchored protein CD59, cholera toxin B subunit (CTxB) (Glebov et al., 2006), cationic polyplexes (Vercauteren et al., 2011) and CPP polyarginine (Payne et al., 2007). In addition to membrane trafficking processes, flotillins have also been revealed to function in several other cellular contexts including cell adhesion, signal transduction e.g. by receptor tyrosine kinases and regulation of the cortical cytoskeleton (Banning et al., 2014, Ludwig et al., 2010).

Flotillins are expressed in all mammalian cells studied to date, and are thought to associate with specific cholesterol-enriched membrane microdomains constitutively through acylation, oligomerisation and cholesterol-binding (reviewed in (Meister and Tikkanen, 2014)). Studies of Frick *et al.* suggested that upon certain stimuli, flotillin-1 and -2 located on the plasma membrane coassemble into higher-ordered oligomers to form flotillin-enriched microdomains that are distinct from those defined by caveolins. These oligomerised flotillins then recruit certain transmembrane cargo proteins such as EGFR into these newly generated microdomains to cluster them prior to endocytosis. These microdomains also exhibited some of the classical hallmarks of lipid rafts and showed the capacity to induce membrane curvature, the formation of membrane invaginations and thus membrane budding towards the cell interior (Frick et al., 2007). The distribution of flotillin microdomains and the flotillin functions during endocytosis are potentially regulated by tyrosine phosphorylation via certain Src family kinases (Neumann-Giesen et al., 2007, Riento et al., 2009). However, the exact role of flotillin-positive microdomains in endocytic uptake has not been fully clarified.

5.1.4 Macropinocytosis

Macropinocytosis is a process that cells can use to nonselectively engulf large amount of extracellular fluid containing nutrients. The most studied macropinocytosis process is that occurs in cells activated by growth factors such as EGF but there is also a belief that many cells types can perform constitutive macropinocytosis via membrane ruffling (Jones, 2007). Identified macropinocytosis regulators include the Na^+/H^+ exchanger, p21-actibvated kinase 1 (PAK-1) and a dynamic actin cytoskeleton to mediate the changes that occur on the plasma membrane. (Lim and Gleeson, 2011, Mercer and Helenius, 2012). The functional relationship between Na^+/H^+ exchange and macropinocytosis is not apparent. One possible mechanism is that the activity of Na^+/H^+ exchanger has influence on cytosolic pH and the pH changes could in turn lead to alterations in the signalling and/or actin reorganisation required for macropinocytosis (Koivusalo et al., 2010). PAK-1 is the best-characterized member of the PAK family of serine/threonine kinases that are activated by Rho family GTPases Rac 1 and Cdc42 (Manser et al., 1994). It binds to the GTP-bound forms of Rac 1/Cdc42, and functions as downstream effector in several Rac- and Cdc42- regulated signalling events including the modulation of the actin cytoskeleton (Figure 4.1). Apart from the small GTPases, several other signalling proteins such as PAK interacting exchange factor (PIX) have been identified as key players in PAK activation (reviewed in (Rane and Minden, 2014). Upon activation, PAK-1 can phosphorylate a serine residue on the light chain of regulatory myosins, and thus stabilise filamentous actin and contribute to the formation of actin-rich structures such as dendritic spine in neuronal cells (Zhang et al., 2005) or to some other actin-based functions such as membrane trafficking and cell migration (Kichina et al., 2010). However, in other cell types including fibroblasts, endothelial cells and epithelial cells, PAK-1 has been shown to have opposite effect on actin structures (Sanders et al., 1999, Goeckeler et al., 2000). In these cell lines, PAK-1 phosphorylates myosin light chain kinase (MLCK), blocking its kinase activity resulting in decreased phosphorylation of myosin light chain and the subsequent dissolution of stress fibres.

PAK-1 has been shown to stimulate the formation of actin-rich dorsal membrane ruffles that were similar to those implicated in the process of macropinocytosis (Dharmawardhane et al., 1997, Edwards et al., 1999). Additionally, inhibition of endogenous PAK activity was reported to impede growth factor induced macropinocytosis (Liberali et al., 2008, Dharmawardhane et al., 2000) and the uptake of vaccinia virus by macropinocytosis (Mercer and Helenius, 2008). These data provide strong evidence for the direct regulatory role of PAK-1 in macropinocytosis, through its actin mediating activity.

Rho GTPases, including Rac1 and Cdc42 are essential for appropriate organisation of actin cytoskeleton and in various endocytic pathways. These Rho family members have different roles in regulating actin dynamics. Specially, Rac1 promotes the formation of lamellipodia and membrane ruffles, whereas Cdc42 is primarily involved in the formation of filopodia, but both GTPases are required for at least some forms of endocytosis, especially macropinocytosis through their regulation of actin assembly factors like ARP2/3 complex and the ARP2/3 activator of WAVE and WASP (Figure 4.1). For example, Cdc42 localised at the plasma membrane can bind to WASP, and the activated WASP in turn interacts with and activates the ARP2/3 complex, which then initiates the assembly of branched actin (Chesarone and Goode, 2009, Takenawa and Suetsugu, 2007). Mammalian diaphanous (mDia) proteins, which belong to the formin family, also act as downstream targets for Cdc42, and their activity is required to induce the polymerisation of unbranched actin filaments (Peng et al., 2003). Another actin regulatory factor cofilin is known to stimulate actin disassembly and actin filament severing. There is still no valid evidence for the direct link between cofilin and Cdc42 but Cdc42 was suggested to indirectly inhibit the activity of cofilin via LIM kinase (Wang et al., 2007). Several recent studies have revealed crosstalk regulation between Rac1 and Cdc42 in regulating actin dynamics (Yang et al., 2006, Steffen et al., 2013). These actin reorganisation events regulated by Cdc42 is the main force to drive membrane deformation and the subsequent vesicle formation required for macropinocytosis.

Cdc42 was first identified in budding yeast, and loss of Cdc42 resulted in failure for budding and mating projection (Etienne-Manneville, 2004). In mammalian cells, in addition to macropinocytosis, fluid-phase endocytosis and clathrin-independent carrier pathway (CLIC-GEEC) have also been reported to rely on the involvement of Cdc42 (Hansen and Nichols, 2009, Howes et al., 2010), and depletion of Cdc42 through RNA interference inhibited the endocytosis of transferrin in human HeLa cells (Balklava et al., 2007).

Aims

Previous studies shown in Chapter 3 and 4 have reported that actin disruption/reorganisation in A431 cells led to dramatic increase of cellular uptake of CPP conjugate EGFP-R8 and of the fluid-phase probe dextran, whereas the opposite effects were seen in HeLa cells. These observations were mainly based on the use of chemical inhibitors such as Cyt D. The aims of this chapter were to attempt to siRNA silence the expression of two proteins, PAK-1 and Cdc42 that have been implicated in regulating actin assembly and specifically macropinocytosis. These cells could then be tested for their ability to internalise EGFP-R8 compared with cells treated with chemicals that have been shown to inhibit macropinocytosis. A further aim was to investigate the potential of siRNA sequences targeting CME, caveolae and flotillin pathways through silencing AP2μ2, caveolin-1 and flotillin-1 respectively to influence EGFP-R8 uptake. Together, these results in HeLa and A431 cells would then provide valuable information regarding the differences observed in their processing of CPPs and fluid phase probes and the roles of different endocytic pathways and specifically actin on the cellular uptake of this CPP-conjugate.

5.2 Results

5.2.1 Inhibition of caveolae-dependent endocytosis through siRNA depletion of caveolin-1

The involvement of caveolae-dependent pathway in EGFP-R8 internalisation by HeLa or A431 cells was initially studied using siRNA transfection targeting caveolin-1. A validated sequence was investigated using a previously described method developed in the laboratory (Al Soraj et al., 2012).

Briefly cells (HeLa or A431 cells) were seeded onto 12-well plates and transfected with 100 nM siRNA for 48 hr. Cells were then lysed and aliquots of the cell lysate was separated by SDS-PAGE. Expression of caveolin-1 and tubulin was detected by Western blotting. In addition, siRNA against GFP (si-GFP) was employed as non-targeting control siRNA.

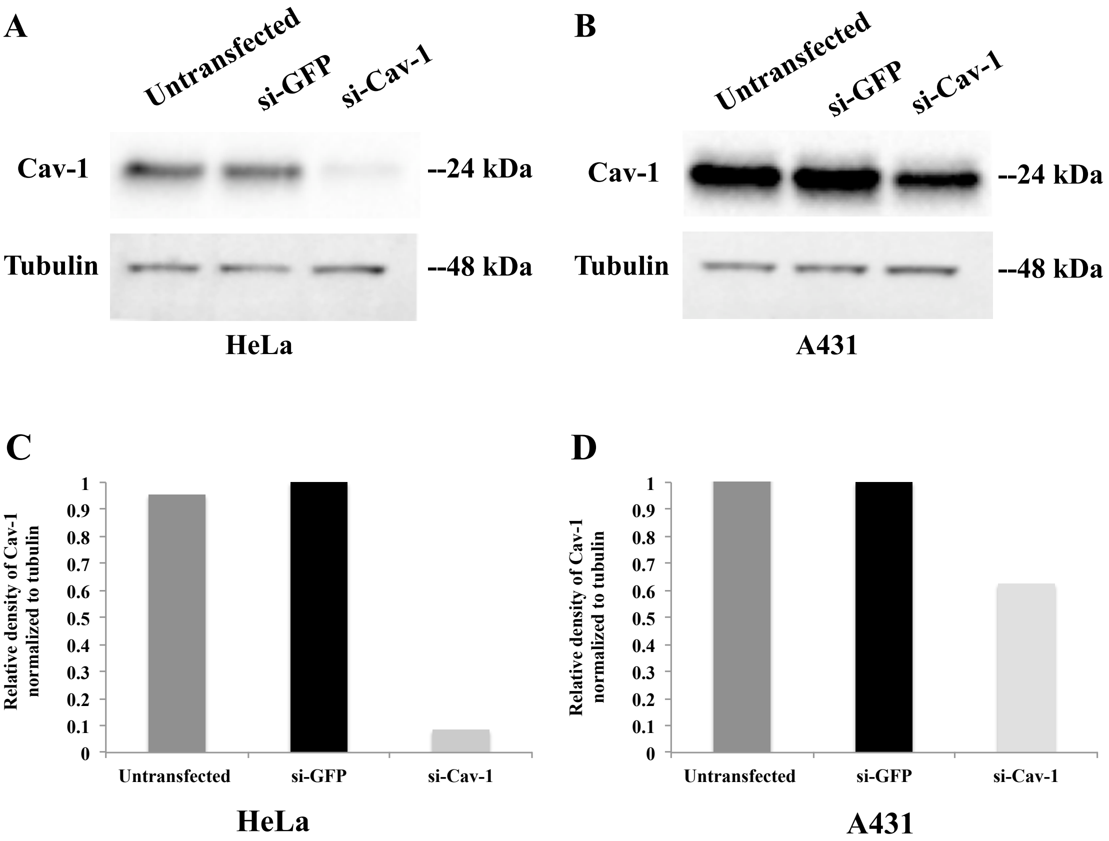

Figure 5.1 siRNA-based caveolin-1 depletion from HeLa (A/C) and A431 (B/D) cells. A-B) Immunoblots for caveolin-1 and tubulin in untransfected cells or cells treated with Cav-1 targeting siRNA (si-Cav-1) or GFP control siRNA (si-GFP). **C-D)** Relative protein expression was quantified using ImageJ software by densitometry and normalised to tubulin loading control.

The expression of caveolin-1 from the blots was normalised to tubulin loading control and the effectiveness of siRNA depletion of the target protein was quantified using ImageJ software. Figure 5.1 demonstrates effective depletion of the target protein from HeLa cells (Figure 5.1A) as ~92% reduction in caveolin-1 expression was observed (Figure 5.1C). The data in Figure 5.1B and D highlights that per µg of loaded protein that Cav-1 expression was higher in A431 cells and that silencing efficiency only reached ~38%. As Cav-1 depletion using this siRNA sequence is well characterised in the laboratory (Al Soraj et al., 2012), this experiment confirming depletion of the protein in HeLa cells was only performed once before then conducting CPP uptake assays. Despite the fact that only partial silencing of Cav-1 expression was noted in

A431 cells it was determined that investigations were performed to observe any effects of this partial depletion on CPP uptake.

Untransfected HeLa cells or cells transfected with control siRNA (si-GFP) or siRNA targeting caveolin-1 (si-Cav-1) for 48 hr as described above were washed and then incubated with 2 μM EGFP-R8 for 1 hr at 37°C/5% CO_2. Cells were then washed three times with 0.5 mg/ml heparin solution and once with PBS prior to live cell imaging confocal microscopy. As shown in Figure 5.2, in comparison to si-GFP treatment, caveolin-1 depletion did not result in any obvious difference in EGFP-R8 uptake with respects to overall fluorescence intensity or intracellular distribution. This agrees with previous studies showing no effect of Cav-1 depletion on the cellular uptake of R8-Alexa 488. Cav-1 studies in this cell line were not carried out further. This experiment was repeated and the fluorescence intensities from both experiments were then calculated using a fluorescence intensity quantification method recently developed in the laboratory (Moody et al., 2015) (*see Appendix 4 for method details*). As this represents an n=2 (due to time limitation), thus no statistical analysis could be performed but the data clearly shows that uptake of this protein is not heavily influenced by Cav-1 expression.

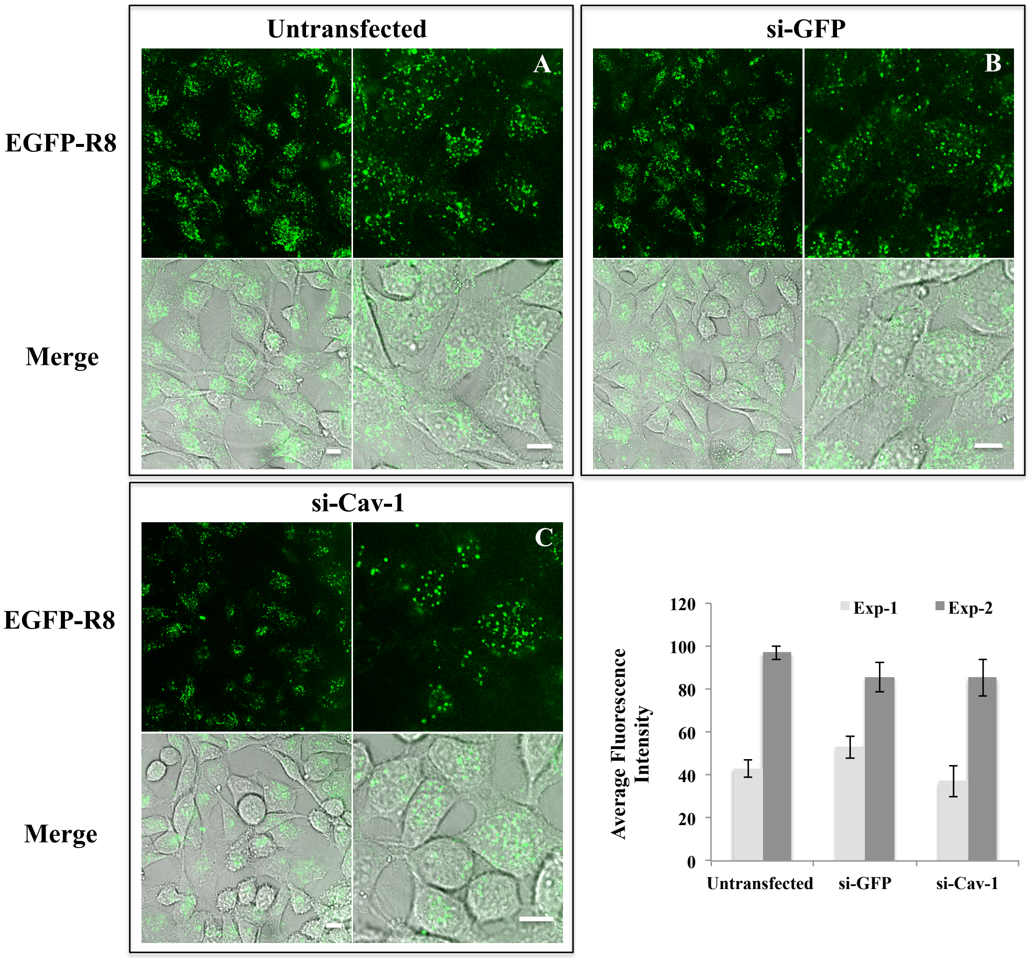

Figure 5.2 Effects of caveolin-1 depletion on the cellular uptake of EGFP-R8 in HeLa cells. Untransfected cells and cells transfected with control siRNA (si-GFP) or siRNA targeting caveolin-1 (si-Cav-1) were incubated for 1 hr with 2 μM EGFP-R8 at 37°C/5% CO_2, and washed with heparin. Cell-associated fluorescence was analysed by confocal microscopy and shown are representative single projection images of fluorescence only (top rows) and merges of fluorescence and DIC of the same cells (bottom rows). Shown in Column A, B, and C are zoomed images of 5-8 cells from different fields of view. Scale bars 10 μm. Quantification data shown at bottom right represents the average fluorescence intensity +/- S.D. indicating intra-experimental variations from two independent experiments.

Despite the fact that this siRNA targeting approach only partially reduced Cav-1 expression in A431 cells, the same experiments were performed three times to investigate whether this loss influenced EGFP-R8 uptake. Confocal microscopy data shown in Figure 5.3 suggest that this depletion did also not influence EGFP-R8 uptake in this cell line. The calculated fluorescence intensity values for control cells and cells transfected with si-GFP or si-Cav-1 were compared and there was no significant difference in fluorescence values between these conditions.

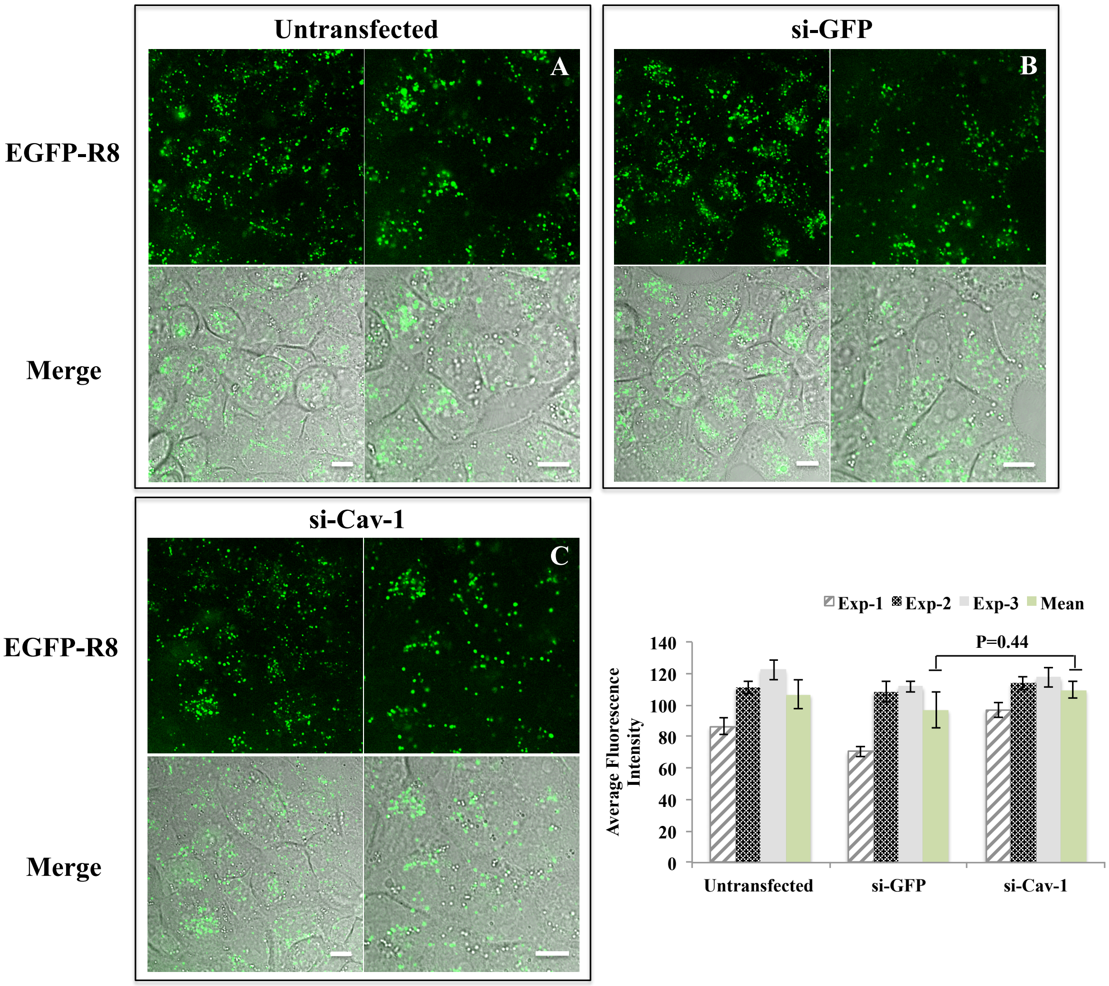

Figure 5.3 Effects of caveolin-1 depletion on the cellular uptake of EGFP-R8 in A431 cells. Untransfected cells and cells transfected with control siRNA (si-GFP) or siRNA targeting caveolin-1 (si-Cav-1) were incubated for 1 hr with 2 µM EGFP-R8 at 37°C/5% CO_2, and washed with heparin. Cell-associated fluorescence then was analysed by confocal microscopy and shown are representative single projection images of fluorescence only (top rows) and merges of fluorescence and DIC of the same cells. Shown in Column A, B, and C are zoomed images of 5-8 cells from different fields of view. Scale bars 10 µm. Quantification data shown at bottom right represents the average fluorescence intensity +/- S.D. from three independent experiments (Exp 1-3; error bars indicate the intra-experimental variations) and the mean fluorescence intensity +/- S.D. of these three experiments (highlighted in green colour; error bars indicate the inter-experimental variations). Student's independent T-Tests were performed to determine the significance of differences between two means. Statistical significance p=0.44.

5.2.2 Inhibition of the flotillin endocytic pathway through siRNA depletion of flotillin-1

Experiments, using the same methodology (section 2.5) were then conducted in order to deplete flotillin-1 from HeLa and A431 cells to assess the contribution of this protein and the pathway in regulating the internalisation of EGFP-R8. Here, a laboratory validated siRNA sequence against flotillin-1 (si-Flot-1) was employed together with control siRNA (si-GFP). The expression of flotillin-1 and GAPDH were finally detected by Western blotting and ECL and the relative intensities of the bands were quantified as described and normalised to the intensity of GAPDH as a loading control. Figure 5.4 demonstrates that the expression of flotillin-1 was reduced by ~96% and ~70% respectively in HeLa and A431 cells.

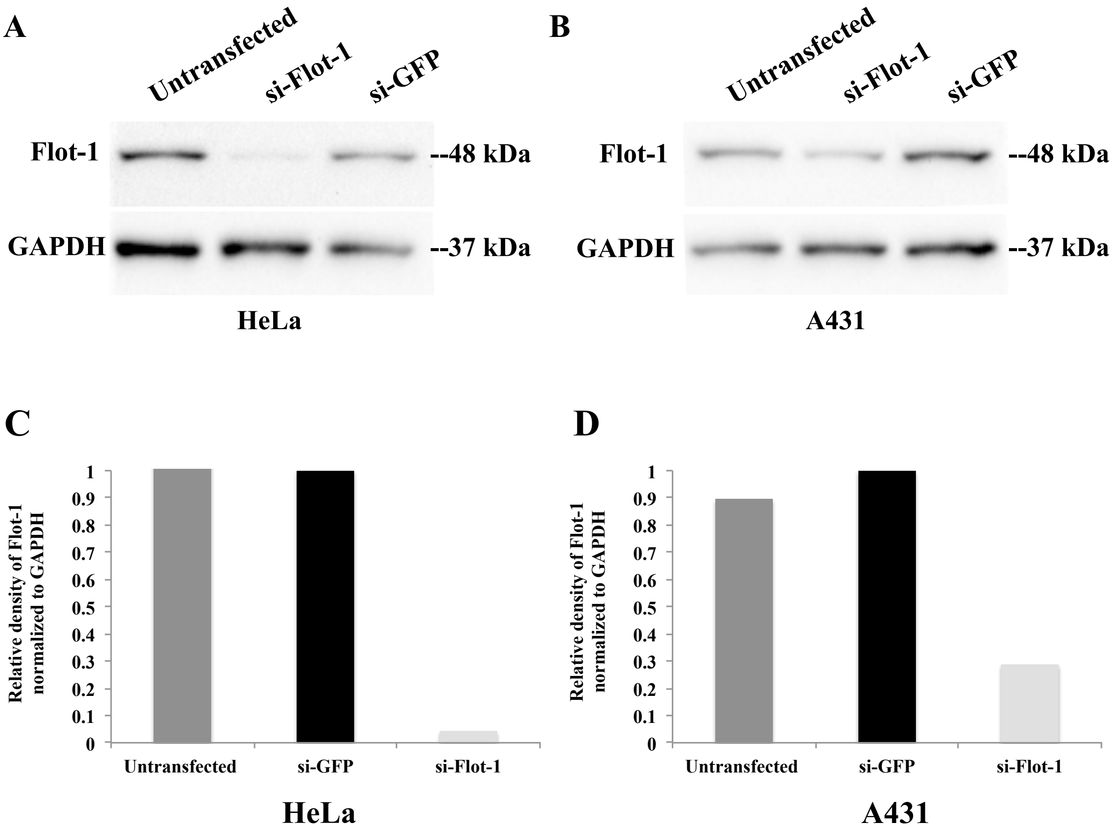

Figure 5.4 siRNA-based flotillin-1 depletion from HeLa (A/C) and A431 (B/D) cells. A-B) Immunoblots for flotillin-1 and GAPDH in untransfected cells or cells treated with flotillin-1 targeting siRNA (si-Flot-1) or GFP non-targeting control siRNA (si-GFP). **C-D)** Relative protein expression was quantified using ImageJ software and normalised to GAPDH loading control.

These experiments were then repeated with HeLa and A431 cells gown in 35mm MatTek dishes that were then further incubated with 2 µM EGFP-R8 to assess whether depletion of flotillin-1 had any influence on uptake of this protein.

Similar to results obtained with si-Cav-1 transfected cells there was, in both cell lines, no obvious difference in EGFP-R8 uptake between control cells and those depleted on flotillin-1 (Figures 5.5-5.6). Quantification data from three independent experiments in A431 cells confirmed that there was no statistical difference between these experimental conditions but highlighted some variation in fluorescence intensity between separate individual experiments (Figure 5.6). From two separate experiments it is also clear that flotillin-1 is not a major regulator of the uptake of EGFP-R8 in HeLa cells (Figure 5.5).

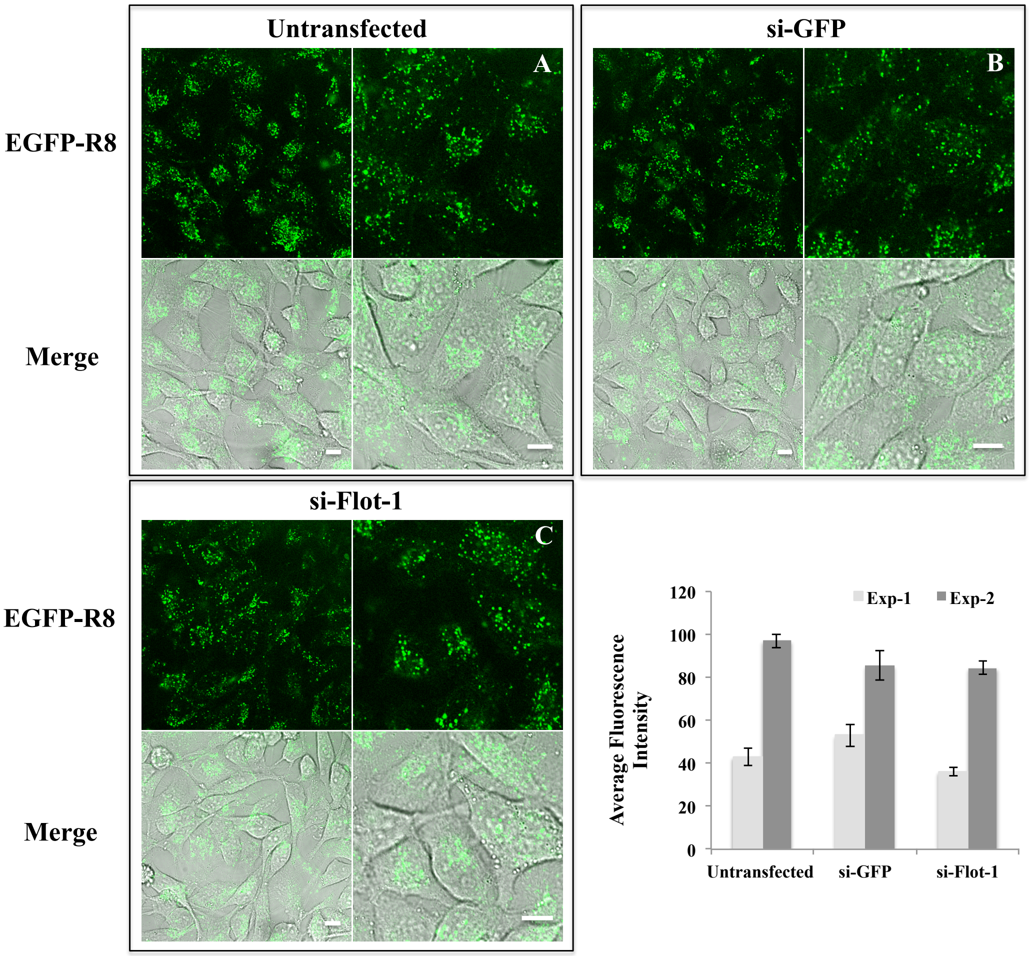

Figure 5.5 Effects of flotillin-1 depletion on the cellular uptake of EGFP-R8 in HeLa cells. Untransfected cells and cells transfected with control siRNA (si-GFP) or siRNA targeting flotillin-1 (si-Flot-1) were incubated for 1 hr with 2 μM EGFP-R8 at 37°C/5% CO_2, and washed with heparin. Cell-associated fluorescence was analysed by confocal microscopy and shown are representative single projection images of fluorescence only (top rows) and merges of fluorescence and DIC of the same cells. Shown in Column A, B, and C are zoomed images of ~5 cells from different fields of view. Scale bars 10 μm. Quantification data shown at bottom right represents the average fluorescence intensity +/- S.D. indicating intra-experimental variations from two independent experiments.

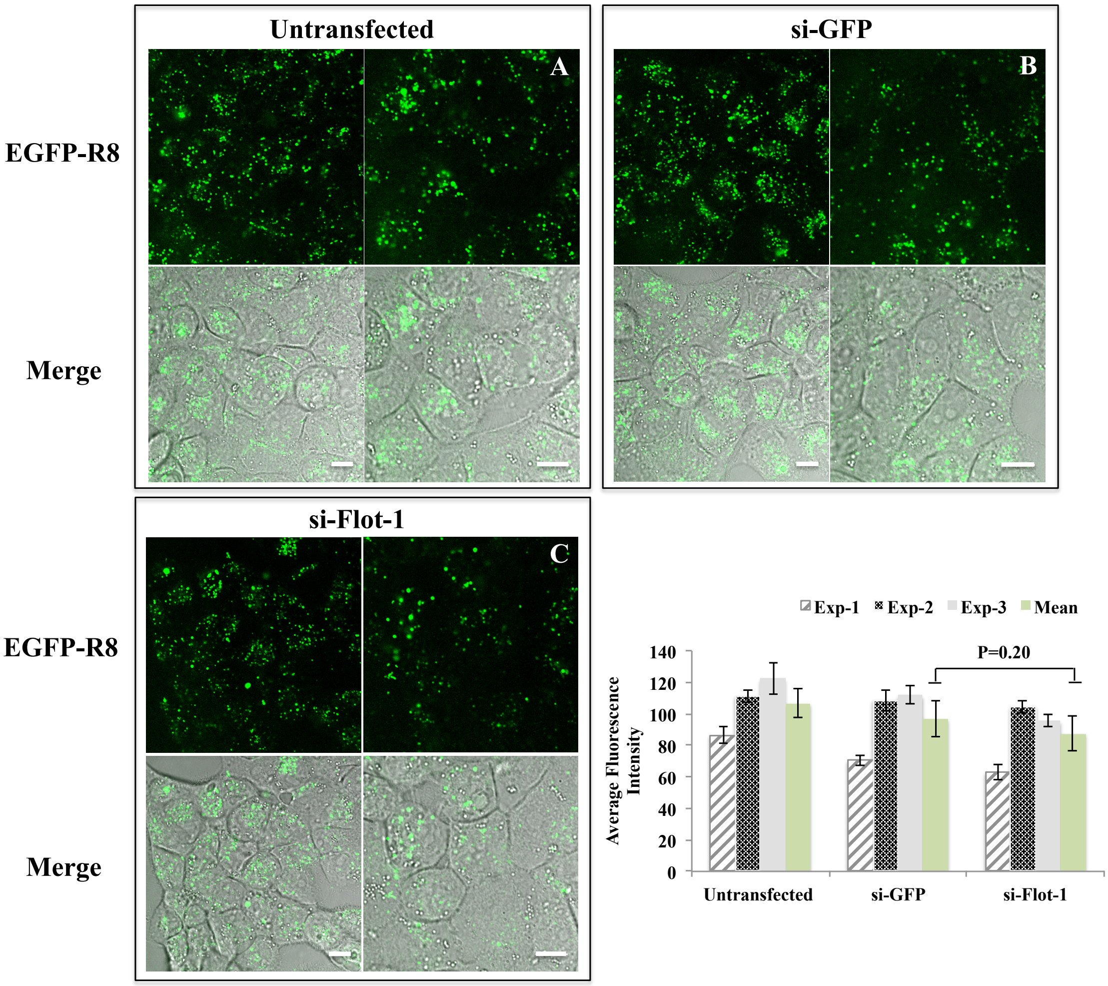

Figure 5.6 Effects of flotillin-1 depletion on the cellular uptake of EGFP-R8 in A431 cells. Untransfected cells and cells transfected with control siRNA (si-GFP) or siRNA targeting flotillin-1 (si-Flot-1) were incubated for 1 hr with 2 µM EGFP-R8 at 37°C/5% CO_2, and washed with heparin. Cell-associated fluorescence then was analysed by confocal microscopy and shown are representative single projection images of fluorescence only (top rows) and merges of fluorescence and DIC of the same cells. Shown in Column A, B, and C are zoomed images of 5-8 cells from different fields of view. Scale bars 10 µm. Quantification data shown at bottom right represents the average fluorescence intensity +/- S.D. from three independent experiments (Exp 1-3; error bars indicate the intra-experimental variations) and the mean fluorescence intensity +/- S.D. of these three experiments (highlighted in green colour; error bars indicate the inter-experimental variations). Student's independent T-Tests were performed to determine the significance of differences between two means. Statistical significance p=0.20.

5.2.3 Inhibition of endocytic pathways regulated by PAK-1 through siRNA depletion of PAK-1

PAK-1 is a well-characterised regulator of actin dynamics. It is also strongly linked with the functioning of macropinocytosis that has a strong requirement for actin reorganisation to accomplish the fluid engulfing and internalisation processes. Attempts were therefore made to silence the expression of this protein in HeLa and A431 cells using the method described in section 2.5 and validated siRNA (Al Soraj et al., 2012).

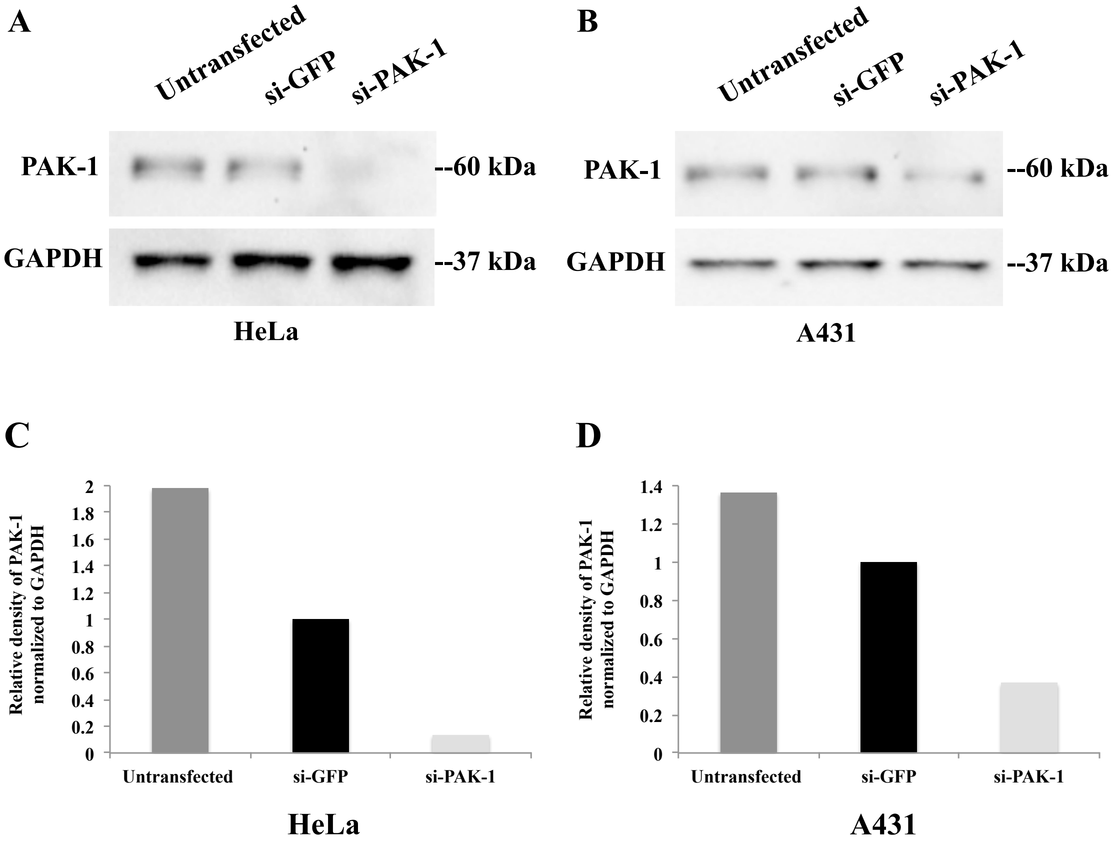

Figure 5.7 siRNA-based PAK-1 depletion from HeLa (A/C) and A431 (B/D) cells. A-B) Immunoblots for PAK-1 and GAPDH in untransfected cells or cells treated with PAK-1 targeting siRNA (si-PAK-1) or GFP non-targeting control siRNA (si-GFP). **C-D)** Relative protein expression was quantified using ImageJ software and normalised to GAPDH loading control.

Results in Figure 5.7 showed that PAK-1 expression was reduced by ~87% in the si-PAK-1 treated HeLa cells (Figure 5.7A and C), and by ~63% in the si-PAK-1 treated A431 cells (Figure 5.7B and D). Here it should be noted that there was also some silencing of PAK-1 with the control transfection using si-GFP; the reason for this is unknown. This method was then used to test the functionality of these cells for uptake of EGFP-R8 using live cell imaging confocal microscopy as described above for si-Cav-1 and si-Flot-1 transfected cells.

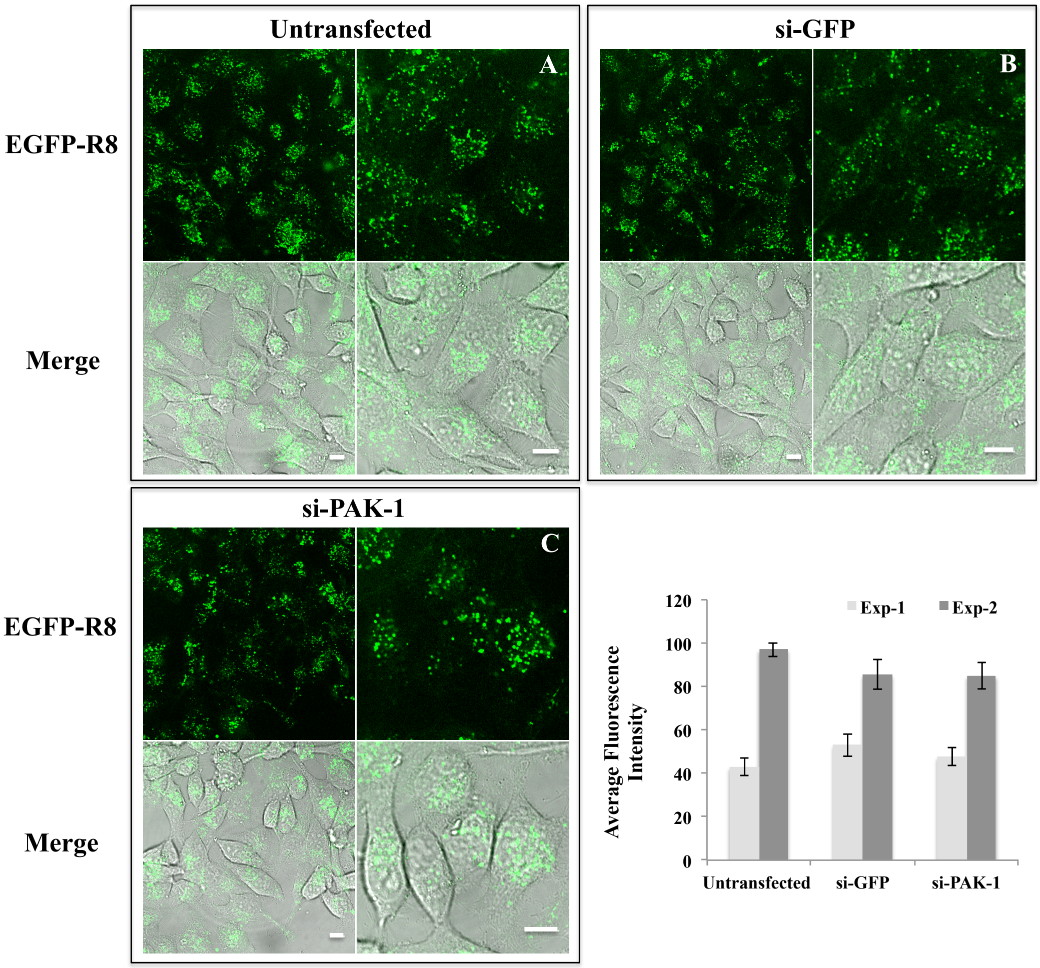

Figure 5.8 Effects of PAK-1 depletion on the cellular uptake of EGFP-R8 in HeLa cells. Untransfected cells and cells transfected with control siRNA (si-GFP) or siRNA targeting PAK-1 (si-PAK-1) were incubated for 1 hr with 2 µM EGFP-R8 at 37°C/5% CO_2, and washed with heparin. Cell-associated fluorescence was analysed by confocal microscopy and shown are representative single projection images of fluorescence only (top rows) and merges of fluorescence and DIC of the same cells. Shown in Column A, B, and C are zoomed images of ~5 cells from different fields of view. Scale bars 10 µm. Quantification data shown at bottom right represents the average fluorescence intensity +/- S.D. indicating intra-experimental variations from two independent experiments.

In both HeLa and A431 cells there was no noticeable difference in EGFP-R8 uptake between si-PAK-1 treated and control cells (Figure 5.8-5.9). Statistical analysis from data obtained in A431 cells showed that any difference was not statistically significant.

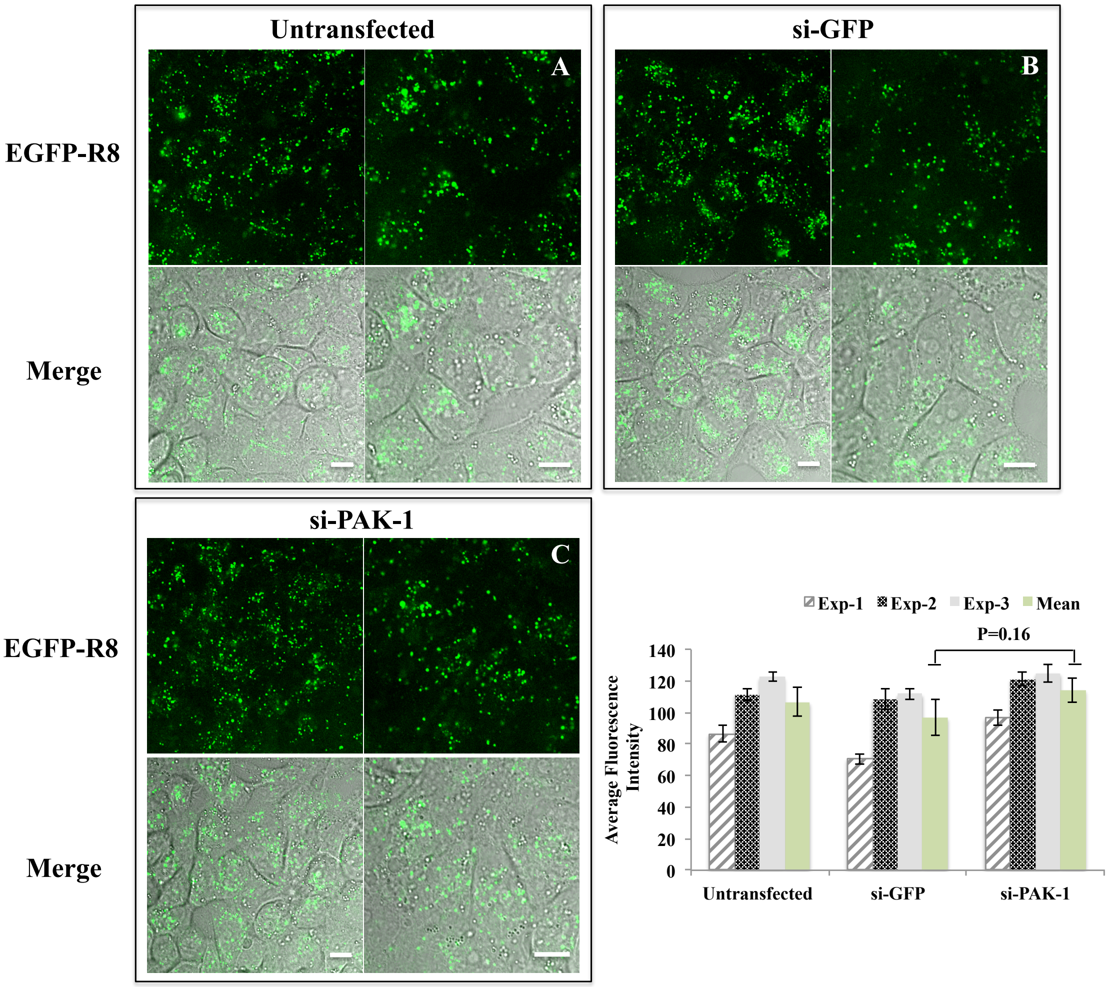

Figure 5.9 Effects of PAK-1 depletion on the cellular uptake of EGFP-R8 in A431 cells. Untransfected cells and cells transfected with control siRNA (si-GFP) or siRNA targeting PAK-1 (si-PAK-1) were incubated for 1 hr with 2 μM EGFP-R8 at 37°C/5% CO_2, and washed with heparin. Cell-associated fluorescence then was analysed by confocal microscopy and shown are representative single projection images of fluorescence only (top rows) and merges of fluorescence and DIC of the same cells. Shown in Column A, B, and C are representative zoomed images of 5-8 cells from different fields of view. Scale bars 10 μm. Quantification data shown at bottom right represents the average fluorescence intensity +/- S.D. from three independent experiments (Exp 1-3; error bars indicate the intra-experimental variations) and the mean fluorescence intensity +/- S.D. of these three experiments (highlighted in green colour; error bars indicate the inter-experimental variations). Student's independent T-Tests were performed to determine the significance of differences between two means. Statistical significance p=0.16.

5.2.4 Inhibition of endocytic pathways regulated by Cdc42 through siRNA depletion of Cdc42

As one of the upstream regulators of PAK-1 activity, Cdc42 functions in the regulation of actin remodelling and in various endocytic pathways. To investigate whether EGFP-R8 uptake is affected by Cdc42-mediated pathways, Cdc42 expression in HeLa and

A431 cells was depleted using siRNA prior to cellular uptake assays. Prior to this thesis no Cdc42 silencing had been attempted in the laboratory. Two MWG/Eurofin custom siRNAs were purchased and tested and one gave very good silencing of this protein (>90%) in both cell lines (Figure 5.10). In contrast to other experiments the control siRNA appeared to increase Cdc42 expression levels.

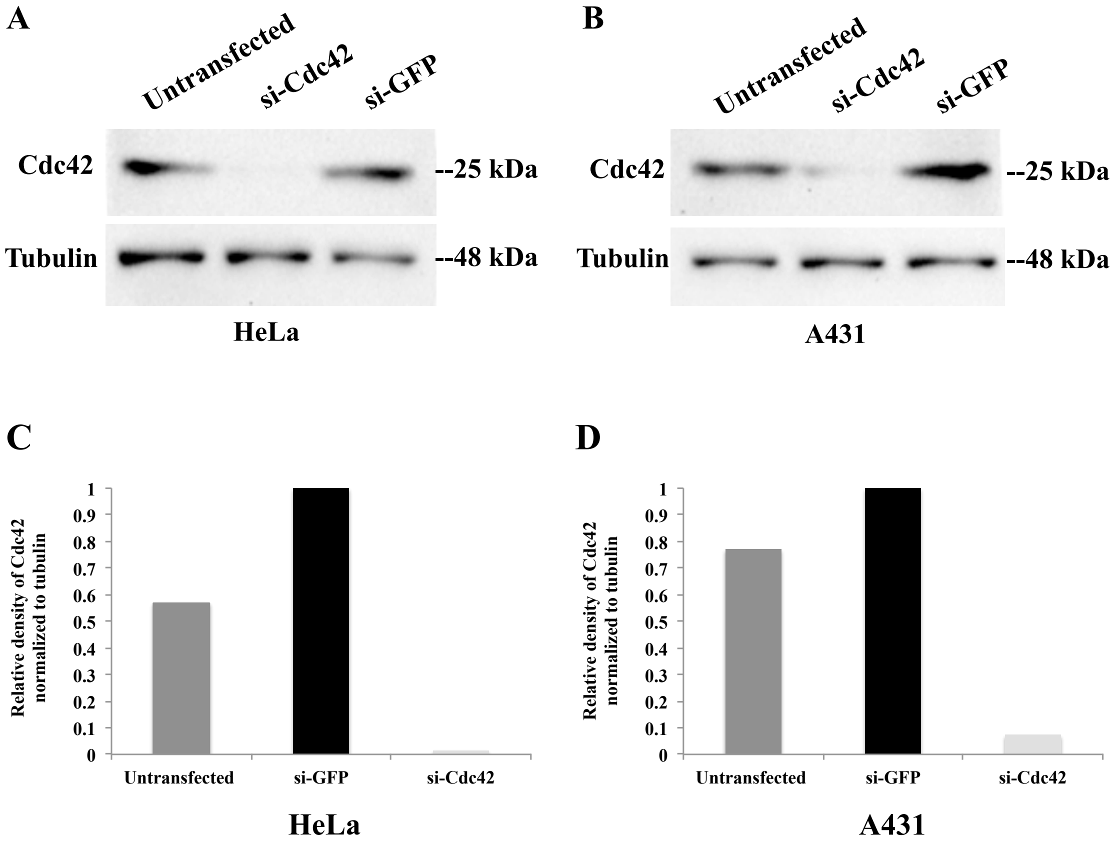

Figure 5.10 siRNA-based Cdc42 depletion from HeLa (A/C) and A431 (B/D) cells. A-B) Immunoblots for Cdc42 and tubulin in untransfected cells or cells treated with Cdc42 targeting siRNA (si-Cdc42) or GFP non-targeting control siRNA (si-GFP). **C-D)** Relative protein expression was quantified using ImageJ software and normalised to tubulin loading control.

These cells were then tested for their ability to internalise EGFP-R8. From initial analysis of the cells by DIC microscopy it was clear that Cdc42 depletion resulted in morphological changes (Figure 5.11-5.12). A proportion of HeLa cells were elongated and these are highlighted with white arrows in the Figure 5.11. A more complex observation was seen in A431 cells that also adopted an elongated shape (a typical example is shown in the bottom left image of Figure 5.12). Additionally the formation of long cell protrusions akin to long filopodia, were also observed in some of these cells. Interestingly, cells imaged in some other regions were a lot more circular in appearance than control cells (see bottom middle image of Figure 5.12). For both cell lines the total fluorescence intensity was quantified from separate experiments (n=2 for HeLa and n=3 for A431) to show that depletion of Cdc42 did not result in major differences in cellular uptake of EGFP-R8. Statistical analysis from data obtained in A431 cells showed that any difference was not statistically significant. It should be highlighted that the rounded A431 were characterised by having low fluorescence (Figure 5.12) that was more polar in localisation compared to the very scattered fluorescence in control and si-GFP treated cells.

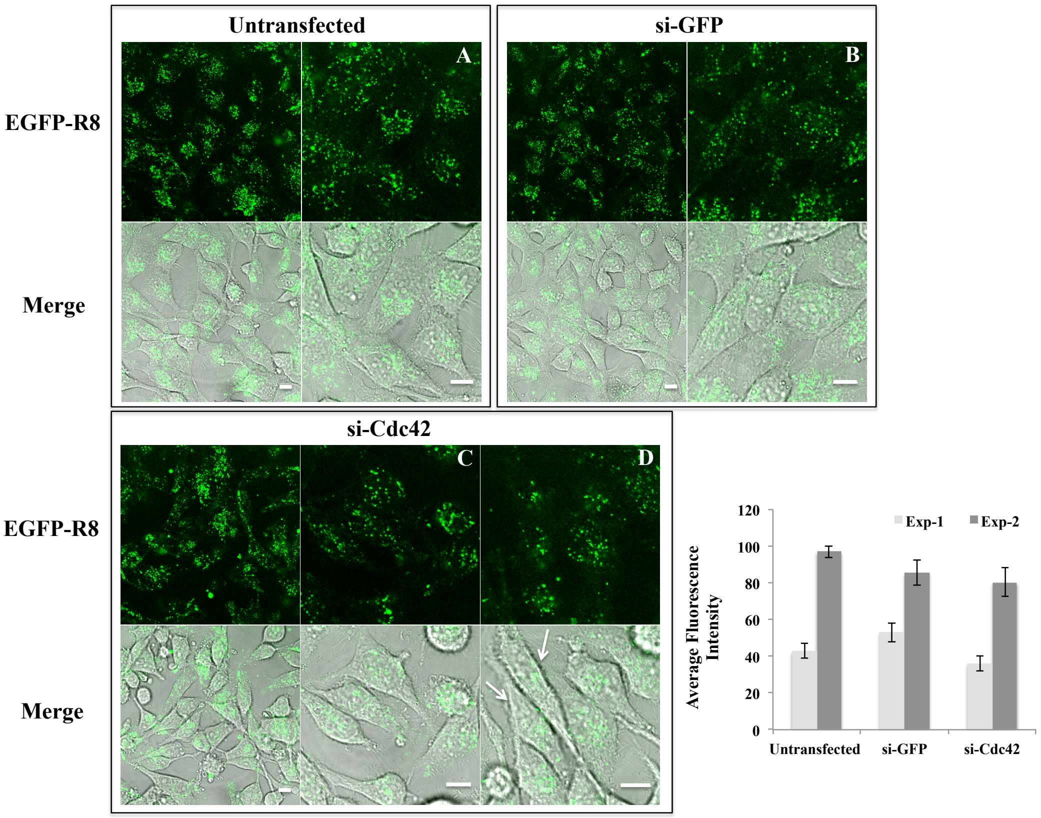

Figure 5.11 Effects of Cdc42 depletion on the cellular uptake of EGFP-R8 in HeLa cells. Untransfected cells and cells transfected with control siRNA (si-GFP) or siRNA targeting Cdc42 (si-Cdc42) were incubated for 1 hr with 2 µM EGFP-R8 at 37°C/5% CO_2, and washed with heparin. Cell-associated fluorescence was analysed by confocal microscopy and shown are representative single projection images of fluorescence only (top rows) and merges of fluorescence and DIC of the same cells. Shown in Column A, B, and C and D are zoomed images of ~5 cells from different fields of view. Scale bars 10 µm. Quantification data shown at bottom right represents the average fluorescence intensity +/- S.D. indicating intra-experimental variations from two independent experiments.

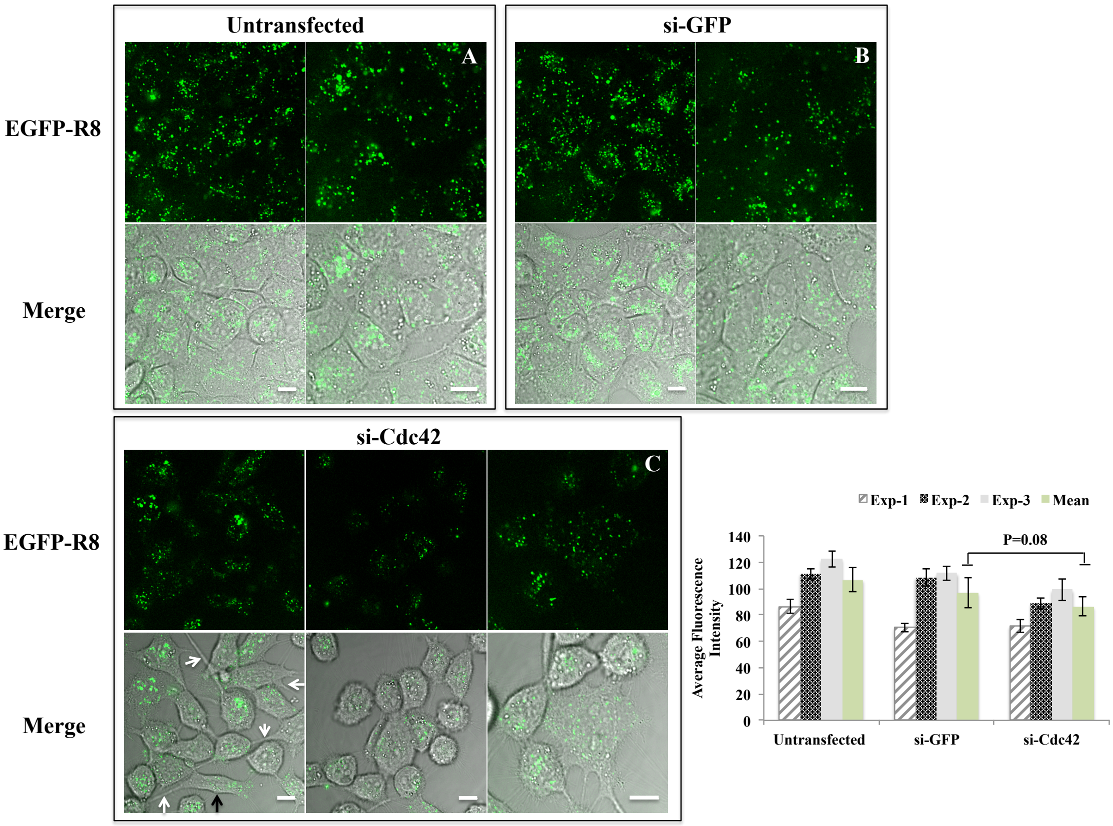

Figure 5.12 Effects of Cdc42 depletion on the cellular uptake of EGFP-R8 in A431 cells. Untransfected cells and cells transfected with control siRNA (si-GFP) or siRNA targeting Cdc42 (si-Cdc42) were incubated for 1 hr with 2 μM EGFP-R8 at 37°C/5% CO_2, and washed with heparin. Cell-associated fluorescence then was analysed by confocal microscopy and shown are representative single projection images of fluorescence only (top rows) and merges of fluorescence and DIC of the same cells. Shown in Column A, B, and C are zoomed images of 5-8 cells from different fields of view. Scale bars 10 μm. Quantification data shown at bottom right represents the average fluorescence intensity +/- S.D. from three independent experiments (Exp 1-3; error bars indicate the intra-experimental variations) and the mean fluorescence intensity +/- S.D. of these three experiments (highlighted in green colour; error bars indicate the inter-experimental variations). Student's independent T-Tests were performed to determine the significance of differences between two means. Statistical significance p=0.08.

As previously shown by DIC microscopy, si-Cdc42 transfected HeLa and A431 cells had visible morphological changes compared to control cells and this was most pronounced in A431 cells. To further investigate whether these cell shape alterations are related to or mediated by actin cytoskeleton rearrangements, untransfected A431 cells or cells incubated with either control siRNA (si-GFP) or siRNA targeting Cdc42 (si-Cdc42) at 37°C/5% CO_2 for 72 hr were fixed and labelled for the nucleus and F-actin, and imaged by the confocal microscopy method described in chapter 4. The cells were incubated for 72 hr rather than 48 hr to maximise the possibility of clearly seeing morphological/actin effects. In Figure 5.13, two typical phenotypes of actin cytoskeleton organisation are shown side by side for each experimental condition - untransfected cells, si-GFP and si-Cdc42 treated cells. A fraction of imaged cells were observed to assemble pronounced long actin fibres (Figure 5.13 B, D and F), particularly noticeable in the basal cell region. In other cells (Figure 5.13 A, C and E) these structures were absent but both phenotypes highlighted the cortical actin that has been described in chapter 4. The F-actin distribution in si-Cdc42 treated cells did not exhibit detectable alterations, compared with those of control cells.

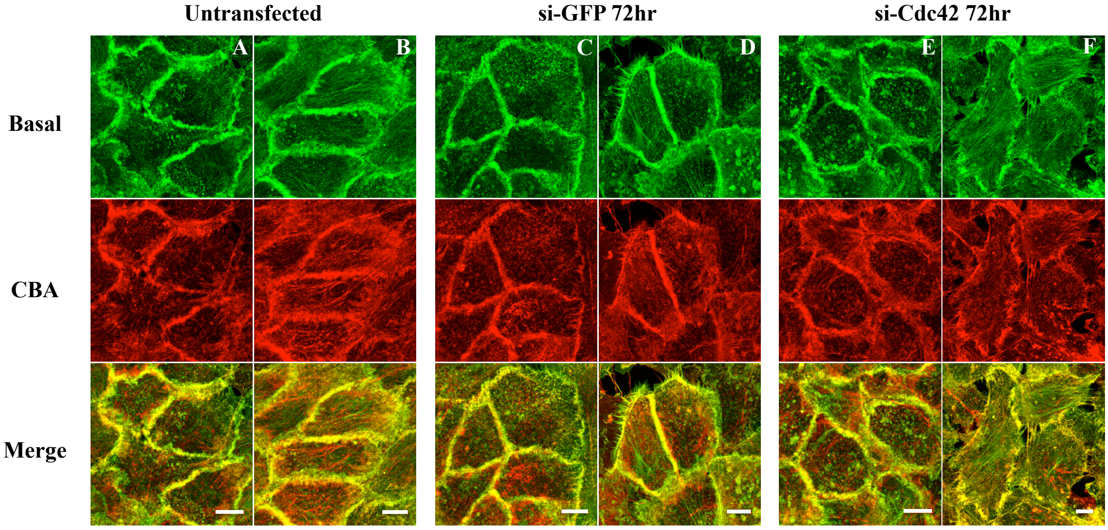

Figure 5.13 Effects of Cdc42 depletion on the actin architecture in A431 cells. Untransfected cells and cells transfected with control siRNA (si-GFP) or siRNA targeting Cdc42 (si-Cdc42) were fixed and stained with Rh-P. Images were acquired as described in section 4.3.1. Scale bars 10 μm.

In chapter 4 A431 cells pre-treated with PP2 did not respond to Cyt D with respects to EGFP-R8 uptake. Experiments were then prepared to investigate whether si-Cdc42 transfected cells were responsive to Cyt D effects. Cells were cultured and untransfected or transfected with siRNA targeting Cdc42 (si-Cdc42) for 48 hr at 37°C/5% CO_2. Some of these cells were further incubated with 10 μM Cyt D for 15 min prior to addition of 2 μM EGFP-R8 for 1 hr in the continued presence of 10 μM Cyt D. The cells were then washed with heparin, and cell-associated fluorescence was analysed by live cell imaging confocal microscopy. As shown in Figure 5.14 and as expected, Cyt D treatment alone dramatically enhanced the EGFP-R8 uptake by A431 cells. Cells transfected with si-Cdc42 were equally responsive to this drug (Figure 5.14 A-B). This was irrespective of their shape.

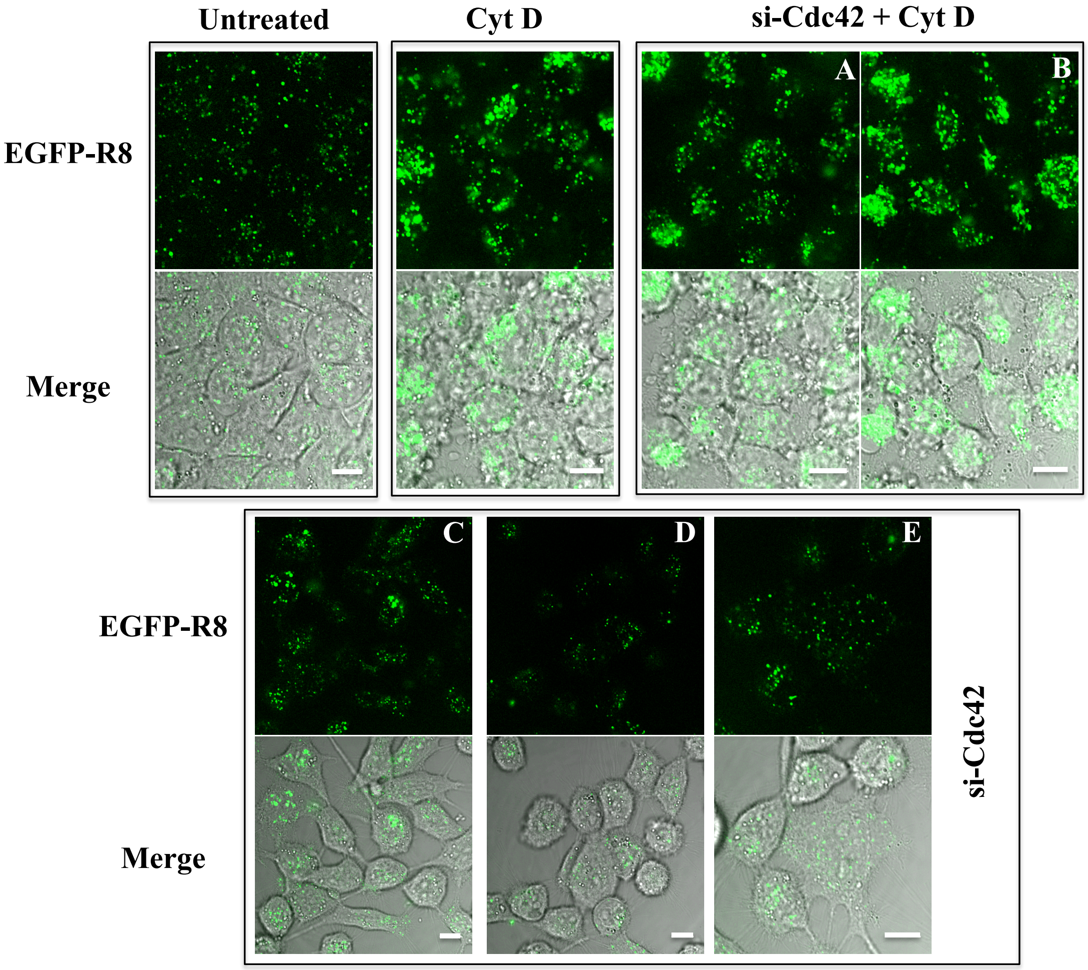

Figure 5.14 Effects of Cdc42 depletion alone and the combination of Cdc42 depletion and Cyt D on the cellular uptake of EGFP-R8 in A431 cells. Cells were cultured and untransfected or transfected with siRNA targeting Cdc42 (si-Cdc42) for 48 hr at 37°C/CO_2. Cells were then incubated with or without 10 µM Cyt D for 15 min prior to incubation with 2 µM EGFP-R8 for 1 hr in the presence or absence of Cyt D. Cells were then washed with heparin, and cell-associated fluorescence was analysed by confocal microscopy. Shown are representative single projection images of fluorescence only (top rows) and merges of fluorescence and DIC of the same cells. Shown in column A and B are images obtained from two different fields of view, and in column E are zoomed images from a different field of view of C/D. Scale bars 10 µm.

5.3 Discussion

The overall aim of this chapter was to support data obtained in chapters 3 and 4 via the development of alternative techniques to study the cellular uptake of CPP-protein conjugates. For clear reasons EGFP was used as a model cargo that allowed for direct analysis of fluorescence inside cells using live cell confocal microscopy. This was the preferred method here over flow cytometry that had previously been used to detail the cellular uptake of Alexa 488 conjugated R8 used here and also HIV-Tat (Al Soraj et al., 2012). Microscopy allows researchers the added benefit of seeing the localisation of CPPs and cargos inside cells and also highlighted in this study is the high degree of heterogeneity in cell phenotype of fluorescence seen within a single experiment within a single population. Ideally flow cytometry and microscopy should be used in tandem but this requires more time that was not available for this thesis.

A large number of investigations on internalisation mechanisms of CPPs attached to small or large cargos have been made, and the vast majority of these studies have relied on the use of chemical inhibitors of endocytosis. Their inherent lack of specificity makes data interpretation very difficult and this is why the laboratory invested time to develop molecular, siRNA targeting strategies, not to totally replace inhibitor work but to supplement research performed with these agents. In this chapter, a number of different siRNA sequences were used as an attempt to block pathways regulated by AP2μ2, caveolin-1, flotillin-1, PAK-1 and Cdc42, and therefore to evaluate the involvement of these pathways in the cellular uptake of EGFP-R8. However optimisation of all siRNA-based silencing was not performed for this PhD project due to time constraints; this includes the inability to silence >50% expression of Cav-1 in A431 cells. This raises the concern that some negative data from CPP uptake assays may be due to the fact that there was insufficient depletion of a protein to mediate a cellular effect on endocytosis.

Initially, several attempts using a siRNA sequence were carried out to deplete the expression of AP2μ2 subunit that forms part of the AP2 complex that is vital for CME. Unfortunately these experiments were unsuccessful due to the poor quality of the purchased AP2μ2 antibodies that gave multiple bands by Western blotting (data not shown). Towards the end of my experimental period Dr Paul Moody in the laboratory was able to characterise AP2μ2 silencing in HeLa cells (Moody et al., 2015). This approach will now be of significant interest to test this very important pathway in cellular uptake of EGFP-R8.

The siRNA sequence employed in this section to target caveolin-1 successfully depleted caveolin-1 expression in HeLa cells. However, this depletion had no detectable effects on EGFP-R8 internalisation. HeLa cells have been reported to utilize caveolar endocytosis to internalise different cargos including lipoplexes (Rejman et al., 2005) and nanoparticles (Bohmer and Jordan, 2015). In a separate study depletion of caveolin-1 in this cell line via siRNA targeting was found to reduce the uptake of a transportan-streptavidin conjugate by up to 50% and interestingly flotillin-1 depletion increased transportan mediated uptake of the same cargo (Säälik et al., 2009). For these types of experiments it should not be overlooked that inhibition of a particular pathway may activate other pathway(s), which then act as compensatory mechanism(s) to perform cargo internalisation. Caveolin-1 depletion has been reported to increase the levels of activated Cdc42 at the plasma membrane (Doherty and McMahon, 2009), and stimulated the Cdc42-dependent fluid phase endocytosis in epithelial ovarian hamster cells (Cheng et al., 2010). An efficient siRNA transfection usually requires at least 24 hr to achieve effective depletion of a protein and in this time the inhibition of one targeted pathway may lead to an up-regulation in the activity of an alternative endocytic pathway. One of the advantages of using pharmacological inhibitors is that the agent only needs to be added to cells for a short period of time to mediate an effect on endocytosis. The problem is that this effect is unlikely to be confined to one endocytic pathway.

Pharmacological inhibitors also affect all cells in the experimental population and effects seen with siRNA transfections will only be obvious if the transfection efficiency is high. This was not the case in A431 cells incubated with si-Cav-1 and it still remains to be determined whether caveolae play an important role in EGFP-R8 uptake in this cell line.

Although flotillin-1 expression was successfully depleted in both HeLa and A431 cells, the lack of this endocytic protein did not exhibit notable effects on EGFP-R8 internalisation in these two cell types. It indicates that the cargo EGFP-R8 does not use flotillin-mediated endocytic pathway for cell entry in these cells. This finding was consistent with our previously published studies where flotillin-1 knockdown with siRNA showed no effects on the cellular uptake of Alexa 488 conjugates of HIV-Tat or R8 (Al Soraj et al., 2012). A major obstacle underlying the investigations of flotillin-mediated pathway is the lack of specific and easy available probes to label this pathway inside cells and also the lack of specific chemical inhibitors to perturb this entry route. To date in addition to flotillin itself, only a limited number of molecules including anti-CD59 antibody have been reported to employ this pathway to enter into cells (Glebov et al., 2006).

It should also be mentioned that both caveolin-1 and flotillin-1 may be regulating the integrity of the plasma membrane via organising lipid rafts to where they both reside. Silencing the expression of these proteins may therefore have effects beyond their roles in mediating endocytic effects as the cells may have very different plasma membrane organisation. The very same is likely to be true in cells incubated with cholesterol sequestering drugs such as methyl β-cyclodextrin that is often used in CPP and other drug delivery research to target endocytosis mediating from lipid rafts (Kaplan et al., 2005, Li et al., 2012, Lim et al., 2013). Great care should be given to interpreting this data.

The siRNA-mediated depletion of the macropinocytosis regulator PAK-1 was shown to reduce the internalisation of R8-Alexa 488 and HIV-Tat by up to 50% in A431 cells (Al Soraj et al., 2012). Growth factor induced entry (i.e. macropinocytosis) of the fluid phase probe dextran into the same cell line was also shown in another study to be inhibited by endogenous PAK-1 silencing (Liberali et al., 2008), indicating that the PAK-1 activity is required for macropinocytic uptake. A recent study examining the molecular mechanisms of the cell entry of Herpes simplex virus1 suggested that the virus internalisation by HeLa cells was dependent on PAK-1 activity either for macropinocytosis or for the reorganisation of local cortical actin cytoskeleton allowing for passage through the plasma membrane and the actin cortex (Devadas et al., 2014). In contrast to these earlier observations, we found that cellular entry of EGFP-R8 was unaffected in PAK-1 depleted cells. The reason for this CPP PAK-1 discrepancy is unknown but may be due to differences in cargo (Alexa 488 vs EGFP) and/or methodology (flow cytometry vs confocal microscopy) and/or a higher level of PAK-1 silencing. Further mention to this is given in the final discussion.

As previously discussed in Section 5.1, Cdc42 plays a crucial role in regulating actin remodelling, thereby controlling cell migration, invasion and morphology (Heasman and Ridley, 2008). This GTPase is mainly responsible for promoting filopodia formation, and two models including convergent elongation and tip nucleation have been suggested to underlie this (Mellor, 2010, Mattila and Lappalainen, 2008). The tip nucleation model involves the formin family of proteins, which stimulate nucleation and the subsequent assembly of linear actin filaments that are required to generate cellular actin structures such as filopodia (Yang and Svitkina, 2011). Upon activation, active Cdc42 can bind to and stimulate the formin family members mDia2 and formin-like protein 3, which in turn induce the formation and extension of filopodia (Wakayama et al., 2015). In a recently published study, the increased activation of Cdc42 (constitutively activated by the Cdc42 GEF Dock10 protein) in HeLa cells induced a morphological transition from polygonal elongated to non-polygonal but more rounded cell shape, with the accompany of inducible formation of filopodia (Ruiz-Lafuente et al., 2015). This is consistent with the proposed role of Cdc42 for filopodia formation. Moreover, this report on the loss of morphological elongation was consistent with a previous study by Gadea and coworkers (Gadea et al., 2008), where siRNA-mediated Dock10 knockdown resulted in a decreased level of activated Cdc42 and thereby a morphology alteration from rounded to elongated in amoeboid cells. This cell elongation also occurred in a population of our si-Cdc42 treated HeLa and A431 cells. Therefore, these observations together confirm the role of Cdc42 for the maintenance of normal cell shape that requires the coordination of membrane remodelling and actin cytoskeleton dynamics at the cell edge. It should be noted that in migrating cells, Cdc42 also contributes to the regulation of the polarity of microtubules through a distinct pathway from that modulating actin cytoskeleton (Cau and Hall, 2005).

An unusual observation discovered in this thesis was the rounding of A431 cells transfected with siRNA targeting Cdc42. This did not extend across the total cell population and may only be observed in cells at a certain stage in cell division. These cells also appeared to have decreased EGFP-R8 fluorescence and it remains to be determined whether this is a due to their position in the cell cycle or the fact that they were depleted of Cdc42. By labelling cells with rhodamine-phalloidin it was expected that actin effects would be highlighted but this was not the case as it was impossible to identify differences between control and si-Cdc42 treated cells. This suggests that the effects are subtle and that alternative microscopy systems such as super resolution systems may be required to observe them. It should be noted here that the siRNA approach used here was very efficient at depleting Cdc42 (>90%) thus criticisms regarding poor silencing (e.g. caveolin-1 in A431 cells) do not really apply.

In a collaborative study with our group Cdc42 depletion impaired the internalisation of glycol chitosan nanogels (Pereira et al., 2015) and similar effects again in HeLa cells were noted for uptake studies characterising the cellular uptake of silica-coated iron oxide nanoparticles (Bohmer and Jordan, 2015) and the entry of vaccine into bladder cancer cells (Redelman-Sidi et al., 2013). This highlighted the involvement of actin dynamics in these events and most probably macropinocytosis. Additionally, in HeLa cells depleted of Cdc42, dextran uptake through clathrin-independent fluid phase endocytosis was markedly reduced (Francis et al., 2015). However, our data obtained from cells with loss of Cdc42 expression implied that the endocytic route(s) regulated by Cdc42 were not necessarily implicated in EGFP-R8 uptake. Moreover, the role of macropinocytosis in EGFP-R8 internalisation could not be confirmed from results presented in this chapter.

Chapter 6: General discussion

It has been more than twenty years since the identification of the first cell penetrating peptide (CPP) (Derossi et al., 1994). This was penetratin and this peptide represents one of the most studied CPPs in the literature as studies on this peptide now span twenty-two years (Gartziandia et al., 2016). A growing number of reports on the capacity of CPPs to deliver a wide range of cargos from small molecular entities to macromolecules including large bioactive complexes into the cell interior reflect the continued interest in them for therapeutic/clinical applications. It should be noted, however, that despite this great effort the number of CPP delivery systems that have made it from bench to clinical trial is disappointingly low and none of these have made it all the way to market.

A major issue that contributes to this poor translation to clinic is the lack of detailed knowledge on the membrane translocation mechanisms that CPPs or CPP-cargos employ. Most of the known CPPs, especially those attached to large cargo such as proteins (Säälik et al., 2009) or being part of nanoparticle formulations (Khalil et al., 2006, Torchilin, 2008) are assumed to rely on endocytic pathways to enter into cells. For some CPPs that are attached to small cargos, non-endocytic direct translocation has been clearly shown to mediate their cellular entry (Duchardt et al., 2007, Tünnemann et al., 2006, Jones and Sayers, 2012). All known endocytic pathways are accompanied by cell cortex remodelling during the internalisation processes; by membrane invagination (e.g. CME and caveolar endocytosis) or membrane protrusion (e.g. macropinocytosis). The literature highlights the very strong link between endocytic pathways and actin and describes how the actin cytoskeleton associates with components of the endocytic machinery during endocytosis (Qualmann et al., 2000, Roth, 2007, Taylor et al., 2012). For example, actin regulators such as ARP2/3 and N-WASP are observed to relocate to clathrin-coated vesicles to facilitate CME (Merrifield et al., 2004). Overall, with the exception of macropinocytosis that involves extensive actin reorganisation, there is little consensus in the literature regarding the exact role of the actin network for endocytic processes (Mooren et al., 2012). The strong link between CPPs and actin has been described in Chapter 3 and 4, and was a major focus of the previous studies in our laboratory (Al Soraj et al., 2012) leading up to the thesis presented here. Further information on this poorly characterised link would hopefully contribute to CPP knowledge with respects to mechanisms of action of cell entry.

A major focus of this PhD project was to perform comparative analysis of the reliance on actin of the internalisation of CPP-conjugates R8-Alexa 488 and EGFP-R8 into two different cell lines HeLa and A431 cells that had been previously shown to have major differences in uptake profiles of R8-Alexa 488. Two major questions were asked with respects to elucidating how these CPP conjugates comparatively rely on, or influence actin dynamics to gain access into cells.

Previous work in the laboratory had focused on CPP-fluorophores and this project initially developed and optimised a protein purification protocol to obtain EGFP-R8 of high yield and also of high purity from *E.coli* cultures. This was developed and the final product achieved a purity of >99% allowing us to confidently study its mechanism(s) of cell entry.

As well as studying CPPs the thesis was also interested in studying the uptake of dextran, a well characterised probe that enters cells via a non receptor process (fluid phase uptake) and also by macropinocytosis (Jones, 2007). As CPPs have also been shown to enter via these pathways dextran represents a good endocytic model for parallel studies with the two selected R8 conjugates. As noted, previous studies performed in the laboratory demonstrated a major difference in the results obtained in dextran uptake in HeLa and A431 cells when actin was disrupted with Cyt D (Al Soraj et al., 2012).

To extend the previous work that the laboratory had performed on both CPPs and dextran with Cyt D, a variety of other actin inhibitors including Lat B and JAS working via different mechanisms were utilized in this thesis and the results were compared with those obtained with Cyt D. In HeLa cells, Cyt D reduced the cellular uptake of both CPP conjugates (R8-Alexa 488 and EGFP-R8) and dextran, but had little effects on the internalisation of CME marker transferrin (TF). Similar to the case in HeLa cells, entry of TF in A431 cells was unaffected by Cyt D. Although this drug did not exert notable influence on the uptake level of R8-Alexa 488 in A431 cells, it altered the distribution of labelled punctate structures from scattered to clustered. It is only by using microscopy based technologies that these subtle changes are observed as flow cytometry would generally not be able to provide this level of information. By contrast, the internalisation of both EGFP-R8 and dextran into vesicles in A431 cells was dramatically enhanced by Cyt D, and a vast majority of these fluorescent vesicles were observed to aggregate in perinuclear regions rather than be scattered throughout the cytoplasm in control cells. This data was unexpected and had not been previously shown. It was also absent form a very large study on twenty-two different CPPs in four cell lines (including HeLa, but not A431 cells) using a number of endocytosis inhibitors where no data on actin-dependent uptake was presented (Mueller et al., 2008). This study did, however, highlight the different responses of the four cell lines to the chosen endocytic inhibitors and also major differences in peptide uptake in the absence of drugs.

CME mediated TF uptake in both cell cells, under the experimental conditions used in this project, did not appear to be sensitive to actin disruption and again the involvement of actin in TF endocytosis is known to be cell line dependent (Fujimoto et al., 2000). In this thesis uptake of the two CPP conjugates and dextran in HeLa cells, by endocytosis, required a functional actin system. In A431 cells, EGFP-R8 and R8-Alexa 488 seemed to utilize different uptake mechanisms (possibly endocytic pathways) to gain access to the cells and uptake characteristics of dextran very closely resembled that of EGFP-R8. However, the low degree of co-localisation obtained after simultaneous incubation of EGFP-R8 and dextran indicated that more than one endocytic routes were utilized by this CPP conjugate. It should be mentioned that dextran as a fluid phase probe also has the capacity to enter cells via multiple pathways. The same co-incubation experiment was then performed in Cyt D treated A431 cells. This study quite dramatically highlighted the increased uptake of both probes and this time they were very strongly co-localised. The underlying mechanism involved in this process still remains unclear. It should be noted that the dextran used in this project is anionic and additional experiments using neutral dextran could be performed to minimise the potential electrostatic interactions between anionic dextran and cationic R8 in the extracellular environment and thus avoid their co-internalisation as complexes into the same endocytic vesicles.

The striking difference between these two cell lines in response to Cyt D with respects to uptake of both EGFP-R8 and dextran may lie in their difference in actin cytoskeleton as previously noted (Al Soraj et al., 2012) and also shown in this thesis. Actin in HeLa cells is prominent in long filaments while cortical actin, associated with the plasma membrane is much more abundant in A431 cells. Therefore, in this thesis, the interesting increased EGFP-R8 uptake in A431 cells by Cyt D was further investigated;

noting that actin is usually regarded as a promoter of endocytosis. Like Cyt D, two other actin-targeting reagents, JAS and Lat B directly interact with actin and modify the actin cytoskeleton as described in Section 4.1. Initially, the effects of these three agents on actin were analysed using confocal fluorescence microscopy in fixed A431 cells labelled with rhodamine-phalloidin. At certain concentrations, all these three drugs showed pronounced disruption of the actin cytoskeleton: they caused the actin reorganisation into amorphous masses and thinned out or even completely destroyed the cortical actin meshwork. Confirming data shown for Cyt D, a marked increase in uptake of EGFP-R8 was also observed in cells treated with Lat B or JAS. The plasma membrane tension of mammalian cells is mainly maintained by actin network, and reduced membrane tension resulted from actin disruption may actually favor the formation of invaginations during the step of endocytosis initiation (Greene and Gao, 2009). Additionally the cortical actin network located immediately beneath the plasma membrane is tightly associated with the membrane via linking proteins such as cortactin (Weed and Parsons, 2001, Cao et al., 2010), and may facilitate membrane invagination and the subsequent scission by providing the mechanical force that is required for membrane deformation (Kaksonen et al., 2006). Studies have also shown that the cortical actin network could function as a physical barrier for exocytosis in chormaffin cells as the transient and focal disruption of actin cytoskeleton underneath the plasma membrane facilitated these secretion processes (Cheek and Burgoyne, 1986, Trifaró and Vitale, 1993, Jog et al., 2007, Johnson et al., 2012). These previous findings together with data in this thesis suggest that this tight mesh of actin is a general barrier to membrane trafficking events close to the plasma membrane.

The other two chemical inhibitors Y27632 and PP2 do not directly interact with actin filaments and influence the actin cytoskeleton in A431 cells via inhibition of ROCKs and Src kinases respectively. The formation of a large number of actin needles that were mostly running perpendicular to the plasma membrane was clearly shown in cells treated with Y27632 of relatively high concentrations and in contrast to the previously discussed actin disruptors, the cortical actin network was still evident in these drug treated cells. In addition to its effects on actin organisation, Y27632 also increased the internalisation of EGFP-R8 into vesicular structures. But unlike those observed in Cyt D or Lat B or JAS treated cells, these fluorescent punctate structures were found to distribute throughout the cytoplasm in a scattered fashion. These observations obtained in cells treated with Y27632 would appear to challenge our hypothesis regarding the role of cortical actin in endocytosis. However it may well be that this drug was able to interfere with cortical actin but in a manner that did not allow for easy identification using confocal microscopy.

Previous studies, mainly from the Futaki laboratory have shown that cationic CPPs such as R8 influence actin arrangement and that this is linked to the possibility that this influences peptide uptake into cells – induction of macropinocytosis (Nakase et al., 2004, Nakase et al., 2007). The effects of EGFP-R8 (2 μM) on the actin architecture of control cells or cells treated with different actin drugs were also investigated to determine whether CPP effects on actin could influence the ability of these drugs to disrupt the cytoskeleton. This was not observed, initially the data shows that EGFP-R8 itself at this concentration did not induce visible actin rearrangement that would be expected to either inhibit or promote uptake via macropinocytosis. Therefore, actin reorganisation/disruption caused by these actin inhibitors working directly or indirectly is the major factor governing this enhanced uptake. These studies allowed for repeating some of the earlier studies shown for R8 and this was performed whilst developing the microscopy assay for visualising actin that was later published (He et al., 2015). It was discovered that the capacity of this CPP to modify actin is highly dependent on the state of the cells and that serum-starved cells were much more sensitive than control cells. This explains why so many studies on macropinocytosis as a cellular event and as a putative response to CPPs are done in serum-starved cells. Caution should however, be given to interpreting the data from these studies as they are done in highly stressed cells.

The results from studies using the Src kinase inhibitor PP2 were surprising and very interesting. PP2 did not cause marked changes in actin arrangement in HeLa cells, whereas in A431 cells, actin filaments became very apparent and the drug also stimulated actin assembly into filamentous bundles. This may be due to the effects of this drug on the Raf-MEK-ERK signalling cascade. The activation of Raf-1, a cytoplasmic serine/threonine protein kinase, involves interaction with active Ras (Ras-GTP) that recruits the protein, in an autoinhibited state, from the cytosol to the plasma membrane and activates it (Marshall, 1995, Desideri et al., 2015). Raf-1 has also been localised to endosomes (Rizzo et al., 2000, McKay et al., 2011) and efficient activation of this protein also requires additional phosphorylation on tyrosine residues by Src kinases and serine residues by PAKs (Tran and Frost, 2003). Activated Raf-1 has been reported to bind to mitogen and extracellular signal-regulated kinase (MEKs) and trigger the phosphorylation and activation of these MEKs and also the extracellular signal-regulated kinases (ERKs) (Pritchard et al., 2004). Together these as the Raf-MEK-ERK pathway have a role in regulating actin remodelling (Nussinov and Jang, 2014). A number of published studies have demonstrated that the constitutive activation of Src by v-Src kinase overexpression lead to a loss of actin stress fibres and other alterations in cytoskeletal architecture, and that v-Src-induced actin disruptions were linked to the activation of MEK and ERK, and the subsequent inhibition of Rho GTPases and their downstream effector ROCKs (Pawlak and Helfman, 2002, Fincham et al., 1999, Mayer et al., 1999, Pullikuth and Catling, 2007, Guarino, 2010). As previously discussed in Chapter 4, the activation of ROCKs by Rho is involved in the formation and stabilisation of actin stress fibres via interactions with a variety of substrates such as LIMK. Considering these together, it is possible that the pharmacological inhibition of Src kinases by PP2 induced a sequential inhibition of Raf, MEKs and then ERKs and in turn stimulated ROCK-mediated actin assembly into fibres. PP2, like Y27632 had not previously been studied in our laboratory and exerted no visible influence on EGFP-R8 uptake in HeLa or A431 cells. However, we were very surprised to observe that pre-incubation of this inhibitor in A431 cells abrogated or completely abolished the Cyt D mediated increase in cellular uptake of this R8 protein conjugate. Importantly the drug was unable to prevent Cyt D mediated actin disruption. The underlying mechanisms governing these surprising findings are unknown but suggest that further cell biology analysis should be performed with PP2 and other actin inhibitors to shed more light on how actin regulates endocytosis and other cellular functions.

In other CPP studies Cyt D alone is used to highlight the role of actin in cell uptake, but based on the results presented in this thesis there is certainly an argument for looking at more actin modifiers to get a higher level of understanding as summarised for R8 conjugates, TF and dextran in Figure 6.1.

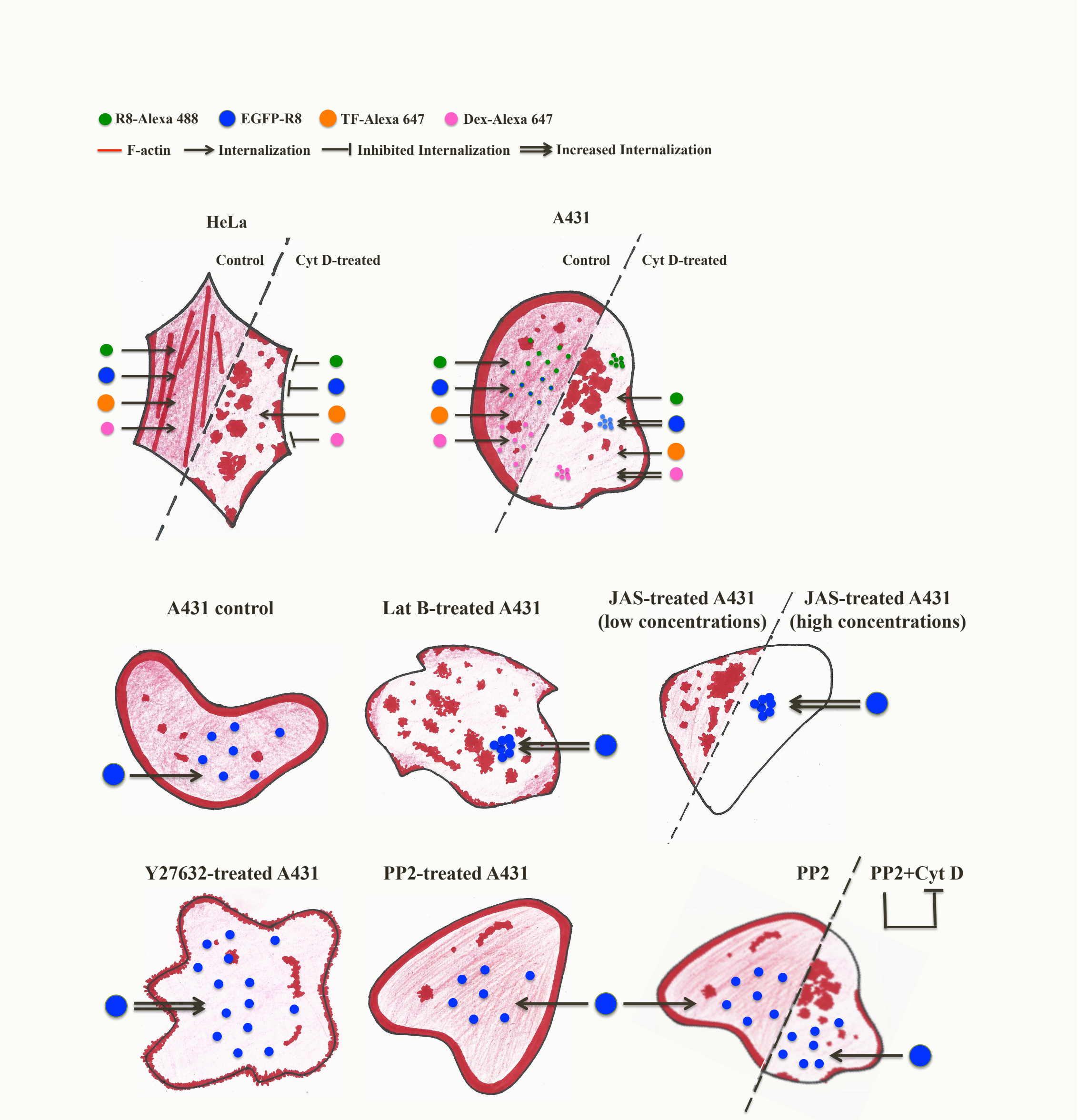

Figure 6.1 Summary of the effects of different actin inhibitors on the actin cytoskeleton and the cellular uptake of CPP conjugates and endocytic probes. Cortical actin is represented as a thick red line that is associated with the plasma membrane.

Supplementation of inhibitor studies with siRNA-based targeting of endocytic proteins and pathways were performed in the last results chapter, in some cases using uncharacterised siRNA and cell models. There was no strong evidence showing that caveolin-1 or flotillin-1 mediated endocytic pathways were implicated in the EGFP-R8 uptake by both HeLa and A431 cells. Caveolar endocytosis was reported to be involved in internalisation of transportan-avidin complexes into HeLa cells (Säälik et al., 2009), but there is no strong data to suggest that this CPP and R8 share identical uptake mechanisms. As PAK-1 is such an important regulator of actin it was rather surprising to observe that si-PAK-1 treated cells had a visibly normal actin phenotype, and that EGFP-R8 uptake seemed to be independent of PAK-1 expression. This may be seen as evidence that macropinocytosis does not regulate uptake of EGFP-R8 in these studied cells. PAK-1 and Cdc42 function in actin organisation is linked and the depletion of Cdc42 from HeLa cells resulted in morphological changes (elongation), which is in agreement with earlier observations from different laboratories (described in section 5.3). Some rather unusual morphological alterations were detected in our si-Cdc42 treated A431 cells with cell rounding and the formation of filopodia-like structures being observed; the latter was unexpected based on the described role of this GTPase in promoting filopodia formation (Chapter 5). These global effects on cells were not reflected in any observable changes on actin cytoskeleton that was visualised by rhodamine-phalloidin staining. Cdc42 is a well-established actin regulator, but in contrast to PAK-1, it may not be essential for macropinocytosis (Amstutz et al., 2008, Koivusalo et al., 2010). In line with observations of an apparently normal actin arrangement in these cells, EGFP-R8 uptake was not evidently affected by Cdc42 depletion.

The importance of the actin cytoskeleton in endocytic processes cannot be underestimated and this PhD project provides new insights into the role(s) of actin for the endocytic uptake of R8 conjugates. We should no longer assume that proper actin assembly is required for R8 uptake in all cell lines. In our hands, as Alexa 488 conjugates, R8 and HIV-Tat peptide behave very similarly (Fretz et al., 2007, Al Soraj et al., 2012) and we suggest here that similar effects would be seen with HIV-Tat when actin is directly disrupted. Remaining to be seen are data from experiments using other more complex CPPs such as penetratin that are likely to use different uptake mechanisms. Interpretation of data on EGFP-R8 uptake following actin disruption/reorganisation is clearly dependent on several factors including the choice of cell line (tissue), the mechanism of actin interfering agent and the nature of the attached cargo. It is very likely that in HeLa cells, this protein cargo employs macropinocytosis/fluid phase uptake to enter into the cell interior. However, for A431 cells, the situation is more complex because of the way these cells and quite possibly others arrange the actin to serve its multiple functions including endocytosis. For future CPP development, the work presented in this thesis further highlights that characterisation of cell uptake is needed in more than one cell model to provide a better understanding of their potential as drug delivery vectors for delivering therapeutics to different tissues.

References

ADELMAN, M. R. & TAYLOR, E. W. 1969. Isolation of an actomyosin-like protein complex from slime mold plasmodium and the separation of the complex into actin- and myosin-like fractions. *Biochemistry,* 8**,** 4964-4975.

AKHMANOVA, A. & HAMMER III, J. A. 2010. Linking molecular motors to membrane cargo. *Current Opinion in Cell Biology,* 22**,** 479-487.

AL SORAJ, M., HE, L., PEYNSHAERT, K., COUSAERT, J., VERCAUTEREN, D., BRAECKMANS, K., DE SMEDT, S. C. & JONES, A. T. 2012. siRNA and pharmacological inhibition of endocytic pathways to characterize the differential role of macropinocytosis and the actin cytoskeleton on cellular uptake of dextran and cationic cell penetrating peptides octaarginine (R8) and HIV-Tat. *Journal of Controlled Release,* 161**,** 132-141.

AL-TAEI, S., PENNING, N. A., SIMPSON, J. C., FUTAKI, S., TAKEUCHI, T., NAKASE, I. & JONES, A. T. 2006. Intracellular traffic and fate of protein transduction domains HIV-1 TAT peptide and octaarginine. Implications for their utilization as drug delivery vectors. *Bioconjugate Chemistry,* 17**,** 90-100.

ALVES, I. D., GOASDOUÉ, N., CORREIA, I., AUBRY, S., GALANTH, C., SAGAN, S., LAVIELLE, S. & CHASSAING, G. 2008. Membrane interaction and perturbation mechanisms induced by two cationic cell penetrating peptides with distinct charge distribution. *Biochimica et Biophysica Acta (BBA) - General Subjects,* 1780**,** 948-959.

ÅMAND, H. L., FANT, K., NORDÉN, B. & ESBJÖRNER, E. K. 2008. Stimulated endocytosis in penetratin uptake: Effect of arginine and lysine. *Biochemical and Biophysical Research Communications,* 371**,** 621-625.

AMSTUTZ, B., GASTALDELLI, M., KÄLIN, S., IMELLI, N., BOUCKE, K., WANDELER, E., MERCER, J., HEMMI, S. & GREBER, U. F. 2008. Subversion of CtBP1-controlled macropinocytosis by human adenovirus serotype 3. *The EMBO Journal,* 27**,** 956-969.

AMYERE, M., PAYRASTRE, B., KRAUSE, U., SMISSEN, P. V. D., VEITHEN, A. & COURTOY, P. J. 2000. Constitutive macropinocytosis in oncogene-transformed fibroblasts depends on sequential permanent activation of phosphoinositide 3-kinase and phospholipase C. *Molecular Biology of the Cell,* 11**,** 3453-3467.

ANDERSON, R. G. W. 1998. The caveloae membrane system. *Annual Review of Biochemistry,* 67**,** 199-225.

ANGERS-LOUSTAU, A., HERING, R., WERBOWETSKI, T. E., KAPLAN, D. R. & DEL MAESTRO, R. F. 2004. SRC regulates actin dynamics and invasion of malignant glial cells in three dimensions. *Molecular Cancer Research,* 2**,** 595-605.

ANITEI, M. & HOFLACK, B. 2012. Bridging membrane and cytoskeleton dynamics in the secretory and endocytic pathways. *Nature Cell Biology,* 14**,** 11-19.

ARAKI, N., HATAE, T., YAMADA, T. & HIROHASHI, S. 2000. Actinin-4 is preferentially involved in circular ruffling and macropinocytosis in mouse macrophages: analysis by fluorescence ratio imaging. *Journal of Cell Science,* 113**,** 3329-3340.

BALKLAVA, Z., PANT, S., FARES, H. & GRANT, B. D. 2007. Genome-wide analysis identifies a general requirement for polarity proteins in endocytic traffic. *Nature Cell Biology,* 9**,** 1066-1073.

BALLESTREM, C., WEHRLE-HALLER, B. & IMHOF, B. A. 1998. Actin dynamics in living mammalian cells. *Journal of Cell Science,* 111**,** 1649-1658.

BANGHAM, A. D., STANDISH, M. M. & WATKINS, J. C. 1965. Diffusion of univalent ions across the lamellae of swollen phospholipids. *Journal of Molecular Biology,* 13**,** 227-238.

BANNING, A., KURRLE, N., MEISTER, M. & TIKKANEN, R. 2014. Flotillins in receptor tyrosine kinase signaling and cancer. *Cells,* 3**,** 129-149.

BARYLKO, B., BINNS, D. D. & ALBANESI, J. P. 2000. Regulation of the enzymatic and motor activities of myosin I. *Biochimica et Biophysica Acta (BBA) - Molecular Cell Research,* 1496**,** 23-35.

BAUER, M. & PELKMANS, L. 2006. A new paradigm for membrane-organizing and -shaping scaffolds. *FEBS Letters,* 580**,** 5559-5564.

BECHARA, C. & SAGAN, S. 2013. Cell-penetrating peptides: 20 years later, where do we stand? *FEBS Letters,* 587**,** 1693-1702.

BOHMER, N. & JORDAN, A. 2015. Caveolin-1 and CDC42 mediated endocytosis of silica-coated iron oxide nanoparticles in HeLa cells. *Beilstein Journal of Nanotechnology,* 6**,** 167-176.

BONIFACINO, J. S. & GLICK, B. S. 2004. The mechanisms of vesicle budding and fusion. *Cell,* 116**,** 153-166.

BOUCROT, E., SAFFARIAN, S., ZHANG, R. & KIRCHHAUSEN, T. 2010. Roles of AP-2 in clathrin-mediated endocytosis. *PLoS ONE,* 5**,** e10597.

BRAEKMAN, J. C., DALOZE, D., MOUSSIAUX, B. & RICCIO, R. 1987. Jaspamide from the marine sponge Jaspis johnstoni. *Journal of Natural Products,* 50**,** 994-995.

BRAET, F., SPECTOR, I., DE ZANGER, R. & WISSE, E. 1998. A novel structure involved in the formation of liver endothelial cell fenestrae revealed by using the actin inhibitor misakinolide. *Proceedings of the National Academy of Sciences of the United States of America,* 95**,** 13635-13640.

BRANDVOLD, K. R., STEFFEY, M. E., FOX, C. C. & SOELLNER, M. B. 2012. Development of a highly selective c-Src kinase inhibitor. *ACS chemical biology,* 7**,** 1393-1398.

BREITSPRECHER, D., JAISWAL, R., BOMBARDIER, J. P., GOULD, C. J., GELLES, J. & GOODE, B. L. 2012. Rocket launcher mechanism of collaborative actin assembly defined by single-molecule imaging. *Science,* 336**,** 1164-1168.

BUBB, M. R., SENDEROWICZ, A. M., SAUSVILLE, E. A., DUNCAN, K. L. & KORN, E. D. 1994. Jasplakinolide, a cytotoxic natural product, induces actin polymerization and competitively inhibits the binding of phalloidin to F-actin. *Journal of Biological Chemistry,* 269**,** 14869-14871.

BUBB, M. R., SPECTOR, I., BEYER, B. B. & FOSEN, K. M. 2000. Effects of jasplakinolide on the kinetics of actin polymerization. An explanation for certain in vivo observations. *Journal of Biological Chemistry,* 275**,** 5163-5170.

CAMPELLONE, K. G. & WELCH, M. D. 2010. A nucleator arms race: cellular control of actin assembly. *Nature Reviews Molecular Cell Biology,* 11**,** 237-251.

CAMPELLONE, K. G., WEBB, N. J., ZNAMEROSKI, E. A. & WELCH, M. D. 2008. WHAMM is an Arp2/3 complex activator that binds microtubules and functions in ER to Golgi transport. *Cell,* 134**,** 148-161.

CAO, H., CHEN, J., KRUEGER, E. W. & MCNIVEN, M. A. 2010. Src-mediated phosphorylation of dynamin and cortactin regulates the “constitutive” endocytosis of transferrin. *Molecular and Cellular Biology,* 30**,** 781-792.

CARLIER, M. F., LAURENT, V., SANTOLINI, J., MELKI, R., DIDRY, D., XIA, G. X., HONG, Y., CHUA, N. H. & PANTALONI, D. 1997. Actin depolymerizing factor (ADF/cofilin) enhances the rate of filament turnover: implication in actin-based motility. *The Journal of Cell Biology,* 136, 1307-1322.

CARLTON, J., BUJNY, M., PETER, B. J., OORSCHOT, V. M. J., RUTHERFORD, A., MELLOR, H., KLUMPERMAN, J., MCMAHON, H. T. & CULLEN, P. J. 2004. Sorting Nexin-1 mediates tubular endosome-to-TGN transport through coincidence sensing of high-curvature membranes and 3-phosphoinositides. *Current Biology,* 14**,** 1791-1800.

CARTER, S. B. 1967. Effects of cytochalasins on mammalian cells. *Nature,* 213**,** 261-264.

CASELLA, J. F., FLANAGAN, M. D. & LIN, S. 1981. Cytochalasin D inhibits actin polymerization and induces depolymerization of actin filaments formed during platelet shape change. *Nature,* 293**,** 302-305.

CAU, J. & HALL, A. 2005. Cdc42 controls the polarity of the actin and microtubule cytoskeletons through two distinct signal transduction pathways. *Journal of Cell Science,* 118**,** 2579-2587.

CHADDA, R., HOWES, M. T., PLOWMAN, S. J., HANCOCK, J. F., PARTON, R. G. & MAYOR, S. 2007. Cholesterol-sensitive Cdc42 activation regulates actin polymerization for endocytosis via the GEEC pathway. *Traffic,* 8**,** 702-717.

CHALOIN, L., VIDAL, P., HEITZ, A., VAN MAU, N., MÉRY, J., DIVITA, G. & HEITZ, F. 1997. Conformations of primary amphipathic carrier peptides in membrane mimicking environments. *Biochemistry,* 36**,** 11179-11187.

CHEEK, T. R. & BURGOYNE, R. D. 1986. Nicotine-evoked disassembly of cortical actin filaments in adrenal chromaffin cells. *FEBS Letters,* 207**,** 110-114.

CHEN, B. C., LEGANT, W. R., WANG, K., SHAO, L., MILKIE, D. E., DAVIDSON, M. W., JANETOPOULOS, C., WU, X. S., HAMMER, J. A., LIU, Z., ENGLISH, B. P., MIMORI-KIYOSUE, Y., ROMERO, D. P., RITTER, A. T., LIPPINCOTT-SCHWARTZ, J., FRITZ-LAYLIN, L., MULLINS, R. D., MITCHELL, D. M., BEMBENEK, J. N., REYMANN, A. C., BÖHME, R., GRILL, S. W., WANG, J. T., SEYDOUX, G., TULU, U. S., KIEHART, D. P. & BETZIG, E. 2014. Lattice light-sheet microscopy: Imaging molecules to embryos at high spatiotemporal resolution. *Science,* 346.

CHENG, Z. J., SINGH, R. D., HOLICKY, E. L., WHEATLEY, C. L., MARKS, D. L. & PAGANO, R. E. 2010. Co-regulation of caveolar and Cdc42-dependent fluid phase endocytosis by phosphocaveolin-1. *The Journal of Biological Chemistry,* 285**,** 15119-15125.

CHEREAU, D., KERFF, F., GRACEFFA, P., GRABAREK, Z., LANGSETMO, K. & DOMINGUEZ, R. 2005. Actin-bound structures of Wiskott–Aldrich syndrome protein (WASP)-homology domain 2 and the implications for filament assembly. *Proceedings of the National Academy of Sciences of the United States of America,* 102**,** 16644-16649.

CHESARONE, M. A. & GOODE, B. L. 2009. Actin nucleation and elongation factors: mechanisms and interplay. *Current Opinion in Cell Biology,* 21**,** 28-37.

CHESARONE, M. A., DUPAGE, A. G. & GOODE, B. L. 2010. Unleashing formins to remodel the actin and microtubule cytoskeletons. *Nature Reviews Molecular Cell Biology,* 11**,** 62-74.

CHESARONE, M., GOULD, C. J., MOSELEY, J. B. & GOODE, B. L. 2009. Displacement of formins from growing barbed ends by Bud14 is critical for actin cable architecture and function. *Developmental cell,* 16**,** 292-302.

CHIRCOP, M. 2014. Rho GTPases as regulators of mitosis and cytokinesis in mammalian cells. *Small GTPases,* 5**,** e29770.

CHO, K., WANG, X., NIE, S., CHEN, Z. & SHIN, D. M. 2008. Therapeutic nanoparticles for drug delivery in cancer. *Clinical Cancer Research,* 14**,** 1310-1316.

CHOI, C. H. J., HAO, L., NARAYAN, S. P., AUYEUNG, E. & MIRKIN, C. A. 2013. Mechanism for the endocytosis of spherical nucleic acid nanoparticle conjugates. *Proceedings of the National Academy of Sciences,* 110**,** 7625-7630.

CLEAL, K., HE, L., D. WATSON, P. & T. JONES, A. 2013. Endocytosis, intracellular traffic and fate of cell penetrating peptide based conjugates and nanoparticles. *Current Pharmaceutical Design,* 19**,** 2878-2894.

COLLINS, B. M., MCCOY, A. J., KENT, H. M., EVANS, P. R. & OWEN, D. J. 2002. Molecular architecture and functional model of the endocytic AP2 complex. *Cell,* 109**,** 523-535.

CONDEELIS, J. 2001. How is actin polymerization nucleated in vivo? *Trends in Cell Biology,* 11**,** 288-293.

CONNER, S. D. & SCHMID, S. L. 2003. Regulated portals of entry into the cell. *Nature,* 422**,** 37-44.

COOPER, J. A. & SCHAFER, D. A. 2000. Control of actin assembly and disassembly at filament ends. *Current Opinion in Cell Biology,* 12**,** 97-103.

COPOLOVICI, D. M., LANGEL, K., ERISTE, E. & LANGEL, Ü. 2014. Cell-penetrating peptides: design, synthesis, and applications. *ACS Nano,* 8**,** 1972-1994.

DARENFED, H., DAYANANDAN, B., ZHANG, T., HSIEH, S. H. K., FOURNIER, A. E. & MANDATO, C. A. 2007. Molecular characterization of the effects of Y-27632. *Cell Motility and the Cytoskeleton,* 64**,** 97-109.

DE LA CRUZ, E. M. & OSTAP, E. M. 2004. Relating biochemistry and function in the myosin superfamily. *Current Opinion in Cell Biology,* 16**,** 61-67.

DERIVERY, E., SOUSA, C., GAUTIER, J. J., LOMBARD, B., LOEW, D. & GAUTREAU, A. 2009. The Arp2/3 activator WASH controls the fission of endosomes through a large multiprotein complex. *Developmental Cell,* 17**,** 712-723.

DEROSSI, D., CALVET, S., TREMBLEAU, A., BRUNISSEN, A., CHASSAING, G. & PROCHIANTZ, A. 1996. Cell internalization of the third helix of the Antennapedia homeodomain is receptor-independent. *Journal of Biological Chemistry,* 271**,** 18188-18193.

DEROSSI, D., JOLIOT, A. H., CHASSAING, G. & PROCHIANTZ, A. 1994. The third helix of the Antennapedia homeodomain translocates through biological membranes. *Journal of Biological Chemistry,* 269**,** 10444-50.

DESHAYES, S., MORRIS, M. C., DIVITA, G. & HEITZ, F. 2006. Interactions of amphipathic CPPs with model membranes. *Biochimica et Biophysica Acta (BBA) - Biomembranes,* 1758**,** 328-335.

DESHAYES, S., PLÉNAT, T., ALDRIAN-HERRADA, G., DIVITA, G., LE GRIMELLEC, C. & HEITZ, F. 2004. Primary amphipathic cell-penetrating peptides: structural requirements and interactions with model membranes. *Biochemistry,* 43**,** 7698-7706.

DESIDERI, E., CAVALLO, ANNA L. & BACCARINI, M. 2015. Alike but different: RAF paralogs and their signaling outputs. *Cell,* 161**,** 967-970.

DEVADAS, D., KOITHAN, T., DIESTEL, R., PRANK, U., SODEIK, B. & DÖHNER, K. 2014. Herpes simplex virus internalization into epithelial cells requires Na+/H+ exchangers and p21-activated kinases but neither clathrin- nor caveolin-mediated endocytosis. *Journal of Virology,* 88**,** 13378-13395.

DHARMAWARDHANE, S., SANDERS, L. C., MARTIN, S. S., DANIELS, R. H. & BOKOCH, G. M. 1997. Localization of p21-activated knase 1 (PAK1) to pinocytic vesicles and cortical actin structures in stimulated cells. *The Journal of Cell Biology,* 138**,** 1265-1278.

DHARMAWARDHANE, S., SCHÜRMANN, A., SELLS, M. A., CHERNOFF, J., SCHMID, S. L. & BOKOCH, G. M. 2000. Regulation of macropinocytosis by p21-activated kinase-1. *Molecular Biology of the Cell,* 11**,** 3341-3352.

DIDRY, D., CARLIER, M. F. & PANTALONI, D. 1998. Synergy between actin depolymerizing factor/cofilin and profilin in increasing actin filament turnover. *Journal of Biological Chemistry,* 273**,** 25602-25611.

DOHERTY, G. J. & MCMAHON, H. T. 2009. Mechanisms of endocytosis. *Annual Review of Biochemistry,* 78**,** 857-902.

DOMINGUEZ, R. & HOLMES, K. C. 2011. Actin structure and function. *Annual Review of Biophysics,* 40**,** 169-186.

DOMINGUEZ, R. 2004. Actin-binding proteins-a unifying hypothesis. *Trends in Biochemical Sciences,* 29**,** 572-578.

DONALDSON, J. G. 2005. Arfs, phosphoinositides and membrane traffic. *Biochemical Society Transactions,* 33**,** 1276-1278.

DRAB, M., VERKADE, P., ELGER, M., KASPER, M., LOHN, M., LAUTERBACH, B., MENNE, J., LINDSCHAU, C., MENDE, F., LUFT, F. C., SCHEDL, A., HALLER, H. & KURZCHALIA, T. V. 2001. Loss of caveolae, vascular dysfunction, and pulmonary defects in caveolin-1 gene-disrupted mice. *Science,* 293**,** 2449-2452.

DUCHARDT, F., FOTIN-MLECZEK, M., SCHWARZ, H., FISCHER, R. & BROCK, R. 2007. A comprehensive model for the cellular uptake of cationic cell-penetrating peptides. *Traffic,* 8**,** 848-866.

DUESS, J., PURI, P. & THOMPSON, J. 2016. Impaired cytoskeletal arrangements and failure of ventral body wall closure in chick embryos treated with rock inhibitor (Y-27632). *Pediatric Surgery International,* 32**,** 45-58.

DULEH, S. N. & WELCH, M. D. 2010. WASH and the Arp2/3 complex regulate endosome shape and trafficking. *Cytoskeleton (Hoboken, N.J.),* 67**,** 193-206.

EDWARDS, D. C., SANDERS, L. C., BOKOCH, G. M. & GILL, G. N. 1999. Activation of LIM-kinase by Pak1 couples Rac/Cdc42 GTPase signalling to actin cytoskeletal dynamics. *Nature Cell Biology,* 1**,** 253-259.

EL-ANDALOUSSI, S., JOHANSSON, H. J., HOLM, T. & LANGEL, U. 2007. A novel cell-penetrating peptide, M918, for efficient delivery of proteins and peptide nucleic acids. *Molecular Therapy,* 15**,** 1820-1826.

EL-SAYED, A., KHALIL, I. A., KOGURE, K., FUTAKI, S. & HARASHIMA, H. 2008. Octaarginine- and octalysine-modified nanoparticles have different modes of endosomal escape. *Journal of Biological Chemistry,* 283**,** 23450-23461.

ENGQVIST-GOLDSTEIN, Å. E. Y. & DRUBIN, D. G. 2003. Actin assembly and endocytosis: from yeast to mammals. *Annual Review of Cell and Developmental Biology,* 19**,** 287-332.

ETIENNE-MANNEVILLE, S. 2004. Cdc42 - the centre of polarity. *Journal of Cell Science,* 117**,** 1291-1300.

EZZAT, K., EL ANDALOUSSI, S., ZAGHLOUL, E. M., LEHTO, T., LINDBERG, S., MORENO, P. M. D., VIOLA, J. R., MAGDY, T., ABDO, R., GUTERSTAM, P., SILLARD, R., HAMMOND, S. M., WOOD, M. J. A., ARZUMANOV, A. A., GAIT, M. J., SMITH, C. I. E., HÄLLBRINK, M. & LANGEL, Ü. 2011. PepFect 14, a novel cell-penetrating peptide for oligonucleotide delivery in solution and as solid formulation. *Nucleic Acids Research,* 39**,** 5284-5298.

FALCONE, S., COCUCCI, E., PODINI, P., KIRCHHAUSEN, T., CLEMENTI, E. & MELDOLESI, J. 2006. Macropinocytosis: regulated coordination of endocytic and exocytic membrane traffic events. *Journal of Cell Science,* 119**,** 4758-4769.

FELICE, B., PRABHAKARAN, M. P., RODRÍGUEZ, A. P. & RAMAKRISHNA, S. 2014. Drug delivery vehicles on a nano-engineering perspective. *Materials Science and Engineering: C,* 41**,** 178-195.

FELS, J., JEGGLE, P., KUSCHE-VIHROG, K. & OBERLEITHNER, H. 2012. Cortical actin nanodynamics determines nitric oxide release in vascular endothelium. *PLoS ONE,* 7**,** e41520.

FERGUSON, S., RAIMONDI, A., PARADISE, S., SHEN, H., MESAKI, K., FERGUSON, A., DESTAING, O., KO, G., TAKASAKI, J., CREMONA, O., O' TOOLE, E. & DE CAMILLI, P. 2009. Coordinated actions of actin and BAR proteins upstream of dynamin at endocytic clathrin-coated pits. *Developmental Cell,* 17**,** 811-822.

FERRARI, A., PELLEGRINI, V., ARCANGELI, C., FITTIPALDI, A., GIACCA, M. & BELTRAM, F. 2003. Caveolae-mediated internalization of extracellular HIV-1 tat fusion proteins visualized in real time. *Molecular Therapy,* 8**,** 284-294.

FINCHAM, V. J., CHUDLEIGH, A. & FRAME, M. C. 1999. Regulation of p190 Rho-GAP by v-Src is linked to cytoskeletal disruption during transformation. *Journal of Cell Science,* 112**,** 947-956.

FITTIPALDI, A., FERRARI, A., ZOPPÉ, M., ARCANGELI, C., PELLEGRINI, V., BELTRAM, F. & GIACCA, M. 2003. Cell membrane lipid rafts mediate caveolar endocytosis of HIV-1 Tat fusion proteins. *Journal of Biological Chemistry,* 278**,** 34141-34149.

FLETCHER, D. A. & MULLINS, R. D. 2010. Cell mechanics and the cytoskeleton. *Nature,* 463**,** 485-492.

FOERG, C., ZIEGLER, U., FERNANDEZ-CARNEADO, J., GIRALT, E. & MERKLE, H. P. 2007. Differentiation restricted endocytosis of cell penetrating peptides in MDCK cells corresponds with activities of Rho-GTPases. *Pharmaceutical research,* 24**,** 628-642.

FORD, M. G. J., MILLS, I. G., PETER, B. J., VALLIS, Y., PRAEFCKE, G. J. K., EVANS, P. R. & MCMAHON, H. T. 2002. Curvature of clathrin-coated pits driven by epsin. *Nature,* 419**,** 361-366.

FOTIN, A., CHENG, Y., SLIZ, P., GRIGORIEFF, N., HARRISON, S. C., KIRCHHAUSEN, T. & WALZ, T. 2004. Molecular model for a complete clathrin lattice from electron cryomicroscopy. *Nature,* 432**,** 573-579.

FRA, A. M., WILLIAMSON, E., SIMONS, K. & PARTON, R. G. 1994. Detergent-insoluble glycolipid microdomains in lymphocytes in the absence of caveolae. *Journal of Biological Chemistry,* 269**,** 30745-8.

FRANCIS, C. L., RYAN, T. A., JONES, B. D., SMITH, S. J. & FALKOW, S. 1993. Ruffles induced by Salmonella and other stimuli direct macropinocytosis of bacteria. *Nature,* 364**,** 639-642.

FRANCIS, M. K., HOLST, M. R., VIDAL-QUADRAS, M., HENRIKSSON, S., SANTARELLA-MELLWIG, R., SANDBLAD, L. & LUNDMARK, R. 2015. Endocytic membrane turnover at the leading edge is driven by a transient interaction between Cdc42 and GRAF1. *Journal of Cell Science,* 128**,** 4183-4195.

FRANKEL, A. D. & PABO, C. O. 1988. Cellular uptake of the tat protein from human immunodeficiency virus. *Cell,* 55**,** 1189-1193.

FRAUENSTEIN, K., TIGGES, J., SOSHILOV, A., KADO, S., RAAB, N., FRITSCHE, E., HAENDELER, J., DENISON, M., VOGEL, C. A. & HAARMANN-STEMMANN, T. 2015. Activation of the aryl hydrocarbon receptor by the widely used Src family kinase inhibitor 4-amino-5-(4-chlorophenyl)-7-(dimethylethyl)pyrazolo[3,4-d]pyrimidine (PP2). *Archives of Toxicology,* 89**,** 1329-1336.

FRETZ, M. M., PENNING, N. A., AL-TAEI, S., FUTAKI, S., TAKEUCHI, T., NAKASE, I., STORM, G. & JONES, A. T. 2007. Temperature-, concentration- and cholesterol-dependent translocation of L- and D-octa-arginine across the plasma and nuclear membrane of CD34(+) leukaemia cells. *Biochemical Journal,* 403**,** 335-342.

FRICK, M., BRIGHT, N. A., RIENTO, K., BRAY, A., MERRIFIED, C. & NICHOLS, B. J. 2007. Coassembly of flotillins induces formation of membrane microdomains, membrane curvature, and vesicle budding. *Current Biology,* 17**,** 1151-1156.

FUJIMOTO, L. M., ROTH, R., HEUSER, J. E. & SCHMID, S. L. 2000. Actin assembly plays a variable, but not obligatory role in receptor-mediated endocytosis in mammalian cells. *Traffic,* 1**,** 161-171.

FUJITA, H., YASUDA, K., NIITSU, S., FUNATSU, T. & ISHIWATA, S. 1996. Structural and functional reconstitution of thin filaments in the contractile apparatus of cardiac muscle. *Biophysical Journal,* 71**,** 2307-2318.

FUTAKI, S., NAKASE, I., TADOKORO, A., TAKEUCHI, T. & JONES, A. 2007. Arginine-rich peptides and their internalization mechanisms. *Biochemical Society transactions,* 35**,** 784-787.

FUTAKI, S., NIWA, M., NAKASE, I., TADOKORO, A., ZHANG, Y., NAGAOKA, M., WAKAKO, N. & SUGIURA, Y. 2004. Arginine carrier peptide bearing Ni(II) chelator to promote cellular uptake of histidine-tagged proteins. *Bioconjugate Chemistry,* 15**,** 475-481.

FUTAKI, S., SUZUKI, T., OHASHI, W., YAGAMI, T., TANAKA, S., UEDA, K. & SUGIURA, Y. 2001. Arginine-rich peptides. An abundant source of membrane-permeable peptides having potential as carriers for intracellular protein delivery. *Journal of Biological Chemistry,* 276**,** 5836-5840.

GABRIELSON, N. P. & PACK, D. W. 2009. Efficient polyethylenimine-mediated gene delivery proceeds via a caveolar pathway in HeLa cells. *Journal of Controlled Release,* 136**,** 54-61.

GADEA, G., SANZ-MORENO, V., SELF, A., GODI, A. & MARSHALL, C. J. 2008. DOCK10-mediated Cdc42 activation is necessary for amoeboid invasion of melanoma cells. *Current Biology,* 18**,** 1456-1465.

GALBIATI, F., ENGELMAN, J. A., VOLONTE, D., ZHANG, X. L., MINETTI, C., LI, M., HOU, H., KNEITZ, B., EDELMANN, W. & LISANTI, M. P. 2001. Caveolin-3 null mice show a loss of caveolae, changes in the microdomain distribution of the dystrophin-glycoprotein complex, and t-tubule abnormalities. *Journal of Biological Chemistry,* 276**,** 21425-21433.

GAMBIN, Y., ARIOTTI, N., MCMAHON, K. A., BASTIANI, M., SIERECKI, E., KOVTUN, O., POLINKOVSKY, M. E., MAGENAU, A., JUNG, W., OKANO, S., ZHOU, Y., LENEVA, N., MUREEV, S., JOHNSTON, W., GAUS, K., HANCOCK, J. F., COLLINS, B. M., ALEXANDROV, K. & PARTON, R. G. 2014. Single-molecule analysis reveals self assembly and nanoscale segregation of two distinct cavin subcomplexes on caveolae. *eLife,* 3**,** e01434.

GAO, S., SIMON, M. J., MORRISON III, B. & BANTA, S. 2009. Bifunctional chimeric fusion proteins engineered for DNA delivery: Optimization of the protein to DNA ratio. *Biochimica et Biophysica Acta (BBA) - General Subjects,* 1790**,** 198-207.

GARRETT, W. S., CHEN, L. M., KROSCHEWSKI, R., EBERSOLD, M., TURLEY, S., TROMBETTA, S., GALÁN, J. E. & MELLMAN, I. 2000. Developmental control of endocytosis in dendritic cells by Cdc42. *Cell,* 102**,** 325-334.

GARTZIANDIA, O., EGUSQUIAGUIRRE, S. P., BIANCO, J., PEDRAZ, J. L., IGARTUA, M., HERNANDEZ, R. M., PRÉAT, V. & BELOQUI, A. 2016. Nanoparticle transport across in vitro olfactory cell monolayers. *International Journal of Pharmaceutics,* 499**,** 81-89.

GEKLE, M., MILDENBERGER, S., FREUDINGER, R., SCHWERDT, G. & SILBERNAGL, S. 1997. Albumin endocytosis in OK cells: dependence on actin and microtubules and regulation by protein kinases. *American Journal of Physiology,* 272**,** F668–F677.

GIACCA, M. & ZACCHIGNA, S. 2012. Virus-mediated gene delivery for human gene therapy. *Journal of Controlled Release,* 161**,** 377-388.

GLEBOV, O. O., BRIGHT, N. A. & NICHOLS, B. J. 2006. Flotillin-1 defines a clathrin-independent endocytic pathway in mammalian cells. *Nature Cell Biology,* 8**,** 46-54.

GOECKELER, Z. M., MASARACCHIA, R. A., ZENG, Q., CHEW, T. L., GALLAGHER, P. & WYSOLMERSKI, R. B. 2000. Phosphorylation of myosin light chain kinase by p21-activated kinase PAK2. *Journal of Biological Chemistry,* 275**,** 18366-18374.

GOFF, S. P. & BERG, P. 1976. Construction of hybrid viruses containing SV40 and λ phage DNA segments and their propagation in cultured monkey cells. *Cell,* 9**,** 695-705.

GOLEY, E. D. & WELCH, M. D. 2006. The ARP2/3 complex: an actin nucleator comes of age. *Nature Reviews Molecular Cell Biology,* 7**,** 713-726.

GOMEZ, T. S. & BILLADEAU, D. D. 2009. A FAM21-containing WASH complex regulates retromer-dependent sorting. *Developmental Cell,* 17**,** 699-711.

GREEN, M. & LOEWENSTEIN, P. M. 1988. Autonomous functional domains of chemically synthesized human immunodeficiency virus tat trans-activator protein. *Cell,* 55**,** 1179-1188.

GREEN, M., ISHINO, M. & LOEWENSTEIN, P. M. 1989. Mutational analysis of HIV-1 Tat minimal domain peptides: Identification of trans-dominant mutants that suppress HIV-LTR-driven gene expression. *Cell,* 58**,** 215-223.

GREENE, W. & GAO, S.-J. 2009. Actin dynamics regulate multiple endosomal steps during Kaposi's sarcoma-associated herpesvirus entry and trafficking in endothelial cells. *PLoS Pathogens,* 5**,** e1000512.

GRIMMER, S., VAN DEURS, B. & SANDVIG, K. 2002. Membrane ruffling and macropinocytosis in A431 cells require cholesterol. *Journal of Cell Science,* 115**,** 2953-2962.

GUARINO, M. 2010. Src signaling in cancer invasion. *Journal of Cellular Physiology,* 223**,** 14-26.

GUMP, J. M., JUNE, R. K. & DOWDY, S. F. 2010. Revised role of glycosaminoglycans in TAT protein transduction domain-mediated cellular transduction. *The Journal of Biological Chemistry,* 285**,** 1500-1507.

GUPTA, B., LEVCHENKO, T. S. & TORCHILIN, V. P. 2005. Intracellular delivery of large molecules and small particles by cell-penetrating proteins and peptides. *Advanced Drug Delivery Reviews,* 57**,** 637-651.

GUTERSTAM, P., MADANI, F., HIROSE, H., TAKEUCHI, T., FUTAKI, S., EL ANDALOUSSI, S., GRÄSLUND, A. & LANGEL, Ü. 2009. Elucidating cell-penetrating peptide mechanisms of action for membrane interaction, cellular uptake, and translocation utilizing the hydrophobic counter-anion pyrenebutyrate. *Biochimica et Biophysica Acta (BBA) - Biomembranes,* 1788**,** 2509-2517.

HAIGLER, H. T., MCKANNA, J. A. & COHEN, S. 1979. Rapid stimulation of pinocytosis in human carcinoma cells A-431 by epidermal growth factor. *The Journal of Cell Biology,* 83**,** 82-90.

HALBERT, C. L., RUTLEDGE, E. A., ALLEN, J. M., RUSSELL, D. W. & MILLER, A. D. 2000. Repeat transduction in the mouse lung by using adeno-associated virus vectors with different serotypes. *Journal of Virology,* 74**,** 1524-1532.

HAMASAKI, M., ARAKI, N. & HATAE, T. 2004. Association of early endosomal autoantigen 1 with macropinocytosis in EGF-stimulated a431 cells. *The Anatomical Record Part A: Discoveries in Molecular, Cellular, and Evolutionary Biology,* 277**,** 298-306.

HANKE, J. H., GARDNER, J. P., DOW, R. L., CHANGELIAN, P. S., BRISSETTE, W. H., WERINGER, E. J., POLLOK, B. A. & CONNELLY, P. A. 1996. Discovery of a novel, potent, and Src family-selective tyrosine kinase inhibitor. Study of Lck- and FynT-dependent T cell activation. *Journal of Biological Chemistry,* 271**,** 695-701.

HANSEN, C. G. & NICHOLS, B. J. 2009. Molecular mechanisms of clathrin-independent endocytosis. *Journal of Cell Science,* 122**,** 1713-1721.

HARTMAN, M. A. & SPUDICH, J. A. 2012. The myosin superfamily at a glance. *Journal of Cell Science,* 125**,** 1627-1632.

HATANO, S. & OOSAWA, F. 1966. Isolation and characterization of plasmodium actin. *Biochimica et Biophysica Acta (BBA) - General Subjects,* 127**,** 488-498.

HAYER, A., STOEBER, M., RITZ, D., ENGEL, S., MEYER, H. H. & HELENIUS, A. 2010. Caveolin-1 is ubiquitinated and targeted to intralumenal vesicles in endolysosomes for degradation. *The Journal of Cell Biology,* 191**,** 615-629.

HE, L., WATSON, P. D. & JONES, A. T. 2015. Visualizing actin architectures in cells incubated with cell-penetrating peptides. *Methods in molecular biology (Clifton, N.J.),* 1324**,** 247-259.

HEASMAN, S. J. & RIDLEY, A. J. 2008. Mammalian Rho GTPases: new insights into their functions from in vivo studies. *Nature Reviews Molecular Cell Biology,* 9**,** 690-701.

HENLEY, J. R., KRUEGER, E. W. A., OSWALD, B. J. & MCNIVEN, M. A. 1998. Dynamin-mediated internalization of caveolae. *The Journal of Cell Biology,* 141**,** 85-99.

HENNE, W. M., BOUCROT, E., MEINECKE, M., EVERGREN, E., VALLIS, Y., MITTAL, R. & MCMAHON, H. T. 2010. FCHo proteins are nucleators of clathrin-mediated endocytosis. *Science,* 328**,** 1281-1284.

HENQUIN, J. C., MOURAD, N. I. & NENQUIN, M. 2012. Disruption and stabilization of β-cell actin microfilaments differently influence insulin secretion triggered by intracellular Ca2+ mobilization or store-operated Ca2+ entry. *FEBS Letters,* 586**,** 89-95.

HERBIG, M. E., WELLER, K., KRAUSS, U., BECK-SICKINGER, A. G., MERKLE, H. P. & ZERBE, O. 2005. Membrane surface-associated helices promote lipid interactions and cellular uptake of human calcitonin-derived cell penetrating peptides. *Biophysical Journal,* 89**,** 4056-4066.

HERCE, H. D. & GARCIA, A. E. 2007. Molecular dynamics simulations suggest a mechanism for translocation of the HIV-1 TAT peptide across lipid membranes. *Proceedings of the National Academy of Sciences,* 104**,** 20805-20810.

HERCE, H. D., GARCIA, A. E., LITT, J., KANE, R. S., MARTIN, P., ENRIQUE, N., REBOLLEDO, A. & MILESI, V. 2009. Arginine-rich peptides destabilize the plasma membrane, consistent with a pore formation translocation mechanism of cell penetrating peptides. *Biophysical Journal,* 97**,** 1917-1925.

HERRMANN, H., BAR, H., KREPLAK, L., STRELKOV, S. V. & AEBI, U. 2007. Intermediate filaments: from cell architecture to nanomechanics. *Nature Reviews Molecular Cell Biology,* 8**,** 562-573.

HERTZOG, M., VAN HEIJENOORT, C., DIDRY, D., GAUDIER, M., COUTANT, J., GIGANT, B. T., DIDELOT, G., PRÉAT, T., KNOSSOW, M., GUITTET, E. & CARLIER, M.-F. 2004. The beta-thymosin/WH2 domain; structural basis for the switch from inhibition to promotion of actin assembly. *Cell,* 117**,** 611-623.

HEWLETT, L., PRESCOTT, A. & WATTS, C. 1994. The coated pit and macropinocytic pathways serve distinct endosome populations. *The Journal of Cell Biology,* 124**,** 689-703.

HILL, M. M., BASTIANI, M., LUETTERFORST, R., KIRKHAM, M., KIRKHAM, A., NIXON, S. J., WALSER, P., ABANKWA, D., OORSCHOT, V. M. J., MARTIN, S., HANCOCK, J. F. & PARTON, R. G. 2008. PTRF-Cavin, a conserved cytoplasmic protein required for caveola formation and function. *Cell,* 132**,** 113-124.

HIROSE, H., TAKEUCHI, T., OSAKADA, H., PUJALS, S., KATAYAMA, S., NAKASE, I., KOBAYASHI, S., HARAGUCHI, T. & FUTAKI, S. 2012. Transient focal membrane deformation induced by arginine-rich peptides leads to their direct penetration into cells. *Molecular Therapy,* 20**,** 984-993.

HOANG, M. V., WHELAN, M. C. & SENGER, D. R. 2004. Rho activity critically and selectively regulates endothelial cell organization during angiogenesis. *Proceedings of the National Academy of Sciences of the United States of America,* 101**,** 1874-1879.

HÖNING, S., RICOTTA, D., KRAUSS, M., SPÄTE, K., SPOLAORE, B., MOTLEY, A., ROBINSON, M., ROBINSON, C., HAUCKE, V. & OWEN, D. J. 2005. Phosphatidylinositol-(4,5)-bisphosphate regulates sorting signal recognition by the clathrin-associated adaptor complex AP2. *Molecular Cell,* 18**,** 519-531.

HOPKINS, C. R., MILLER, K. & BEARDMORE, J. M. 1985. Receptor-mediated endocytosis of transferrin and epidermal growth factor receptors: a comparison of constitutive and ligand-induced uptake. *Journal of Cell Science,* 1985**,** 173-186.

HOWES, M. T., MAYOR, S. & PARTON, R. G. 2010. Molecules, mechanisms, and cellular roles of clathrin-independent endocytosis. *Current Opinion in Cell Biology,* 22**,** 519-527.

HUANG, F., KHVOROVA, A., MARSHALL, W. & SORKIN, A. 2004. Analysis of clathrin-mediated endocytosis of epidermal growth factor receptor by RNA interference. *Journal of Biological Chemistry,* 279**,** 16657-16661.

ISHIZAKI, T., MAEKAWA, M., FUJISAWA, K., OKAWA, K., IWAMATSU, A., FUJITA, A., WATANABE, N., SAITO, Y., KAKIZUKA, A., MORII, N. & NARUMIYA, S. 1996. The small GTP-binding protein Rho binds to and activates a 160 kDa Ser/Thr protein kinase homologous to myotonic dystrophy kinase. *The EMBO Journal,* 15**,** 1885-1893.

ISHIZAKI, T., UEHATA, M., TAMECHIKA, I., KEEL, J., NONOMURA, K., MAEKAWA, M. & NARUMIYA, S. 2000. Pharmacological properties of Y-27632, a specific inhibitor of Rho-associated kinases. *Molecular Pharmacology,* 57**,** 976-983.

IVANOV, A. 2008. Pharmacological inhibition of endocytic pathways: is it specific enough to be useful? *In:* IVANOV, A. (ed.) *Exocytosis and Endocytosis.* Humana Press.

IVANOV, A. I. 2008. Pharmacological inhibition of endocytic pathways: is it specific enough to be useful? *Methods in molecular biology (Clifton, N.J.),* 440**,** 15-33.

JÄRVER, P., MÄGER, I. & LANGEL, Ü. 2010. In vivo biodistribution and efficacy of peptide mediated delivery. *Trends in Pharmacological Sciences,* 31**,** 528-535.

JO, J., HONG, S., CHOI, W. Y. & LEE, D. R. 2014. Cell-penetrating peptide (CPP)-conjugated proteins is an efficient tool for manipulation of human mesenchymal stromal cells. *Scientific Reports,* 4**,** 4378.

JOG, N. R., RANE, M. J., LOMINADZE, G., LUERMAN, G. C., WARD, R. A. & MCLEISH, K. R. 2007. The actin cytoskeleton regulates exocytosis of all neutrophil granule subsets. *American Journal of Physiology - Cell Physiology,* 292**,** C1690-C1700.

JOHNSON, F. H., SHIMOMURA, O., SAIGA, Y., GERSHMAN, L. C., REYNOLDS, G. T. & WATERS, J. R. 1962. Quantum efficiency of Cypridina luminescence, with a note on that of Aequorea. *Journal of Cellular and Comparative Physiology,* 60**,** 85-103.

JOHNSON, J. L., MONFREGOLA, J., NAPOLITANO, G., KIOSSES, W. B. & CATZ, S. D. 2012. Vesicular trafficking through cortical actin during exocytosis is regulated by the Rab27a effector JFC1/Slp1 and the RhoA-GTPase–activating protein Gem-interacting protein. *Molecular Biology of the Cell,* 23**,** 1902-1916.

JOLIOT, A., PERNELLE, C., DEAGOSTINI-BAZIN, H. & PROCHIANTZ, A. 1991. Antennapedia homeobox peptide regulates neural morphogenesis. *Proceedings of the National Academy of Sciences of the United States of America,* 88**,** 1864-1868.

JONES, A. T. & SAYERS, E. J. 2012. Cell entry of cell penetrating peptides: tales of tails wagging dogs. *Journal of Controlled Release,* 161**,** 582-591.

JONES, A. T. 2007. Macropinocytosis: searching for an endocytic identity and role in the uptake of cell penetrating peptides. *Journal of Cellular and Molecular Medicine,* 11**,** 670-684.

JONES, A. T. 2010. Uptake and intracellular dynamics of proteins internalized by cell-penetrating peptides. *Organelle-Specific Pharmaceutical Nanotechnology.* John Wiley & Sons, Inc.

KABSCH, W., MANNHERZ, H. G., SUCK, D., PAI, E. F. & HOLMES, K. C. 1990. Atomic structure of the actin: DNase I complex. *Nature,* 347**,** 37-44.

KAKSONEN, M., TORET, C. P. & DRUBIN, D. G. 2006. Harnessing actin dynamics for clathrin-mediated endocytosis. *Nature Reviews Molecular Cell Biology,* 7**,** 404-414.

KALIA, M., KUMARI, S., CHADDA, R., HILL, M. M., PARTON, R. G. & MAYOR, S. 2006. Arf6-independent GPI-anchored protein-enriched early endosomal compartments fuse with sorting endosomes via a Rab5/phosphatidylinositol-3'-kinase-dependent machinery. *Molecular Biology of the Cell,* 17**,** 3689-3704.

KAPLAN, I. M., WADIA, J. S. & DOWDY, S. F. 2005. Cationic TAT peptide transduction domain enters cells by macropinocytosis. *Journal of Controlled Release,* 102**,** 247-253.

KASAHARA, K., NAKAYAMA, Y., SATO, I., IKEDA, K., HOSHINO, M., ENDO, T. & YAMAGUCHI, N. 2007. Role of Src-family kinases in formation and trafficking of macropinosomes. *Journal of Cellular Physiology,* 211**,** 220-232.

KASAS, S., WANG, X., HIRLING, H., MARSAULT, R., HUNI, B., YERSIN, A., REGAZZI, R., GRENNINGLOH, G., RIEDERER, B., FORRÒ, L., DIETLER, G. & CATSICAS, S. 2005. Superficial and deep changes of cellular mechanical properties following cytoskeleton disassembly. *Cell motility and the cytoskeleton,* 62**,** 124-132.

KELLY, B. T., MCCOY, A. J., SPATE, K., MILLER, S. E., EVANS, P. R., HONING, S. & OWEN, D. J. 2008. A structural explanation for the binding of endocytic dileucine motifs by the AP2 complex. *Nature,* 456**,** 976-979.

KERR, M. C. & TEASDALE, R. D. 2009. Defining macropinocytosis. *Traffic,* 10**,** 364-371.

KHALIL, I. A., KOGURE, K., FUTAKI, S. & HARASHIMA, H. 2006. High density of octaarginine stimulates macropinocytosis leading toefficient intracellular trafficking for gene expression. *Journal of Biological Chemistry,* 281**,** 3544-3551.

KICHINA, J. V., GOC, A., AL-HUSEIN, B., SOMANATH, P. R. & KANDEL, E. S. 2010. PAK1 as a therapeutic target. *Expert opinion on therapeutic targets,* 14**,** 703-725.

KIM, A., SHIN, T. H., SHIN, S. M., PHAM, C. D., CHOI, D. K., KWON, M. H. & KIM, Y. S. 2012. Cellular internalization mechanism and intracellular trafficking of filamentous M13 phages displaying a cell-penetrating transbody and TAT peptide. *PLoS ONE,* 7**,** e51813.

KIRKHAM, M. & PARTON, R. G. 2005. Clathrin-independent endocytosis: New insights into caveolae and non-caveolar lipid raft carriers. *Biochimica et Biophysica Acta (BBA) - Molecular Cell Research,* 1746**,** 350-363.

KIRKHAM, M., FUJITA, A., CHADDA, R., NIXON, S. J., KURZCHALIA, T. V., SHARMA, D. K., PAGANO, R. E., HANCOCK, J. F., MAYOR, S. & PARTON, R. G. 2005. Ultrastructural identification of uncoated caveolin-independent early endocytic vehicles. *The Journal of Cell Biology,* 168**,** 465-476.

KOIVUSALO, M., KAPUS, A. & GRINSTEIN, S. 2009. Sensors, transducers, and effectors that regulate cell size and shape. *The Journal of Biological Chemistry,* 284**,** 6595-6599.

KOIVUSALO, M., WELCH, C., HAYASHI, H., SCOTT, C. C., KIM, M., ALEXANDER, T., TOURET, N., HAHN, K. M. & GRINSTEIN, S. 2010. Amiloride inhibits macropinocytosis by lowering submembranous pH and preventing Rac1 and Cdc42 signaling. *The Journal of Cell Biology,* 188**,** 547-563.

KOLODNEY, M. & WYSOLMERSKI, R. 1992. Isometric contraction by fibroblasts and endothelial cells in tissue culture: a quantitative study. *The Journal of Cell Biology,* 117**,** 73-82.

KOLOKOLTSOV, A. A., DENIGER, D., FLEMING, E. H., ROBERTS, N. J., KARPILOW, J. M. & DAVEY, R. A. 2007. Small interfering RNA profiling reveals key role of clathrin-mediated endocytosis and early endosome formation for infection by respiratory syncytial virus. *Journal of Virology,* 81**,** 7786-7800.

KOREN, E. & TORCHILIN, V. P. 2012. Cell-penetrating peptides: breaking through to the other side. *Trends in Molecular Medicine,* 18**,** 385-393.

KOSUGE, M., TAKEUCHI, T., NAKASE, I., JONES, A. T. & FUTAKI, S. 2008. Cellular internalization and distribution of arginine-rich peptides as a function of extracellular peptide concentration, serum, and plasma membrane associated proteoglycans. *Bioconjugate Chemistry,* 19**,** 656-664.

KOVTUN, O., TILLU, V. A., ARIOTTI, N., PARTON, R. G. & COLLINS, B. M. 2015. Cavin family proteins and the assembly of caveolae. *Journal of Cell Science,* 128**,** 1269-1278.

KOVTUN, O., TILLU, VIKAS A., JUNG, W., LENEVA, N., ARIOTTI, N., CHAUDHARY, N., MANDYAM, RAMYA A., FERGUSON, C., MORGAN, GARRY P., JOHNSTON, WAYNE A., HARROP, STEPHEN J., ALEXANDROV, K., PARTON, ROBERT G. & COLLINS, BRETT M. 2014. Structural insights into the organization of the cavin membrane coat complex. *Developmental Cell,* 31**,** 405-419.

KRAUSE, M. & GAUTREAU, A. 2014. Steering cell migration: lamellipodium dynamics and the regulation of directional persistence. *Nature Reviews Molecular Cell Biology,* 15**,** 577-590.

KRENDEL, M. F. & BONDER, E. M. 1999. Analysis of actin filament bundle dynamics during contact formation in live epithelial cells. *Cell motility and the cytoskeleton,* 43**,** 296-309.

KRENDEL, M., OSTERWEIL, E. K. & MOOSEKER, M. S. 2007. Myosin 1E interacts with synaptojanin-1 and dynamin via its SH3 domain. *FEBS letters,* 581**,** 644-650.

KRISTENSEN, M., BIRCH, D. & MØRCK NIELSEN, H. 2016. Applications and challenges for use of cell-penetrating peptides as delivery vectors for peptide and protein cargos. *International Journal of Molecular Sciences,* 17**,** 185.

KRONLAGE, C., SCHÄFER-HERTE, M., BÖNING, D., OBERLEITHNER, H. & FELS, J. 2015. Feeling for filaments: quantification of the cortical actin web in live vascular endothelium. *Biophysical Journal,* 109**,** 687-698.

KURZCHALIA, T. V., DUPREE, P., PARTON, R. G., KELLNER, R., VIRTA, H., LEHNERT, M. & SIMONS, K. 1992. VIP21, a 21-kD membrane protein is an integral component of trans-Golgi-network-derived transport vesicles. *The Journal of Cell Biology,* 118**,** 1003-1014.

KWIK, J., BOYLE, S., FOOKSMAN, D., MARGOLIS, L., SHEETZ, M. P. & EDIDIN, M. 2003. Membrane cholesterol, lateral mobility, and the phosphatidylinositol 4,5-bisphosphate-dependent organization of cell actin. *Proceedings of the National Academy of Sciences of the United States of America,* 100**,** 13964-13969.

LAKADAMYALI, M., RUST, M. J. & ZHUANG, X. 2006. Ligands for clathrin-mediated endocytosis are differentially sorted into distinct populations of early endosomes. *Cell,* 124**,** 997-1009.

LANG, D. M., LOMMEL, S., JUNG, M., ANKERHOLD, R., PETRAUSCH, B., LAESSING, U., WIECHERS, M. F., PLATTNER, H. & STUERMER, CLAUDIA A. O. 1998. Identification of Reggie-1 and Reggie-2 as plasmamembrane-associated proteins which cocluster with activated GPI-anchored cell adhesion molecules in non-caveolar micropatches in neurons. *Journal of Neurobiology* 37**,** 502-523.

LANZETTI, L., PALAMIDESSI, A., ARECES, L., SCITA, G. & DI FIORE, P. P. 2004. Rab5 is a signalling GTPase involved in actin remodelling by receptor tyrosine kinases. *Nature,* 429**,** 309-314.

LAVOIE, J. N., LANDRY, M.-C., FAURE, R. L. & CHAMPAGNE, C. 2010. Src-family kinase signaling, actin-mediated membrane trafficking and organellar dynamics in the control of cell fate: Lessons to be learned from the adenovirus E4orf4 death factor. *Cellular Signalling,* 22**,** 1604-1614.

LE CLAINCHE, C., PAULY, B. S., ZHANG, C. X., ENGQVIST-GOLDSTEIN, Å. E. Y., CUNNINGHAM, K. & DRUBIN, D. G. 2007. A Hip1R–cortactin complex negatively regulates actin assembly associated with endocytosis. *The EMBO Journal,* 26**,** 1199-1210.

LE, P. U. & NABI, I. R. 2003. Distinct caveolae-mediated endocytic pathways target the Golgi apparatus and the endoplasmic reticulum. *Journal of Cell Science,* 116**,** 1059-1071.

LECLAIRE, L. L., BAUMGARTNER, M., IWASA, J. H., MULLINS, R. D. & BARBER, D. L. 2008. Phosphorylation of the Arp2/3 complex is necessary to nucleate actin filaments. *The Journal of Cell Biology,* 182**,** 647-654.

LEUNG, T., MANSER, E., TAN, L. & LIM, L. 1995. A novel serine/threonine kinase binding the Ras-related RhoA GTPase which translocates the kinase to peripheral membranes. *Journal of Biological Chemistry,* 270**,** 29051-29054.

LEWIS, C. M., SMITH, A. K. & KAMEN, B. A. 1998. Receptor-mediated folate uptake is positively regulated by disruption of the actin cytoskeleton. *Cancer Research,* 58**,** 2952-2956.

LEWIS, W. H. 1931. Pinocytosis. *Bulletin of the Johns Hopkins Hospital,* 49**,** 17-27.

LI, G. H., LI, W., MUMPER, R. J. & NATH, A. 2012. Molecular mechanisms in the dramatic enhancement of HIV-1 Tat transduction by cationic liposomes. *The FASEB Journal,* 26**,** 2824-2834.

LIBERALI, P., KAKKONEN, E., TURACCHIO, G., VALENTE, C., SPAAR, A., PERINETTI, G., BÖCKMANN, R. A., CORDA, D., COLANZI, A., MARJOMAKI, V. & LUINI, A. 2008. The closure of Pak1-dependent macropinosomes requires the phosphorylation of CtBP1/BARS. *The EMBO Journal,* 27**,** 970-981.

LIM, J. P. & GLEESON, P. A. 2011. Macropinocytosis: an endocytic pathway for internalising large gulps. *Immunology and Cell Biology* 89**,** 836-843.

LIM, J. P., WANG, J. T. H., KERR, M. C., TEASDALE, R. D. & GLEESON, P. A. 2008. A role for SNX5 in the regulation of macropinocytosis. *BMC Cell Biology,* 9**,** 58-58.

LIM, K. J., SUNG, B. H., SHIN, J. R., LEE, Y. W., KIM, D. J., YANG, K. S. & KIM, S. C. 2013. A cancer specific cell-penetrating peptide, BR2, for the efficient delivery of an scFv into cancer cells. *PLoS ONE,* 8**,** e66084.

LIN, Y. Z., YAO, S., VEACH, R. A., TORGERSON, T. R. & HAWIGER, J. 1995. Inhibition of nuclear translocation of transcription factor NF-kappa B by a synthetic peptide containing a cell membrane-permeable motif and nuclear localization sequence. *Journal of Biological Chemistry,* 270**,** 14255-14258.

LIU, K. Y., TIMMONS, S., LIN, Y. Z. & HAWIGER, J. 1996. Identification of a functionally important sequence in the cytoplasmic tail of integrin beta 3 by using cell-permeable peptide analogs. *Proceedings of the National Academy of Sciences of the United States of America,* 93**,** 11819-11824.

LIU, N. Q., LOSSINSKY, A. S., POPIK, W., LI, X., GUJULUVA, C., KRIEDERMAN, B., ROBERTS, J., PUSHKARSKY, T., BUKRINSKY, M., WITTE, M., WEINAND, M. & FIALA, M. 2002. Human immunodeficiency virus type 1 enters brain microvascular endothelia by macropinocytosis dependent on lipid rafts and the mitogen-activated protein kinase signaling pathway. *Journal of Virology,* 76**,** 6689-6700.

LODISH, H., BERK, A. & ZIPURSKY, S. L. 2000. Intermediate Filaments. *In:* FREEMAN, W. H. (ed.) *Molecular Cell Biology.* 4th ed. New York: W. H. Freeman.

LU, J., MENG, W., POY, F., MAITI, S., GOODE, B. L. & ECK, M. J. 2007. Structure of the FH2 domain of Daam1: implications for formin regulation of actin assembly. *Journal of Molecular Biology,* 369**,** 1258-1269.

LUDWIG, A., OTTO, G. P., RIENTO, K., HAMS, E., FALLON, P. G. & NICHOLS, B. J. 2010. Flotillin microdomains interact with the cortical cytoskeleton to control uropod formation and neutrophil recruitment. *The Journal of Cell Biology,* 191**,** 771-781.

LUKINAVICIUS, G., REYMOND, L., D'ESTE, E., MASHARINA, A., GOTTFERT, F., TA, H., GUTHER, A., FOURNIER, M., RIZZO, S., WALDMANN, H., BLAUKOPF, C.,

SOMMER, C., GERLICH, D. W., ARNDT, H.-D., HELL, S. W. & JOHNSSON, K. 2014. Fluorogenic probes for live-cell imaging of the cytoskeleton. *Nature Methods,* 11**,** 731-733.

LUNDBERG, M. & JOHANSSON, M. 2002. Positively charged DNA-binding proteins cause apparent cell membrane translocation. *Biochemical and Biophysical Research Communications,* 291**,** 367-371.

LUNDBERG, M., WIKSTROM, S. & JOHANSSON, M. 2003. Cell surface adherence and endocytosis of protein transduction domains. *Molecular Therapy,* 8**,** 143-150.

LUNDMARK, R., DOHERTY, G. J., HOWES, M. T., CORTESE, K., VALLIS, Y., PARTON, R. G. & MCMAHON, H. T. 2008a. The GTPase-activating protein GRAF1 regulates the CLIC/GEEC endocytic pathway. *Current Biology,* 18**,** 1802-1808.

LUNDMARK, R., DOHERTY, GARY J., VALLIS, Y., PETER, BRIAN J. & MCMAHON, HARVEY T. 2008b. Arf family GTP loading is activated by, and generates, positive membrane curvature. *Biochemical Journal,* 414**,** 189-194.

MÄGER, I., EIRÍKSDÓTTIR, E., LANGEL, K., EL ANDALOUSSI, S. & LANGEL, Ü. 2010. Assessing the uptake kinetics and internalization mechanisms of cell-penetrating peptides using a quenched fluorescence assay. *Biochimica et Biophysica Acta (BBA) - Biomembranes,* 1798**,** 338-343.

MAI, J. C., SHEN, H., WATKINS, S. C., CHENG, T. & ROBBINS, P. D. 2002. Efficiency of protein transduction is cell type-dependent and is enhanced by dextran sulfate. *Journal of Biological Chemistry,* 277**,** 30208-30218.

MANIAK, M. 2001. Fluid-phase uptake and transit in axenic Dictyostelium cells. *Biochimica et Biophysica Acta (BBA) - General Subjects,* 1525**,** 197-204.

MANSER, E., LEUNG, T., SALIHUDDIN, H., ZHAO, Z. S. & LIM, L. 1994. A brain serine/threonine protein kinase activated by Cdc42 and Rac1. *Nature,* 367**,** 40-46.

MARGUS, H., PADARI, K. & POOGA, M. 2012. Cell-penetrating peptides as versatile vehicles for oligonucleotidedelivery. *Molecular Therapy,* 20**,** 525-533.

MARKS, J. R., PLACONE, J., HRISTOVA, K. & WIMLEY, W. C. 2011. Spontaneous membrane-translocating peptides by orthogonal high-throughput screening. *Journal of the American Chemical Society,* 133**,** 8995-9004.

MARSHALL, M. 1995. Interactions between Ras and Raf: Key regulatory proteins in cellular transformation. *Molecular Reproduction and Development,* 42**,** 493-499.

MATSUZAKI, K., YONEYAMA, S., MURASE, O. & MIYAJIMA, K. 1996. Transbilayer transport of ions and lipids coupled with mastoparan X translocation. *Biochemistry,* 35**,** 8450-8456.

MATTILA, P. K. & LAPPALAINEN, P. 2008. Filopodia: molecular architecture and cellular functions. *Nature Reviews Molecular Cell Biology,* 9**,** 446-454.

MAXFIELD, F. R. & MCGRAW, T. E. 2004. Endocytic recycling. *Nature Reviews Molecular Cell Biology,* 5**,** 121-132.

MAYER, T., MEYER, M., JANNING, A., SCHIEDEL, A. C. & BARNEKOW, A. 1999. A mutant form of the rho protein can restore stress fibers and adhesion plaques in v-src transformed fibroblasts. *Oncogene,* 18**,** 2117-2128.

MCGRATH, J. L., TARDY, Y., DEWEY JR, C. F., MEISTER, J. J. & HARTWIG, J. H. 1998. Simultaneous measurements of actin filament turnover, filament fraction, and monomer diffusion in endothelial cells. *Biophysical Journal,* 75**,** 2070-2078.

MCKAY, J., WANG, X., DING, J., BUSS, J. E. & AMBROSIO, L. 2011. H-ras resides on clathrin-independent ARF6 vesicles that harbor little RAF-1, but not on clathrin-dependent endosomes. *Biochimica et Biophysica Acta (BBA) - Molecular Cell Research,* 1813**,** 298-307.

MCKAYED, K. K. & SIMPSON, J. C. 2013. Actin in action: imaging approaches to study cytoskeleton structure and function. *Cells,* 2**,** 715-731.

MCMAHON, H. T. & BOUCROT, E. 2011. Molecular mechanism and physiological functions of clathrin-mediated endocytosis. *Nature Reviews Molecular Cell Biology,* 12**,** 517-533.

MEIER, O., BOUCKE, K., HAMMER, S. V., KELLER, S., STIDWILL, R. P., HEMMI, S. & GREBER, U. F. 2002. Adenovirus triggers macropinocytosis and endosomal leakage together with its clathrin-mediated uptake. *The Journal of Cell Biology,* 158**,** 1119-1131.

MEISTER, M. & TIKKANEN, R. 2014. Endocytic trafficking of membrane-bound cargo: a flotillin point of view. *Membranes,* 4**,** 356-371.

MELLOR, H. 2010. The role of formins in filopodia formation. *Biochimica et Biophysica Acta (BBA) - Molecular Cell Research,* 1803**,** 191-200.

MENDOZA, M. C., EMRAH, E., ZHANG, W., BALLIF, B. A., ELLIOTT, H. L., DANUSER, G. & BLENIS, J. 2011. ERK-MAPK drives lamellipodia protrusion by activating the WAVE2 regulatory complex. *Molecular cell,* 41**,** 661-671.

MERCER, J. & HELENIUS, A. 2008. Vaccinia virus uses macropinocytosis and apoptotic mimicry to enter host cells. *Science,* 320**,** 531-535.

MERCER, J. & HELENIUS, A. 2009. Virus entry by macropinocytosis. *Nature Cell Biology,* 11**,** 510-520.

MERCER, J. & HELENIUS, A. 2012. Gulping rather than sipping: macropinocytosis as a way of virus entry. *Current Opinion in Microbiology,* 15**,** 490-499.

MERRIFIELD, C. J., MOSS, S. E., BALLESTREM, C., IMHOF, B. A., GIESE, G., WUNDERLICH, I. & ALMERS, W. 1999. Endocytic vesicles move at the tips of actin tails in cultured mast cells. *Nature Cell Biology,* 1**,** 72-74.

MERRIFIELD, C. J., QUALMANN, B., KESSELS, M. M. & ALMERS, W. 2004. Neural Wiskott Aldrich Syndrome Protein (N-WASP) and the Arp2/3 complex are recruited to sites of clathrin-mediated endocytosis in cultured fibroblasts. *European Journal of Cell Biology,* 83**,** 13-18.

MIKI, H., MIURA, K. & TAKENAWA, T. 1996. N-WASP, a novel actin-depolymerizing protein, regulates the cortical cytoskeletal rearrangement in a PIP2-dependent manner downstream of tyrosine kinases. *The EMBO Journal,* 15**,** 5326-5335.

MILLETTI, F. 2012. Cell-penetrating peptides: classes, origin, and current landscape. *Drug Discovery Today,* 17**,** 850-860.

MINGOZZI, F. & HIGH, K. A. 2013. Immune responses to AAV vectors: overcoming barriers to successful gene therapy. *Blood,* 122**,** 23-36.

MISHRA, A., LAI, G. H., SCHMIDT, N. W., SUN, V. Z., RODRIGUEZ, A. R., TONG, R., TANG, L., CHENG, J., DEMING, T. J., KAMEI, D. T. & WONG, G. C. L. 2011. Translocation of HIV TAT peptide and analogues induced by multiplexed membrane and cytoskeletal interactions. *Proceedings of the National Academy of Sciences of the United States of America,* 108**,** 16883-16888.

MIYATA, Y., NISHIDA, E., KOYASU, S., YAHARA, I. & SAKAI, H. 1989. Protein kinase C-dependent and -independent pathways in the growth factor-induced cytoskeletal reorganization. *Journal of Biological Chemistry,* 264**,** 15565-8.

MONIER, S., PARTON, R. G., VOGEL, F., BEHLKE, J., HENSKE, A. & KURZCHALIA, T. V. 1995. VIP21-caveolin, a membrane protein constituent of the caveolar coat, oligomerizes in vivo and in vitro. *Molecular Biology of the Cell,* 6**,** 911-927.

MOODY, P. R., SAYERS, E. J., MAGNUSSON, J. P., ALEXANDER, C., BORRI, P., WATSON, P. & JONES, A. T. 2015. Receptor crosslinking: a general method to trigger internalization and lysosomal targeting of therapeutic receptor:ligand complexes. *Molecular Therapy,* 23**,** 1888-1898.

MOOREN, O. L., GALLETTA, B. J. & COOPER, J. A. 2012. Roles for actin assembly in endocytosis. *Annual Review of Biochemistry,* 81**,** 661-686.

MORÉN, B., SHAH, C., HOWES, M. T., SCHIEBER, N. L., MCMAHON, H. T., PARTON, R. G., DAUMKE, O. & LUNDMARK, R. 2012. EHD2 regulates caveolar dynamics via ATP-driven targeting and oligomerization. *Molecular Biology of the Cell,* 23**,** 1316-1329.

MOTLEY, A., BRIGHT, N. A., SEAMAN, M. N. J. & ROBINSON, M. S. 2003. Clathrin-mediated endocytosis in AP-2–depleted cells. *The Journal of Cell Biology,* 162**,** 909-918.

MUELLER, J., KRETZSCHMAR, I., VOLKMER, R. & BOISGUERIN, P. 2008. Comparison of cellular uptake using 22 CPPs in 4 different cell lines. *Bioconjugate Chemistry,* 19**,** 2363-2374.

MUFAMADI, M. S., PILLAY, V., CHOONARA, Y. E., DU TOIT, L. C., MODI, G., NAIDOO, D. & NDESENDO, V. M. K. 2011. A review on composite liposomal technologies for specialized drug delivery. *Journal of Drug Delivery,* 2011**,** 939851.

NABI, I. R. & LE, P. U. 2003. Caveolae/raft-dependent endocytosis. *The Journal of Cell Biology,* 161**,** 673-677.

NAKASE, I., NIWA, M., TAKEUCHI, T., SONOMURA, K., KAWABATA, N., KOIKE, Y., TAKEHASHI, M., TANAKA, S., UEDA, K., SIMPSON, J. C., JONES, A. T., SUGIURA, Y. & FUTAKI, S. 2004. Cellular uptake of arginine-rich peptides: roles for macropinocytosis and actin rearrangement. *Molecular Therapy,* 10**,** 1011-1022.

NAKASE, I., TADOKORO, A., KAWABATA, N., TAKEUCHI, T., KATOH, H., HIRAMOTO, K., NEGISHI, M., NOMIZU, M., SUGIURA, Y. & FUTAKI, S. 2007. Interaction of arginine-rich peptides with membrane-associated proteoglycans is crucial for induction of actin organization and macropinocytosis. *Biochemistry,* 46**,** 492-501.

NAM, J. S., INO, Y., SAKAMOTO, M. & HIROHASHI, S. 2002. Src family kinase inhibitor PP2 restores the E-cadherin/catenin cell adhesion system in human cancer cells and reduces cancer metastasis. *Clinical Cancer Research,* 8**,** 2430-2436.

NEUMANN-GIESEN, C., FERNOW, I., AMADDII, M. & TIKKANEN, R. 2007. Role of EGF-induced tyrosine phosphorylation of reggie-1/flotillin-2 in cell spreading and signaling to the actin cytoskeleton. *Journal of Cell Science,* 120**,** 395-406.

NGUYEN, L. T., HANEY, E. F. & VOGEL, H. J. 2011. The expanding scope of antimicrobial peptide structures and their modes of action. *Trends in Biotechnology,* 29**,** 464-472.

NICHOLS, B. J. & LIPPINCOTT-SCHWARTZ, J. 2001. Endocytosis without clathrin coats. *Trends in Cell Biology,* 11**,** 406-412.

NICHOLS, B. J. 2002. A distinct class of endosome mediates clathrin-independent endocytosis to the Golgi complex. *Nature Cell Biology,* 4**,** 374-378.

NIEDERMAN, R. & POLLARD, T. D. 1975. Human platelet myosin. II. In vitro assembly and structure of myosin filaments. *The Journal of Cell Biology,* 67**,** 72-92.

NISCHAN, N., HERCE, H. D., NATALE, F., BOHLKE, N., BUDISA, N., CARDOSO, M. C. & HACKENBERGER, C. P. R. 2015. Covalent attachment of cyclic TAT peptides to GFP results in protein delivery into live cells with immediate bioavailability. *Angewandte Chemie International Edition,* 54**,** 1950-1953.

NORBURY, C. C. 2006. Drinking a lot is good for dendritic cells. *Immunology,* 117**,** 443-451.

NUSSINOV, R. & JANG, H. 2014. Dynamic multiprotein assemblies shape the spatial structure of cell signaling. *Progress in biophysics and molecular biology,* 116**,** 158-164.

OCHOCKI, J. D., MULLEN, D. G., WATTENBERG, E. V. & DISTEFANO, M. D. 2011. Evaluation of a cell penetrating prenylated peptide lacking an intrinsic fluorophore via in situ click reaction. *Bioorganic & Medicinal Chemistry Letters,* 21**,** 4998-5001.

OEHLKE, J., SCHELLER, A., JANEK, K., WIESNER, B., KRAUSE, E., BEYERMANN, M. & BIENERT, M. 2002. Rapid translocation of amphipathic βhelical and β-sheet-forming peptides through plasma membranes of endothelial cells. *In:* SHIMONISHI, Y. (ed.) *Peptide Science — Present and Future.* Springer Netherlands.

OEHLKE, J., SCHELLER, A., WIESNER, B., KRAUSE, E., BEYERMANN, M., KLAUSCHENZ, E., MELZIG, M. & BIENERT, M. 1998. Cellular uptake of an α-helical amphipathic model peptide with the potential to deliver polar compounds into the cell interior non-endocytically. *Biochimica et Biophysica Acta (BBA) - Biomembranes,* 1414**,** 127-139.

OHNO, H., STEWART, J., FOURNIER, M. C., BOSSHART, H., RHEE, I., MIYATAKE, S., SAITO, T., GALLUSSER, A., KIRCHHAUSEN, T. & BONIFACINO, J. S. 1995. Interaction of tyrosine-based sorting signals with clathrin-associated proteins. *Science,* 269**,** 1872-1875.

OIKAWA, T., YAMAGUCHI, H., ITOH, T., KATO, M., IJUIN, T., YAMAZAKI, D., SUETSUGU, S. & TAKENAWA, T. 2004. PtdIns(3,4,5)P3 binding is necessary for WAVE2-induced formation of lamellipodia. *Nature Cell Biology,* 6, 420-426.

OLIVARES, M. J., GONZÁLEZ-JAMETT, A. M., GUERRA, M. J., BAEZ-MATUS, X., HARO-ACUÑA, V., MARTÍNEZ-QUILES, N. & CÁRDENAS, A. M. 2014. Src kinases regulate de novo actin polymerization during exocytosis in neuroendocrine chromaffin cells. *PLoS ONE,* 9, e99001.

OTTO, G. P. & NICHOLS, B. J. 2011. The roles of flotillin microdomains – endocytosis and beyond. *Journal of Cell Science,* 124, 3933-3940.

PADARI, K., SÄÄLIK, P., HANSEN, M., KOPPEL, K., RAID, R., LANGEL, Ü. & POOGA, M. 2005. Cell transduction pathways of transportans. *Bioconjugate Chemistry,* 16, 1399-1410.

PALADE, G. E. 1953. Fine structure of blood capillaries. *Journal of Applied Physics,* 24, 1424.

PANNELL, D. & ELLIS, J. 2001. Silencing of gene expression: implications for design of retrovirus vectors. *Reviews in Medical Virology,* 11, 205-217.

PANTALONI, D., CLAINCHE, C. L. & CARLIER, M.-F. 2001. Mechanism of actin-based motility. *Science,* 292, 1502-1506.

PAPAKONSTANTI, E. A. & STOURNARAS, C. 2002. Association of PI-3 kinase with PAK1 leads to actin phosphorylation and cytoskeletal reorganization. *Molecular Biology of the Cell,* 13, 2946-2962.

PARK, F., OHASHI, K., CHIU, W., NALDINI, L. & KAY, M. A. 2000. Efficient lentiviral transduction of liver requires cell cycling in vivo. *Nature Genetics,* 24, 49-52.

PARRINI, M. C., MATSUDA, M. & DE GUNZBURG, J. 2005. Spatiotemporal regulation of the Pak1 kinase. *Biochemical Society Transactions,* 33, 646-648.

PARSONS, S. J. & PARSONS, J. T. 2004. Src family kinases, key regulators of signal transduction. *Oncogene,* 23, 7906-7909.

PARTON, R. G. & DEL POZO, M. A. 2013. Caveolae as plasma membrane sensors, protectors and organizers. *Nature Reviews Molecular Cell Biology,* 14, 98-112.

PARTON, R. G. & HOWES, M. T. 2010. Revisiting caveolin trafficking: the end of the caveosome. *The Journal of Cell Biology,* 191, 439-441.

PARTON, R. G. & RICHARDS, A. A. 2003. Lipid rafts and caveolae as portals for endocytosis: new insights and common mechanisms. *Traffic,* 4, 724-738.

PARTON, R. G., HANZAL-BAYER, M. & HANCOCK, J. F. 2006. Biogenesis of caveolae: a structural model for caveolin-induced domain formation. *Journal of Cell Science,* 119, 787-796.

PAWLAK, G. & HELFMAN, D. M. 2002. MEK mediates v-Src-induced disruption of the actin cytoskeleton via inactivation of the Rho-ROCK-LIM kinase pathway. *Journal of Biological Chemistry,* 277, 26927-26933.

PAYNE, C. K., JONES, S. A., CHEN, C. & ZHUANG, X. 2007. Internalization and trafficking of cell surface proteoglycans and proteoglycan-binding ligands. *Traffic,* 8, 389-401.

PELHAM, R. J. & WANG, Y. L. 1999. High resolution detection of mechanical forces exerted by locomoting fibroblasts on the substrate. *Molecular Biology of the Cell,* 10, 935-945.

PELKMANS, L. & HELENIUS, A. 2002. Endocytosis via caveolae. *Traffic,* 3, 311-320.

PELKMANS, L. & ZERIAL, M. 2005. Kinase-regulated quantal assemblies and kiss-and-run recycling of caveolae. *Nature,* 436, 128-133.

PELKMANS, L. 2005. Secrets of caveolae- and lipid raft-mediated endocytosis revealed by mammalian viruses. *Biochimica et Biophysica Acta (BBA) - Molecular Cell Research,* 1746, 295-304.

PELKMANS, L., KARTENBECK, J. & HELENIUS, A. 2001. Caveolar endocytosis of simian virus 40 reveals a new two-step vesicular-transport pathway to the ER. *Nature Cell Biology,* 3, 473-483.

PENG, G. E., WILSON, S. R. & WEINER, O. D. 2011. A pharmacological cocktail for arresting actin dynamics in living cells. *Molecular Biology of the Cell,* 22, 3986-3994.

PENG, J., WALLAR, B. J., FLANDERS, A., SWIATEK, P. J. & ALBERTS, A. S. 2003. Disruption of the Diaphanous-related formin Drf1 gene encoding mDia1 reveals a role for Drf3 as an effector for Cdc42. *Current Biology,* 13, 534-545.

PEREIRA-LEAL, J. B., HUME, A. N. & SEABRA, M. C. 2001. Prenylation of Rab GTPases: molecular mechanisms and involvement in genetic disease. *FEBS Letters,* 498, 197-200.

PEREIRA, P., PEDROSA, S. S., WYMANT, J. M., SAYERS, E., CORREIA, A., VILANOVA, M., JONES, A. T. & GAMA, F. M. 2015. siRNA inhibition of endocytic pathways to characterize the cellular uptake mechanisms of folate functionalized glycol chitosan nanogels. *Molecular Pharmaceutics,* 12, 1970-1979.

PERRET, F., NISHIHARA, M., TAKEUCHI, T., FUTAKI, S., LAZAR, A. N., COLEMAN, A. W., SAKAI, N. & MATILE, S. 2005. Anionic fullerenes, calixarenes, coronenes, and pyrenes as activators of oligo/polyarginines in model membranes and live cells. *Journal of the American Chemical Society,* 127, 1114-1115.

PESEN, D. & HOH, J. H. 2005. Micromechanical architecture of the endothelial cell cortex. *Biophysical Journal,* 88, 670-679.

PETER, B. J., KENT, H. M., MILLS, I. G., VALLIS, Y., BUTLER, P. J. G., EVANS, P. R. & MCMAHON, H. T. 2004. BAR domains as sensors of membrane curvature: the amphiphysin BAR structure. *Science,* 303, 495-499.

POLLARD, T. D. & BORISY, G. G. 2003. Cellular motility driven by assembly and disassembly of actin filaments. *Cell,* 112, 453-465.

POLLARD, T. D. & COOPER, J. A. 2009. Actin, a central player in cell shape and movement. *Science,* 326, 1208-1212.

POLLARD, T. D. 2007. Regulation of actin filament assembly by Arp2/3 complex and formins. *Annual Review of Biophysics and Biomolecular Structure,* 36, 451-477.

POUNY, Y., RAPAPORT, D., MOR, A., NICOLAS, P. & SHAI, Y. 1992. Interaction of antimicrobial dermaseptin and its fluorescently labeled analogs with phospholipid membranes. *Biochemistry,* 31, 12416-12423.

PRAEFCKE, G. J. K. & MCMAHON, H. T. 2004. The dynamin superfamily: universal membrane tubulation and fission molecules? *Nature Reviews Molecular Cell Biology,* 5, 133-147.

PRITCHARD, C. A., HAYES, L., WOJNOWSKI, L., ZIMMER, A., MARAIS, R. M. & NORMAN, J. C. 2004. B-Raf acts via the ROCKII/LIMK/cofilin pathway to maintain actin stress fibers in fibroblasts. *Molecular and Cellular Biology,* 24, 5937-5952.

PULLIKUTH, A. K. & CATLING, A. D. 2007. Scaffold mediated regulation of MAPK signaling and cytoskeletal dynamics: A perspective. *Cellular Signalling,* 19, 1621-1632.

QUALMANN, B., KESSELS, M. M. & KELLY, R. B. 2000. Molecular links between endocytosis and the actin cytoskeleton. *The Journal of Cell Biology,* 150, 111-116.

RÄÄGEL, H. & POOGA, M. 2011. Chapter 10 - Peptide and Protein Delivery with Cell-penetrating Peptides. *In:* WALLE, C. V. D. (ed.) *Peptide and Protein Delivery.* Boston: Academic Press.

RÄÄGEL, H., SÄÄLIK, P., HANSEN, M., LANGEL, Ü. & POOGA, M. 2009. CPP–protein constructs induce a population of non-acidic vesicles during trafficking through endo-lysosomal pathway. *Journal of Controlled Release,* 139, 108-117.

RACOOSIN, E. L. & SWANSON, J. A. 1993. Macropinosome maturation and fusion with tubular lysosomes in macrophages. *The Journal of Cell Biology,* 121, 1011-1020.

RADHAKRISHNA, H., AL-AWAR, O., KHACHIKIAN, Z. & DONALDSON, J. G. 1999. ARF6 requirement for Rac ruffling suggests a role for membrane trafficking in cortical actin rearrangements. *Journal of Cell Science,* 112, 855-866.

RAJAKYLÄ, E. K. & VARTIAINEN, M. K. 2014. Rho, nuclear actin, and actin-binding proteins in the regulation of transcription and gene expression. *Small GTPases,* 5, e27539.

RANE, C. K. & MINDEN, A. 2014. P21 activated kinases: structure, regulation, and functions. *Small GTPases,* 5, e28003.

RAO, P. V., DENG, P. F., KUMAR, J. & EPSTEIN, D. L. 2001. Modulation of aqueous humor outflow facility by the Rho kinase–specific inhibitor Y-27632. *Investigative Ophthalmology & Visual Science,* 42**,** 1029-1037.

RAPOSO, G. & STOORVOGEL, W. 2013. Extracellular vesicles: Exosomes, microvesicles, and friends. *The Journal of Cell Biology,* 200**,** 373-383.

RAUCHER, D. & RYU, J. S. 2015. Cell-penetrating peptides: strategies for anticancer treatment. *Trends in Molecular Medicine,* 21**,** 560-570.

RAVIKUMAR, B., MOREAU, K., JAHREISS, L., PURI, C. & RUBINSZTEIN, D. C. 2010. Plasma membrane contributes to the formation of pre-autophagosomal structures. *Nature Cell Biology,* 12**,** 747-757.

RAZANI, B., WANG, X. B., ENGELMAN, J. A., BATTISTA, M., LAGAUD, G., ZHANG, X. L., KNEITZ, B., HOU, H., CHRIST, G. J., EDELMANN, W. & LISANTI, M. P. 2002. Caveolin-2-deficient mice show evidence of severe pulmonary dysfunction without disruption of caveolae. *Molecular and Cellular Biology,* 22**,** 2329-2344.

REDELMAN-SIDI, G., IYER, G., SOLIT, D. & GLICKMAN, M. S. 2013. Oncogenic activation of Pak1-dependent pathway of macropinocytosis determines BCG entry into bladder cancer cells. *Cancer research,* 73**,** 1156-1167.

REINECKE, J. & CAPLAN, S. 2014. Endocytosis and the Src family of non-receptor tyrosine kinases. *Biomolecular concepts,* 5**,** 143-155.

REJMAN, J., BRAGONZI, A. & CONESE, M. 2005. Role of clathrin- and caveolae-mediated endocytosis in gene transfer mediated by lipo- and polyplexes. *Molecular Therapy,* 12**,** 468-474.

REWATKAR, P. V., PARTON, R. G., PAREKH, H. S. & PARAT, M. O. 2015. Are caveolae a cellular entry route for non-viral therapeutic delivery systems? *Advanced Drug Delivery Reviews,* 91**,** 92-108.

RHEE, M. & DAVIS, P. 2006. Mechanism of uptake of C105Y, a novel cell-penetrating peptide. *Journal of Biological Chemistry,* 281**,** 1233-1240.

RICHARD, J. P., MELIKOV, K., BROOKS, H., PREVOT, P., LEBLEU, B. & CHERNOMORDIK, L. V. 2005. Cellular uptake of unconjugated TAT peptide involves clathrin-dependent endocytosis and heparan sulfate receptors. *Journal of Biological Chemistry,* 280**,** 15300-15306.

RICHARD, J. P., MELIKOV, K., VIVES, E., RAMOS, C., VERBEURE, B., GAIT, M. J., CHERNOMORDIK, L. V. & LEBLEU, B. 2003. Cell-penetrating peptides. A reevaluation of the mechanism of cellular uptake. *Journal of Biological Chemistry,* 278**,** 585-590.

RIDLEY, A. J. & HALL, A. 1992. The small GTP-binding protein rho regulates the assembly of focal adhesions and actin stress fibers in response to growth factors. *Cell,* 70**,** 389-399.

RIDLEY, A. J. 2006. Rho GTPases and actin dynamics in membrane protrusions and vesicle trafficking. *Trends in Cell Biology,* 16**,** 522-529.

RIDLEY, A. J., PATERSON, H. F., JOHNSTON, C. L., DIEKMANN, D. & HALL, A. 1992. The small GTP-binding protein rac regulates growth factor-induced membrane ruffling. *Cell,* 70**,** 401-410.

RIDLEY, ANNE J. 2011. Life at the leading edge. *Cell,* 145**,** 1012-1022.

RIENTO, K. & RIDLEY, A. J. 2003. ROCKs: multifunctional kinases in cell behaviour. *Nature Reviews Molecular Cell Biology,* 4**,** 446-456.

RIENTO, K., FRICK, M., SCHAFER, I. & NICHOLS, B. J. 2009. Endocytosis of flotillin-1 and flotillin-2 is regulated by Fyn kinase. *Journal of Cell Science,* 122**,** 912-918.

RINGSDORF, H. 1975. Structure and properties of pharmacologically active polymers. *Journal of Polymer Science: Polymer Symposia,* 51**,** 135-153.

RINGSTAD, N., NEMOTO, Y. & DE CAMILLI, P. 1997. The SH3p4/Sh3p8/SH3p13 protein family: Binding partners for synaptojanin and dynamin via a Grb2-like Src homology 3 domain. *Proceedings of the National Academy of Sciences of the United States of America,* 94**,** 8569-8574.

RIZZO, M. A., SHOME, K., WATKINS, S. C. & ROMERO, G. 2000. The recruitment of Raf-1 to membranes is mediated by direct interaction with phosphatidic acid and is independent of association with Ras. *Journal of Biological Chemistry,* 275**,** 23911-23918.

ROBERTS, R. L., BARBIERI, M. A., ULLRICH, J. & STAHL, P. D. 2000. Dynamics of rab5 activation in endocytosis and phagocytosis. *Journal of Leukocyte Biology,* 68**,** 627-632.

ROBERTSON, A., SMYTHE, E. & AYSCOUGH, K. 2009. Functions of actin in endocytosis. *Cellular and Molecular Life Sciences,* 66**,** 2049-2065.

ROHATGI, R., MA, L., MIKI, H., LOPEZ, M., KIRCHHAUSEN, T., TAKENAWA, T. & KIRSCHNER, M. W. 1999. The interaction between N-WASP and the Arp2/3 complex links Cdc42-dependent signals to actin assembly. *Cell,* 97**,** 221-231.

ROSS, J. L., ALI, M. Y. & WARSHAW, D. M. 2008. Cargo transport: molecular motors navigate a complex cytoskeleton. *Current Opinion in Cell Biology,* 20**,** 41-47.

ROSSMAN, K. L., DER, C. J. & SONDEK, J. 2005. GEF means go: turning on RHO GTPases with guanine nucleotide-exchange factors. *Nature Reviews Molecular Cell Biology,* 6**,** 167-180.

ROTH, M. G. 2007. Integrating actin assembly and endocytosis. *Developmental Cell,* 13**,** 3-4.

ROTHBARD, J. B., JESSOP, T. C., LEWIS, R. S., MURRAY, B. A. & WENDER, P. A. 2004. Role of membrane potential and hydrogen bonding in the mechanism of translocation of guanidinium-rich peptides into cells. *Journal of the American Chemical Society,* 126**,** 9506-9507.

ROTHBERG, K. G., HEUSER, J. E., DONZELL, W. C., YING, Y. S., GLENNEY, J. R. & ANDERSON, R. G. W. 1992. Caveolin, a protein component of caveolae membrane coats. *Cell,* 68**,** 673-682.

ROTHBERG, K. G., YING, Y. S., KAMEN, B. A. & ANDERSON, R. G. 1990. Cholesterol controls the clustering of the glycophospholipid-anchored membrane receptor for 5-methyltetrahydrofolate. *The Journal of Cell Biology,* 111**,** 2931-2938.

ROUILLER, I., XU, X.-P., AMANN, K. J., EGILE, C., NICKELL, S., NICASTRO, D., LI, R., POLLARD, T. D., VOLKMANN, N. & HANEIN, D. 2008. The structural basis of actin filament branching by the Arp2/3 complex. *The Journal of Cell Biology,* 180**,** 887-895.

RUIZ-LAFUENTE, N., ALCARAZ-GARCÍA, M. J., GARCÍA-SERNA, A. M., SEBASTIÁN-RUIZ, S., MOYA-QUILES, M. R., GARCÍA-ALONSO, A. M. & PARRADO, A. 2015. Dock10, a Cdc42 and Rac1 GEF, induces loss of elongation, filopodia, and ruffles in cervical cancer epithelial HeLa cells. *Biology Open,* 4**,** 627-635.

RUPPER, A., LEE, K., KNECHT, D. & CARDELLI, J. 2001. Sequential activities of phosphoinositide 3-kinase, PKB/Aakt, and Rab7 during macropinosome formation in Dictyostelium. *Molecular Biology of the Cell,* 12**,** 2813-2824.

RYSER, H. J. P. & HANCOCK, R. 1965. Histones and basic polyamino acids stimulate the uptake of albumin by tumor cells in culture. *Science,* 150**,** 501-503.

SÄÄLIK, P., PADARI, K. R., NIINEP, A., LORENTS, A., HANSEN, M., JOKITALO, E., LANGEL, Ü. & POOGA, M. 2009. Protein Delivery with Transportans Is Mediated by Caveolae Rather Than Flotillin-Dependent Pathways. *Bioconjugate Chemistry,* 20**,** 877-887.

SAAR, K., LINDGREN, M., HANSEN, M., EIRÍKSDÓTTIR, E., JIANG, Y., ROSENTHAL-AIZMAN, K., SASSIAN, M. & LANGEL, Ü. 2005. Cell-penetrating peptides: a comparative membrane toxicity study. *Analytical Biochemistry,* 345**,** 55-65.

SABHARANJAK, S., SHARMA, P., PARTON, R. G. & MAYOR, S. 2002. GPI-anchored proteins are delivered to recycling endosomes via a distinct cdc42-regulated, clathrin-independent pinocytic pathway. *Developmental Cell,* 2**,** 411-423.

SAFFARIAN, S., COCUCCI, E. & KIRCHHAUSEN, T. 2009. Distinct dynamics of endocytic clathrin-coated pits and coated plaques. *PLoS Biology,* 7**,** e1000191.

SALAS-CORTES, L., YE, F., TENZA, D., WILHELM, C., THEOS, A., LOUVARD, D., RAPOSO, G. & COUDRIER, E. 2005. Myosin Ib modulates the morphology and the protein transport within multi-vesicular sorting endosomes. *Journal of Cell Science,* 118, 4823-4832.

SANDERS, L. C., MATSUMURA, F., BOKOCH, G. M. & DE LANEROLLE, P. 1999. Inhibition of myosin light chain kinase by p21-activated kinase. *Science,* 283, 2083-2085.

SARGIACOMO, M., SCHERER, P. E., TANG, Z., KÜBLER, E., SONG, K. S., SANDERS, M. C. & LISANTI, M. P. 1995. Oligomeric structure of caveolin: implications for caveolae membrane organization. *Proceedings of the National Academy of Sciences of the United States of America,* 92, 9407-9411.

SAWITZKY, H., LIEBE, S., WILLINGALE-THEUNE, J. & MENZEL, D. 1999. The anti-proliferative agent jasplakinolide rearranges the actin cytoskeleton of plant cells. *European Journal of Cell Biology,* 78, 424-433.

SAYERS, E. J., CLEAL, K., EISSA, N. G., WATSON, P. & JONES, A. T. 2014. Distal phenylalanine modification for enhancing cellular delivery of fluorophores, proteins and quantum dots by cell penetrating peptides. *Journal of Controlled Release,* 195, 55-62.

SCHAFER, D. A., JENNINGS, P. B. & COOPER, J. A. 1996. Dynamics of capping protein and actin assembly in vitro: uncapping barbed ends by polyphosphoinositides. *The Journal of Cell Biology,* 135, 169-179.

SCHAFMEISTER, C. E., PO, J. & VERDINE, G. L. 2000. An all-hydrocarbon crosslinking system for enhancing the helicity and metabolic stability of peptides. *Journal of the American Chemical Society,* 122, 5891-5892.

SCHELLER, A., OEHLKE, J., WIESNER, B., DATHE, M., KRAUSE, E., BEYERMANN, M., MELZIG, M. & BIENERT, M. 1999. Structural requirements for cellular uptake of α-helical amphipathic peptides. *Journal of Peptide Science,* 5, 185-194.

SCHINDELIN, J., ARGANDA-CARRERAS, I., FRISE, E., KAYNIG, V., LONGAIR, M., PIETZSCH, T., PREIBISCH, S., RUEDEN, C., SAALFELD, S., SCHMID, B., TINEVEZ, J. Y., WHITE, D. J., HARTENSTEIN, V., ELICEIRI, K., TOMANCAK, P. & CARDONA, A. 2012. Fiji - an open source platform for biological image analysis. *Nature methods,* 9, 10.1038/nmeth.2019.

SCHLOSSMAN, D. M., SCHMID, S. L., BRAELL, W. A. & ROTHMAN, J. E. 1984. An enzyme that removes clathrin coats: purification of an uncoating ATPase. *The Journal of Cell Biology,* 99, 723-733.

SCHLÜTER, K., JOCKUSCH, B. M. & ROTHKEGEL, M. 1997. Profilins as regulators of actin dynamics. *Biochimica et Biophysica Acta (BBA) - Molecular Cell Research,* 1359, 97-109.

SCHMID, E. M. & MCMAHON, H. T. 2007. Integrating molecular and network biology to decode endocytosis. *Nature,* 448, 883-888.

SCHNATWINKEL, C., CHRISTOFORIDIS, S., LINDSAY, M. R., UTTENWEILER-JOSEPH, S., WILM, M., PARTON, R. G. & ZERIAL, M. 2004. The Rab5 effector Rabankyrin-5 regulates and coordinates different endocytic mechanisms. *PLoS Biology,* 2, e261.

SCHNITZER, J. E. 2001. Caveolae: from basic trafficking mechanisms to targeting transcytosis for tissue-specific drug and gene delivery in vivo. *Advanced Drug Delivery Reviews,* 49, 265-280.

SENDEROWICZ, A. M. J., KAUR, G., SAINZ, E., LAING, C., INMAN, W. D., RODRIGUEZ, J., CREWS, P., MALSPEIS, L., GREVER, M. R., SAUSVILLE, E. A. & DUNCAN, K. L. K. 1995. Jasplakinolide's inhibition of the growth of prostate carcinoma cells in vitro with disruption of the actin cytoskeleton. *Journal of the National Cancer Institute,* 87, 46-51.

SENJU, Y., ITOH, Y., TAKANO, K., HAMADA, S. & SUETSUGU, S. 2011. Essential role of PACSIN2/syndapin-II in caveolae membrane sculpting. *Journal of Cell Science,* 124, 2032-2040.

SERRESI, M., BIZZARRI, R., CARDARELLI, F. & BELTRAM, F. 2009. Real-time measurement of endosomal acidification by a novel genetically encoded biosensor. *Analytical and Bioanalytical Chemistry,* 393, 1123-1133.

SHAH, K. & VINCENT, F. 2005. Divergent roles of c-Src in controlling platelet-derived growth factor-dependent signaling in fibroblasts. *Molecular Biology of the Cell,* 16, 5418-5432.

SHARMA, D. K., BROWN, J. C., CHOUDHURY, A., PETERSON, T. E., HOLICKY, E., MARKS, D. L., SIMARI, R., PARTON, R. G. & PAGANO, R. E. 2004. Selective stimulation of caveolar endocytosis by glycosphingolipids and cholesterol. *Molecular Biology of the Cell,* 15, 3114-3122.

SHAW, M. K. & TILNEY, L. G. 1999. Induction of an acrosomal process in Toxoplasma gondii: visualization of actin filaments in a protozoan parasite. *Proceedings of the National Academy of Sciences,* 96, 9095-9099.

SHIMOMURA, O., JOHNSON, F. H. & SAIGA, Y. 1962. Extraction, purification and properties of aequorin, a bioluminescent protein from the luminous hydromedusan, Aequorea. *Journal of Cellular and Comparative Physiology,* 59, 223-239.

SHURETY, W., STEWART, N. L. & STOW, J. L. 1998. Fluid-phase markers in the basolateral endocytic pathway accumulate in response to the actin assembly-promoting drug Jasplakinolide. *Molecular Biology of the Cell,* 9, 957-975.

SIGISMUND, S., CONFALONIERI, S., CILIBERTO, A., POLO, S., SCITA, G. & DI FIORE, P. P. 2012. Endocytosis and signaling: cell logistics shape the eukaryotic cell plan. *Physiological Reviews,* 92, 273-366.

SIGISMUND, S., WOELK, T., PURI, C., MASPERO, E., TACCHETTI, C., TRANSIDICO, P., DI FIORE, P. P. & POLO, S. 2005. Clathrin-independent endocytosis of ubiquitinated cargos. *Proceedings of the National Academy of Sciences of the United States of America,* 102, 2760-2765.

SIMON, M. J., GAO, S., KANG, W. H., BANTA, S. & MORRISON, B. 2009. TAT-mediated intracellular protein delivery to primary brain cells is dependent on glycosaminoglycan expression. *Biotechnology and bioengineering,* 104, 10-19.

SIT, S. T. & MANSER, E. 2011. Rho GTPases and their role in organizing the actin cytoskeleton. *Journal of Cell Science,* 124, 679-683.

SOLIS, GONZALO P., HOEGG, M., MUNDERLOH, C., SCHROCK, Y., MALAGA-TRILLO, E., RIVERA-MILLA, E. & STUERMER, CLAUDIA A O. 2007. Reggie/flotillin proteins are organized into stable tetramers in membrane microdomains. *Biochemical Journal,* 403, 313-322.

SOOMETS, U., LINDGREN, M., GALLET, X., HÄLLBRINK, M., ELMQUIST, A., BALASPIRI, L., ZORKO, M., POOGA, M., BRASSEUR, R. & LANGEL, Ü. 2000. Deletion analogues of transportan. *Biochimica et Biophysica Acta (BBA) - Biomembranes,* 1467, 165-176.

SPECTOR, I., BRAET, F., SHOCHET, N. R. & BUBB, M. R. 1999. New anti-actin drugs in the study of the organization and function of the actin cytoskeleton. *Microscopy Research and Technique,* 47, 18-37.

SPECTOR, I., SHOCHET, N. R., BLASBERGER, D. & KASHMAN, Y. 1989. Latrunculins—novel marine macrolides that disrupt microfilament organization and affect cell growth: I. Comparison with cytochalasin D. *Cell Motility and the Cytoskeleton,* 13, 127-144.

STEFFEN, A., LADWEIN, M., DIMCHEV, G. A., HEIN, A., SCHWENKMEZGER, L., ARENS, S., LADWEIN, K. I., HOLLEBOOM, J. M., SCHUR, F., SMALL, J. V., SCHWARZ, J., GERHARD, R., FAIX, J., STRADAL, T. E. B., BRAKEBUSCH, C. & ROTTNER, K. 2013. Rac function is crucial for cell migration but is not required for spreading and focal adhesion formation. *Journal of Cell Science,* 126, 4572-4588.

STIMPSON, H. E. M., TORET, C. P., CHENG, A. T., PAULY, B. S. & DRUBIN, D. G. 2009. Early-arriving Syp1p and Ede1p function in endocytic site placement and formation in budding yeast. *Molecular Biology of the Cell,* 20, 4640-4651.

STRADAL, T. E. B. & SCITA, G. 2006. Protein complexes regulating Arp2/3-mediated actin assembly. *Current Opinion in Cell Biology,* 18, 4-10.

SUETSUGU, S. 2009. The direction of actin polymerization for vesicle fission suggested from membranes tubulated by the EFC/F-BAR domain protein FBP17. *FEBS Letters,* 583**,** 3401-3404.

SUETSUGU, S., YAMAZAKI, D., KURISU, S. & TAKENAWA, T. 2003. Differential roles of WAVE1 and WAVE2 in dorsal and peripheral ruffle formation for fibroblast cell migration. *Developmental Cell,* 5**,** 595-609.

SUHORUTSENKO, J., OSKOLKOV, N., ARUKUUSK, P., KURRIKOFF, K., ERISTE, E., COPOLOVICI, D.-M. & LANGEL, Ü. 2011. Cell-penetrating peptides, PepFects, show no evidence of toxicity and immunogenicity in vitro and in vivo. *Bioconjugate Chemistry,* 22**,** 2255-2262.

SUN, H. Q., YAMAMOTO, M., MEJILLANO, M. & YIN, H. L. 1999. Gelsolin, a multifunctional actin regulatory protein. *Journal of Biological Chemistry,* 274**,** 33179-33182.

SUN, J. Y., ANAND-JAWA, V., CHATTERJEE, S. & WONG, K. K. 2003. Immune responses to adeno-associated virus and its recombinant vectors. *Gene Therapy,* 10**,** 964-976.

SVITKINA, T. M., VERKHOVSKY, A. B. & BORISY, G. G. 1995. Improved procedures for electron microscopic visualization of the cytoskeleton of cultured cells. *Journal of Structural Biology,* 115**,** 290-303.

SVOBODA, K. K. H., MOESSNER, P., FIELD, T. & ACEVEDO, J. 2004. ROCK inhibitor (Y27632) increases apoptosis and disrupts the actin cortical mat in embryonic avian corneal epithelium. *Developmental Dynamics,* 229**,** 579-590.

SWANSON, J. A. & WATTS, C. 1995. Macropinocytosis. *Trends in Cell Biology,* 5**,** 424-428.

SWANSON, J. A. 2008. Shaping cups into phagosomes and macropinosomes. *Nature Reviews Molecular Cell Biology,* 9**,** 639-649.

SWIECICKI, J. M., BARTSCH, A., TAILHADES, J., DI PISA, M., HELLER, B., CHASSAING, G., MANSUY, C., BURLINA, F. & LAVIELLE, S. 2014. The efficacies of cell-penetrating peptides in accumulating in large unilamellar vesicles depend on their ability to form inverted micelles. *ChemBioChem,* 15**,** 884-891.

TAKAYAMA, K., HIROSE, H., TANAKA, G., PUJALS, S., KATAYAMA, S., NAKASE, I. & FUTAKI, S. 2012. Effect of the attachment of a penetration accelerating sequence and the influence of hydrophobicity on octaarginine-mediated intracellular delivery. *Molecular Pharmaceutics,* 9**,** 1222-1230.

TAKENAWA, T. & SUETSUGU, S. 2007. The WASP-WAVE protein network: connecting the membrane to the cytoskeleton. *Nature Reviews Molecular Cell Biology,* 8**,** 37-48.

TAKEUCHI, T., KOSUGE, M., TADOKORO, A., SUGIURA, Y., NISHI, M., KAWATA, M., SAKAI, N., MATILE, S. & FUTAKI, S. 2006. Direct and rapid cytosolic delivery using cell-penetrating peptides mediated by pyrenebutyrate. *ACS Chemical Biology,* 1**,** 299-303.

TAPON, N. & HALL, A. 1997. Rho, Rac and Cdc42 GTPases regulate the organization of the actin cytoskeleton. *Current Opinion in Cell Biology,* 9**,** 86-92.

TAYLOR, M. J., LAMPE, M. & MERRIFIELD, C. J. 2012. A feedback loop between dynamin and actin recruitment during clathrin-mediated endocytosis. *PLoS Biology,* 10**,** e1001302.

TEE, Y. H., SHEMESH, T., THIAGARAJAN, V., HARIADI, R. F., ANDERSON, K. L., PAGE, C., VOLKMANN, N., HANEIN, D., SIVARAMAKRISHNAN, S., KOZLOV, M. M. & BERSHADSKY, A. D. 2015. Cellular chirality arising from the self-organization of the actin cytoskeleton. *Nature Cell Biology,* 17**,** 445-457.

TEHRANI, S., TOMASEVIC, N., WEED, S., SAKOWICZ, R. & COOPER, J. A. 2007. Src phosphorylation of cortactin enhances actin assembly. *Proceedings of the National Academy of Sciences,* 104**,** 11933-11938.

THOMAS, C. E., EHRHARDT, A. & KAY, M. A. 2003. Progress and problems with the use of viral vectors for gene therapy. *Nature Reviews Genetics,* 4**,** 346-358.

THORÉN, P. E. G., PERSSON, D., ISAKSON, P., GOKSÖR, M., ÖNFELT, A. & NORDÉN, B. 2003. Uptake of analogs of penetratin, Tat(48–60) and oligoarginine in live cells. *Biochemical and Biophysical Research Communications,* 307**,** 100-107.

THORN, H., STENKULA, K. G., KARLSSON, M., ÖRTEGREN, U., NYSTROM, F. H., GUSTAVSSON, J. & STRÅLFORS, P. 2003. Cell surface orifices of caveolae and localization of caveolin to the necks of caveolae in adipocytes. *Molecular Biology of the Cell,* 14**,** 3967-3976.

THUMKEO, D., WATANABE, S. & NARUMIYA, S. 2013. Physiological roles of Rho and Rho effectors in mammals. *European Journal of Cell Biology,* 92**,** 303-315.

TORCHILIN, V. P. 2008. Tat peptide-mediated intracellular delivery of pharmaceutical nanocarriers. *Advanced Drug Delivery Reviews,* 60**,** 548-558.

TORGERSEN, M. L., SKRETTING, G., VAN DEURS, B. & SANDVIG, K. 2001. Internalization of cholera toxin by different endocytic mechanisms. *Journal of Cell Science,* 114**,** 3737-3747.

TORRES, E. & ROSEN, M. K. 2006. Protein-tyrosine kinase and GTPase signals cooperate to phosphorylate and activate Wiskott-Aldrich Syndrome Protein (WASP)/neuronal WASP. *Journal of Biological Chemistry,* 281**,** 3513-3520.

TÓTH, J., KOVÁCS, M., WANG, F., NYITRAY, L. & SELLERS, J. R. 2005. Myosin V from Drosophila reveals diversity of motor mechanisms within the myosin V family. *Journal of Biological Chemistry,* 280**,** 30594-30603.

TRAN, N. H. & FROST, J. A. 2003. Phosphorylation of Raf-1 by p21-activated kinase 1 and Src regulates Raf-1 autoinhibition. *Journal of Biological Chemistry,* 278**,** 11221-11226.

TRIFARÓ, J. M. & VITALE, M. L. 1993. Cytoskeleton dynamics during neurotransmitter release. *Trends in Neurosciences,* 16**,** 466-472.

TSIEN, R. Y. 1998. The green fluorescent protein. *Annual Review of Biochemistry,* 67**,** 509-544.

TÜNNEMANN, G., MARTIN, R. M., HAUPT, S., PATSCH, C., EDENHOFER, F. & CARDOSO, M. C. 2006. Cargo-dependent mode of uptake and bioavailability of TAT-containing proteins and peptides in living cells. *The FASEB Journal,* 20**,** 1775-1784.

TÜNNEMANN, G., TER-AVETISYAN, G., MARTIN, R. M., STÖCKL, M., HERRMANN, A. & CARDOSO, M. C. 2008. Live-cell analysis of cell penetration ability and toxicity of oligo-arginines. *Journal of Peptide Science,* 14**,** 469-476.

UEHATA, M., ISHIZAKI, T., SATOH, H., ONO, T., KAWAHARA, T., MORISHITA, T., TAMAKAWA, H., YAMAGAMI, K., INUI, J., MAEKAWA, M. & NARUMIYA, S. 1997. Calcium sensitization of smooth muscle mediated by a Rho-associated protein kinase in hypertension. *Nature,* 389**,** 990-994.

UNGEWICKELL, E., UNGEWICKELL, H., HOLSTEIN, S. E. H., LINDNER, R., PRASAD, K., BAROUCH, W., MARTINI, B., GREENE, L. E. & EISENBERG, E. 1995. Role of auxilin in uncoating clathrin-coated vesicles. *Nature,* 378**,** 632-635.

VAN DEURS, B., VILHARDT, F., TORGERSEN, M., ROEPSTORFF, K., HOMMELGAARD, A. M. & SANDVIG, K. 2006. The role of caveolae and noncaveolar rafts in endocytosis. *Lipid Rafts and Caveolae.* Wiley-VCH Verlag GmbH & Co. KGaA.

VARSHOSAZ, J. 2012. Dextran conjugates in drug delivery. *Expert opinion on drug delivery,* 9**,** 509-523.

VAVYLONIS, D., KOVAR, D. R., O'SHAUGHNESSY, B. & POLLARD, T. D. 2006. Model of formin-associated actin filament elongation. *Molecular Cell,* 21**,** 455-466.

VEITHEN, A., CUPERS, P., BAUDHUIN, P. & COURTOY, P. J. 1996. v-Src induces constitutive macropinocytosis in rat fibroblasts. *Journal of Cell Science,* 109**,** 2005-2012.

VEMURI, S. & RHODES, C. T. 1995. Preparation and characterization of liposomes as therapeutic delivery systems: a review. *Pharmaceutica Acta Helvetiae,* 70**,** 95-111.

VERCAUTEREN, D., PIEST, M., VAN DER AA, L. J., AL SORAJ, M., JONES, A. T., ENGBERSEN, J. F. J., DE SMEDT, S. C. & BRAECKMANS, K. 2011. Flotillin-dependent endocytosis and a phagocytosis-like mechanism for cellular internalization of disulfide-based poly(amido amine)/DNA polyplexes. *Biomaterials,* 32**,** 3072-3084.

VERCAUTEREN, D., VANDENBROUCKE, R. E., JONES, A. T., REJMAN, J., DEMEESTER, J., DE SMEDT, S. C., SANDERS, N. N. & BRAECKMANS, K. 2010.

The use of inhibitors to study endocytic pathways of gene carriers: optimization and pitfalls. *Molecular Therapy,* 18**,** 561-569.

VICENTE-MANZANARES, M., MA, X., ADELSTEIN, R. S. & HORWITZ, A. R. 2009. Non-muscle myosin II takes centre stage in cell adhesion and migration. *Nature Reviews Molecular Cell Biology,* 10**,** 778-790.

VINCENT, S. & SETTLEMAN, J. 1997. The PRK2 kinase is a potential effector target of both Rho and Rac GTPases and regulates actin cytoskeletal organization. *Molecular and Cellular Biology,* 17**,** 2247-2256.

VISEGRÁDY, B., LŐRINCZY, D., HILD, G., SOMOGYI, B. & NYITRAI, M. 2005. A simple model for the cooperative stabilisation of actin filaments by phalloidin and jasplakinolide. *FEBS Letters,* 579**,** 6-10.

VIVÈS, E., BRODIN, P. & LEBLEU, B. 1997. A truncated HIV-1 Tat protein basic domain rapidly translocates through the plasma membrane and accumulates in the cell nucleus. *Journal of Biological Chemistry,* 272**,** 16010-16017.

VIVÈS, E., RICHARD, J., RISPAL, C. & LEBLEU, B. 2003. TAT peptide internalization: seeking the mechanism of entry. *Current protein & peptide science,* 4**,** 125-132.

WADIA, J. S. & DOWDY, S. F. 2003. Modulation of cellular function by TAT mediated transduction of full length proteins. *Current protein & peptide science,* 4**,** 97-104.

WADIA, J. S., STAN, R. V. & DOWDY, S. F. 2004b. Transducible TAT-HA fusogenic peptide enhances escape of TAT-fusion proteins after lipid raft macropinocytosis. *Nature Medicine* 10**,** 310- 315.

WAKAYAMA, Y., FUKUHARA, S., ANDO, K., MATSUDA, M. & MOCHIZUKI, N. 2015. Cdc42 mediates Bmp-induced sprouting angiogenesis through Fmnl3-driven assembly of endothelial filopodia in zebrafish. *Developmental Cell,* 32**,** 109-122.

WANG, M. & CASEY, P. J. 2016. Protein prenylation: unique fats make their mark on biology. *Nat Rev Mol Cell Biol,* 17**,** 110-122.

WANG, W., EDDY, R. & CONDEELIS, J. 2007. The cofilin pathway in breast cancer invasion and metastasis. *Nature reviews. Cancer,* 7**,** 429-440.

WANG, Y., TERAOKA, I., HANSEN, F. Y., PETERS, G. H. & HASSAGER, O. 2010. A theoretical study of the separation principle in size exclusion chromatography. *Macromolecules,* 43**,** 1651-1659.

WANG, Z., EDWARDS, J. G., RILEY, N., PROVANCE JR, D. W., KARCHER, R., LI, X.-D., DAVISON, I. G., IKEBE, M., MERCER, J. A., KAUER, J. A. & EHLERS, M. D. 2008. Myosin Vb mobilizes recycling endosomes and AMPA receptors for postsynaptic plasticity. *Cell,* 135**,** 535-548.

WASSEF, N. M., MATYAS, G. R. & ALVING, C. R. 1991. Complement-dependent phagocytosis of liposomes by macrophages: suppressive effects of "stealth" lipids. *Biochemical and Biophysical Research Communications,* 176**,** 866-874.

WATARAI, M., DERRE, I., KIRBY, J., GROWNEY, J. D., DIETRICH, W. F. & ISBERG, R. R. 2001. Legionella pneumophila is internalized by a macropinocytotic uptake pathway controlled by the Dot/Icm System and the mouse Lgn1 locus. *The Journal of Experimental Medicine,* 194**,** 1081-1096.

WATKINS, C. L., BRENNAN, P., FEGAN, C., TAKAYAMA, K., NAKASE, I., FUTAKI, S. & JONES, A. T. 2009. Cellular uptake, distribution and cytotoxicity of the hydrophobic cell penetrating peptide sequence PFVYLI linked to the proapoptotic domain peptide PAD. *Journal of Controlled Release,* 140**,** 237-244.

WATKINS, C. L., SAYERS, E. J., ALLENDER, C., BARROW, D., FEGAN, C., BRENNAN, P. & JONES, A. T. 2011. Co-operative membrane disruption between cell-penetrating peptide and cargo: implications for the therapeutic use of the Bcl-2 converter peptide D-NuBCP-9-r8. *Molecular Therapy,* 19**,** 2124-2132.

WATKINS, CATHERINE L., SCHMALJOHANN, D., FUTAKI, S. & JONES, ARWYN T. 2009. Low concentration thresholds of plasma membranes for rapid energy-independent translocation of a cell-penetrating peptide. *Biochemical Journal,* 420**,** 179-191.

WEED, S. A. & PARSONS, J. T. 2001. Cortactin: coupling membrane dynamics to cortical actin assembly. *Oncogene,* 20**,** 6418-6434.

WEISENBERG, R. C. 1972. Microtubule formation in vitro in solutions containing low calcium concentrations. *Science,* 177**,** 1104-1105.

WELLS, A. L., LIN, A. W., CHEN, L. Q., SAFER, D., CAIN, S. M., HASSON, T., CARRAGHER, B. O., MILLIGAN, R. A. & SWEENEY, H. L. 1999. Myosin VI is an actin-based motor that moves backwards. *Nature,* 401**,** 505-508.

WESSELLS, N. K., SPOONER, B. S., ASH, J. F., BRADLEY, M. O., LUDUENA, M. A., TAYLOR, E. L., WRENN, J. T. & YAMADA, K. M. 1971. Microfilaments in cellular and developmental processes. *Science,* 171**,** 135-143.

WEST, M. A., BRETSCHER, M. S. & WATTS, C. 1989. Distinct endocytotic pathways in epidermal growth factor-stimulated human carcinoma A431 cells. *The Journal of Cell Biology,* 109**,** 2731-2739.

WIGGE, P., KÖHLER, K., VALLIS, Y., DOYLE, C. A., OWEN, D., HUNT, S. P. & MCMAHON, H. T. 1997. Amphiphysin heterodimers: potential role in clathrin-mediated endocytosis. *Molecular Biology of the Cell,* 8**,** 2003-2015.

WILCZEWSKA, A. Z., NIEMIROWICZ, K., MARKIEWICZ, K. H. & CAR, H. 2012. Nanoparticles as drug delivery systems. *Pharmacological Reports,* 64**,** 1020-1037.

WOLF, A. A., JOBLING, M. G., WIMER-MACKIN, S., FERGUSON-MALTZMAN, M., MADARA, J. L., HOLMES, R. K. & LENCER, W. I. 1998. Ganglioside Structure Dictates Signal Transduction by Cholera Toxin and Association with Caveolae-like Membrane Domains in Polarized Epithelia. *The Journal of Cell Biology,* 141**,** 917-927.

WOOLNER, S. & BEMENT, W. M. 2009. Unconventional myosins acting unconventionally. *Trends in Cell Biology,* 19**,** 245-252.

WYMANT, J. M. 2014. *The role of BCA2 in receptor tyrosine kinase endocytosis and breast cancer.* Ph.D thesis, Cardiff University. Accessible from orca.cf.ac.uk/72275.

YANG, C. & SVITKINA, T. 2011. Filopodia initiation: focus on the Arp2/3 complex and formins. *Cell Adhesion & Migration,* 5**,** 402-408.

YANG, L., WANG, L. & ZHENG, Y. 2006. Gene targeting of Cdc42 and Cdc42GAP affirms the critical involvement of Cdc42 in filopodia induction, directed migration, and proliferation in primary mouse embryonic fibroblasts. *Molecular Biology of the Cell,* 17**,** 4675-4685.

YESYLEVSKYY, S., MARRINK, S. J. & MARK, A. E. 2009. Alternative mechanisms for the interaction of the cell-penetrating peptides penetratin and the TAT peptide with lipid bilayers. *Biophysical Journal,* 97**,** 40-49.

YIN, H., KANASTY, R. L., ELTOUKHY, A. A., VEGAS, A. J., DORKIN, J. R. & ANDERSON, D. G. 2014. Non-viral vectors for gene-based therapy. *Nature Reviews Genetics,* 15**,** 541-555.

YOO, Y., HO, H. J., WANG, C. & GUAN, J. L. 2009. Tyrosine phosphorylation of cofilin at Y68 by v-Src leads to its degradation through ubiquitin-proteasome pathway. *Oncogene,* 29**,** 263-272.

ZHANG, H., WEBB, D. J., ASMUSSEN, H., NIU, S. & HORWITZ, A. F. 2005. A GIT1/PIX/Rac/PAK signaling module regulates spine morphogenesis and synapse formation through MLC. *The Journal of Neuroscience,* 25**,** 3379-3388.

ZIEGLER, A. & SEELIG, J. 2008. Binding and clustering of glycosaminoglycans: a common property of mono- and multivalent cell-penetrating compounds. *Biophysical Journal,* 94**,** 2142-2149.

ZIGMOND, S. H. 2004. Formin-induced nucleation of actin filaments. *Current Opinion in Cell Biology,* 16**,** 99-105.

ZORKO, M. & LANGEL, Ü. 2005. Cell-penetrating peptides: mechanism and kinetics of cargo delivery. *Advanced Drug Delivery Reviews,* 57**,** 529-545.

ZUCHERO, J. B., COUTTS, A. S., QUINLAN, M. E., THANGUE, N. B. L. & MULLINS, R. D. 2009. p53-cofactor JMY is a multifunctional actin nucleation factor. *Nature Cell Biology,* 11**,** 451-459.

Appendix 1: The original SDS-PAGE gel that formed the template for Figure 3.2.

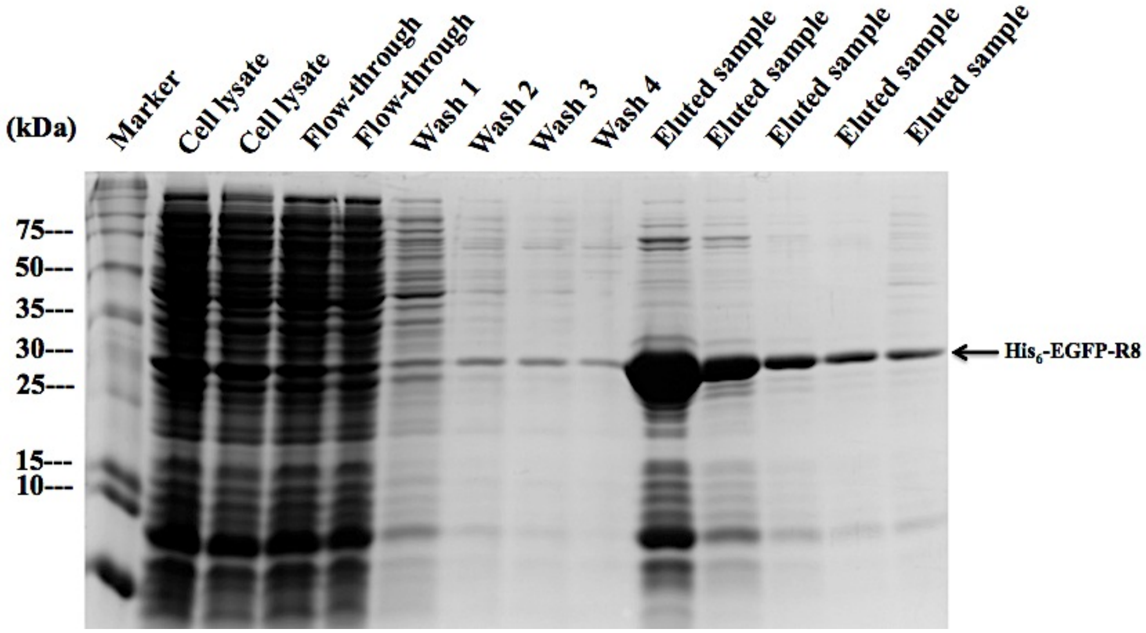

Appendix 2: The effects of cytochalasin D (Cyt D) on internalisation of dextran (40 kDa) labeled with FITC (FITC-Dex40) in A431 and published as Figure 8F in (Al Soraj et al., 2012).

A431 cells seeded on tissue culture plates were washed twice with PBS at room temperature then pre-incubated at 37°C/5% CO_2 for 15 min in serum-free D-MEM in the absence (control) or presence of 10 μM Cyt D. The media was removed and fresh serum-free D-MEM containing 5.0 mg/ml FITC-Dex40 (Sigma-Aldrich, Dorset, UK) as well as 10 μM Cyt D was added and the cells were further incubated for 0–80 min at 37°C/5% CO_2. The plates were then placed on ice to inhibit further uptake and washed twice with ice-cold PBS followed by a 1 min incubation in ice-cold acid wash (0.2 M acetic acid, 0.2 M NaCl, pH 2.0) to remove remaining surface label. Cells were then washed three times with PBS at room temperature, prior to trypsinisation for 4 min at 20°C. The cell suspension was then washed with ice-cold PBS, before measuring cell-associated fluorescence (10,000 gated cells) by flow cytometry on a Becton Dickinson FACScalibur analyser.

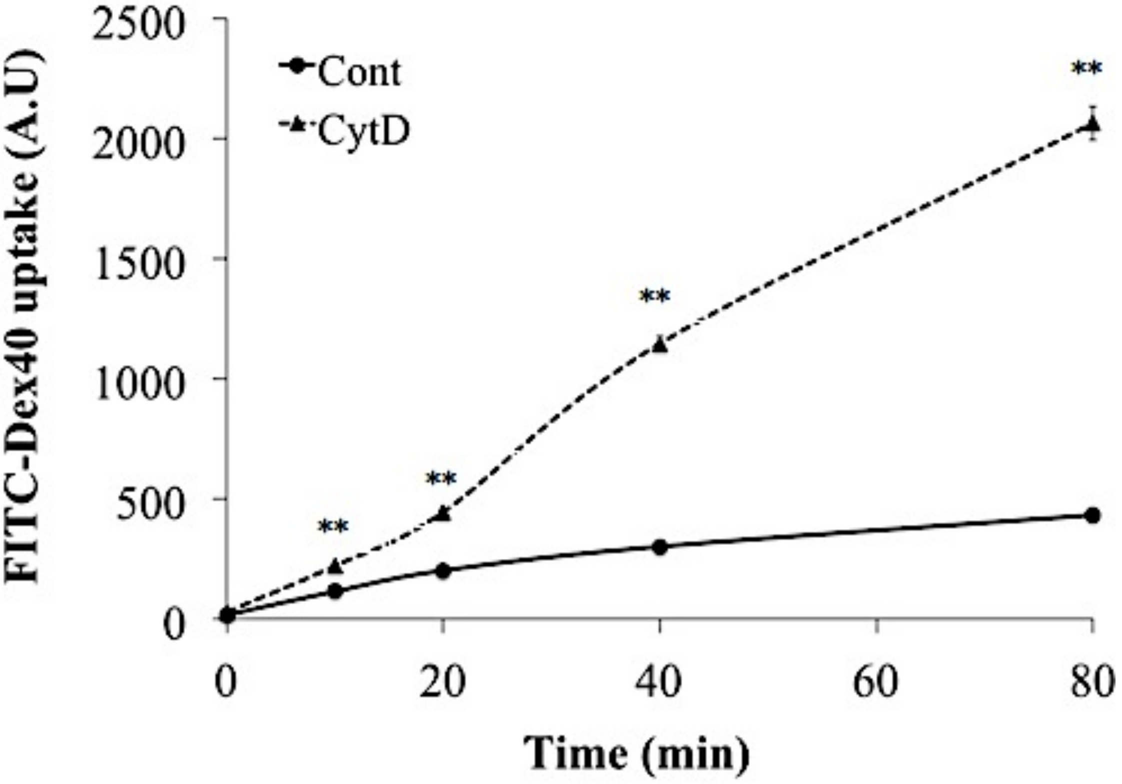

Appendix Figure 2. The effects of cytochalasin D (Cyt D) on internalisation of dextran (40 kDa) labeled with FITC (FITC-Dex40) in A431 cells. Cells were pre-incubated in the absence (Cont) or presence of 10 μM Cyt D prior to incubation with FITC-Dex40 for the indicated time points. The cells were then trypsinised and analysed by flow cytometry. Data represent the geometric means ± S.D. from three separate experiments. Statistical analysis for comparing control cells with treated cells was performed using the Student's t-test. ** $p<0.01$, compared with controls. The cellular uptake of this probe in A431 cells was markedly increased following actin disruption by Cyt D.

Appendix 3: Effects of 0.8 μM JAS on the cellular uptake of EGFP-R8 in A431 cells.

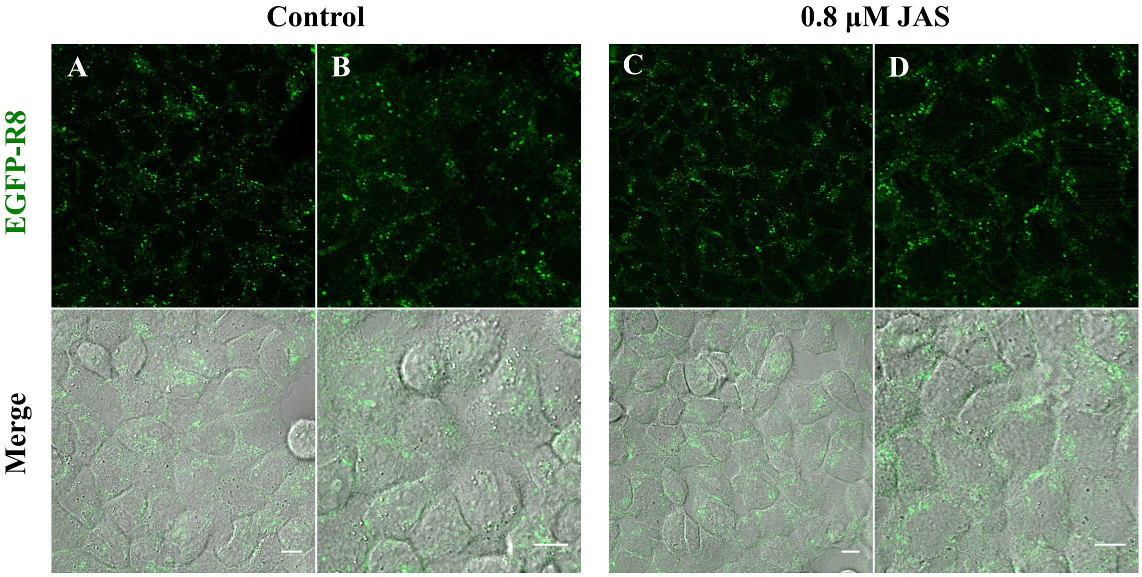

Appendix Figure 3. Effects of JAS on the cellular uptake of EGFP-R8 in A431 cells. Cells (control and those pre-treated with 0.8 μM JAS for 45 min) were incubated with 2 μM EGFP-R8 in the continued absence (control) or presence of 0.8 μM JAS for 1 hr and washed three times with heparin and once with PBS. Cell associated fluorescence was analysed using live-cell confocal microscopy and shown are single projection images of fluorescence only (top rows) and merges of fluorescence and DIC of the same cells. B/D represent zoomed images from different fields of view of A/C. Scale bars 10 μm.

Appendix 4: Calculation of fluorescence intensities (Moody et al., 2015).

Images to be analysed by this quantification method were acquired by live cell confocal microscopy. Single chosen images were analysed using an ImageJ script without manual intervention. Fluorescence intensity was calculated for each channel except the DIC channel. Pixels with intensity greater than an ImageJ Li (Li and Lee, 1993) threshold were considered as "fluorescent", and the mean intensity of these fluorescent pixels was calculated. Pixels having intensity below a Li threshold and being spatially separated by at least 5 pixels from any pixel above this threshold were labelled as "Background". Then the mean background intensity was calculated. The corrected intensity was then calculated by subtracting the mean background intensity value from the mean fluorescence intensity value. For each experimental sample, corrected intensity values were calculated for at least ten images (≥100 cells in total), and the average of these values was then calculated as shown in Chapter 5.

References

AL SORAJ, M., HE, L., PEYNSHAERT, K., COUSAERT, J., VERCAUTEREN, D., BRAECKMANS, K., DE SMEDT, S. C. & JONES, A. T. 2012. siRNA and pharmacological inhibition of endocytic pathways to characterize the differential role of macropinocytosis and the actin cytoskeleton on cellular uptake of dextran and cationic cell penetrating peptides octaarginine (R8) and HIV-Tat. *Journal of Controlled Release,* 161**,** 132-141.

LI, C. H. & LEE, C. K. 1993. Minimum cross entropy thresholding. *Pattern Recognition,* 26**,** 617-625.

MOODY, P. R., SAYERS, E. J., MAGNUSSON, J. P., ALEXANDER, C., BORRI, P., WATSON, P. & JONES, A. T. 2015. Receptor crosslinking: a general method to trigger internalization and lysosomal targeting of therapeutic receptor:ligand complexes. *Molecular Therapy,* 23**,** 1888-1898.